This item was submitted to Loughborough University as a PhD thesis by the author and is made available in the Institutional Repository (https://dspace.lboro.ac.uk/) under the following Creative Commons Licence conditions.

creative commons

COMMONS DEED

Attribution-NonCommercial-NoDerivs 2.5

You are free:

- to copy, distribute, display, and perform the work

Under the following conditions:

Attribution. You must attribute the work in the manner specified by the author or licensor.

Noncommercial. You may not use this work for commercial purposes.

No Derivative Works. You may not alter, transform, or build upon this work.

- For any reuse or distribution, you must make clear to others the license terms of this work.
- Any of these conditions can be waived if you get permission from the copyright holder.

Your fair use and other rights are in no way affected by the above.

This is a human-readable summary of the Legal Code (the full license).

Disclaimer

For the full text of this licence, please go to:
http://creativecommons.org/licenses/by-nc-nd/2.5/

Novel Control of a High Performance Rotary Wood Planing Machine

by

Matthew Chamberlain
4/19/2013

A doctoral thesis submitted in partial fulfilment of the requirements for the award of Doctor of Philosophy of Loughborough University

© Matthew Chamberlain 2013

Loughborough
University

CERTIFICATE OF ORIGINALITY

This is to certify that I am responsible for the work submitted in this thesis, that the original work is my own except as specified in acknowledgments or in footnotes, and that neither the thesis nor the original work contained therein has been submitted to this or any other institution for a degree.

……………………………………………. (Signed)

……………………………………………. (Date)

Abstract

Rotary planing, and moulding, machining operations have been employed within the woodworking industry for a number of years. Due to the rotational nature of the machining process, cuttermarks, in the form of waves, are created on the machined timber surface. It is the nature of these cuttermarks that determine the surface quality of the machined timber. It has been established that cutting tool inaccuracies and vibrations are a prime factor in the form of the cuttermarks on the timber surface. A principal aim of this thesis is to create a control architecture that is suitable for the adaptive operation of a wood planing machine in order to improve the surface quality of the machined timber.

In order to improve the surface quality, a thorough understanding of the principals of wood planing is required. These principals are stated within this thesis and the ability to manipulate the rotary wood planing process, in order to achieve a higher surface quality, is shown. An existing test rig facility is utilised within this thesis, however upgrades to facilitate higher cutting and feed speeds, as well as possible future implementations such as extended cutting regimes, the test rig has been modified and enlarged. This test rig allows for the dynamic positioning of the centre of rotation of the cutterhead during a cutting operation through the use of piezo electric actuators, with a displacement range of ±15µm.

A new controller for the system has been generated. Within this controller are a number of tuneable parameters. It was found that these parameters were dependant on a high number external factors, such as operating speeds and run-out of the cutting knives. A novel approach to the generation of these parameters has been developed and implemented within the overall system.

Both cutterhead inaccuracies and vibrations can be overcome, to some degree, by the vertical displacement of the cutterhead. However a crucial information element is not known, the particular displacement profile. Therefore a novel approach, consisting of a subtle change to the displacement profile and then a pattern matching approach, has been implemented onto the test rig.

Within the pattern matching approach the surface profiles are simplified to a basic form. This basic form allows for a much simplified approach to the pattern matching whilst producing a result suitable for the subtle change approach. In order to compress the data levels a Principal Component Analysis was performed on the measured surface data. Patterns were found to be present in the resultant data matrix and so investigations into defect classification techniques have been carried out using both K-Nearest Neighbour techniques and Neural Networks.

The application of these novel approaches has yielded a higher system performance, for no additional cost to the mechanical components of the wood planing machine, both in terms of wood throughput and machined timber surface quality.

Acknowledgements

The work described within this thesis was carried out at Innovative Manufacturing Research Centre at Loughborough University, during the period 2008-2012. I have been supervised by Professors Mike Jackson and Rob Parkin. I am very grateful for their continued support and encouragement throughout my PhD period. The feedback you have given to me during this time has been both to a greater understanding of this subject matter and also to develop more confidence in myself and my abilities. I would like to also thank the administrative staff, particularly Jo Mason, for her help and understanding. I must also thank the EPSRC for the funding for this project work, without this funding this project, and my PhD, would not have been possible. I would also like to thank Bob Wood. Your comments on my written work were always spot on, if not what I wanted to hear, and I thank you for having confidence in me to progress through this journey.

To all my friends and colleagues within the research centre must also go must sincerest thanks. To allow me to bounce ideas off you was essential for me, and without that ability I would truly have suffered.

I am very much indebted to my family for their continued support. It has been a long journey for us all to take, but we are finally there and hopefully it has been worth it! I thank you all for your support, both morale and financial. I will never be able to put into words what it has meant to me, but all I can say is a thank you.

4 Contents

TABLE OF FIGURES 10

TABLE OF TABLES 14

NOMENCLATURE 15

GLOSSARY OF TERMS 17

1. CHAPTER 1 – INTRODUCTION 1

1.1 Wood Planing Fundamentals 3

1.2 Demonstrator 6

1.3 Research Aims and Objectives 11

1.4 Proposed Control Architecture 13

1.5 Project Scope, Work Breakdown and Methodology 14

1.6 Research Achievements 16

1.7 Overview of Thesis 18

2 CHAPTER 2 - LITERATURE REVIEW 21

2.1 Material Removal Techniques 22

2.2 Metal Machining 22

2.3 Wood Machining 28
2.3.1 Rotary Wood Planing 30

2.4 Semi Active Vibration Reduction 37

2.5 Surface Inspection 40
2.5.1 Contact Measurement 41
2.5.2 Non-Contact Measurement 41

2.6 Data Processing 45

2.7 Adaptive Techniques 46

2.8 Research Gap 57
2.8.1 Proposed New Architecture 57

3 CHAPTER 3 – SURFACE WAVINESS OF PLANED WOOD 60

3.1 Circular Arcs Approximation 60

3.2 Surface Defects and Their Appearance Forms on Machined Timber 65
  3.2.1 The Effect of a Proud Knife on the Surface Form 65
  3.2.2 The Effect of Cutterhead Vibration on the Surface Form 68

3.3 Summary and Conclusions 70

4 METHODOLOGY 71

4.1 Summary of Current Drawbacks 71

4.2 Overall Project Flow Diagram 73
  4.2.1 Model Based Tuning Methodology Flow Diagram 74
  4.2.2 Defect Measurement and Classification Methodology Flow Diagram 75
  4.2.3 Subtle Change Methodology Flow Diagram 77

4.3 Summary 78

5 CHAPTER 5 - SMALL SCALE PLANER TEST RIG LAYOUT AND MODIFICATIONS 79

5.1 Piezo Electric Actuator 79

5.2 Eddy Current Probes 82

5.3 Mechanical Design of the Small Scale Planer 82
  5.3.1 Smart Spindle Unit 83
  5.3.2 Actuator Arrangement 88
  5.3.3 Sensor Arrangement 93

5.4 Small Scale Planer Modifications 97
  5.4.1 Feed Table Length 97
  5.4.2 Cutterheads 98
  5.4.3 Motor Upgrades 99
  5.4.4 WSMS Integration 101

5.5 New Small Scale Planer Test Rig 103

5.6 Commissioning Testing 104
  5.6.1 Motor Speed Tests 104
  5.6.2 Cutterhead Vibration Tests 106

6 CHAPTER 6 – MODEL BASED TUNING 108

6.1 Inner Control Architecture 108

6.2 System Identification 112

6.3 Input-Output Data **113**

6.4 State Based Model Parameter Estimation **117**

6.5 LQG Controller Parameter Tuning **120**

6.6 System Tracking Performance **121**
  6.6.1. An Adaptive Approach 128
  6.6.2 Data Generation 128
  6.6.3 Network Training 131

6.7 Network Parameter Generation Performance **133**

6.8 Summary and Conclusion **152**

7 CHAPTER 7 – DEFECT MEASUREMENT AND CLASSIFICATION TECHNIQUES **154**

7.1 Measurement Techniques **155**
  7.1.1 Wood Surface Measurement System Principals of Operation 155

7.2 Principal Component Analysis **162**
  7.2.1 Principal Component Analysis Implementation 163
  7.2.2 Use of Principal Components 164

7.3 A-Priori Knowledge Base **173**

7.4 Defect Classification Tools **174**
  7.4.1 K-Nearest Neighbor 175
  7.4.2 Pattern Recognition Neural Network 178
  7.4.3 Performance Differences between K-Nearest Neighbour and Pattern Recognition Neural Network 179

7.5 A-Priori Data Considerations **181**

7.6 Conclusions **182**

8 CHAPTER 8 – A NEW APPROACH, SUBTLE CHANGES **184**

8.1 Corrective Action Complication **185**

8.2 Generation of Further Data in Real Time **186**

8.3 Requirements for Subtle Change Approach **187**

8.4 Principal of Subtle Change Technique **189**
  8.4.1 Step 1 – Initial Cutting Test 192
  8.4.2 Step 2 – Initial Surface Waveform Analysis 193
  8.4.3 Step 3 – Modification of reference path 193
  8.4.4 Step 4 – Second Cutting Test 193
  8.4.5 Step 5 – Secondary Surface Waveform Analysis 194

8.4.6 Step 6 – Identification and Generation of Link 194

8.5 Potential Complications 197
8.5.1 Measurement Dependency 197
8.5.2 Lost Links 198
8.5.3 Number of Knives Around the Cutterhead 198
8.5.4 Missing Cuttermarks 198
8.5.5 Input Geometry 200
8.5.6 Knife Displacement Magnitude 204

8.6 Alternative Applications for the Technique 206
8.6.1 Rotary Machining Applications 206
8.6.2 Further Applications 207

9 CHAPTER 9 – THE CONNECTED SOLUTION 209

9.1 Two Knife Cutterhead 209
9.1.1 Cutting Parameters 209
9.1.2 System Identification 210
9.1.3 Initial Cutting Test 210
9.1.4 Heuristic Approach 211

9.2 Four Knife Cutterhead 212
9.2.1 Cutting Parameters 212
9.2.2 Initial Cutting Test 213
9.2.3 Heuristic Approach 213

9.3 Surface Quality Assessment 215

10 CHAPTER 10 – CONCLUSIONS AND RECOMMENDATIONS 217

10.1 Achievements from Aims 217
10.1.1 Test Rig Upgrade 217
10.1.2 Real-Time Controller Adjustment 217
10.1.3 Defect Classification Software Tool Development 218
10.1.4 Real-Time Reference Path Modification 219
10.1.5 Overall Assessment 219

10.2 Recommendations for Further Work 220
10.2.1 Measurement System 220
10.2.2 Defect Characterisation 220
10.2.3 Heuristic Subtle Change Approach 221

11 REFERENCES 222

12 APPENDIX A – COMPUTATIONAL MODELS 231

12.1 Simulink Model for Setpoint Tracker Controller 231

13 APPENDIX B – ALICONA INFINATE FOCUS MACHINE 232

14 APPENDIX C – PURCHASED COMPONENTS 234

14.1 Table of Suppliers 234

14.3 Component Data Sheets 235

15 APPENDIX D – TECHNICAL DRAWINGS 252

16 APPENDIX E – PUBLICATION 253

Table of Figures

FIGURE 1-1 - CNC LATHE 1
FIGURE 1-2 - SURFACE FEATURES - (HYNEK 2004) 3
FIGURE 1-3 - PRINCIPLE OF ROTARY MACHINING PROCESS - (ELMAS 2008) 5
FIGURE 1-4 - TEST RIG SCHEMATIC, (HYNEK 2004) 6
FIGURE 1-5 - WOOD MACHINING PROCESS 7
FIGURE 1-6 - CUTTERHEAD DETAIL - (HYNEK 2004) 8
FIGURE 1-7 - SURFACE WAVINESS - (ELMAS 2008) 9
FIGURE 1-8 - EXISTING WOOD PLANING EXPERIMENTAL MACHINE 9
FIGURE 1-9 - PROPOSED KNOWLEDGE BASED CONTROL ARCHITECTURE 13
FIGURE 1-10- PROJECT BREAKDOWN STRUCTURE 15
FIGURE 2-1 - PIEZO-DRIVEN FLEXURE-BASED MECHANISM, (TIAN, ZHANG ET AL. 2011) 23
FIGURE 2-2 - SCHEMATIC DIAGRAM OF WORKPIECE MICRO-POSITIONING TABLE, (GAO, ZHANG ET AL. 2001) 24
FIGURE 2-3 - SET-UP OF THE ROTARY DRIVEN TOOL ON A LATHE, (LEI, LIU 2002) 25
FIGURE 2-4 - ASSEMBLED PROTOTYPE ROTARY-AXIAL SPINDLE, (LU, PAONE ET AL. 2009) 27
FIGURE 2-5 - STRUCTURE OF CIRCULAR SAW TEST RIG FOR VIBRATION CONTROL, (CHEN, WANG ET AL. 2003)) 29
FIGURE 2-6 - CUTTERMARK SHAPE INFLUENCED BY HORIZONTAL CUTTERHEAD MOVEMENT ((HYNEK 2004)) 32
FIGURE 2-7 - VERTICAL CUTTERHEAD MOVEMENT ((HYNEK 2004)) 33
FIGURE 2-8 - PRINCIPALS OF THE CUTTERHEAD INACCURACIES COMPENSATION ((OGUN 2012)) 35
FIGURE 2-9 - CONTROL SYSTEM WITH BOTH FEED-FORWARD AND FEEDBACK CONTROL, (OGUN 2012)37
FIGURE 2-10 - ER DAMPER, (LIM, PARK ET AL. 2005) 38
FIGURE 2-11 - PRINCIPAL OF LIGHT SECTIONING, (YANG, JACKSON ET AL. 2006) 42
FIGURE 2-12 - SCHEMATIC OF THE TWO-IMAGE PHOTOMETRIC STEREO SETUP, (OGUN, JACKSON ET AL. 2012) 43
FIGURE 2-13 - ON-LINE INVERSE LEARNING, (DENAI, PALIS ET AL. 2004) 52
FIGURE 2-14 - PROPOSED SYSTEM ARCHITECTURE 58
FIGURE 3-1 - ROTARY MACHINING PROCESS VELOCITY RELATIONSHIPS - (HYNEK 2004) 61
FIGURE 3-2 - CIRCULAR ARCS APPROXIMATION – (HYNEK 2004) 62
FIGURE 3-3 - THE EFFECT OF SINGLE AND TWO KNIFE FINISH ON THE IDEAL SURFACE FORM 66
FIGURE 3-4 - EFFECT OF TIR ON SURFACE FINISH 67
FIGURE 3-5 - JOINTED CUTTER WITH JOINT LAND 68
FIGURE 3-6 - EFFECT OF 1 PER REVOLUTION VIBRATION ON THE SURFACE FORM 69
FIGURE 4-1 - OVERALL PROJECT METHODOLOGY FLOWCHART 73
FIGURE 4-2 - MODEL BASED TUNING METHODOLOGY FLOWCHART 74
FIGURE 4-3 - DEFECT MEASUREMENT AND CLASSIFICATION METHODOLOGY FLOWCHART 75
FIGURE 4-4 - SUBTLE CHANGE TECHNIQUE METHODOLOGY FLOWCHART 77
FIGURE 5-1 - PIEZO HYSTERESIS CURVE, (OGUN 2012) 80
FIGURE 5-2 - SPINDLE RESPONSES TO DIFFERING STEP INPUT VOLTAGES 81
FIGURE 5-3 - SMALL SCALE PLANER, (HYNEK 2004) 83
FIGURE 5-4 - OVERHUNG SPINDLE 84
FIGURE 5-5 - RATIO $Y_K/Y_{V,}$ (HYNEK 2004) 86
FIGURE 5-6 – SMART SPINDLE UNIT CUT-THROUGH, (HYNEK 2004) 87
FIGURE 5-7 - SPINDLE SUPPORT 88
FIGURE 5-8 - SMART SPINDLE UNIT ARRANGEMENT 89
FIGURE 5-9 - ACTUATOR ARRANGEMENT 90

FIGURE 5-10 - DISPLACEMENT VERSUS VOLTAGE, (HYNEK 2004) 91
FIGURE 5-11 - ACTUATOR MOUNTING, (HYNEK 2004) 92
FIGURE 5-12 - EFFECT OF PRELOAD, Γ=0, (HYNEK 2004) 93
FIGURE 5-13 - SPINDLE SENSOR ARRANGEMENT, (HYNEK 2004) 94
FIGURE 5-14 - SPINDLE DEFLECTION TESTING SETUP 96
FIGURE 5-15 - EXAMPLE TORQUE VS TIME GRAPH AT 6000RPM 100
FIGURE 5-16 - INTEGRATION OF WSMS TO THE SMALL SCALAR PLANING MACHINE 102
FIGURE 5-17 - UPDATED SMALL SCALE PLANER TEST RIG 103
FIGURE 5-18 - SPEED-TIME GRAPH FOR FEED MOTOR 105
FIGURE 5-19 - SPINDLE VIBRATION TEST AT 3000RPM 106
FIGURE 6-1- INNER CONTROL SYSTEM USING BOTH FEEDFORWARD AND FEEDBACK CONTROL (OGUN, JACKSON ET AL. 2012, OGUN 2012) 108
FIGURE 6-2 - IMBALANCE MASS ATTACHED TO THE CUTTERHEAD 115
FIGURE 6-3- TIME DOMAIN RESPONSE - 106G CUTTERHEAD 115
FIGURE 6-4 - TIME DOMAIN RESPONSE - 190G CUTTERHEAD 116
FIGURE 6-5 - TIME DOMAIN RESPONSE - 293G CUTTERHEAD 116
FIGURE 6-6- MEASURED AND PREDICTED OUTPUTS FOR SECOND ORDER MODEL 118
FIGURE 6-7 - MEASURED AND PREDICTED OUTPUTS FOR FOURTH ORDER MODEL 119
FIGURE 6-8 - MEASURED AND PREDICTED OUTPUTS FOR SIXTH ORDER MODEL 119
FIGURE 6-9 - GRAPH SHOWING OVERSHOOT, SETTLING TIME AND RISE TIME EXAMPLES 122
FIGURE 6-10 - MEASURED VS DESIRED CUTTERHEAD POSITIONS, TIR 0.005M, 1000RPM, HIGH FEEDBACK GAIN (K_{FF} = 15) 123
FIGURE 6-11 - MEASURED VS DESIRED CUTTERHEAD POSITIONS, TIR 0.005M, 1000RPM, HIGH FEEDBACK GAIN (K_{FF} = 15) ZOOMED 123
FIGURE 6-12 - MEASURED VS DESIRED CUTTERHEAD POSITIONS, TIR 0.005M, 1000RPM, LOW FEEDBACK GAIN (K_{FF} = 1) 124
FIGURE 6-13 - MEASURED VS DESIRED CUTTERHEAD POSITIONS, TIR 0.005M, 1000RPM, LOW FEEDBACK GAIN (K_{FF} = 1), ZOOMED 125
FIGURE 6-14 - MEASURED VS DESIRED CUTTERHEAD POSITIONS, TIR 0.005M, 3000RPM, POORLY TUNED 125
FIGURE 6-15 - MEASURED VS DESIRED CUTTERHEAD POSITIONS, TIR 0.005M, 3000RPM, POORLY TUNED, ZOOMED 126
FIGURE 6-16 - MEASURED VS DESIRED CUTTERHEAD POSITIONS, TIR 0.005M, 3000RPM, TUNED 127
FIGURE 6-17 - MEASURED VS DESIRED CUTTERHEAD POSITIONS, TIR 0.005M, 3000RPM, TUNED, ZOOMED 127
FIGURE 6-18 - MANUAL PARAMETER GENERATION FOR OPTIMAL CONTROL 130
FIGURE 6-19 - SMALL NETWORK (20 HIDDEN NODES) K_{FF} GENERATION PERFORMANCE USING SMALLER DATA SET (5 ENTRIES) FOR TIR OF 10µM 136
FIGURE 6-20 - SMALL NETWORK (20 HIDDEN NODES) K_{FF} GENERATION PERFORMANCE USING SMALLER DATA SET (5 ENTRIES) FOR TIR OF 15µM 136
FIGURE 6-21 - LARGE NETWORK (50 HIDDEN NODES) K_{FF} GENERATION PERFORMANCE USING SMALLER DATA SET (5 ENTRIES) FOR TIR OF 10µM 138
FIGURE 6-22 - LARGE NETWORK (50 HIDDEN NODES) K_{FF} GENERATION PERFORMANCE USING SMALLER DATA SET (5 ENTRIES) FOR TIR OF 15µM 138
FIGURE 6-23 - SMALL NETWORK (20 HIDDEN NODES) K_{FF} GENERATION PERFORMANCE USING LARGER DATA SET (21 ENTRIES) FOR TIR OF 10µM 140
FIGURE 6-24 - SMALL NETWORK (20 HIDDEN NODES) K_{FF} GENERATION PERFORMANCE USING LARGER DATA SET (21 ENTRIES) FOR TIR OF 15µM 140

FIGURE 6-25 - LARGE NETWORK (50 HIDDEN NODES) K_{FF} GENERATION PERFORMANCE USING LARGER DATA SET (21 ENTRIES) FOR TIR OF 10µM 142
FIGURE 6-26 - LARGE NETWORK (50 HIDDEN NODES) K_{FF} GENERATION PERFORMANCE USING LARGER DATA SET (21 ENTRIES) FOR TIR OF 15µM 142
FIGURE 6-27 - SMALL NETWORK (20 HIDDEN NODES) Q GENERATION PERFORMANCE USING SMALLER DATA SET (5 ENTRIES) FOR TIR OF 10µM 144
FIGURE 6-28 - SMALL NETWORK (20 HIDDEN NODES) Q GENERATION PERFORMANCE USING SMALLER DATA SET (5 ENTRIES) FOR TIR OF 15µM 144
FIGURE 6-29 - LARGE NETWORK (50 HIDDEN NODES) Q GENERATION PERFORMANCE USING SMALLER DATA SET (5 ENTRIES) FOR TIR OF 10µM 146
FIGURE 6-30 - LARGE NETWORK (50 HIDDEN NODES) Q GENERATION PERFORMANCE USING SMALLER DATA SET (5 ENTRIES) FOR TIR OF 15µM 146
FIGURE 6-31 - SMALL NETWORK (20 HIDDEN NODES) Q GENERATION PERFORMANCE USING LARGER DATA SET (21 ENTRIES) FOR TIR OF 10µM 148
FIGURE 6-32 - SMALL NETWORK (20 HIDDEN NODES) Q GENERATION PERFORMANCE USING LARGER DATA SET (21 ENTRIES) FOR TIR OF 15µM 148
FIGURE 6-33 - LARGE NETWORK (50 HIDDEN NODES) Q GENERATION PERFORMANCE USING LARGER DATA SET (21 ENTRIES) FOR TIR OF 10µM 150
FIGURE 6-34 - LARGE NETWORK (50 HIDDEN NODES) Q GENERATION PERFORMANCE USING LARGER DATA SET (21 ENTRIES) FOR TIR OF 15µM 150
FIGURE 7-1 - IDEALISED SPECULAR AND DIFFUSE REFLECTION - A LAMBERTIAN SURFACE - (JACKSON, YANG ET AL. 2007) 156
FIGURE 7-2 - SCHEMATIC OF LAMBERTIAN REFLECTION 157
FIGURE 7-3 - SCHEMATIC OF THE TWO IMAGE PHOTOMETRIC STEREO METHOD, (JACKSON, YANG ET AL. 2007) 159
FIGURE 7-4 - CUTTERHEAD NUMBERING CONVENTION 165
FIGURE 7-5 - FOUR KNIFE FINISH WITH ONCE PER REVOLUTION VIBRATION (Φ = 0) 166
FIGURE 7-6 - FOUR KNIFE FINISH WITH ONCE PER REVOLUTION VIBRATION (Φ = Π/2) 167
FIGURE 7-7 - FOUR KNIFE FINISH WITH ONCE PER REVOLUTION VIBRATION (Φ = Π/4) 167
FIGURE 7-8 - FOUR KNIFE FINISH WITH ONCE PER REVOLUTION VIBRATION (Φ = Π/6) 168
FIGURE 7-9 - FOUR KNIFE FINISH WITH ONCE PER REVOLUTION VIBRATION (Φ = Π/8) 168
FIGURE 7-10 - FOUR KNIFE FINISH WITH TWICE PER REVOLUTION VIBRATION 170
FIGURE 7-11 - EXTENDED PRINCIPAL COMPONENT ANALYSIS TO INCLUDE A THIRD INPUT DATA STREAM, THE AVERAGE OF THE UPPER AND LOWER ENVELOPES 171
FIGURE 7-12 - K-NEAREST NEIGHBOR GRAPHICAL EXAMPLE, K = 3 176
FIGURE 7-13 - MODIFIED K-NEAREST NEIGHBOR APPROACH 177
FIGURE 7-14 - SIMPLIFIED PATTERNNET NETWORK SHOWING BOTH IDEAL AND REAL TYPE OUTPUTS 179
FIGURE 8-1 - EXAMPLE CUTTERHEAD GEOMETRY 184
FIGURE 8-2 - EXAMPLE TIMBER SURFACE CUT WITH A SINGLE PROUD KNIFE ON A FOUR KNIFE CUTTERHEAD 185
FIGURE 8-3 - REQUIRED REPETITIVE CUTTERMARKS ON TIMBER SURFACE 188
FIGURE 8-4 - NON REPEATING SURFACE FORM 189
FIGURE 8-5 - FLOW DIAGRAM OF HEURISTIC APPROACH 191
FIGURE 8-6 - EXAMPLE IDEALISED SURFACE DEFECTS 194
FIGURE 8-7 - EXAMPLE INITIAL SURFACE FORM 195
FIGURE 8-8 - PLUNGE KNIFE 1 SURFACE DEFECT EXAMPLE 195
FIGURE 8-9 - MATCHED IDEALISED SURFACE DEFECTS 196
FIGURE 8-10 - POSSIBLE SURFACE FORMS PRODUCED BY A SINGLE PLUNGED KNIFE REFERENCE PATH 200

FIGURE 8-11 - FURTHER POSSIBLE SURFACE FORMS PRODUCED BY A SINGLE PLUNGED KNIFE REFERENCE PATH 202
FIGURE 8-12 – TIMBER SURFACE BASED ON OUTPUT A 203
FIGURE 8-13 - KNIFE DISPLACEMENT COMPLICATION EXAMPLE........ 205
FIGURE 8-14 - COMPARISON BETWEEN DISCRETE AND NON DISCRETE CUTTING POSITIONS, LEFT - WOOD PLANING MACHINE FOUR KNIFE CUTTERHEAD, RIGHT - SURFACE GRINDING WHEEL...... 206
FIGURE 9-1 - 2 KNIFE CUTTING TEST WITHOUT COMPENSATION 210
FIGURE 9-2 - 2 KNIFE CUTTING TEST WITH COMPENSATION........ 212
FIGURE 9-3 - INITIAL CUTTING TEST SURFACE PROFILE 213
FIGURE 9-4 - SURFACE PROFILE WITH KNIFE 3 PLUNGED 14µM........ 214
FIGURE 9-5 - FINAL MACHINED TIMBER SURFACE 215

Table of Tables

TABLE 1-1 - SURFACE QUALITY CLASSIFICATION - (ELMAS 2008) 5
TABLE 5-1 - PIEZO ELECTRIC ACTUATOR SPECIFICATION 79
TABLE 5-2 - EDDY CURRENT SENSOR/DRIVER SPECIFICATION 82
TABLE 5-3 - ACTUATOR SPECIFICATION (SAME AS TABLE 5-1) 89
TABLE 5-4 - SPINDLE DISPLACEMENT RESULTS 96
TABLE 5-5 - CUTTERHEAD KNIFE TIP RADII MEASUREMENTS 99
TABLE 5-6 - SPINDLE VIBRATION AMPLITUDE DUE TO IMBALANCE 107
TABLE 6-1 - OPTIMAL CONTROL CHARACTERISTICS 129
TABLE 6-2 - K_{FF} GENERATION NETWORK FIGURES 134
TABLE 6-3 - Q GENERATION NETWORK FIGURES 134
TABLE 6-4 - DIFFERENT NETWORK SIZES AND INPUTS 135
TABLE 7-1 - PRINCIPAL COMPONENTS FOR FOUR KNIFE FINISH WITH ONCE PER REVOLUTION VIBRATION 166
TABLE 7-2 - PRINCIPAL COMPONENTS FOR FOUR KNIFE FINISH WITH ONCE PER REVOLUTION VIBRATIONS AT VARYING OUT OF BALANCE POSITIONS 168
TABLE 7-3 - PRINCIPAL COMPONENTS FOR A FOUR KNIFE FINISH WITH TWICE PER REVOLUTION VIBRATION 170
TABLE 7-4 - EXTENDED PCA RESULTS FOR FOUR KNIFE FINISH WITH ONCE PER REVOLUTION VIBRATIONS AT VARYING OUT OF BALANCE POSITIONS USING SIMULATED DATA, BASED ON SIMULATION DATA 172
TABLE 7-5 - EXTENDED PCA RESULTS FOR FOUR KNIFE FINISH WITH DIFFERING OPERATING CONDITIONS 172
TABLE 7-6 - K NEAREST NEIGHBOUR CLASSIFICATION RESULTS 179
TABLE 7-7 - NEURAL NETWORK CLASSIFICATION RESULTS 180
TABLE 7-8 - K-NEAREST NEIGHBOUR CLASSIFICATION SUCCESS BASED ON MODIFIED A-PRIORI KNOWLEDGE BASE 182
TABLE 9-1- STANDARD DEVIATION RESULTS 216

Nomenclature

d_t	Distance moved by cutterhead (mm)
E_h	Error is surface height between circular arcs approximation and actual height (mm)
h	Cuttermark height (mm)
h_a	Cuttermark actual height (mm)
h_c	Circular arcs surface height (mm)
k	Effective stiffness of actuators and spindle support (N m^{-1})
N	Number of knives
p	Cuttermark pitch (mm)
R	Knife radius (mm)
t	Time (s)
V_c	Cutterhead linear speed (mm s^{-1})
V_f	Feed speed (mm s^{-1})
V_o	Knife tip speed (mm s^{-1})
w	Cuttermark width (mm)
x_s, y_s	Spindle displacement measured in sensor co-ordinate system (mm)
y_v	Vertical cutterhead movement
α	Angle of knife tilt (rad)

ω	Cutting speed (rev s^{-1})
ω_c	Cutterhead angular speed (rad s^{-1})
ϕ	Angle between sensor axis and actuator axis (°)
τ	Light source azimuth (rad)
θ	Cutterhead angular position (rad)
σ	Light source zenith (rad)

Glossary of Terms

Albedo	A measure of the reflectivity of a surface. It is defined as the proportion of incident light that is reflected by the surface.
Chatter	Vibration of the machining process due to the difference in displacement between the cutting tool and the workpiece.
Cuttermarks	Waves cut into the surface caused by the kinematics of the rotary machining process
Jointing	A process employed in the wood planing industry to true all the cutting knives around the cutterhead to a common cutting circle
Kerf	The width of the groove generated by a cutting tool, such as a saw

1. Chapter 1 – Introduction

With world competition forcing all manufacturers to become more efficient and reduce cost whilst increasing both performance and reliability, we are forced to re-evaluate all the processes involved with the production of goods. This document is concerned principally with the production machine, more specifically, intelligent production machines. Figure 1-1 shows a current computer numerically controlled, CNC, lathe, although the same impetus are relevant upon all machining processes.

Figure 1-1 - CNC Lathe

In recent years there has been a move towards 'Lights Out Machining' (Noël, Sodhi et al. 2007)(Noël, Sodhi et al. 2007)(Noël, Sodhi et al. 2007)(Noël, Sodhi et al. 2007)(Noël, Sodhi et al. 2007)(Noël, Sodhi et al. 2007)(Noël, Sodhi et al. 2007)(Noël, Sodhi et al. 2007)(Noël, Sodhi et al. 2007) where, to increase machine utilisation, the machines are left running overnight without operators. This type of process was slow to take hold initially, as there were doubts over reliability and whether the machines could be 'trusted' to carry out all operations without the guidance of an experienced operator, however the fledgling technology more than proved itself and has now been adopted by a large proportion of manufacturing centres. This has obvious advantages, with reduced lead times and increased productivity being perhaps the most obvious, but it has also allowed companies to make, and obtain, bids for otherwise non commercially viable contracts, (Rooks 2003).

It has been estimated that an intelligent manufacturing machine system would improve utilisation by 100% and further increase productivity/quality by a factor of two in certain industry sectors, if the full capabilities of the machine were harnessed at all times. With such large possible improvements over current processes this type of system cannot be ignored or side-lined. The current methodology involves computer numerically controlled, CNC, machines, running to preloaded programs. This allows a certain amount of flexibility and indeed a much greater level of utilisation of the machine over a machine with a constant brief by the operator.

Also hypothesised is that if machine health and the process health were established and monitored during use operating parameters could be adjusted to exploit the best possible performance for the actual operating conditions, leading to increased production and reliability. This type of automatic process adjustment is set to dramatically change existing process machinery performance, from the current total dependence on mechanical and material characteristics of the process-workpiece interaction to a scenario where the advanced sensing, a-priori knowledge base, real-time determined process and machine/tool condition knowledge and dependant control actions, will result in a high speed adaptive intelligent machine capable of managing strategy and forming tactical decisions about process performance and delivery schedules.

1.1 Wood Planing Fundamentals

Surface quality is characterised by two features (Jackson, Parkin et al. 2002), surface roughness and surface waviness. Surface roughness being defined as the shorter-wavelength component of the surface form, primarily due to two factors, timber properties such as wood species and moisture content, and cutting edge geometry. Surface waviness is defined as the longer-wavelength component of the surface form (Hynek 2004) . These defects are illustrated in Figure 1-2 below. Surface waviness is caused through the fundamental kinematics on the rotating knives. As they remove the material they leave circular impressions in the material surface, often referred to as cuttermarks.

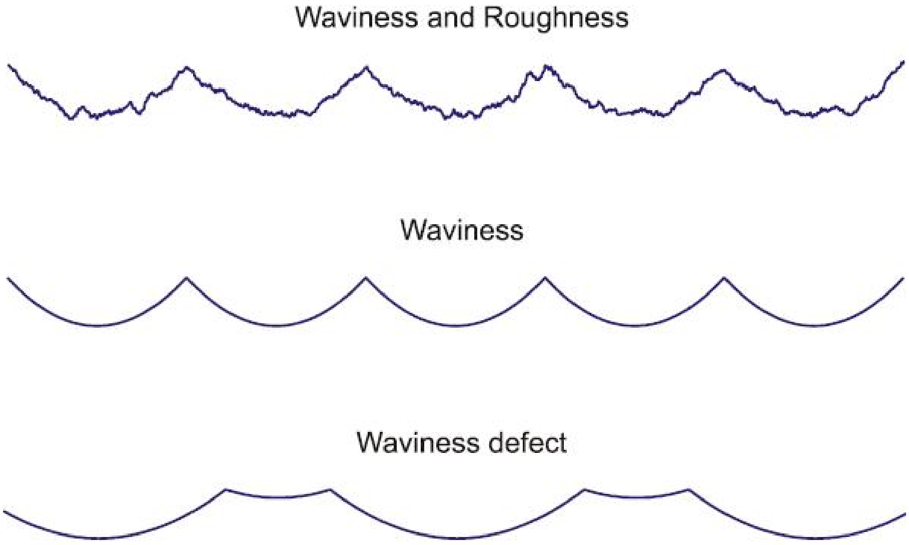

Figure 1-2 - Surface Features - (Hynek 2004)

Factors such as the type of cutterhead, machining parameters and machine condition can influence the surface waviness. (Goodchild 1963) studied the influence of vertical cutterhead harmonic movement with frequency equal to several multiples of spindle speed, and introduced a parameter which describes sensitivity of the cutting process to vertical vibration. This factor was defined as a critical amplitude of vertical cutterhead movement that causes the resultant surface finish to appear as if it were machined with fewer knives. Multiple critical amplitudes can be defined dependant on the number of actual knives on the cutterhead. As an example three critical amplitudes can be defined for a four knife cutterhead. The circular arc theory allows the derivation of the equations for the critical amplitudes. However this theory does not allow for the study of more general cases of cutterhead movement, cutterhead inaccuracies or a combination of the two.

Another factor that can have an effect on the surface quality are the cutting forces generated by the machining process. Large forces occur each time a cutting tooltip engages with the wood surface. These forces have been measured in the order of 30-1000N. Factors such as cutting direction, sharpness of knife, angle of knife engagement, chip thickness, cutting depth and timber properties all effect the cutting forces, (Jackson 1986), (Beer, Sinn et al. 2005).

The current wood planing technique is to feed the timber towards the rotating cutterhead at speed v_f, illustrated in Figure 1-3. The cutting speed typically lies within the range 30 - 80 ms^{-1}, with the feed speed also high, when compared to metals, typically within the range 0.08 – 1.6 ms^{-1} (Elmas 2008).

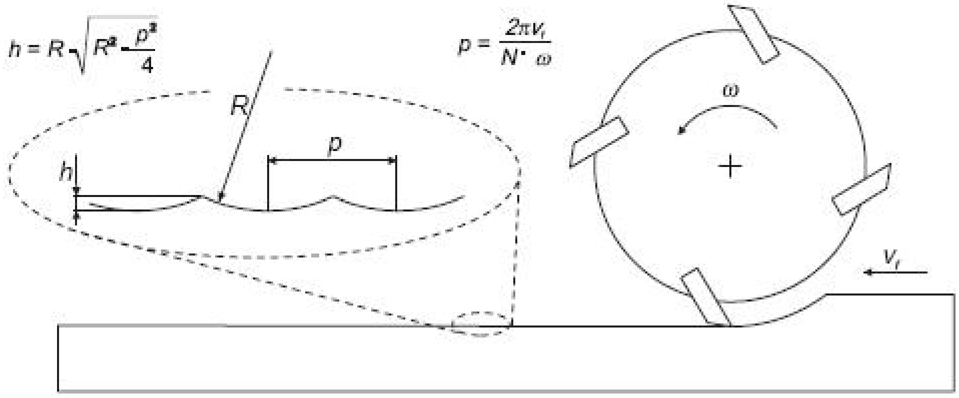
$h = R - \sqrt{R^2 - \frac{p^2}{4}}$
$p = \frac{2\pi v_f}{N \cdot \omega}$
R
h
p
ω
v_f

Figure 1-3 - Principle of Rotary Machining Process - (Elmas 2008)

Figure 1-3 illustrates the detrimental effect surface waviness can have on machined timber. The length of these cuttermarks, p, also known as the pitch, is usually taken as a measure of surface quality. Table 1-1 shows typical cuttermark lengths together with cuttermark heights for three different quality levels produced by a cutterhead with a 120mm diameter.

Table 1-1 - Surface Quality Classification - (Elmas 2008)

Surface quality	Cuttermark length (mm)	Cuttermark height (µm) (cutterhead radius R=60 mm)
Average	2.0 - 2.5	8.3 - 13
Good	1.5 - 1.8	4.7 – 6.8
High	1 .0 or less	2 or less

A high quality surface finish should have cuttermarks of <1mm length in a regular manner. This profile is almost undetectable by the human eye and the regularity of the wave appears ‘wave free’, (Jackson 1986).

1.2 Demonstrator

Within the Intelligent Automation Centre at Loughborough University exists a vast amount of experience with wood machining, particularly wood planing, and a rotary wood planing test rig to use for experimentation. It has been decided that the practical demonstrator for this project will be this wood planing machine. This will both help reduce costs and lead time as the machine will not have to be designed, assembled and tested, see Figure 1-8. The schematic of the test rig is given below.

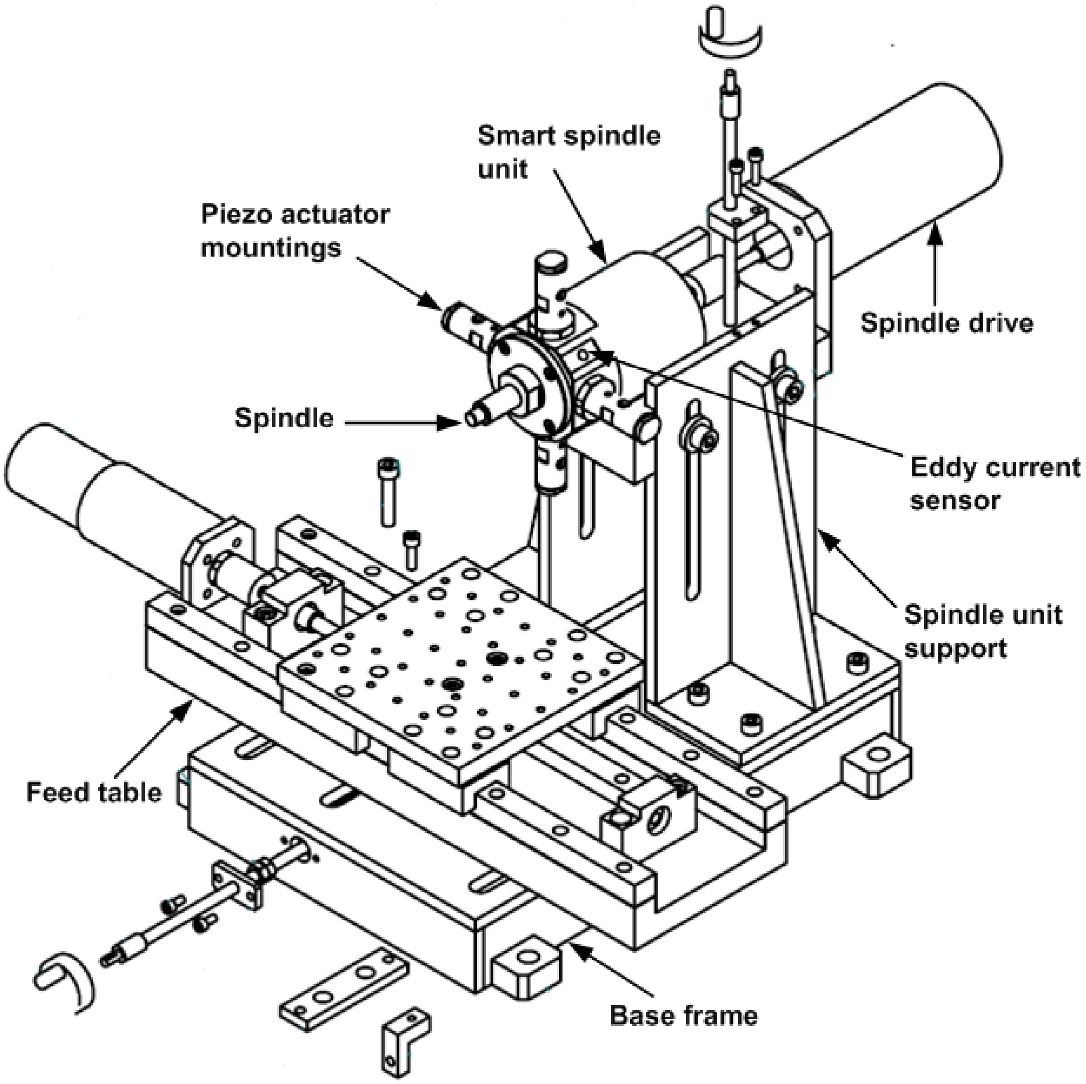
Smart spindle unit
Piezo actuator mountings
Spindle drive
Spindle
Eddy current sensor
Spindle unit support
Feed table
Base frame

Figure 1-4 - Test Rig Schematic, (Hynek 2004)

This test rig is capable of small scale wood planing, see chapter 4 for further details.

The fundamental principle of the rotary machining process lies in separation of the material by knives which are clamped in a rotating cutterhead as shown in Figure 1-5.

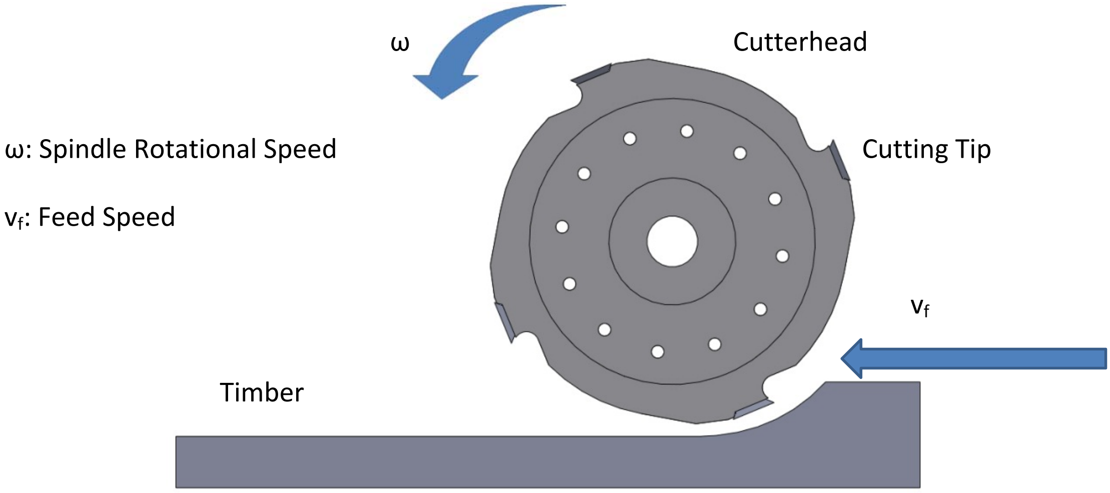
ω
Cutterhead
ω: Spindle Rotational Speed
Cutting Tip
v_f: Feed Speed
v_f
Timber

Figure 1-5 - Wood Machining Process

Figure 1-6 shows a photo of a real production machine cutterhead.

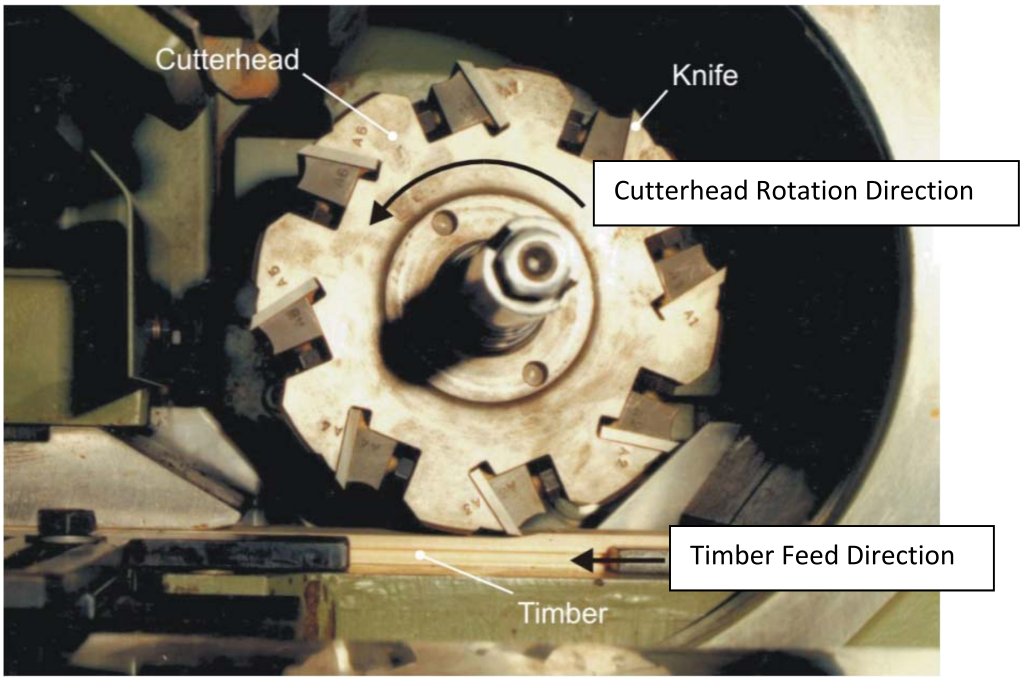

Figure 1-6 - Cutterhead Detail - (Hynek 2004)

A timber surface machined by rotary process consists of a number of waves due to the kinematics of the rotary machining process. In many applications it is desirable to reduce, or eradicate totally, these waves, such as furniture or window frame manufacture, (Malkoçoğlu 2007). The machining method and quality may also have an effect on the structural properties of an assembled wooden product. Typically wooden structures are bonded together and in these cases the machining method and surface quality are a major factor in the bonding strength, (Özçifçi, Yapici 2008). Figure 1-7 shows an example of surface quality that would not be acceptable where a high quality surface finish was required. If the surface quality was similar to that shown, further processing of the timber is required, such as sanding, (TAYLOR J, CARRANO A et al. 1999, Sulaiman, Hashim et al. 2009) . In the figure, as orientated below, the cuttermarks are clearly visible as vertical lines on the timber surface. These cuttermarks attract the eye, and detract from the overall impression of timber surface quality.

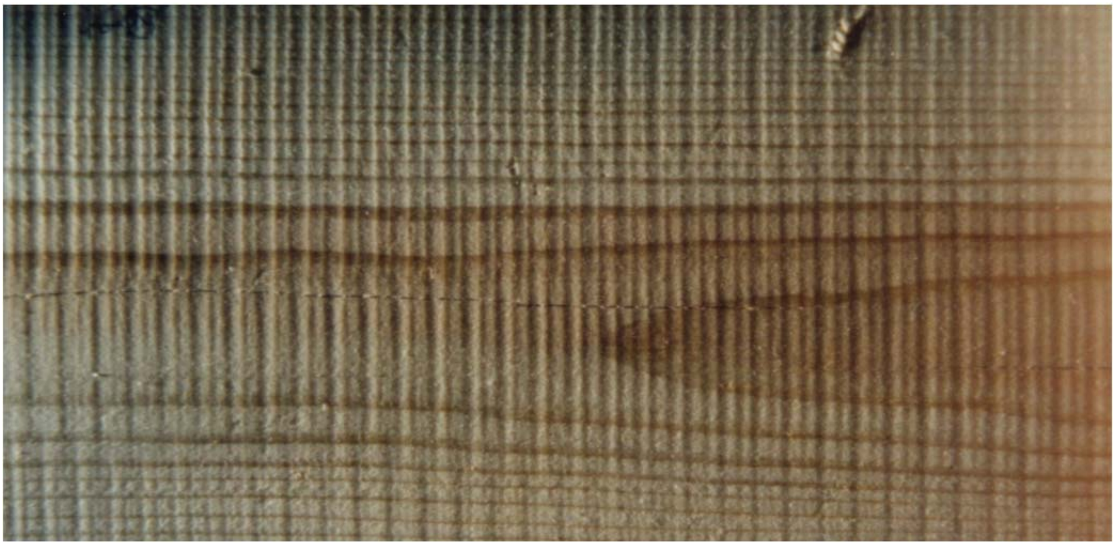

Figure 1-7 - Surface Waviness - (Elmas 2008)

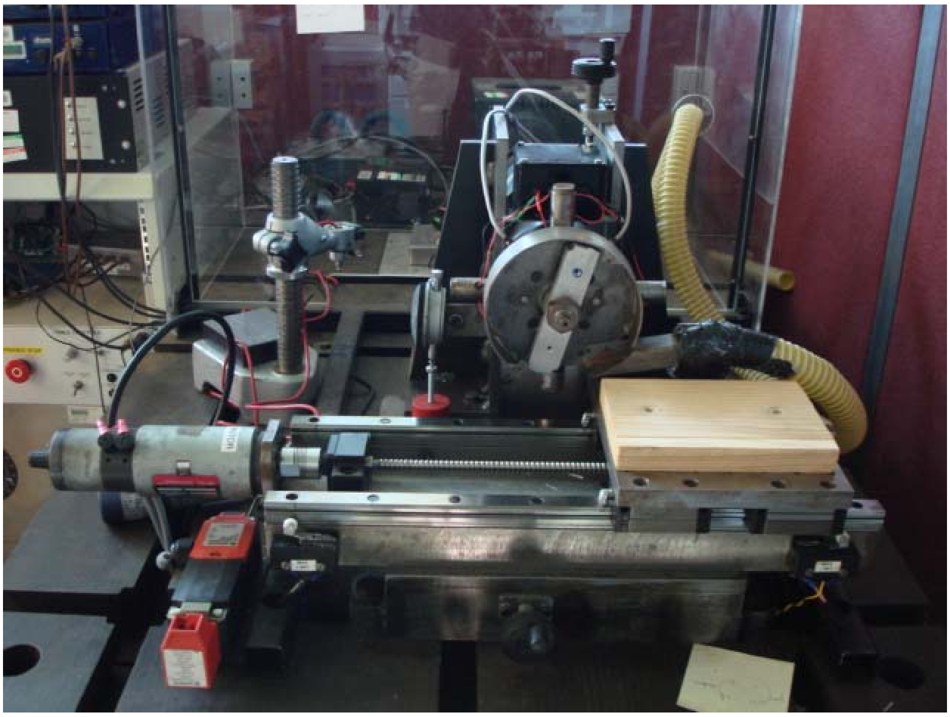

Figure 1-8 - Existing Wood Planing Experimental Machine

Although an existing test rig has been selected as the demonstrator for this research, Figure 1-8, modifications have been carried out to overcome certain limitations with the existing setup. The existing test rig has been used to design, and test, active vibration control (Elmas 2008), with limited actual cutting test being carried out. The control of the motor speeds was therefore fairly primitive, the system employed a variac to set the no load speed but no feedback was implemented such that when cutting commences the speed dramatically reduces. It was decided to modify the test rig in order to allow for a feedback loop for motor speeds to be employed, whilst at the same time extending the rotational speed range of the system. In order to measure the surface profile in real time and then take account of the measured surface, a larger slide length was required. This allows the timber to pass below the cutterhead and then into the visible range of the camera system, whilst timber is still being cut. Changes can then be made to the control system and these changes observed on a single piece of timber.

1.3 Research Aims and Objectives

The overall aim of this research is to develop a control architecture that is suitable for adaptive operation of a high performance rotary wood planing machine, in order to improve the surface quality of the machined timber surface. Within this research the specific research areas are:

- Test Rig Upgrade
    - To upgrade the small scale planer test rig in order to allow an increased scope of operation
    - Carry out commissioning tests to validate the updated test rig setup
- Real-Time Controller Parameter Adjustment
    - To investigate the effect of parameter adjustments to the controllers operation
    - To develop a system capable of predicting the required parameter requirements based on known a-priori conditions
    - To implement a system that can apply the predicted parameter conditions
- Defect Characterisation
    - To develop a software tool to understand the nature of the causes of the defects on the timber surface
- Real-Time Reference Path Modification
    - To develop a novel system to generate links between specific knives and their respective cuttermarks
    - To design and implement a system that can modify an existing reference path to implement the additional data generated by the link between specific knives and their cuttermarks
- Overall Assessment

- To perform cutting tests on the small scale planer test rig in order to ascertain the effectiveness of the path modification techniques

1.4 Proposed Control Architecture

In order to achieve the aims as set out in section 1.3, a new control architecture has been proposed. This single control system is able to compensate for cutterhead inaccuracies and process disturbances, such as vibrations. Although these have been studied independently, (Elmas 2008, Hynek 2004), this is the first attempt to design a control architecture combining this previous research with new approached developed here.

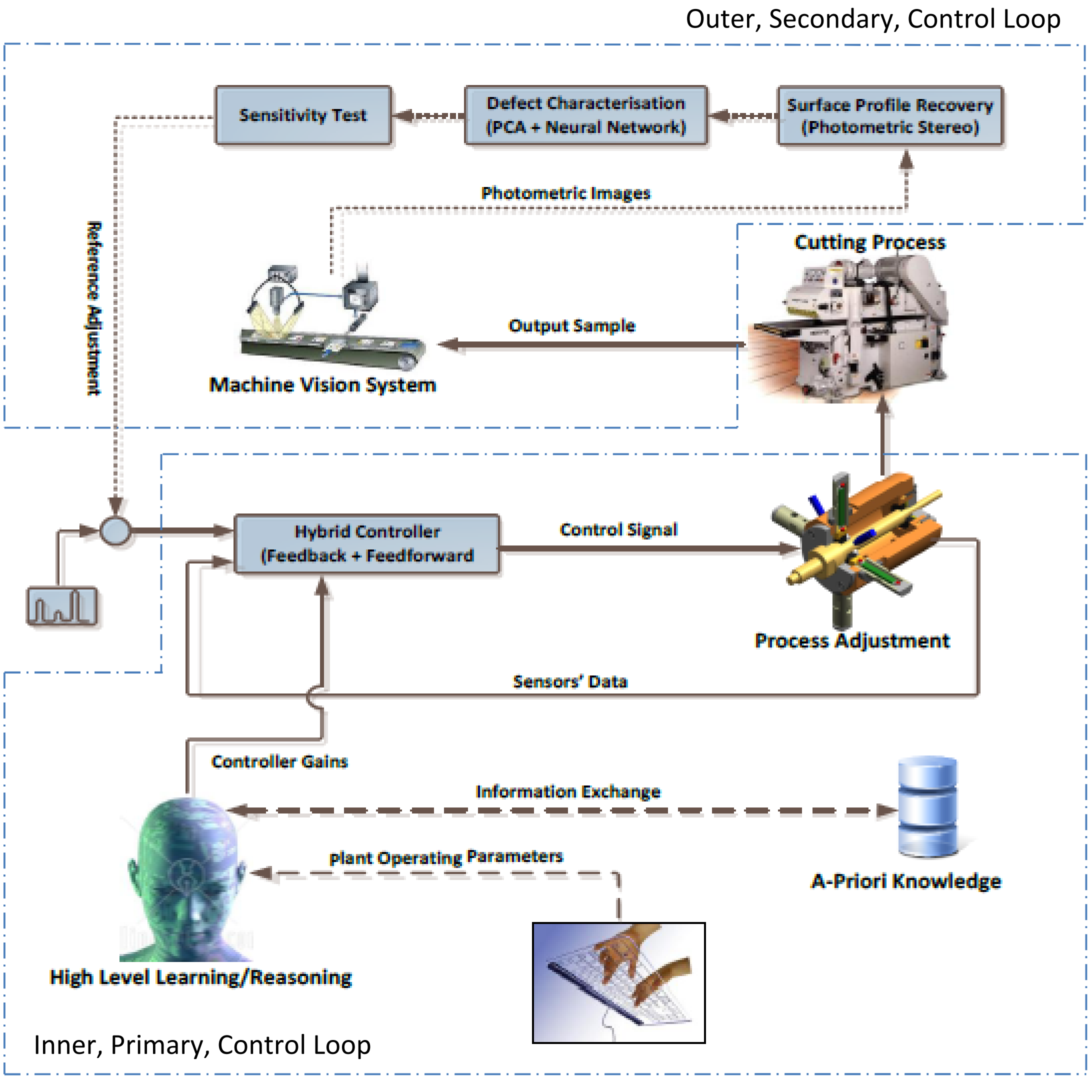
Outer, Secondary, Control Loop
Sensitivity Test
Defect Characterisation
(PCA + Neural Network)
Surface Profile Recovery
(Photometric Stereo)
Photometric Images
Reference Adjustment
Cutting Process
Output Sample
Machine Vision System
Hybrid Controller
(Feedback + Feedforward
Control Signal
Process Adjustment
Sensors' Data
Controller Gains
Information Exchange
Plant Operating Parameters
A-Priori Knowledge
High Level Learning/Reasoning
Inner, Primary, Control Loop

Figure 1-9 - Proposed Knowledge Based Control Architecture

The proposed control architecture is shown in Figure 1-9. The architecture consists of an inner, primary, control loop and an outer, secondary, control loop. The primary control loop concerns real-time monitoring and minor process adjustments of the plants process parameters. Within this loop sensors are used to measure the dynamic state of the plant with the signals passed to a controller driving the plant to the desired state. The desired state is pre-determined based on a-priori knowledge concerning the plant, as well as process disturbances.

Feedback is measured using a vision system focussed on the actual surface output. This measured surface output is then passed to the outer, secondary, control loop. Here the surface is characterised and the controller parameters are altered in a heuristic manner in order to achieve the system goal, an improved surface finish. This approach allows the plant to produce high quality surface finishes through the adjustment of controller parameters in real-time.

1.5 Project Scope, Work Breakdown and Methodology

The overall project involves a large amount of work, far more than can be reasonably achieved within the time constraints of the authors placement, and as such forms part of a team project, involving the author (MRC) and P. S. Ogun (PSO). This thesis considers the adaptive areas of the overall project, involving decision making and guidance planning. In order to achieve this, with the underlying emphasis being the usage of a-priori knowledge, an a-priori knowledge base for certain aspects of the work is also considered.

Figure 1-10 gives a breakdown of the separate work packages. These work packages are split as follows:

• Creation of process model for wood planing	(PSO)
• Synthetic data creation for defect characterisation	(MRC)
• Wood surface defect characterisation	(MRC)
• Visual based wood surface measurement	(PSO)
• Creation of heuristic process adjustment technique	(MRC)
• Test rig upgrade	(MRC)
• System identification	(PSO & MRC)
• Adaptive gain generation	(MRC)
• Controller design	(MRC & PSO)
• Experimental testing	(MRC & PSO)

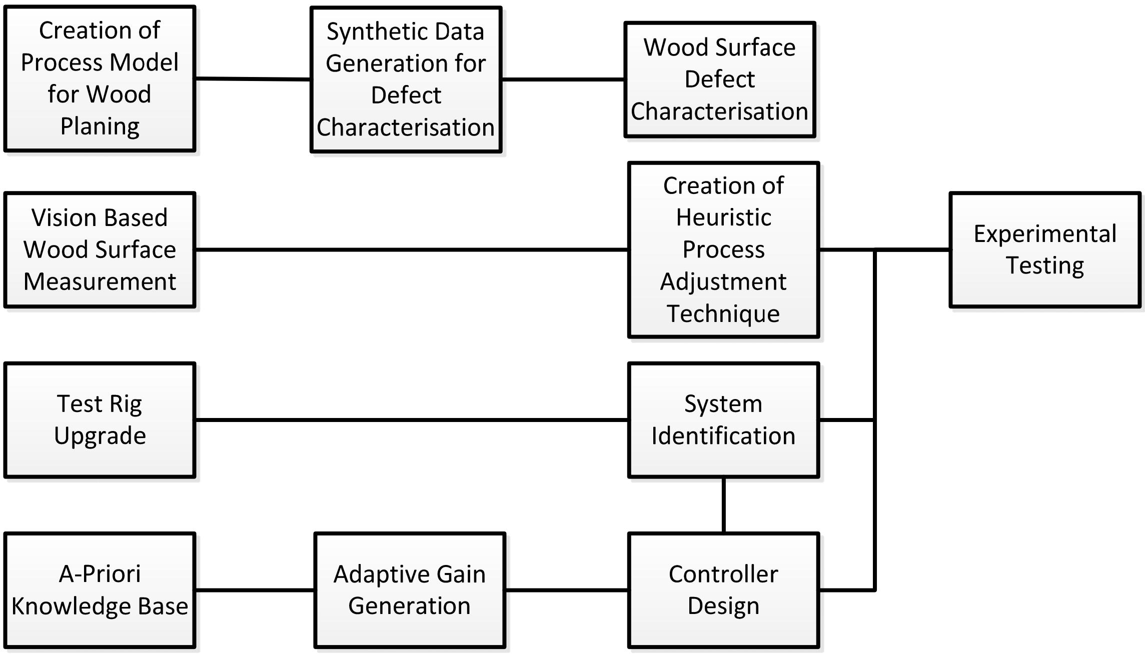
Creation of Process Model for Wood Planing
Synthetic Data Generation for Defect Characterisation
Wood Surface Defect Characterisation
Vision Based Wood Surface Measurement
Creation of Heuristic Process Adjustment Technique
Experimental Testing
Test Rig Upgrade
System Identification
A-Priori Knowledge Base
Adaptive Gain Generation
Controller Design

Figure 1-10- Project Breakdown Structure

The research reported in this thesis utilises multiple modelling and simulation techniques in order to gain an understanding of the processes involved with rotary wood planing. The model based approach has been selected as it allows rapid development of multiple solutions to the areas of specific interest. However, certain aspects of the work reported here have employed real world data recorded from the small-scale planer test rig. Due to the complexity, and multiple unknown conditions, which would have made the creation of an accurate model difficult, this method allowed measurement of the required parameters in a high speed manner without the need for the creation of a model. However, not having an accurate model of the plant may lead to difficulties when attempting to test further control approaches.

Using the real-world measured data, a system has been created that alters certain parameters of the main plant controller in order for accurate implementation of rectifying actions across a wide range of operating conditions. Utilising a generic rotary wood planing model, a large synthetic a-priori data base has been created and the data held within this database used to create models of the controller. This has allowed the development of a tool to classify both the defect cause and, separately, rectifying actions to overcome those defects. Finally, a new heuristic subtle change approach has been created in order to generate missing links between specific cutting knives and their cuttermarks. Once these links have been generated, rectifying actions can be taken in order to machine an improved surface quality.

1.6 Research Achievements

This novel research has resulted in a new control structure consisting of a heuristic subtle change technique combined with a simple pattern matching approach. Although the underlying approach employs iterative techniques with significant trial and error, the newly linked approaches of deliberately introducing a known defect causing error, and then the comparison of a simplified surface form, provide a powerful tool for the introduction of intelligent control. This new structure allows intelligent control to be applied to processes where previously the lack of system knowledge prohibited its implementation. This technique can also be applied continuously in real time, thereby advancing previous work in this area.

A new software tool has been created that both provides additional information suitable for application within the new control structure and subsequent 'blocks' and for an end user. For the user the software tool will enable a more accurate identification of the cause of the surface defect, and although within the control structure the end use is the same, identification of the defect, the novel software tool will suggest a set of rectifying actions to generate a more ideal surface waveform. It is also the case that once an ideal surface waveform has been generated, a particular surface defect type, that may be desired for a particular application, can be more easily introduced.

The original small scale planer test rig, which in itself has a high degree of novelty with piezo electric actuators mounted around the rotating shaft to effect the centre of rotation of the cutterhead, has been significantly upgraded. The test rig is now significantly more capable in terms of both processing speeds and cutting power. Although this facility has been used to enable the research within this thesis, the capability of the test rig is such that it now opens up further research into complimentary areas such as surface measurement, using different camera based system, of moving timber and sinusoidal based displacement based control strategies in order to achieve a higher quality machined timber surface.

1.7 Overview of Thesis

This thesis consists of nine chapters.

Chapter one gives an introduction to this research. The main research aims are stated as well as the structure of this report. The overall theme of the group project is presented and the work split given.

Chapter two explores the literature regarding wood machining in general, and 'sets the scene' of the current technology base. Importance has been given to wood planing and specific focus on adaptive technologies. The chapter focus remains however on the actual implementation of techniques rather than the more abstract.

Chapter three focuses on the wood planing technology and physical implications of the rotary wood planing process on the surface quality of the wood. The wood planing process is explained in detail with the governing equations given.

Chapter four sets out the drawbacks with the current systems and describes the proposed solutions. Flow diagrams are also given describing the methodology used within this thesis.

Chapter five describes in detail the small scalar planer test rig capabilities. The upgrades carried out are described, with further technical drawings given in the appendix. Commissioning tests are described and results presented.

Chapter six gives details of some work carried out by other research members linked with this project, as this is necessary to fit the main body of work for this chapter into context, that being the work on the LQG controller. It explains some of the limitations with the controller, and hence the need for a more adaptive and intelligent system. The main focus of this chapter is the Q to R ratio generation and selection and the differing effects of the different ratios. This work is mainly simulated due to time restraints and complications with the actual test rig. Descriptions are given about the database generation, requirements and the final system implementation.

Chapter seven studies the extraction of meaningful, real world, scenarios from the principal component analysis data, such as ‘single proud knife’ etc. This is brought about by the use of K-nearest neighbor algorithms and pattern recognition algorithms. Advantages and disadvantages of both are discussed and examples given. A final selection is made based upon initial performance and then further testing carried out. Again the requirements of a database are shown and again the data provided has been artificially simulated to speed up the process.

Chapter eight develops a new novel type of control system, the heuristic subtle change approach. This type of control system makes small changes to controlling signals in real time and attempts to extract more meaningful data about the health of the machining process whilst also attempting to increase the quality of surface profile produced.

Chapter nine summarises the work and combines all the aspects carried out by the author and collegues together into a single combined system. This shows the overall performance of the new architecture and more easily shows the benefit of the work done with this thesis rather than the individual parts being shown in isolation. Performance gain is demonstrated with particular emphasis on the work carried out within this thesis, but other members' work will be highlighted in order to gain a full understanding of the complete system. This chapter is intended to group all the separate areas of work into a single combined system, showing the data flows throughout the system and the impact one subsystem has on the subsequent systems.

Chapter ten discusses the effect this work will have on the wood planing industry, and other associated industries. The benefits of the total body of work are highlighted and future work efforts are put forward. The results are also put into context with the complete architecture and the project relevancy put forward and how this can be employed.

2 Chapter 2 - Literature Review

This chapter is a critical review of previous authors work in the areas of adaptive techniques, tool wear rates and statistical tools as well as general woodworking and metal working technologies. There are also sections establishing a research baseline for mechanical items such as piezo electric actuator as well as a sub-section on data processing. Vibration stabilising techniques are also discussed as these effects have a negative effect on the resultant surface form, as shown in Figure 3-6. This chapter concludes by highlighting a research gap and proposing a new system architecture in an attempt to instigate an intelligent system capable of running in real time.

Authors such as (Hynek 2004) and (Elmas 2008) have proposed real time adjustment of the knife tip trajectory to help reduce the surface waviness. (Vahebi Nojedeh, Habibi et al. 2011) have used similar techniques to enhance the accuracy of a vertical milling machine. These methods involve moving the cutterhead itself with piezo electric actuators. This project is an extension of these works and looks to intelligently alter all parameters to gain a superior surface finish, the ideal being to create a surface free from waves and roughness.

Section 2.7 is an overview of some of the more interesting research being carried out with adaptive techniques. These techniques involve, but are not limited to, neural networks, fuzzy logic, iterative learning, anfis, self-organising maps and K-nearest neighbour.

2.1 Material Removal Techniques

Although the demonstrator for this project is a wood planing machine, it is important to consider the potential for technology transfer between this specific area of implementation and other similar areas, such as grinding, turning and milling, all processes with rotating components and material removal. Most of the research in this area centres on metal working rather than wood machining principally due to the potential markets and possible investment. Much of the research focus is on the new software tool design and innovative methods of control.

2.2 Metal Machining

Metal surface grinding is an efficient machining process for the production of precision surfaces on a workpiece, where the wheel position relative to the workpiece must be accurately controlled in order to achieve the desired surface profile and finish and also the wheel itself have a high quality surface finish (Cao, Lin et al. 2013, Hecker, Liang 2003). A precision positioning mechanism is proposed by (Tian, Zhang et al. 2011), a flexure-based mechanism utilising a piezo-electric actuator to improve both static and dynamic performance, schematically shown in Figure 2-1.

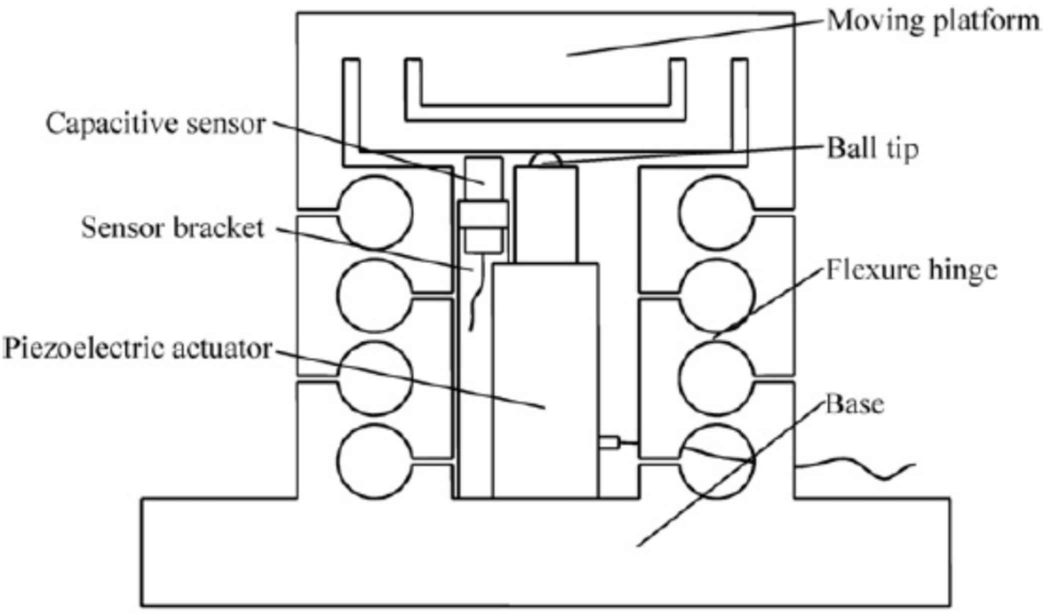

Figure 2-1 - Piezo-driven flexure-based mechanism, (Tian, Zhang et al. 2011)

The author points out that piezo actuators suffer from hysteresis effects, but that these can be overcome through the use of a closed-loop control system. It was found that the overshoot of the system was directly linearly system proportional to the step input size until a critical point was reached at which point the linearity of the system was lost. At this step input size the table was separating from the actuator thereby increasing the level of overshoot. However by increasing the preload of the system this was generally overcome.

Two types of command signal were utilised to drive the piezo actuator, slope and cycloidal, and the resulting overshoot and settling times observed. As the rise time increased, it was noted that the overshoot generally decreased. Below a critical rise time value, the slope command had a lower maximum overshoot than the cycloidal command. As the rise time was increased the maximum overshoot of the slope command became larger than the cycloidal shape. As rise time increased the settling time of the flexure based system reduced, but beyond a critical point, an increase in rise time did not bring about a further reduction in settling time. In a similar result to the overshoot, and very low rise times of the command signal the settling time of the slope command was less than that for the cycloidal command, but at a critical value, dependant on the system characteristic, the cycloidal command generated a reduced settling time.

A similar system was proposed by (Gao, Zhang et al. 2001), however rather than a flexural system to generate the restoring force to the piezo actuator, preloaded springs were used, as shown in Figure 2-2. Both these systems operate by moving the workpiece which has a much reduced mass to the rotating wheel.

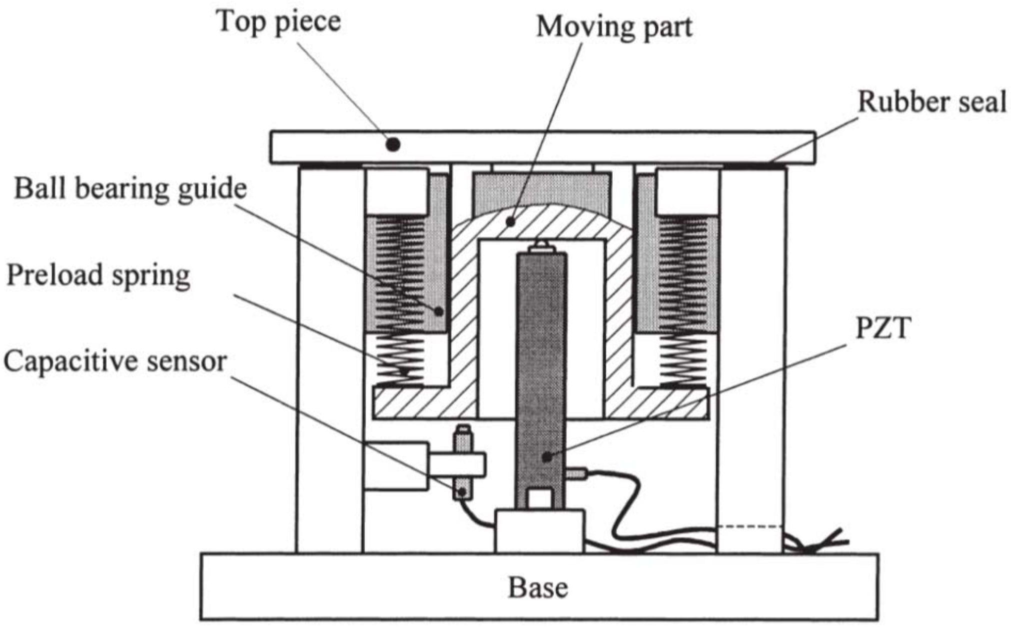

Figure 2-2 - Schematic diagram of workpiece micro-positioning table, (Gao, Zhang et al. 2001)

Traditionally metal turning involves rotating the workpiece and forcing a static tool into the surface to drive off chips of material (Kilic, Raman 2007). Certain materials have developed empirical rules, such as using low cutting speeds, high feed rates and copious amounts of cutting fluid, such as titanium, (An, Fu et al. 2011). In order to increase productivity, and therefore competitiveness in the marketplace, an increase in material removal is sought. One potential solution to this is presented by (Lei, Liu 2002) where a rotating tool is used rather than a stationary one, shown in Figure 2-3. This solution allows much improved cooling to the cutting tool. However the major advantage with this type of system is the independent control of the rotational speed. This results in a tool life that is less sensitive to cutting speed than for the traditional stationary tool. The authors report that the tool life of the rotary driven tool is approximately thirty seven times that of the stationary tool on average. This allows for fewer indexing operations of the tool further increasing productivity over the stationary tool.

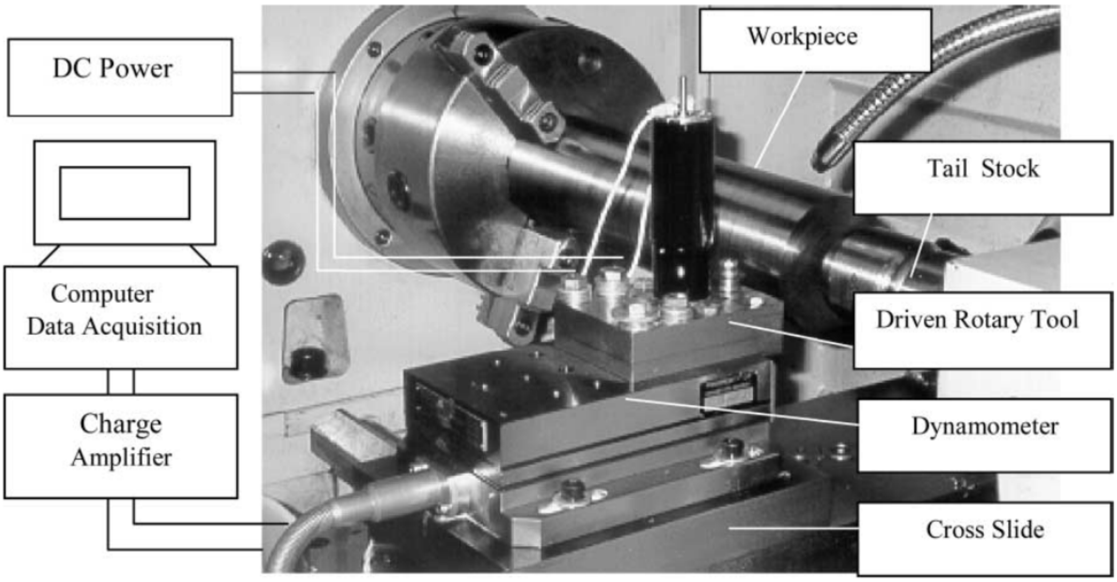

Figure 2-3 - Set-up of the rotary driven tool on a lathe, (Lei, Liu 2002)

It is often agreed that the need to improve quality and productivity in precision manufacturing constantly drives the need for machine spindles with higher performance, (Brecher, Spachtholz et al. 2007). In processes such as milling, turning and grinding, there is typically a rotary spindle for cutting and a Z axis stage to support the spindle for feeding. This often requires the spindle to be supported with its own journal and thrust bearings and the Z axis to be supported by a secondary set of lateral and axial bearings. The serial duplication of radial and axial bearings increases machine cost, reduced overall stiffness and decreases achievable precision, (Lu, Paone et al. 2009). In this work a prototype spindle unit was developed, composed of three separate elements, an aerostatic journal bearing assembly, a permanent magnet brushless motor and an armature plate for a magnetic actuator. Three key control issues are highlighted, the large dynamic range between the mm stroke and nanometre scale resolution, highest possible axial control bandwidth for dynamic stiffness, and rotary speed feedback while allowing axial motion. Mechanical properties were compared with a commercially available aerostatic spindle with standard aerostatic thrust bearings and replacing it with a magnetic thrust bearing. It was found that this prototype advanced spindle achieved a higher load capacity, higher stiffness and less error motion than the standard aerostatic spindle. This potentially allows the use of aerostatic bearings within machine tools to achieve both high accuracy and high stiffness, especially in the axial direction, which is often lacking. The magnetic thrust bearing also benefits from the lack of friction so there is no deficit in performance. The prototype is shown in Figure 2-4.

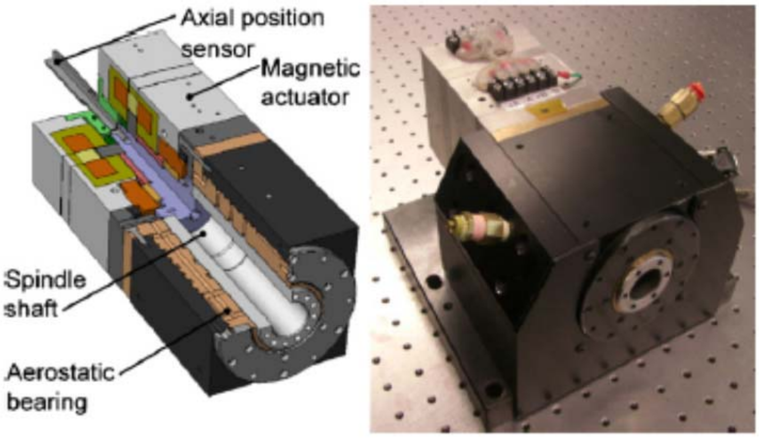

Figure 2-4 - Assembled prototype rotary-axial spindle, (Lu, Paone et al. 2009)

However, (Zuperl, Kiker et al. 2006) discuss the application of an adaptive, neural network based, solution deployed on a standard Heller CNC milling machine. The author reports that using the adaptive system improved both surface finish and tool wear rates. (Cus, Zuperl 2008) further develop these concepts and report that through dynamic adaption of feedrate and spindle speed the system is able to control surface roughness and cutting forces, and that by maintaining constant cutting forces, constant quality of surface is assured.

(Gao, Yao et al. 2002) have successfully employed a piezo electric actuator onto a boring bar. Deflection feedback for the controller was generated through a strain gauge and the piezo actuator was actuated in real time to compensate for any deflections of the boring bar. On line error prediction was generated through the use of forecasting compensatory control, FCC, based on an autoregressive, AR, model of the system. It was found that the errors in the system using this AR model were acceptable, with the forecast errors normally distributed about a zero mean and a maximum value of approximately 3.5µm.

2.3 Wood Machining

Circular saws are widely used in the wood processing industry for applications ranging from primary lumber manufacture to furniture production. Vibrations in the saw blade contribute directly to poor cutting accuracy and poor surface finish, (Nishio, Marui 1996). Vibrations also contribute to material wastage, with approximately 12% of the raw material in woodcutting ending up as waste due to excessive sawing gap caused by vibration. (Chen, Wang et al. 2003, Nishio, Marui 1996). In the above paper the authors describe an LQG controller and a novel test rig utilising two sets of magnetic actuators acting on the outer annuli of the cutting blade. Eddy current probes measure the displacement of the blade at four positions around the blade, with these signals being fed into the LQG controller. This is shown diagrammatically in Figure 2-5.

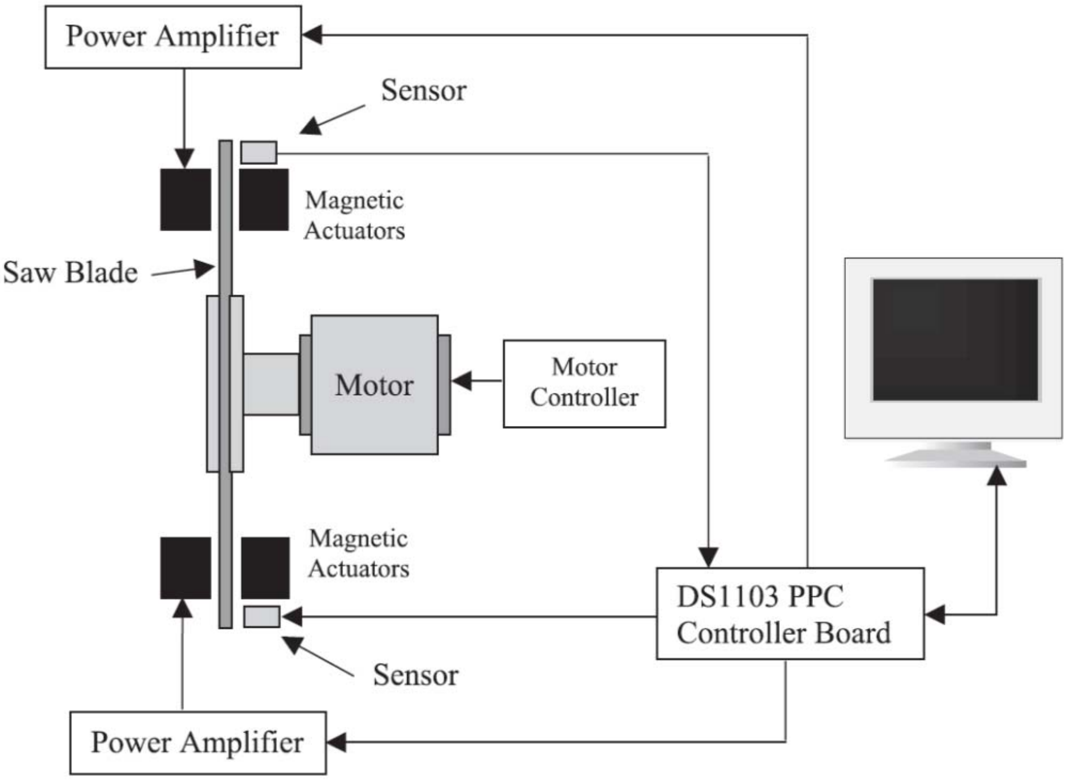
Power Amplifier
Sensor
Magnetic Actuators
Saw Blade
Motor
Motor Controller
Magnetic Actuators
DS1103 PPC Controller Board
Sensor
Power Amplifier

Figure 2-5 - Structure of circular saw test rig for vibration control, (Chen, Wang et al. 2003))

The authors reported that the system reduced vibration by 66%, and that the saw gap, kerf, was reduced by 25%. This resulted in a dramatic reduction in waste and based on 1995 lumber prices would have resulted in an increase of revenue of approximately $645,000 for a mill producing 100 million foot board measure, MMFBM, of lumber annually. (Denaud, Bleron et al. 2007) describe a technique of acoustic analysis to detect errors in the machining process of timber, which is a similar technique as to that employed by (Diniz, Liu et al. 1992) although within this particular research the material under investigation was steel rather than timber. It was reported that acoustic emission were indeed a satisfactory method of establishing tool wear and the online growth of surface roughness.

(Iskra, Hernandez 2012) present a system capable of estimating the surface roughness of paper birch wood while routing. Transducers were mounted on the router spindle and also around the workpiece. Statistical regression was used in conjunction with neural networks to establish links between the measured signals and the actual cutting depth and surface roughness. It was found that a microphone at a constant distance from the workpiece to be the most useful sensor and a model was then generated to predict the surface roughness regardless of the depth of cut. Similar techniques for predicting wood surface finish are also reported in (Iskra, Hernandez 2009, Iskra, Tanaka 2006). Further research correlating tool wear to surface quality, thereby allowing for easier in-direct measurements, has been proposed by (Lemaster, Lu et al. 2000).

2.3.1 Rotary Wood Planing

A number of novel solutions to improving the surface quality of rotary planed timber have been proposed within the research community. These have focused on reducing the cuttermark heights of the machined timber surface caused by three main effects, knife run-out, vibrations, and the geometric effects of the rotary process. As given in equation (3-2) for a given cutterhead, reducing the pitch of the wave reduced the cuttermark height, ignoring vibration effects, and improving the surface quality. A major cause of vibration in any rotating machinery is out of balance masses. These out of balance masses, when rotating at high speed, cause sinusoidal vibrations. In the small planer rig demonstrator at Loughborough Intelligent Automation Centre, these are normal to the cutting plane. One novel technique put forward is dynamic movement of the cutterhead itself. Within this general principal two forms of movement have been proposed, horizontal movement and vertical movement of the cutterhead.

2.3.1.1 Horizontal Cutterhead Movement

(Brown 1999, Brown, Parkin 1999) extensively studied the horizontal cutterhead movement approach. In principal when each knife comes into contact with the wood surface, the cutterhead is advanced in the horizontal direction whilst the cutterhead continues to rotate. As the knife leaves the surface the cutterhead is retracted back and the process repeats for the following knife.

The waviness reduction can be visualised using Figure 3-2, where d_t is the distance travelled by the cutterhead while the knife is in contact with the timber. This distance is usually quite small in comparison with the cuttermark pitch. However introducing the horizontal movement increases the value of d_t, and through the mathematical relations, reduces the waviness height. As can be seen in Figure 2-6, significant reductions can be achieved with horizontal movements of 40% of the wave pitch.

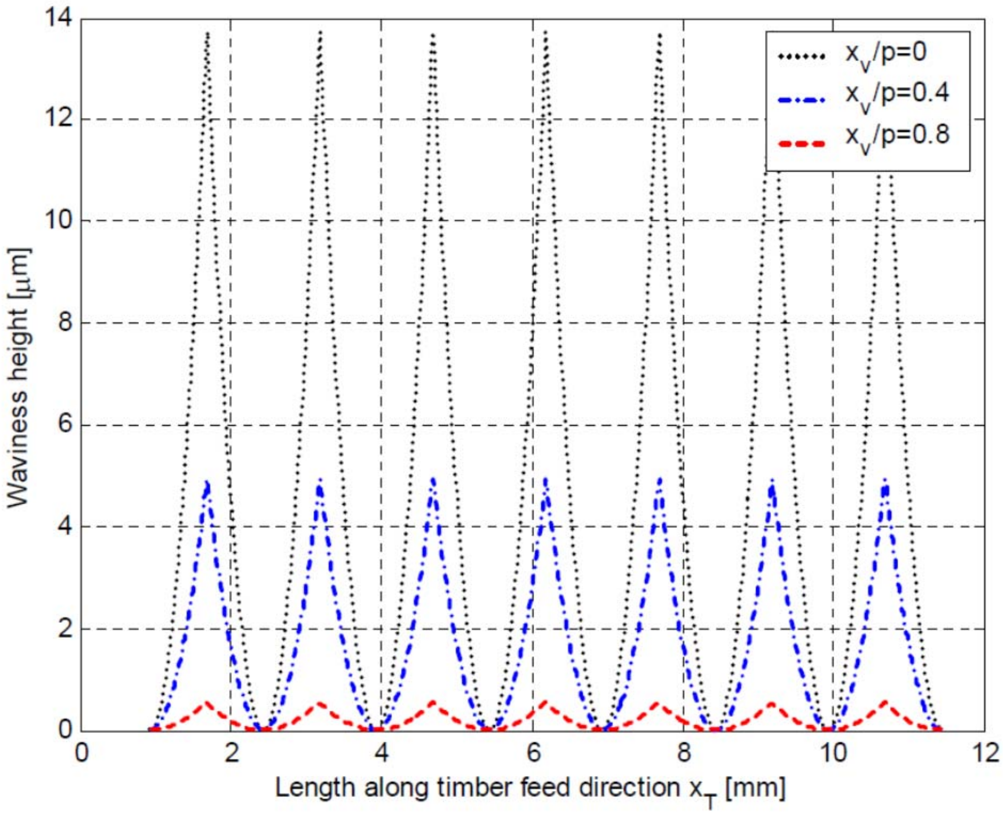

Figure 2-6 - Cuttermark shape influenced by horizontal cutterhead movement ((Hynek 2004))

Significant waviness reduction can be achieved with a horizontal movement of the cutterhead, approaching a 100% reduction when the movement of the cutterhead approaches the same level as the pitch of the wave. However, for practicality reasons this becomes incredibly hard to achieve given the very small time windows available to move the cutterhead, and therefore the large speed required to move the cutterhead within these small time windows, and the relatively large distances required to move the cutterhead.

2.3.1.2 Vertical Cutterhead Movement

Vertical cutterhead movement was proposed by (Hynek 2004). It is similar in general principal to the horizontal cutterhead movement but transposed 90 degrees. As the tooltip contacts the material surface the cutterhead moves vertically upwards reaching a maximum point as the knife reaches its lowest point in the cutterhead revolution. As the cutterhead continues to rotate, it is moved vertically downwards. This is shown in Figure 2-7.

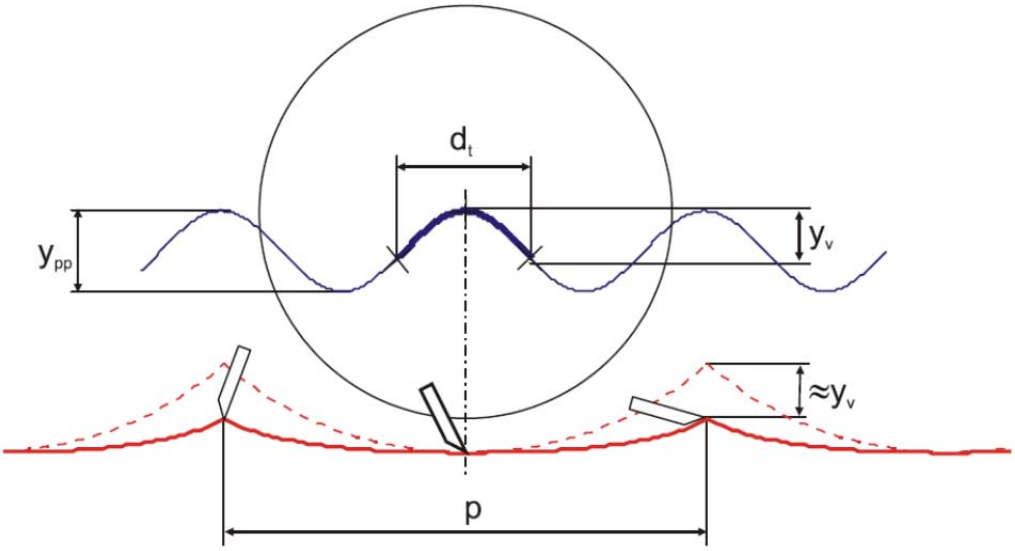

Figure 2-7 - Vertical Cutterhead Movement ((Hynek 2004))

The author points out that this type of cutterhead movement is only applicable for straight knives. Helical knives, as commonly used in metal milling, would not suit this type of movement as at least one cutting edge, or part of one cutting edge, is always in contact with the part. This renders it impossible to synchronise the vertical cutterhead movement with the angular position of the cutterhead.

This analogue type of vertical movement will reduce the waviness by approximately the magnitude of cutterhead movement, y_v. Therefore to reduce the surface waviness by a given factor, vertical movement requires a much reduced cutterhead movement when compared to horizontal movement. The author comments that again, as with horizontal cutterhead movement, it is theoretically possible to totally remove all surface waviness by forcing the knife tip to follow a horizontal line matching the vertical cutterhead movement to the arc path followed by the knife tip when no vertical displacement is applied. However it is noted that to achieve this type of cutterhead movement, actuators with very low response times need to be sought which may not be commercially available.

A development of the vertical cutterhead movement technique is in vibration control. (Elmas 2008). The author continued to use the smart spindle unit, Figure 5-6, with piezo actuators to overcome system vibration. The system operation principal is described here. The vertical displacement of the cutterhead is measured using eddy current probes located within the smart spindle unit. These are located at 45 degrees to the vertical, due to the vertical position of the piezo actuator, so these signals need to be resolved to give a vertical displacement. The level of displacement is then input to an LGQ controller. This controller generates an output signal, fed through amplifiers, to the piezo actuators to apply a corrective force to the spindle to reduce the level of vibration. It was reported that with a closed loop system 68% of the vibration amplitude could be reduced.

However these two proposals each only counter the effects of a single aspect of the machining process, the geometric effects or the undesirable vibration induced through out of balance masses. Neither proposal is able to compensate for knife run-out, or indeed a mixture of all of these effects. The work described by (Ogun 2012) is able to partially overcome all of these negative components on the wood surface profile. This work is an extension of both the work carried out by (Hynek 2004, Elmas 2008) , insofar as it uses vertical displacement of the cutterhead coupled with an LQG controller.

In order to reduce the effect of the TIR, rather than a sinusoidal pulse to the piezo actuator, a digital pulse is deployed. This shifts the cutterhead vertically, changing the effective radius of the knife. This can see seen in Figure 2-8.

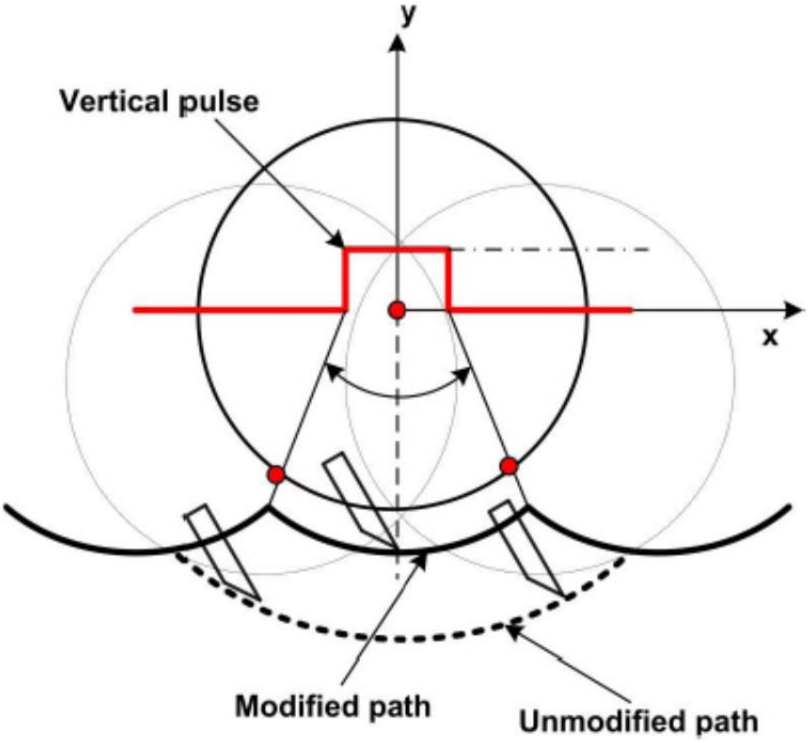

Figure 2-8 - Principals of the cutterhead inaccuracies compensation ((Ogun 2012))

This process eliminates the need for the knives to be jointed saving both time and money for the production process. Again there are limitations to the available cutting speed due to the step response of the actuator, but it is possible to move the cutterhead immediately after the previous knife has left the surface of the timber, to the position required to overcome the TIR of the subsequent knife, thereby extending the time available to move the cutterhead.

The system uses an LQG controller, but rather than attempting to maintain a rotational axis about the zero position, the controller tracks a desired reference path. As the controller is attempting to minimise the error between the reference signal and the actual spindle position it is therefore not only overcoming the effect of TIR, it is also functioning as an active vibration controller simultaneously.

Another key aspect to this work is that it combines a disturbance feed-forward control loop with a feedback LQG control scheme. (Ogun 2012) reports that in the presence of significant disturbances, especially, where there is a long delay between plant output measurements and input pulses, a simple feedback control system alone may not meet the required tracking performance. Significant improvements were made to tracking performance as disturbances can be measured and fed forward into the control loop, giving the controller time to apply corrective action. This is only possible when disturbances can be measured and compensated for before they affect the process performance however. This is shown schematically in Figure 2-9.

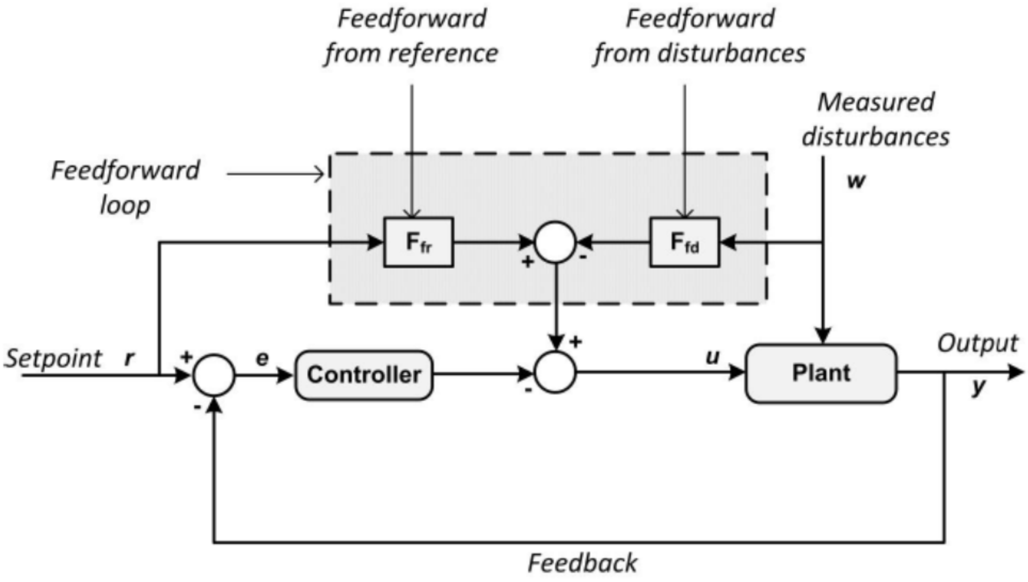
Feedforward from reference
Feedforward from disturbances
Measured disturbances
w
Feedforward loop
F_fr
F_fd
+
-
Setpoint r
e
Controller
u
Plant
Output
y
Feedback

Figure 2-9 - Control system with both feed-forward and feedback control, (Ogun 2012)

2.4 Semi Active Vibration Reduction

Semi active vibration control is an approach that offers the reliability of passive systems, yet maintaining the adaptability and versatility of active system, (Jalili 2002). In addition, semi-active systems do not destabilize the structure, (Kori, Jangid 2009). Active damping has been employed successfully deployed, (Ganguli, Deraemaeker et al. 2007, Zhang, Sims 2005), and others including (Soliman, Ismail 1998) where a simple system was designed such that when chatter was detected the control system ramped up the spindle speed in search of an operating condition where chatter ceased.

(Lim, Park et al. 2005) propose a semi active system using an electrorheological (ER) fluid damper coupled with an AI system to damp rotational motion. The damper, as shown in Figure 2-10 - ER Damper, was designed and manufactured. The properties of the ER fluid can be altered by subjecting the fluid to an electric field. The damper is a thin circular cylinder. Once it is fixed in place the disk inside the damper does not rotate, rather it moves in a vertical direction within the electric field developed between the housing and the disk.

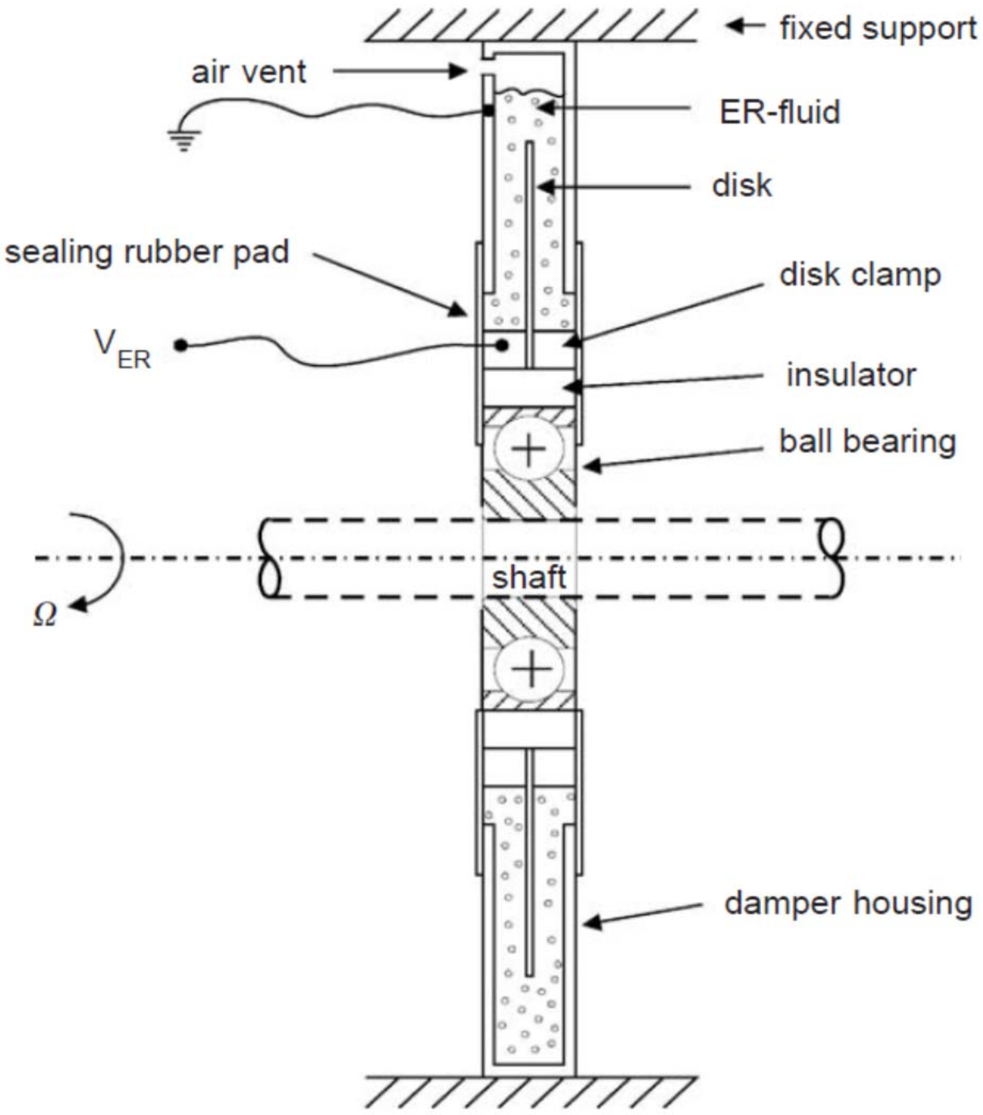
fixed support
air vent
ER-fluid
disk
sealing rubber pad
disk clamp
V_{ER}
insulator
ball bearing
Ω
shaft
damper housing

Figure 2-10 - ER Damper, (Lim, Park et al. 2005)

The author reports that as the electrical field was increased, the damping effect increased and the time constant of oscillation reduced, thereby offering some level of vibration control of the system.

(Lara-Prieto, Parkin et al. 2010) discuss the use of magnetorheological (MR) fluid within beams to adaptively alter the stiffness, thereby modifying the vibration characteristics of the beam. It was found that under the influence of a magnetic field, of 0.11T for this specific example, the beams damping ratio increased considerably from 0.46% in the absence of the magnetic field, to 0.65% with the magnetic field. The effect of activating the MR fluid in a specific region was also reported and the natural frequency of specific area could be increased with the addition of a localised magnetic field. These tuneable MR fluid filled beams could be incorporated into spindles to alter the natural frequencies away from operating conditions if required, thereby altering the chatter characteristics of the spindle.

Boring tool chatter characteristics can also benefit from MR fluids. (Sathianarayanan, Karunamoorthy et al. 2008) present a study utilising an MR fluid filled damper. Magnetic coils within the piston provide the magnetic field. As the piston reciprocates the MR fluid flows through an annular gap offering a damping effect. As the current to the magnetic coils is altered the resulting stiffness of the MR fluid changes and so does the damping effect. This MR fluid damper was applied to a boring bar on a lathe during a boring operation. It was concluded that chatter suppression could be achieved using this technique. (Adkins, Zhiming Huang et al. 1996) have used an electromagnetic absorber successfully to achieve a high level of damping in boring bars. A reduced feedback controller was deployed within the simulation using model control theory with a quadratic performance index.

The disadvantages of the ER fluids is a relatively narrow operating range in terms of temperature, (10-70°C) compared to (-40-150°C), and high operating voltages (2-5KV) whereas MR fluids operate in the region of (12-24V). However the response times of the ER fluids are in the range of a few milliseconds whereas MR fluids systems tend to have larger response times, 25-65ms, (Abele, Altintas et al. 2010, Kavlicoglu, Kavlicoglu et al. 2007).

An interesting application of piezo-electric actuators is described by (Clark 2000) whilst the system is in motion the actuator is held in a high stiffness state, such that energy is stored in the actuator. When the systems motion would cause it to receive energy back from the actuator, the actuator is switched to its low stiffness state, dissipating the energy, thereby inducing a vibration damping motion. A similar technique was deployed to alter the vibrational characteristics of excited mass spring setup, (Ramaratnam, Jalili 2006). The authors again report that this technique of switching the stiffness as the system is moving away from its equilibrium state, to a higher stiffness, and then returning the system to a lower stiffness as it returns to the equilibrium state, was highly successful.

2.5 Surface Inspection

Once a surface has been machined, a crucial element will be some form of surface inspection to ascertain the actual surface profile produced. A requirement of a measurement system is to measure to a suitable accuracy and high reliability, to levels suitable for the application. Within rotary wood planing the pitch of the wave may be between 1-2.5mm with the height of the wave between 2-13µm, Table 1-1, so any measurement system for this machining process would need to be able to capture detail to these levels. Various measurement systems have been proposed, (Sandak, Tanaka 2003), (Leach, Giusca et al.), where broadly two types of measurement system exist, contact and non-contact measurement.

2.5.1 Contact Measurement

Contact measurement is normally carried out using a mechanical stylus, (Kiran, Ramamoorthy et al. 1998, Garratt, Nettleton 1992). The device measures the surface usually by contacting the stylus tip across the surface. The surface profile is then recorded by the vertical displacement of the stylus tip. These devices often have a vertical resolution in the micrometre range and in specific applications, the vertical resolution can be to the nanometre level, (Dietzsch, Gröger et al. 2007). However these mechanical systems do not lend themselves to high levels of automation due to the relatively slow measurement speeds often being a post process approach as the stylus tip can jump at high measuring speeds, often known as ‘bouncing’. (Elmas, Islam et al. 2011). A further disadvantage of this type of system is that is can be destructive to soft surfaces like wood, due to the loading of the stylus and the very small radius tips, generating high tip pressures and ‘ploughing’ into the material surface. (Gröger, Dietzsch et al. 2005) describe in detail a number of issues resulting from stylus measurements including concerns about the reproduction of the real surface due to the mechanical limitations of the stylus tip radii, 2µm. These disadvantages have led to the development of non-contact measurement systems. However, these types of system cannot be used in ‘dirty’ environments, can require high set up times and are not affected by colour of reflectivity of the material under measurement, (Lee, Kim et al. 1987).

2.5.2 Non-Contact Measurement

Various non-contact methods of surface measurement have been proposed, with most being optical including optical profilometers, microscopes, image analysers and optical light sectioning. (Islam, Parkin et al. 2011). It has been proved that many techniques developed for metals are not suitable for timber surface measurement, (Parkin, Jackson 1996) , (Yang, Jackson et al. 2006, Parkin, Jackson 1996) propose a light sectioning method where an oblique light stripe is projected from the side of a sample onto the surface to produce a light section, as shown in Figure 2-11.

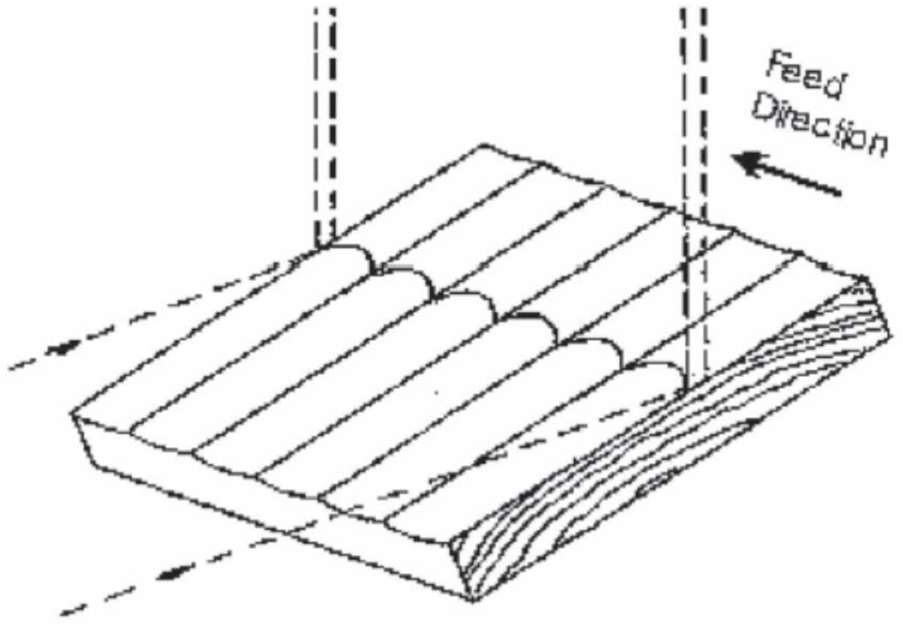

Figure 2-11 - Principal of light sectioning, (Yang, Jackson et al. 2006)

This light section produces a wavy line caused by the wavy nature of the surface. A relationship between the height of the wave and the height of the Cuttermark is described, and with this relationship the heights and widths of the cuttermarks can be calculated. The author reports good correlation between the light sectioning method and laser profilometers. However the setup used within this experimentation projected the laser stripe parallel to the feed direction, which is not always feasible to implement. This misalignment of the laser stripe causes an inclination of the of the wavy line of the material surface, which the author reports can be removed successfully through the use of least squares mean line of the light section. It is possible that this type of measurement system could be implemented on a production machine, but possible errors and distortions may occur due to blurring of the image due to the movement of the surface across the image window, would need to be filtered out.

A further novel non-contact surface inspection method is the photometric stereo technique, (Yang 2006). This setup uses a single camera and two light sources which are illuminated independently of each other, as shown in Figure 2-12.

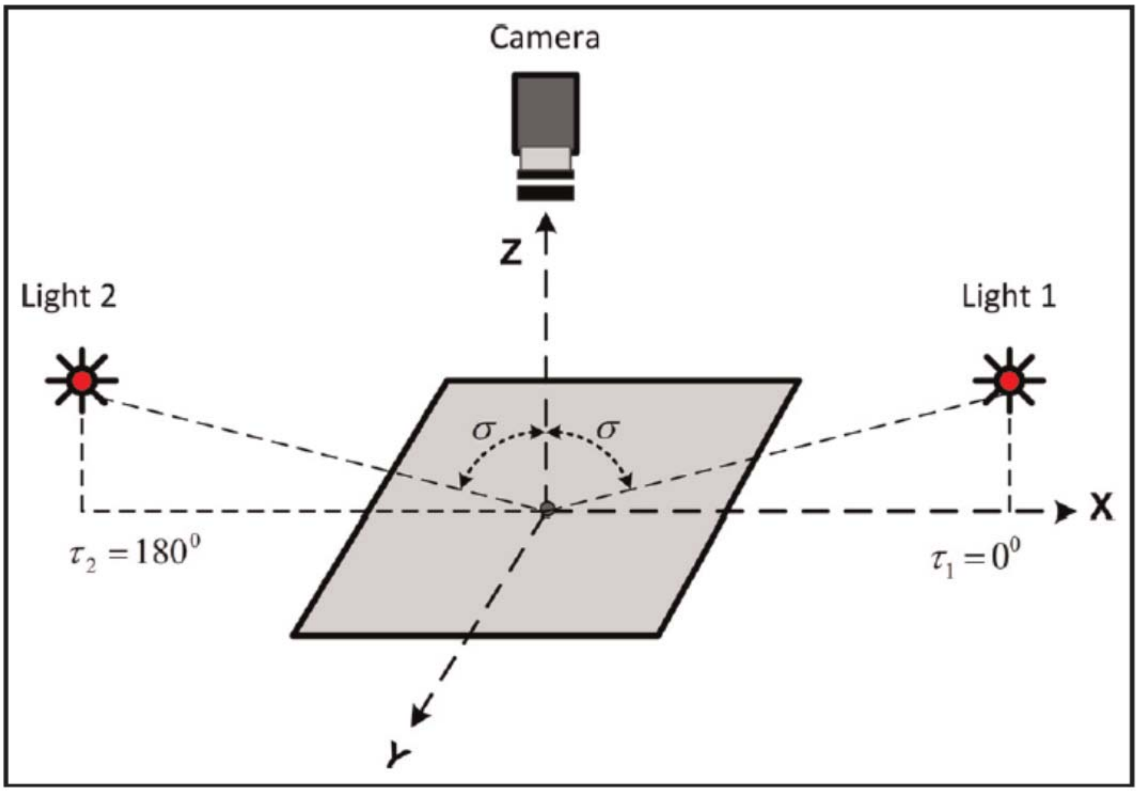

Figure 2-12 - Schematic of the two-image photometric stereo setup, (Ogun, Jackson et al. 2012)

The photometric stereo technique is used to estimate the local gradient of a surface from multiple images captured in a fixed spatial location but under different illumination directions. In this work the illumination sources are set 180° apart and as low as possible to the surface as is realistically achievable. This technique does assume that the wood exhibits a diffuse reflectance, this is nearly the case for unpolished wood, (Maristany, Lebow et al. 1993), which allows the use of this technique. It should be noted that this technique assumes that there is no height variation along the Y axis, and will only produce a two dimensional plot of the surface form. For a rotary wood planing machine this is a fair assumption assuming correct machine setup, (Elmas, Islam et al. 2011).

The two images gathered by the camera will have different reflectance maps, and the assumption that the two illumination sources have similar intensity values allows these two images to be sufficient to compute the gradient of the surface. The images are converted to intensity profiles using column-wise averaging techniques. A frequency domain integration method is then used to extract the surface profile from the gradient data. However, constants of integration may not be solved so offsets in the surface profile may cause a skew in the calculated profile.

This method requires the surface under investigation to remain stationary as to allow the multiple images to be correlated. A temporal multiplexing method was applied to the moving photometric stereo problem. Here the images are taken in quick succession and a method to determine pixel correspondence between successive image to allow the surface to be passing under the camera has been proposed, (Ogun, Jackson et al. 2012). However using this technique the correlation between a 15 pixel offset set of images was only found to be 56%. With a lower 8 pixel offset in the images the correlation between static and dynamic profiles was measured to be 87%. This allows some dynamic movement to be implemented at limited offsets. This limits the passing speed of the surface by the response time of the camera and illumination systems. The results for temporal multiplexing for the higher speed, larger offset images, may be due to limitations due to the need for the high intensity of lighting needed to realise very short image acquisition periods, (Smith, Smith 2005).

2.6 Data Processing

The surface profile measurement systems described in section 2.6 will produce a surface plot. This data however needs to be translated into a form that can be analysed to identify and characterise surface defects. (Gorecki 1990) proposes the uses of an optical transform system using Fourier spectra sampling. This Fourier sampling reduces the dimensionality of the sampled data set, down to a data set of 64 values per sample, which then allows classification techniques to be undertaken. The author reports that the system is capable of surface analysis of machined metal in the wave height range of 0.05 to 2µm. The Fourier spectrum analysis of machined surfaces is able to identify modes and dominant harmonic components of the surface profile. This can extract the fundamental waviness pitch from the surface of a rotary planed timber, (Elmas 2008). This data can then be used to characterise surface profiles. However, the Fourier spectral analysis requires that the input, in this specific case a surface profile, be strictly periodic or stationary. In real machining processes artefacts within the timber, or the natural timber properties, may not be uniform along its length, (Ikonen, Kellomäki et al. 2003). This can lead to a non-periodic surface profile causing the Fourier spectral analysis to fail.

(Lebow, Brunner et al. 1996) present a system using principal component analysis, PCA, to reduce the dimensionality of the data set. The PCA is able to decompose a complex signal into its fundamental patterns in the form of empirical basis functions. PCA can be applied to any type of input signal, which has benefits when considering surfaces with random defects which cannot be foreseen.

2.7 Adaptive Techniques

Recently much research has been carried out in the field of adaptive techniques with researchers approaching this from many different backgrounds, (Park, Kim 1998). However, adaptive control is not without its own problems and complexities. (Anderson, Lee et al. 2005, Anderson, Dehghani 2008) report on a number of potential problems of adaptive control split into two main groups. Firstly a collection of problems where specific difficulties only became apparent sometime after the generation of initial ideas, included in this group are the MIT rule, bursting, the Rohr's counterexample, and iterative control and identification. The second group of problems describe generic problems, such as impractical control objectives, transient instability, and suddenly unstable closed loop, and finally changing experimental conditions.

(Park 2001) has developed a system for continual improvement of cutting conditions for milling operations called GELCC, generation and evolutionary learning of cutting conditions. The technique performs three functions, the modification of cutting conditions obtained from a data handbook, incremental learning of obtained cutting conditions using fuzzy artmap neural networks, FAMNN, and then finally the substitution of these improved parameters to the milling procedure. Within the structure previous data is stored as either tables or graphs, which show the modification of the ratio of cutting conditions for the types and materials of cutters, or other important factors.

A 4-layer neural network, NN, was used to generate the modified cutting conditions. The rate of error convergence was checked by changing the number of hidden layers, the number of neurons within each layer and the learning rate. These values though were arbitrarily changed by a human operator whilst designing the NN. The modified cutting parameters are then passed to two fuzzy ART neural networks. These are configured to work in parallel such that one learns the feedrate and the other the cutting speed. The fuzzy ART NN categories are given learning patterns according to similarities among them. The vigilance parameter and learning rate influence the number of categories.

In general the higher the vigilance parameter the more specific categories are created. The new input pattern is presented to the two ARTMAP's and if the map field receives inputs from both ARTMAP's, the network learns by modifying the weight vectors of the chosen categories for the input layers of the ARTMAP's. If there is a mismatch the vigilance parameter of one of the ARTMAP's is increased, and the system searches again for another category. This continues until either the system finds a matching category or a new one is created. Results from an initial test on a vertical CNC milling machine show that the system facilitates the improvement of cutting parameters through the continual operation of the machine. (CARPENTER 1992) comments that an ARTMAP voting strategy can be used to assign confidence estimates to competing predictions given small, noisy or incomplete training sets. A further advantage to the fuzzy ARTMAP structure is the ability for it to be incrementally trained, (Javadpour 2003).

(Pomerleau 1991) demonstrates the first successful use of a neural network with real-time sensors. The system is used to steer an autonomous land vehicle along a road using a video camera. The network is trained using a backpropogation algorithm so that the networks performance more closely corresponds to the correct steering angle. The system is presented with a series of images as input and the corresponding steering angle as output. The backpropogation algorithm then modifies the weights of neurons to achieve the required outputs. However to speed learning a further algorithm was generated that allowed learning in real time where the system imitated a human operator to achieve the required steering angle whilst watching the video feed input.

However this can lead to problems as if the training data is not fully representative of the full task, the system is not guaranteed able to take successful action when encountering these situations. A further problem was encountered where if a period of straight road was encountered, no changes to the input, it is possible for the system to 'overlearn' due to repetitive inputs, causing the system to 'forget' previously learned data about curved roads, (Chauvin 1990), (Fierro 1998, Chauvin 1990) presents a neural network integrated with a kinematic controller for the control of a nonholonomic mobile robot. The neural network is used as a torque controller, based on the approximation of the non-linear dynamics of the cart. However the system is limited to certain constraints. The neural network can cope with unmodeled disturbances, but only within bounds, and the velocity inputs from the kinematic controller must be smooth. The network uses the gradient algorithm based on backpropagated error to tune the weights of the neurons.

(Rekdalsbakken 2006) demonstrates a novel method of training a neural network for balancing an inverted pendulum. Rather than using the more traditional back propagation method, the author uses a genetic algorithm where the chromosomes are coded with the values of each node within the single hidden layer of the network. Throughout the development of the different generations mutation rates were changed in an attempt to improve the overall performance of the NN, however at the close of the experiment none of the final chromosomes were able to balance the inverted pendulum more successfully than the modal control algorithm. This appears to be due to the population reaching a local suboptimal level after a set number of generations and then failing to adapt further. However it is proposed that changing some test parameters, such as epoch time and mutation probabilities, would cause the chromosomes to leave this suboptimum position.

(Balazinski 2002) has carried out a comparison of three different artificial intelligence methods, feed forward back propagation neural network, fuzzy decision support system and a neural network based inference system, for tool condition monitoring. The system uses cutting force measurements as they are more sensitive to tool wear than either vibration or acoustic methods. However this type of measurement technique is sensitive to the size of uncut chip cross-sectional area, a product of feed rate and depth of cut. However the results presented show very little dependence on the cutting force with tool wear rate, and that the tool wear rate is far more dependent on the cutting parameters.

It was suggested that if the cutting force is to be used as a measure of tool wear rate it must be used in conjunction with the depth of cut. A three layer multi-layer perceptron, MLP, with three input cells in the input layer, five in the hidden layer and a single output and was trained using back propagation. The fuzzy decision support system is used to handle uncertain or imprecise knowledge, (Zadeh 1973), and the fuzzy rules were provided by a human expert. This is a possible draw-back of the fuzzy system as if the rules are either inaccurate or insufficient the system performance will be reduced. The authors conclude that the simple network was not susceptible to overtraining, as all errors stabilised after 100,000 iterations, but that retraining the system is slow, if it is to be used on the factory floor, between 15 – 30 minutes depending on the number of neurons within the hidden layer. Whilst testing the neural network based fuzzy inference system there was no dependence on the number of iterations as a similar result was obtained with just 2 as to 200 iterations. The number of fuzzy rules did have an influence on the system performance, however 5 rules gave an optimum, fewer than 5 to model the learning data and more than 5 resulted in a loss of generalisation of the model. However the training time for this model was much improved over the neural network alone at <1 minute.

Fuzzy Logic, FL, deals with uncertainty by attaching degrees of certainty to the answer, (McKone 2005). An advantage of fuzzy logic is that the rules are conceptually easy to understand and parameters have clear physical meaning, (Altug 1999). However one problem often attributed to the use of fuzzy logic is the generation of these rules. These have to be created by an experienced operator within the area of interest. This can be a time consuming procedure and if the rules are not complete can lead to a mal performing system. (Nagata, Kusumoto et al. 2009) propose the use of a fuzzy controller to modify the feedrate when machining timber cylinders. The proposed controller attempts to prevent the brittle failure of the timber whilst maintaining the highest possible throughput. Here the main factor affecting the feedrate is the relief complexity and the type of timber, however the feedrates are calculated before the actual machining process, and the system is not designed to be run in real-time.

A Fuzzy Neural Network, FNN, has also been used to control a high speed milling machine, (Zhou 2002), specifically maintaining the optimum cutting forces for highest productivity levels. In this work the FNN was designed to overcome specific problems to previous works. The author states that due to scaling factors, the dynamic performance of the system has been ignored, and as such the networks were unable to totally replace the more traditional PID control system. The new FNN proposed also attempts to converge much more quickly and in a stable manner. The FNN proposed main difference is that it has an extra input and output layer where scale conversion can be finished dynamically. Fuzzy conversion is actually carried out within the neurons of the network itself, aswell as the assignment of the membership functions and the rule matching processes. However the 49 fuzzy control rules used by the system were based on data generated by experienced manufacturing engineers. However these membership functions, and indeed the fuzzy control rules can be tuned by online learning. This same FNN approach has been successfully employed in forecasting returns of scrap product, (Marx-Gómez, Rautenstrauch et al. 2002), demonstrating the flexibility of the approach to be used in a wide range of applications.

When plant exhibits time varying dynamics, direct inverse control does not guarantee satisfactory response characteristics and steady state errors may remain, (Denai, Palis et al. 2004). In this paper the control structure shown in Figure 2-13 was proposed.

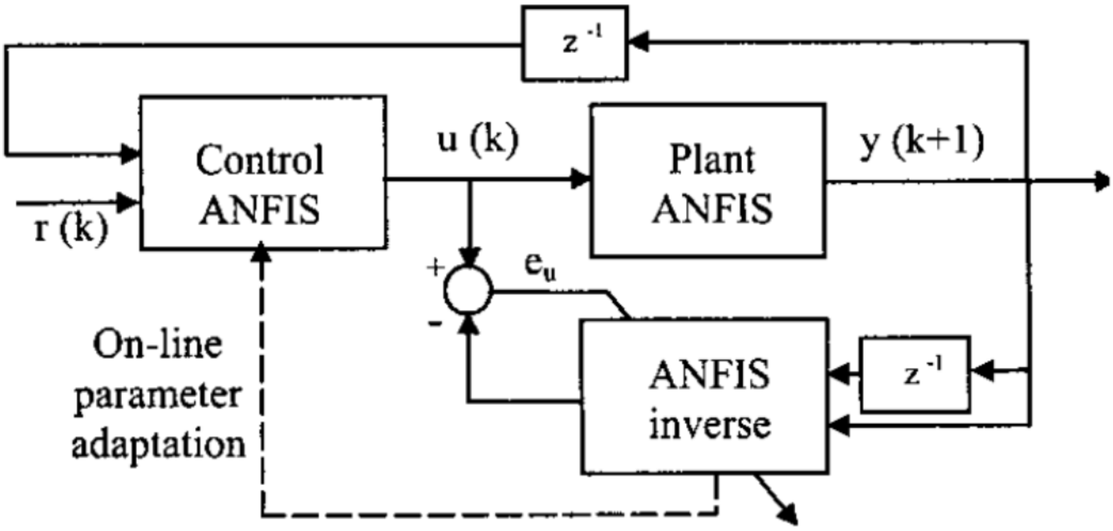

Figure 2-13 - On-Line Inverse Learning, (Denai, Palis et al. 2004)

On line learning of the ANFIS inverse model occurs at each time step to fine tune the membership function parameters of the ANFIS controller. This structure was employed to model neuromuscular systems as an example of a system where there are systems with high degrees of uncertainty, rather than a neural network control scheme as the method of gradient decent cannot guarantee that the output tracking error will converge to zero. The appropriate combination of both neural and fuzzy inference systems provide a valuable modelling approach to complex systems. The on-line inverse learning model, Figure 2-13, does not require an intermediate model of the plant and hence is applicable to any system for which the inverse model can be identified online.

Genetic algorithms have also been used in conjunction with fuzzy logic rules, (Gonzalez, Perez 1999). The system uses a genetic algorithm to extract a set of fuzzy rules, from examples, that best represents the system. This process is developed from an iterative approach, and the new rule obtained is added to a final set of rules for the overall system. In order to select a new rule, the previous rule selected by the system is penalised, by eliminating the examples from the training data covered by this rule, and the process repeated. This is repeated until the set of fuzzy rules adequately covers the training data, although no mention of how this is score is given. The author describes however that the previous versions of SLAVE, (Gonzalez, Perez 1996), (Gonzalez, Perez 1993) and (Gonzalez, Perez 1998) did not take into account the previously selected fuzzy rules when choosing a new rule, which could lead to unexpected interactions between the rules obtained, and so to avoid this a new method is proposed, a method to evaluate the 'goodness' of the rules that takes the cooperation/competition of the rules into account. This is done by splitting the rule set, by applying another concept from the example data, into the rule set that describes this new concept and the rule set that describe the remaining concepts. The maximum positive covering degree is then defined as the maximum covering subset of the rules that describe the new concept example. In the same way the definition of the maximum negative covering degree is given. While the positive covering degree is higher than the negative covering degree the new concept example will be correctly classified. However no information is given about eliminating earlier selected rules, only the choice of new rules depends on the previously selected rules. Therefore an optimum set of rules may be missed if an early selected rule interacts poorly with a remaining rule.

Iterative learning controller, ILC, can also be credited with intelligent learning behaviour. These learn in a similar method to humans and as such are more easily understood. A trial is performed, the error measured and then a retrial carried out based on an update law and the error from the previous attempt. One advantage that these controllers have over others, such as fuzzy logic, neural networks etc, is that the system can operate with or without any previous knowledge or training data. However the nature of an ILC does require a repetitive task to be carried out, hence the solution is not a universally applicable one. These controllers have been used in many environments from motion tracing, (Hamamoto 2001), to stroke rehabilitation, (Hughes, Burridge et al. 2008). (Ziliani 2007) describe an ILC for contour tracking used by an industrial SCARA robot. The ILC strategy is proposed to overcome issues such as the inability to tune the control design parameters of the original PID controller. The controller is also designed to overcome the joint backlash which causes error in the system and to overcome the error assigned to static friction when the manipulator velocity changes sign. A standard ILC strategy requires a pre-specified time-based reference signal, the robot position is predefined at the same time instant in each repetition. However since in contour tracking the piece being tracked is of unknown shape, (Ziliani 2007) has overcome this normal pre-requisite. This is done by modifying the normal force set point according to the normal force error measured in the previous repetition.

Further studies have also shown the even with small reset datuming errors, learning can still be carried out, (Lee 1996). Continuing the work of (Lee 1996), (Sun, Wang 2001) have developed a solution to overcome the initial error using an initial rectifying action. Results show that the techniques employed also improve the overall system robustness. (Madady 2008) have again taken this approach further and explored the use of an ILC for time dependant systems, where the system parameters and initial conditions are variable in various iterations, using a closed loop control law. The system described by (Madady 2008) proposes using the self-tuning iterative learning control systems, STILCS, to solve the time dependant system. The system uses adjustable gains, called learning gains, controlled by both the input and output data of the previous operation. The author mathematically proves the selection of the algorithm step size, which when selected correctly guarantees convergence of the system. The results presented show that after approximately 15 iterations the total learning has plateaued at a low level. The total learning error being the sum of all errors, from each iteration, for that particular testpoint. Further iterations do reduce this further with ever increasing iteration numbers.

When considering pattern recognition a popular solution exists in the form of Self-Organising Maps, SOM, (Jain, Duin et al. 2000, Ridge, Skocaj et al. 2008). SOM's are a form of neural network, also highly popular in data mining and exploring data, grouping similar aspects of the data set together. These patterns can either be images, such as cuttermarks surface profiles, or data set patterns, like those produced by either Fourier analysis of principal component analysis. This type of technique would be able to form a link between data extraction elements and decision making aspects of an integrated system architecture.

If however a model of the system is accessible ILC's can still be used by combining the iterative learning control with Internal Model Control, IMC, (Fan 2006). In this document the author presents a method for combining the two different types of control, for the control of a linear motor, stating that IMC component provides robust performance against unrepeatable disturbances and the ILC portion reduces tracking errors in the early stages of learning. However it is assumed that the internal model can be simplified by disregarding the non-linearity of the system and also the friction. These assumptions are made as when studying a pick and place machine, translator movements take place with high velocities and the large accelerations. However these assumptions do not change the overall method of combining the two model types to create the overall control architecture.

Model Reference Adaptive Control, MRAC, has been used to compensate for the hysteresis effects present in piezo electric actuators, (Liu, Chang et al. 2010). This technique involves updating the parameters of an existing controller based on the actual output of the process. The objective is to find an appropriate control input such that the system output follows the desired input. This type of architecture presents potential when considering the rotary wood planing process, when used in conjunction with a model concerned with vertical cutterhead movement to overcome both cutterhead inaccuracies and out of balance forces of the spindle. If the general MRAC principals are used together with other systems to generate suitable control parameters a truly novel solution could be created.

Flexible manufacturing system, FMS, have been employed to improve efficiency in industry. Loading problems, selecting a subset of jobs from the job pool and allocating these among the available machines, has been proposed to be solved using a heuristic approach. The approach developed by (Nagarjuna, Mahesh et al. 2006) attempted to minimise system unbalance, processing time for the total number of jobs, whilst satisfying constraints such as available machine capability. A set of rules were developed with subsequent choices only made available dependant on previous outcomes. The approach also attempted to consider job sequencing and operation allocations concurrently rather than using predetermined sequencing rules such as shortest processing time. Although the heuristic approach was found to be successful, limitations, such as a limited number of jigs and fixtures, pallets and automated guided vehicles limited the overall success in this specific application. However (Yu, Sarker 2003) report that using heuristic for searches can become computationally inefficient as at time multiple searches may have to be re-run when only a small number have changed from a previous search. However this can be overcome by directionally decomposing the inter-cell, a machine cell here is treated as a machine itself, flows and incrementally computing these. (Guschinskaya, Dolgui 2009) however conclude that when considering line balancing scheduling different approaches should be employed for different sized problems. If there are less than 25 operations, then exact methods should be used, however if the number of operations increases beyond approximately fifty, then heuristic approaches are advised. Further research has investigated the use of differing heuristic approaches to cost reductions in assembly lines, (Amen 2000, Amen 2001)

2.8 Research Gap

The research above has highlighted an area where previously little research has been undertaken. This 'gap' is for an intelligent system monitoring the actual produced surface profile in real time, altering the control parameters in accordance with an a-priori knowledge base, APKN, set of information. Although the system would not have any direct knowledge about which particular cuttermark was caused by any particular knife it would be possible through a series of subtle parameter changes to isolate and then rectify a particular defect cause, such as a proud knife or an imbalance in the rotating shaft assembly. Many of the above systems require in depth knowledge of the cutting process and mechanical measurements of cutting knife radii. This is not often available, and the proposed system of subtle changes coupled to an intelligent system would overcome this problem.

2.8.1 Proposed New Architecture

It is proposed that the new system architecture have two 'control loops' working together in real time to control the overall system performance. This would thereby allow them to work at different speeds carrying out different tasks pertinent to their particular area of 'expertise'. It is also important to note that the feedback into the outer control loop is actual surface profile date rather than spindle position data. This is a more advanced data stream as it is a direct measure of the actual surface rather than a measure if spindle position mathematically transposed to estimate the surface profile. This surface profile data requires then a further system block to attempt to categorise the surface defects between the data stream itself and the 'higher level reasoning' block, as shown in Figure 2-14.

The tighter control loop is the faster loop with the system controller acting out a set of pre designated rules. These rules would include the movement requirements for the cutterhead in order to effectively remove the TIR in order to achieve an improved surface quality. The outer control loop is able to then run at a much reduced iteration speed. This allows this loop to gather data and then make a judgement as to the best course of action to generate an improved surface.

Below is a schematic of the overall proposed intelligent system architecture.

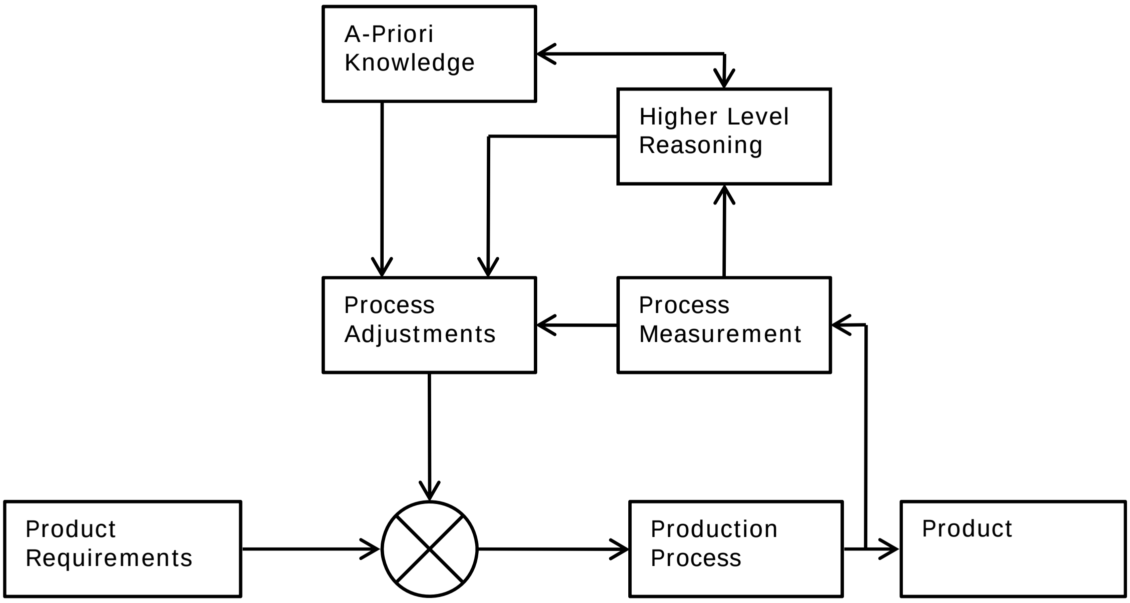
A-Priori Knowledge
Higher Level Reasoning
Process Adjustments
Process Measurement
Product Requirements
Production Process
Product

Figure 2-14 - Proposed System Architecture

The ‘Product Requirements’ block is akin to the product specification. This can be any type of requirement ranging from dimensional requirements through to surface finish. The ‘Production Process’ block may be any type of process; although in this project we are focussing of wood planing. With the ‘Process Measurement’ block any number and/or type of measurements are made upon both the product and machine. These measurements are then processed both by a ‘local’ process control system making ‘Process Adjustments’ and the ‘Higher Level Reasoning’ block. Within this block a more strategically focussed approach is taken to guide the system to operating condition more favourable to the ‘Product Requirements’. The ‘A-Priori Knowledge’ block feeds past data both to the ‘Higher Level Reasoning’ block and the ‘Process Adjustments’ block in order to help develop changes in parameter values through past experiences.

The proposed system combines an A-Priori knowledge base, APKN, with a higher level reasoning ‘engine’ and an innovative control model to make suitable changes to the production process to attain higher levels of both machine utilisation, or production, quality and reliability to seek out a competitive edge.

The higher level reasoning is tightly linked to both the APKN and other process measurements to determine production trends, but when a situation arises that has not been seen before, it should make a judgement using any available data as to what is the best course of action. If this solution is found to be inaccurate, parameters will then be altered until a satisfactory set is found. This new knowledge is then stored for possible future use.

3 Chapter 3 – Surface Waviness of Planed Wood

This chapter of the thesis gives a more in depth view of the principals of rotary wood planing and the mathematical approximations used to predict the surface forms. Some surface defects and their possible causes are also given as well as some of the specific technical language used within the woodworking industry.

3.1 Circular Arcs Approximation

One method to approximate the surface form of the planed material is to use the circular arcs simplification, as can be seen in Figure 3-2. Machining parameters used within the woodworking industry make this approximation possible.

The knives of the cutterhead are rotating at speed v_c, also known as the cutting speed, and the timber is moving toward the cutterhead with speed v_f, known as the feed speed, as shown in Figure 1-5. It is convenient to establish a measure, which can describe the kinematical relationship of the rotary machining process regardless of the actual cutting and feed speeds. The ratio µ is used to describe the rotary machining process.

$$\mu = \frac{v_c}{v_f} \tag{3-1}$$

This ratio µ is typically within the range 50 – 300.

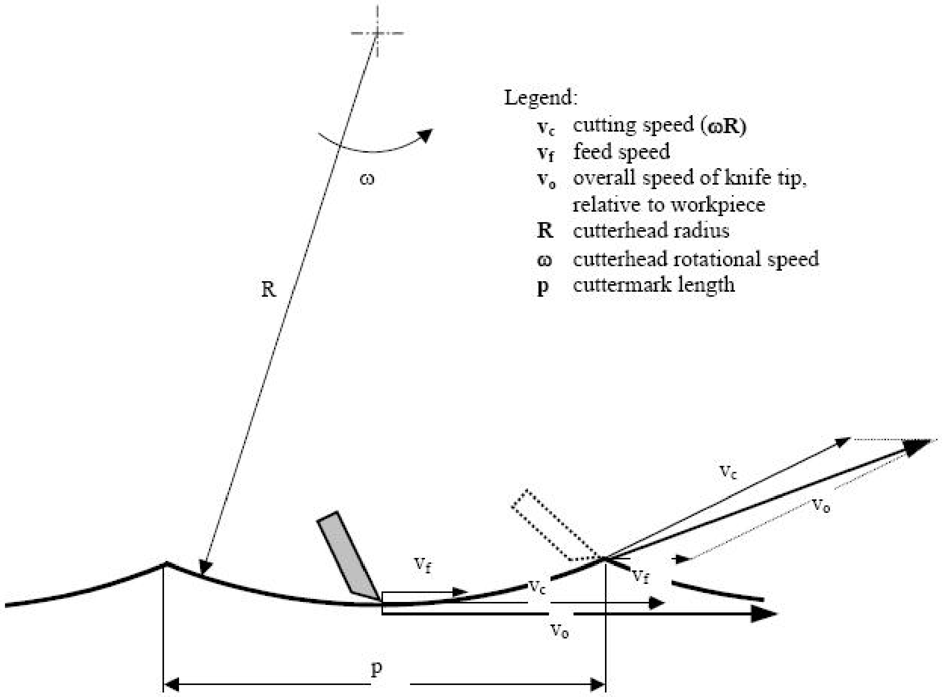
Legend:
v_c cutting speed (ωR)
v_f feed speed
v_o overall speed of knife tip, relative to workpiece
R cutterhead radius
ω cutterhead rotational speed
p cuttermark length
ω
R
v_f
v_c
v_o
p

Figure 3-1 - Rotary Machining Process Velocity Relationships - (Hynek 2004)

The length of the cuttermarks is primarily determined by the following parameters: feed speed v_f, cutterhead angular velocity ω and number of knives N. The relationship between these parameters and the cuttermark length is expressed by the following equation;

$$p = \frac{v_f}{N\omega} \tag{3-2}$$

(Cutri 1991)

It should be noted that the length of the cuttermarks does not depend on the cutterhead diameter R. The pitch of the cuttermarks, p, is the length that the timber travels between two knives.

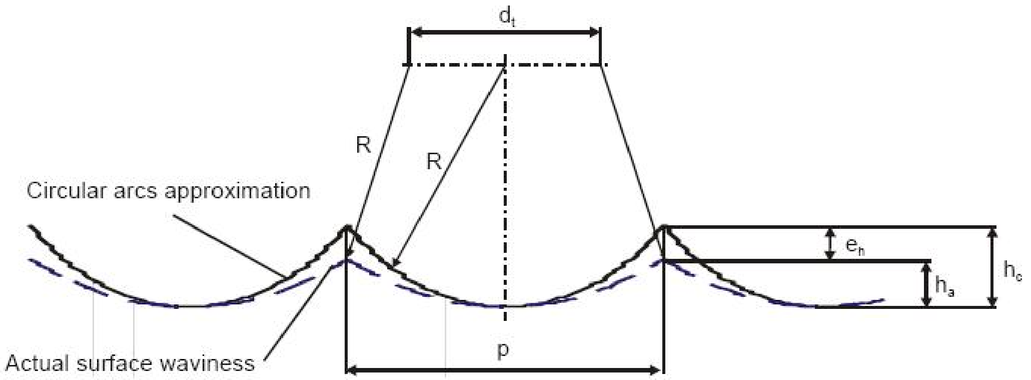
d_t
R
R
Circular arcs approximation
e_h
h_a
h_c
Actual surface waviness
p

Figure 3-2 - Circular Arcs Approximation – (Hynek 2004)

The waviness height of the idealised surface is described by equation (3-3), where R is the cutterhead radius, (Elmas 2008).

$$h_c = R - \sqrt{R^2 - \frac{p^2}{4}} \tag{3-3}$$

Figure 3-2 also shoes the slight inaccuracy of the circular arc approximation, but the actual waviness height can be expressed as follows

$$h_a = R - \sqrt{R^2 - \frac{(p - d_t)^2}{4}} \tag{3-4}$$

Where d_t is the distance the cutterhead travels while the knife is cutting the length of cuttermark p. This distance can be expressed as follows

$$d_t = \int_0^p \frac{v_f}{v_{ox}(x)} dx \tag{3-5}$$

Where v_{ox} is the horizontal component of the knife velocity v_o. The knife tip velocity relative to the work piece, as shown in Figure 3-1, is a vector sum of the cutting speed and the feed speed.

$$\overrightarrow{v_o} = \overrightarrow{v_c} + \overrightarrow{v_f} \tag{3-6}$$

A simplification can be made by assuming the horizontal component of the knife tip velocity to be constant, whereas clearly the velocity varies throughout each revolution, Figure 3-1. This can be made as the angular displacement while the knife is machining a single cuttermark is small. This simplification allows equation (3-6) to be simplified to.

$$v_o = v_c + v_f \tag{3-7}$$

Combining equation (3-1), equation (3-5) and equation (3-7) gives;

$$d_t = \frac{p}{\mu + 1} \tag{3-8}$$

The time that the cutterhead needs to travel distance d_t can be expressed as the follows.

$$\Delta t_c = \frac{d_t}{v_f} \tag{3-9}$$

This time Δt_c is important for improving wood surface form by modification of the machining process, (Hynek 2004). The surface waviness can only be influenced during this time period. Equation (3-9) can be rearranged to a more practical form by substituting equation (3-8) and equation (3-1).

$$\Delta t_c = \frac{p}{v_c + v_f} \tag{3-10}$$

There is an error between the height of the actual surface, h_a, and the waviness height of the idealised surface, h_c. This error can be described through (3-11).

$$E_h = \frac{h_a - h_c}{h_a} \tag{3-11}$$

The actual surface height h_a is approximately 5% lower than the simplified circular approximation height h_c for typical values of µ, (Hynek 2004). This low error justifies the use of the simplification of approximating the surface to a series or circular arcs.

3.2 Surface Defects and Their Appearance Forms on Machined Timber

Spindle vibrations and machine tool inaccuracies, particularly cutting tool inaccuracies, can also lead to surface defects, (Elmas 2008). The work carried out by (Elmas 2008) was the first mechatronic system capable of providing surface defects on demand, in order to more fully isolate and understand which parameters were producing the actual type of defect. In this work both single and two knife finishes were simulated and experimentally demonstrated. The work also included the influence of proud knives and cutterhead vibrations, particularly vertical cutterhead movement.

3.2.1 The Effect of a Proud Knife on the Surface Form

Cutterhead inaccuracies have a significant impact on surface quality, (Jackson, Parkin et al. 2002), especially the Total Indicated Runout, TIR. TIR is the radial difference between the knife with the largest radius and the knife with the smallest radius. Setting cutters up with typical room equipment can result in a TIR of typically 50 µm, (Hynek 2004). If however the cutters are setup and then ground, the TIR can be improved to be within the range 5-10 µm.

The single knife finish produces a surface form determined by the largest radius knife in the cutterhead. This can result from poor tolerances when grinding the knives, or from poor relocation of these knives within the cutterhead. It is not possible to produce cutting tools of all exact proportions however so this type of inaccuracy is important in the study of rotary wood planing. There will however be tolerances between the knives, where the smaller the tolerance band the higher quality of the cutting edge. The TIR can be as much as 50 µm for knives set in a cutterhead using a setting gauge (Jackson, Parkin et al. 2002) . Using the equations in Section 2, if we assume the cutterhead is rotating at 6000 rpm and has a feed rate of 12 m/min, the surface would have a pitch of 2 mm, which would be in the low quality range as described by Figure 3-3, whereas if the TIR was the ideal of 0 m, the surface would have a pitch of 1 mm, which would be in the high quality range.

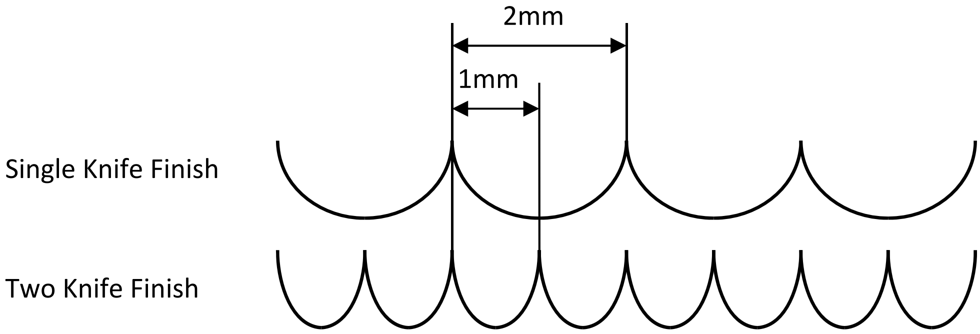

Figure 3-3 - The Effect of Single And Two Knife Finish On the Ideal Surface Form

One solution to minimise the TIR is to grind the knives whilst still in the cutterhead itself. Cutters ground in the cutterhead and then relocated using ‘hydrogrip’ tooling typically results with a TIR of 5 – 10 µm (Hynek 2004), but these inaccuracies cannot be totally eliminated.

Figure 3-4 shows the resultant surface finish from a cutterhead with two different radii knives. The surface form contains shorter cuttermarks, produced by the smaller radii knife, and longer cuttermarks, produced by the larger radii knife. The process of dressing the knives in the cutterhead is also known as ‘jointing’, (Elmas 2008), with an aim to true the cutting edges and to achieve a multi knife finish.

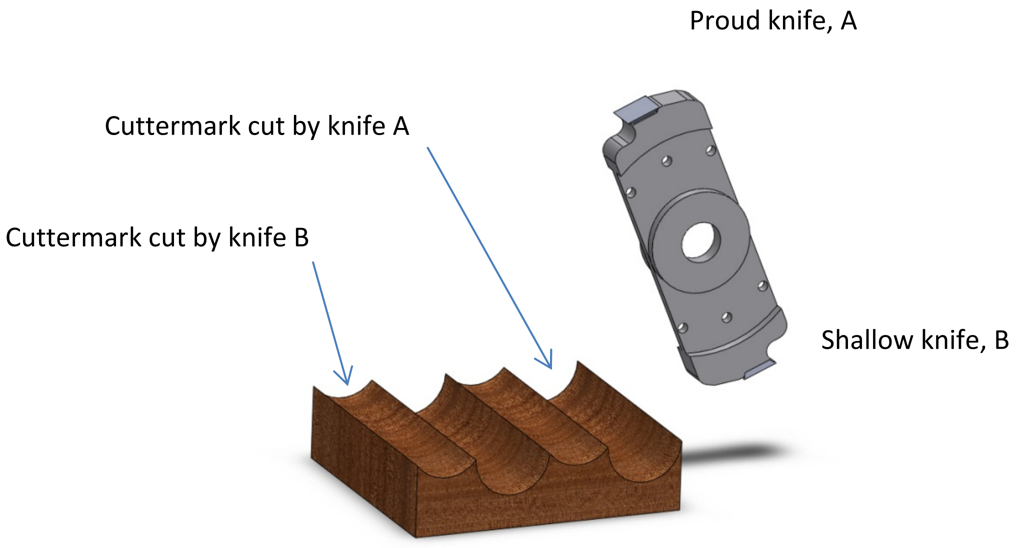
Proud knife, A
Cuttermark cut by knife A
Cuttermark cut by knife B
Shallow knife, B

Figure 3-4 - Effect of TIR on Surface Finish

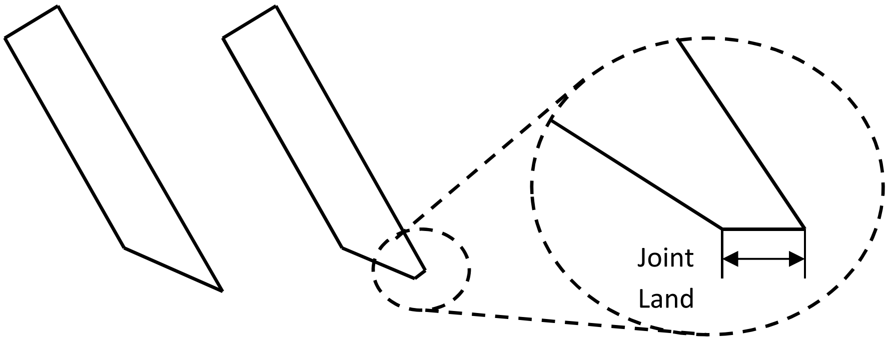

Figure 3-5 - Jointed Cutter with Joint Land

The process of jointing produces a joint land in the cutting edge, Figure 3-5. The difference in radius of the individual cutters results in joint land width variation, which leads to significant force variation and correspondingly poor surface roughness and waviness quality, (Jackson, Parkin et al. 2002) .

3.2.2 The Effect of Cutterhead Vibration on the Surface Form

Cutterhead vibration also has an effect on the surface form. In high speed woodworking machinery the cutterhead can have up to twenty knives. As shown through equation (3-2) the greater the number of knives the higher the feed rate for the same pitch, therefore allowing a higher speed of production for the same surface waviness quality.

The requirement to have an ideal multi knife finish requires all of the knives to have the same radius. To achieve this the knives are often jointed, but this causes the knives to have a zero clearance back angle that rubs the timber surface, which can cause a sealing effect of the timber leading to the timber not accepting many finish types, such as varnish, which is often undesirable. This rubbing effect causes variations in the normal cutting force, which produce cutter spindle deflection and hence variation in the cutter path, (Jackson, Parkin et al. 2002).

A particular example case may be a four knife cutter where all the cutters have been ground to the same radii, is subject to a 1 per revolution displacement at the spindle rotation frequency.

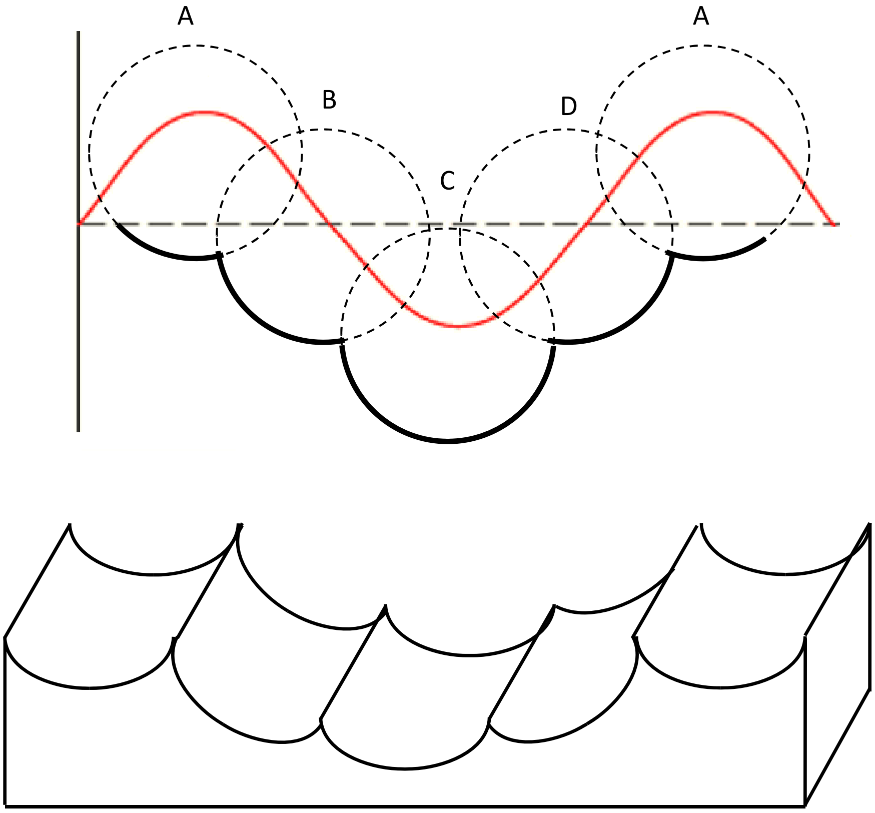

Resultant Surface Defect Caused By 1 per Revolution Vibration

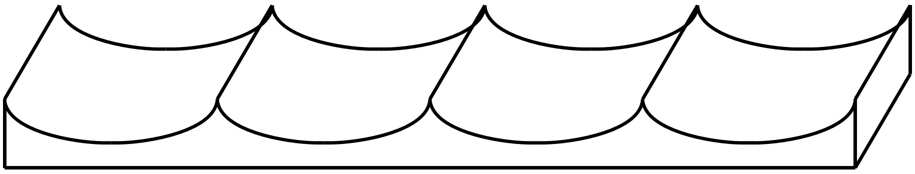

Ideal Surface Form Without Spindle Vibration

Figure 3-6 - Effect of 1 per Revolution Vibration on the Surface Form

Figure 3-6 shows that cutting knives B and D are unaffected by the vibration, whereas cutting knife A is pulled out of the workpiece, leading to a high spot, whereas cutting knife C is pushed into the workpiece, leading to a low spot equal in magnitude to the vibration magnitude. This is shown for the case where the positive maximum vibration displacement aligns with cutter A. The surface form depicted in Figure 3-6 is based on the circular arcs theory. When the vibration surface form is compared to the vibration free surface form we can see that it is an unacceptable surface quality.

3.3 Summary and Conclusions

This chapter has summarised a widely used approximation of surface form within the woodworking industry, the circular arcs approximation. This approximation attempts to predict the surface form of the machined timber surface, from the operating conditions. This approximation is used throughout this thesis and the research covered by it, particularly when choosing the operating conditions for the actual cutting tests carried out.

Also discussed within this chapter are the forms of common surface defects and some potential causes of these defects. This highlights the importance of cutterhead position control in order to achieve optimum surface finish given non-optimum operating conditions such as cutterhead vibrations and run-out of the cutting knives.

4 Methodology

This section will highlight the current drawbacks of the existing system and the proposed approach to address these shortcomings. Flow diagrams are given showing both the overall system and how the separate sub-systems interlink together, and the individual sub systems themselves.

4.1 Summary of Current Drawbacks

The current systems employed within the wood industry, and to the current small scale planer test rig, are all non-adaptive systems. Therefore, if during operation, the operating conditions change, this could be due to one of multiple reasons such as the cutting tip losing its sharp cutting edge and becoming more blunt or wearing away and the run-out of the knife changing, or the desired pitch of the machined timber surface altering, the overall system is not capable, in real-time, of overcoming this and requires a manual reset and tuning. This tuning requires a-priori knowledge of the cutterhead, and operating conditions, in order to optimise the control. Currently the best solution to this is to manually measure the run-out of the knives in order to gain an understanding of the TIR, and a trial and error approach to parameter tuning within the LQG controller.

There is also no existing software tool to analyse the surface profile directly, or indirectly, in order to ascertain the cause and type of surface defect, nor to propose a resolution in order to generate an improved machine timber surface. As the system deployed here by (Ogun 2012) uses a set point tracker the resolution type is that of a modification to the reference path used by the set point tracker.

A final consideration here is that of the test rig itself. Due to the nature of this research requiring actual cutting test rather than simply measuring the vibration of the cutterhead in free air under different operating conditions, the test rig itself is unsuitable to carry out the required tests.

A series of solutions have been proposed to overcome the drawbacks outlined in this section. A flow chart outlining the proposed methodology is given below. Different methodologies are implemented throughout the various sub sections and so this superficial methodology flowchart is then supplemented with additional flowcharts outlining the methodology utilised within each sub section of the work.

4.2 Overall Project Flow Diagram

The flowchart, Figure 4-1, gives a very brief order to the work carried out within this thesis. It follows the system operation and demonstrates the flow of information within the completed system.

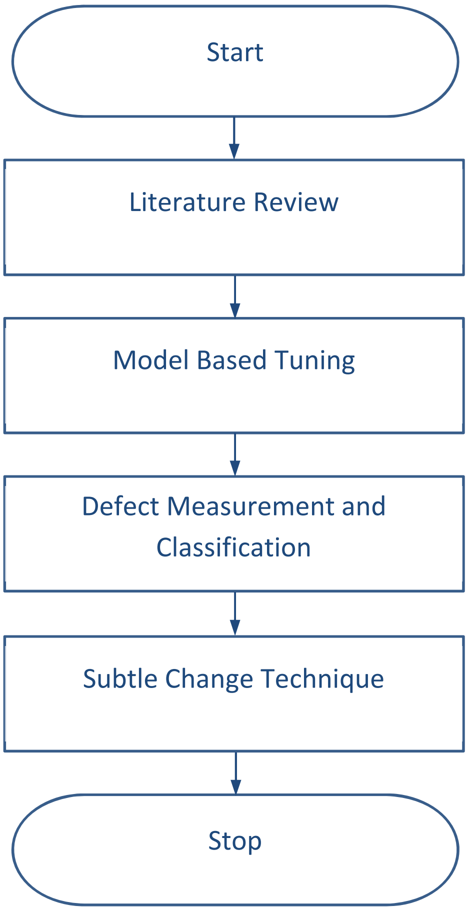
Start
Literature Review
Model Based Tuning
Defect Measurement and Classification
Subtle Change Technique
Stop

Figure 4-1 - Overall Project Methodology Flowchart

4.2.1 Model Based Tuning Methodology Flow Diagram

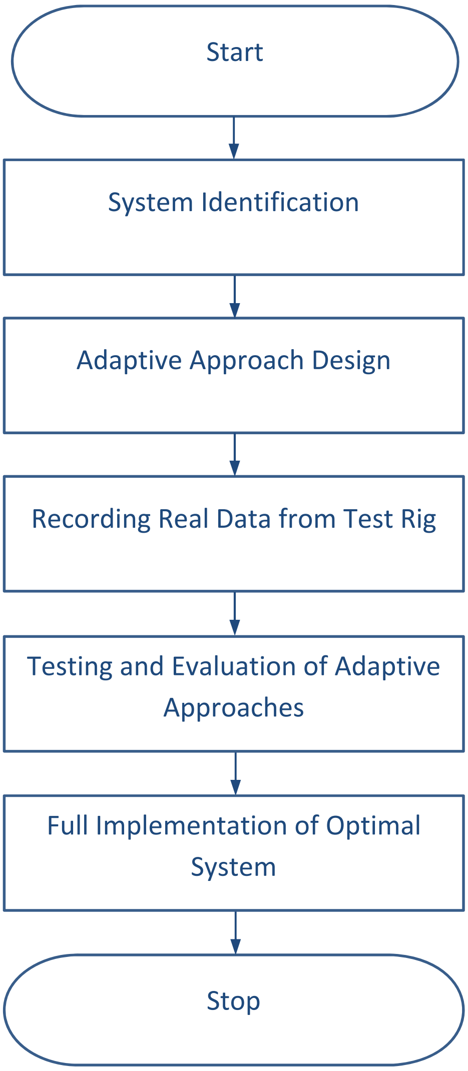
Start
System Identification
Adaptive Approach Design
Recording Real Data from Test Rig
Testing and Evaluation of Adaptive Approaches
Full Implementation of Optimal System
Stop

Figure 4-2 - Model Based Tuning Methodology Flowchart

Figure 4-2 shows the methodology flowchart for the model based tuning sub-system of the overall project methodology flowchart, Figure 4-1. The model based tuning relies on real data collected in a trial and error manner from the test rig. This data is then used to train a number of different adaptive systems. These software solutions overcome the non-adaptive, non-real-time drawback of the current solutions, by allowing for rapidly changing operating conditions to be deployed throughout the machining process.

4.2.2 Defect Measurement and Classification Methodology Flow Diagram

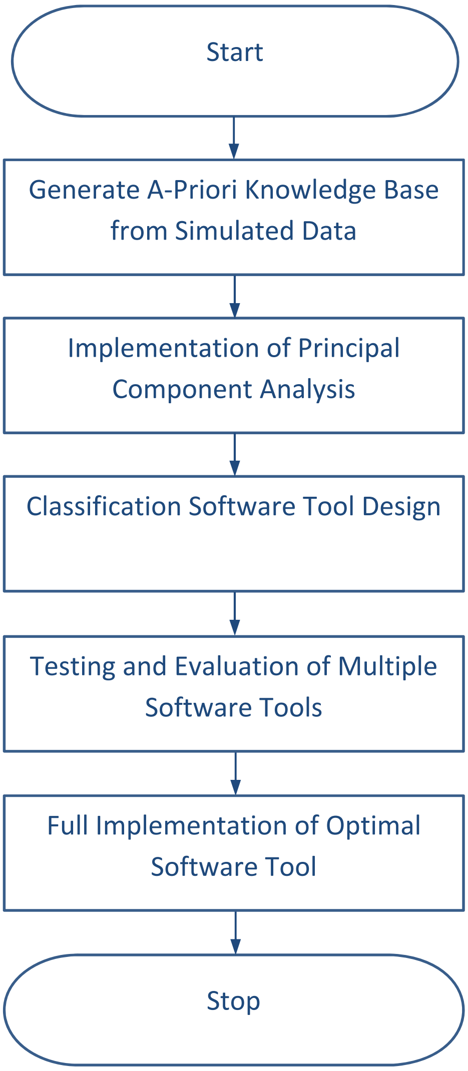
Start
Generate A-Priori Knowledge Base from Simulated Data
Implementation of Principal Component Analysis
Classification Software Tool Design
Testing and Evaluation of Multiple Software Tools
Full Implementation of Optimal Software Tool
Stop

Figure 4-3 - Defect Measurement and Classification Methodology Flowchart

Figure 4-3 shows the methodology flowchart for the defect measurement and characterisation section of this work. This differs from the model based tuning in one major characteristic, the data source. This data source, due to the size and timescale required to collect real world data, is a simulated source. Although without this data no further work would be possible, the main research effort here is the actual defect measurement and classification, rather than the production of thousands of known defect samples. The output of this section of work is a software tool capable of analysing a machined timber surface and outputting a defect cause and reference path capable of overcoming the defect, where possible.

4.2.3 Subtle Change Methodology Flow Diagram

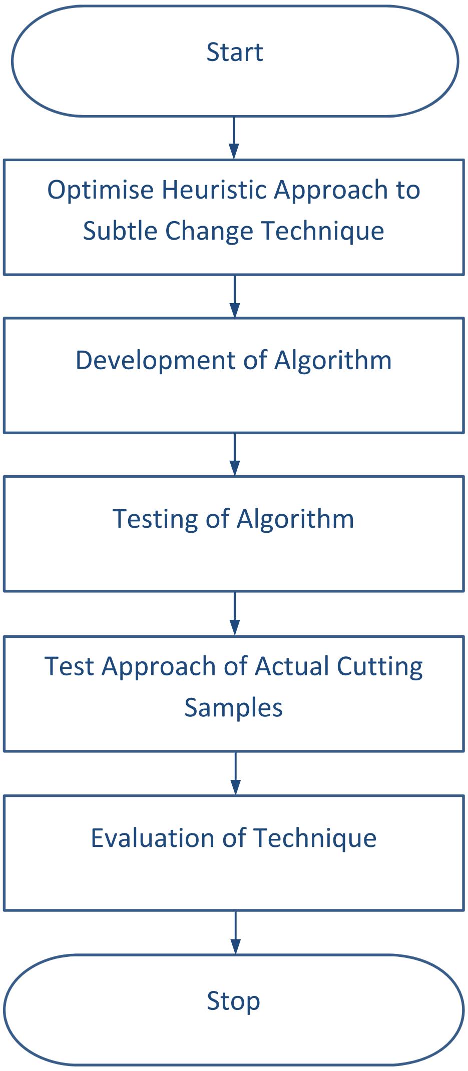
Start
Optimise Heuristic Approach to Subtle Change Technique
Development of Algorithm
Testing of Algorithm
Test Approach of Actual Cutting Samples
Evaluation of Technique
Stop

Figure 4-4 - Subtle Change Technique Methodology Flowchart

Figure 4-4 shows the methodology flowchart for the subtle change approach created and developed within this thesis. This approach again differs from that set out in Figure 4-2 and Figure 4-3, as here there are both simulations and real world tests carried out. The simulation work is used to more rapidly develop the algorithm, whereas the real world testing is used to evaluate the system on the actual test rig.

4.3 Summary

This section has described the different methodologies used within this thesis. The use of completely real world data, completely simulated data and a blend of the both real world and simulated data has enabled both rapid development of the core ideas and thorough evaluation of the techniques on actual data recorded from the test rig itself. Further details of the actual testing and evaluation are given in the thesis chapter designated for the particular section, such as the evaluation metrics used or the specific output from each sub-section of research and how these are used by subsequent ‘blocks’ within the overall system.

5 Chapter 5 - Small Scale Planer Test Rig Layout and Modifications

This theis is an extension to previous work carried out on the small scale wood planer machine at Loughborough University. This chapter aims to introduce the existing test rig and demonstrate the further capabilities added by this work. The original small scale planer rig was designed by (Hynek 2004). The system was designed to utilise vertical and horizontal cutterhead movement to improve the surface finish of the planed timber.

5.1 Piezo Electric Actuator

The actuation on the small scale planer is carried out by four stack type piezo electric actuators. These types of actuators are constructed of n layers of piezoelectric elements, which are connected mechanically in series, but electrically in parallel. The specification for all four actuator is given in Table 5-1.

Table 5-1 - Piezo Electric Actuator Specification

Max input voltage, V	150	V
Actuator stiffness, k_p	14	N/µm
Zero load displacement @ 150V, y_0	40	µm
Blocked force, F_{p0}	0.56	kN
Actuator capacitance, C_p	2.3	µF
Cross-sectional area, A	25	mm^2
Length, L	19.5	mm

The piezoelectric material expands proportionally to the applied voltage, detailed mathematical models are presented by (Hynek 2004).

Further evidence of the requirement to utilise a closed loop system has been generated by, (Ogun 2012). Figure 5-1, where the nonlinear behaviour of the actuators due to their hysteresis characteristics lead to non-repeatable spindle response. However it is stated that a closed loop system constantly driving the spindle to the desired position is capable of overcoming these issues.

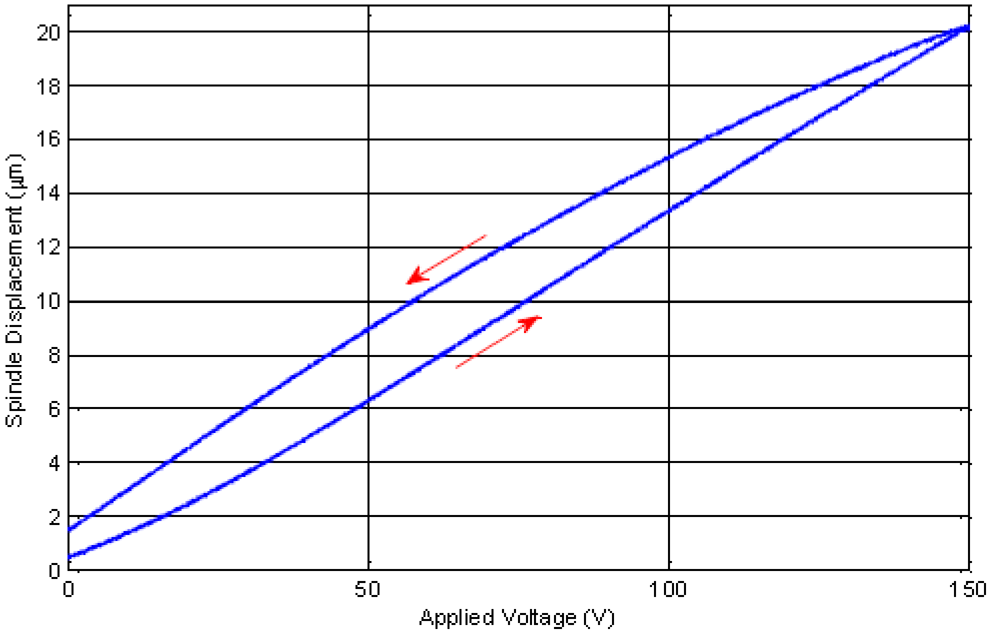

Figure 5-1 - Piezo Hysteresis Curve, (Ogun 2012)

Further tests were carried out on the piezo actuators to ascertain the time response characteristics. This is an important factor to take account of when considering the possible rotational speed of the cutterhead and the triggering position of the actuators to allow the cutterhead time to displace to the required position, Figure 5-2. It was found that the rise time was independent of the displacement value (input voltage), at approximately 1ms. At a rotational speed of 6000rpm the cutterhead will have rotated approximately 36° in this time which is still acceptable when using a four knife cutterhead as the knives are equally spaced around the cutterhead at increments of 90°, therefore the 36° offset is well within the available 90°.

However signal transmission lag of approximately 2ms was measured. This was the time taken from an initial tigger from the computer for that signal to actuate the piezo and then for that displacement to be measured by the computer.

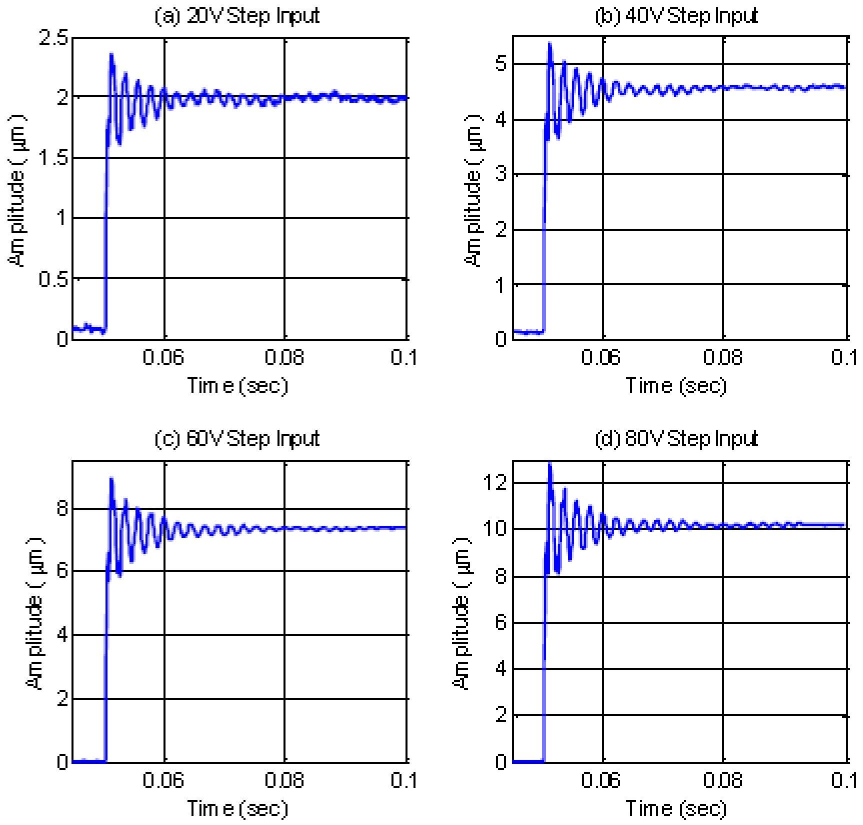

Figure 5-2 - Spindle Responses to Differing Step Input Voltages

5.2 Eddy Current Probes

To measure the position of the spindle two non-contact eddy current probes are installed into the spindle unit. These probes require an external driver unit to amplify the signal. A brief outline specification can be found in Table 5-2. The output from the driver is proportional to the distance between the spindle and the tip of the probe. The amplified signal from the driver also minimises the influence of noise introduced onto the signal line from the probe to the computer input.

Table 5-2 - Eddy Current Sensor/Driver Specification

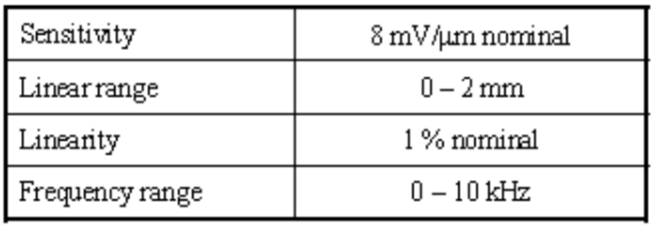

Sensitivity	8 mV/µm nominal
Linear range	0 – 2 mm
Linearity	1 % nominal
Frequency range	0 – 10 kHz

5.3 Mechanical Design of the Small Scale Planer

The existing small scale planer test rig consists of a base frame on which a feed table and smart spindle assembly are mounted. The smart spindle unit can be moved vertically in order to control the depth of cut. The smart spindle unit can also be moved horizontally to affect the surface finish but for this body of work this degree of movement is locked. The feed table has a preloaded ball screw and high precision linear guides to ensure consistent cutting conditions as the table passes across the cutterhead. This is shown in Figure 5-3.

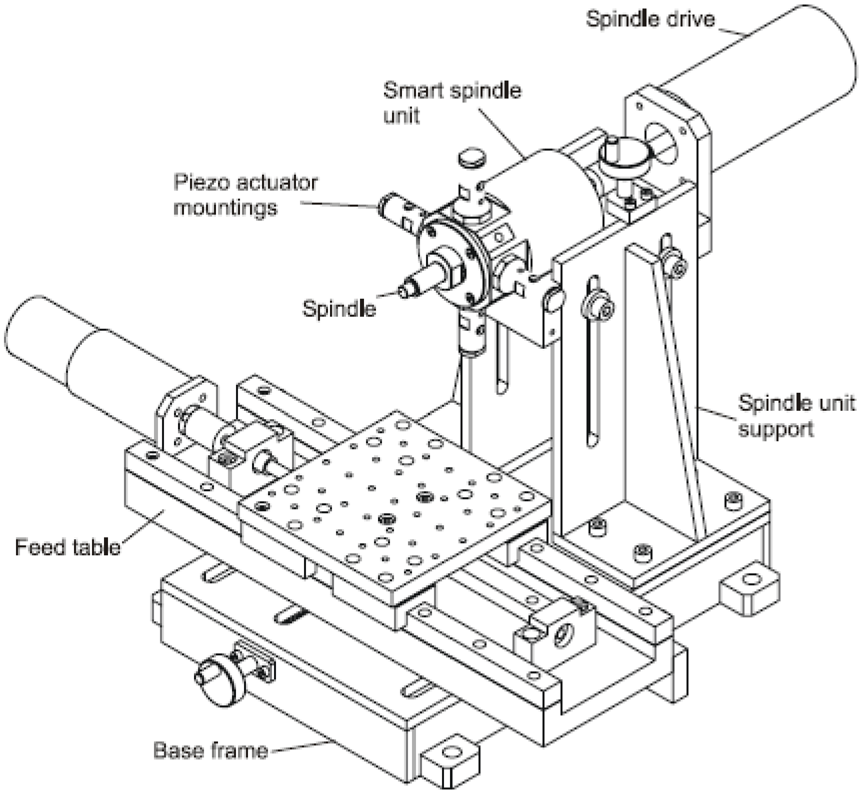
Spindle drive
Smart spindle unit
Piezo actuator mountings
Spindle
Spindle unit support
Feed table
Base frame

Figure 5-3 - Small Scale Planer, (Hynek 2004)

5.3.1 Smart Spindle Unit

The test rig has an overhung smart spindle unit, Figure 5-6. The spindle is supported by two precision angular bearings at the front and rear of the housing, with the cutterhead overhung from the front bearing. To displace the cutterhead vertically the entire front bearing assembly is displaced. This simple arrangement allows a limited cutterhead displacement as only the front bearing is displaced, but requires fewer actuators than displacing both the front and rear bearings. This type of movement does however introduce cutterhead tilt, and therefore knife tilt, as shown in Figure 5-4. The amount of knife tilt needs to be understood as it will have an effect on the machined surface quality.

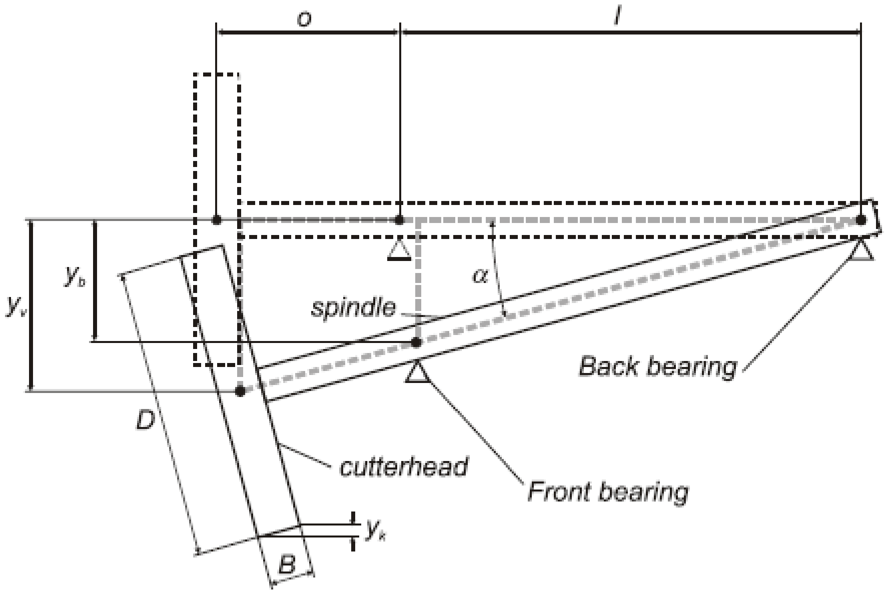
o
l
α
y_b
y_v
spindle
Back bearing
D
cutterhead
Front bearing
y_k
B

Figure 5-4 - Overhung Spindle

The magnitude of knife tilt can be estimated through the geometric relationships of the overhung spindle arrangement. The angle of knife tilt is equal to the angle of spindle tilt α. This angle can be calculated as follows

$$\propto = \sin^{-1}\left(\frac{y_b}{l}\right) \tag{5-1}$$

Where;

l is the length between the two bearings

y_b is the vertical displacement of the front bearing

However the knife tilts influence on the machined timber is more meaningfully described by the vertical displacement of the two edges of the knife, y_k.

$$y_k = y_v \frac{B}{l + O} \tag{5-2}$$

Where;

B is the width of the cutterhead

O is the overhang of the cutterhead from the font bearing

l is the length between the two bearings

In order to minimise the tilt of the knives, and therefore the negative effect upon the wood surface, the value of y_k should be minimised. With the overhung setup it is not possible to achieve zero tilt, and it is reported, (Hynek 2004), that the ratio $\frac{y_k}{y_v}$ should be less than 10%. This ratio depends on the cuttehead width B and the overall spindle length l + O, as given in equation (5-2).

Figure 5-5 shows the relationship between the overall spindle length and the cutterhead width at different $\frac{y_k}{y_v}$ ratio values.

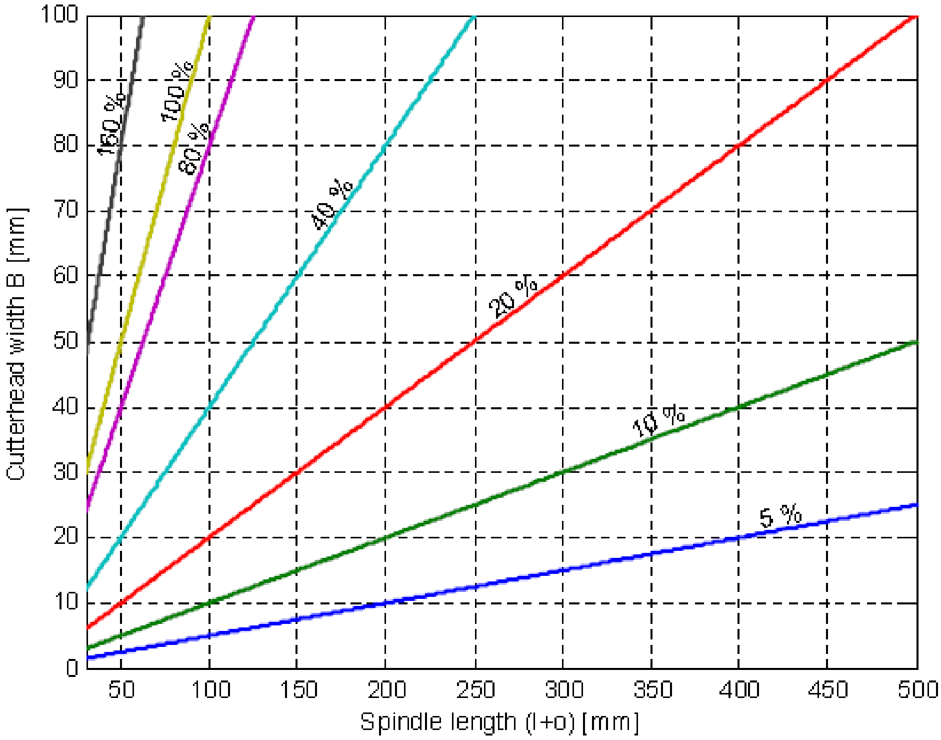

Figure 5-5 - Ratio $y_k/y_{v,}$ (Hynek 2004)

With practical considerations for a small scale planer test rig within the Loughborough research department, the overhung spindle arrangement is only suitable for narrow cutterheads. The current test rig employs a cutterhead that is 10mm in depth, and bearing span of 87mm and a spindle overhang of 47mm. The resulting $\frac{y_k}{y_v}$ ratio is 7.46%. For a 10µm vertical displacement in the cutterhead, the value of y_v is 0.746 µm, which is an acceptably small value, and should not have an appreciable negative effect on the surface quality.

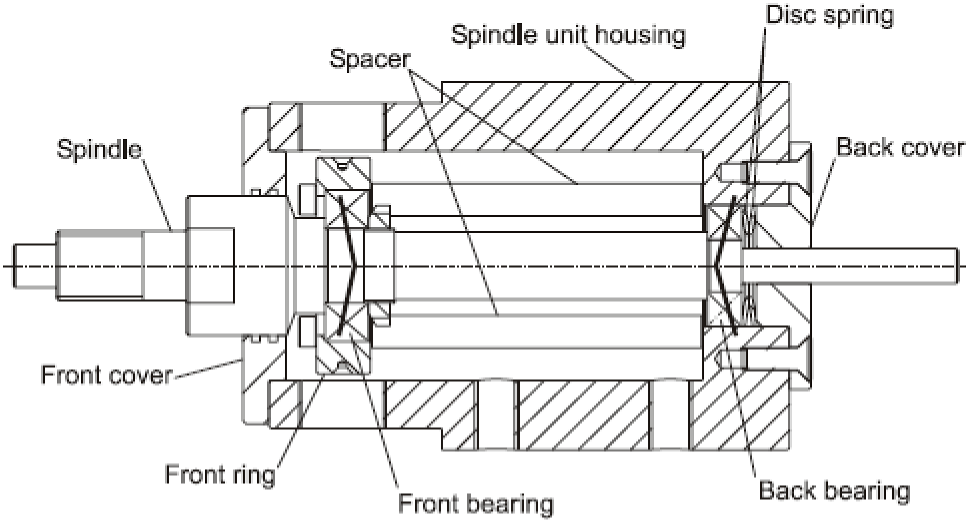
Disc spring
Spindle unit housing
Spacer
Spindle
Back cover
Front cover
Front ring
Front bearing
Back bearing

Figure 5-6 – Smart Spindle Unit Cut-through, (Hynek 2004)

Figure 5-6 shows a cross section of the spindle unit. The two high precision angular contact ball bearings are arranged in a face to face configuration. The rear bearing is fitted to the housing, whereas the front bearing is fitted to the front ring, which is retained axially by four spacers, see Figure 5-7. The two bearings are preloaded by a pair of disc spring to remove any axial float of the spindle.

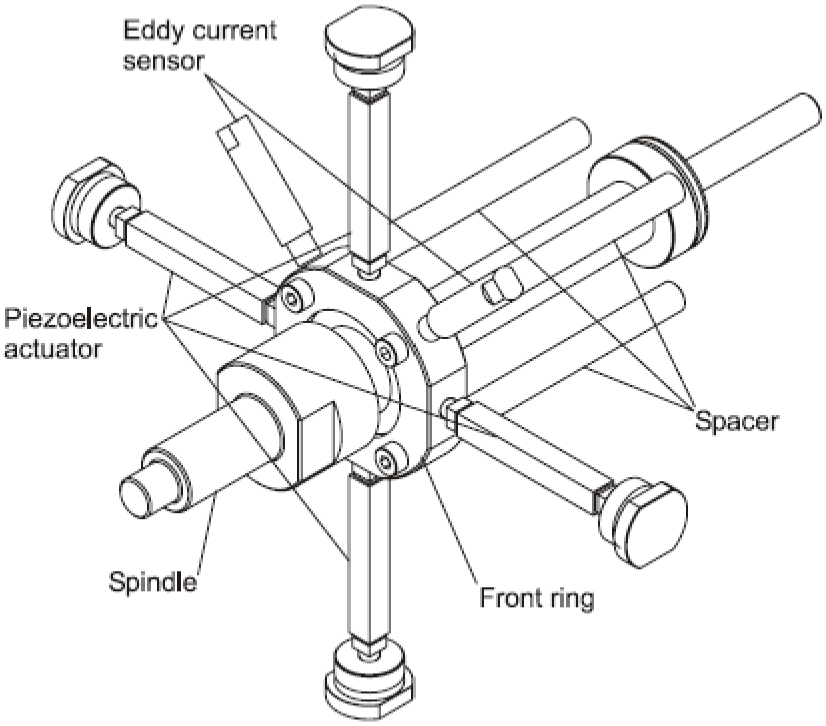

Figure 5-7 - Spindle Support

This arrangement provides a flexible support for the front bearing, which has a low stiffness when the actuators are not fitted, circa 2 N/µm in the radial direction. This low stiffness is an advantage as it provides less resistance to the actuators, therefore the required force to move the spindle is low.

5.3.2 Actuator Arrangement

Four piezoelectric actuators are arranged radially around the spindle, Figure 5-8. These actuators are located both vertically and horizontally opposed to one another. When activated with appropriate voltage inputs, the actuators control movement of the spindle in a plane perpendicular to the axis of spindle rotation.

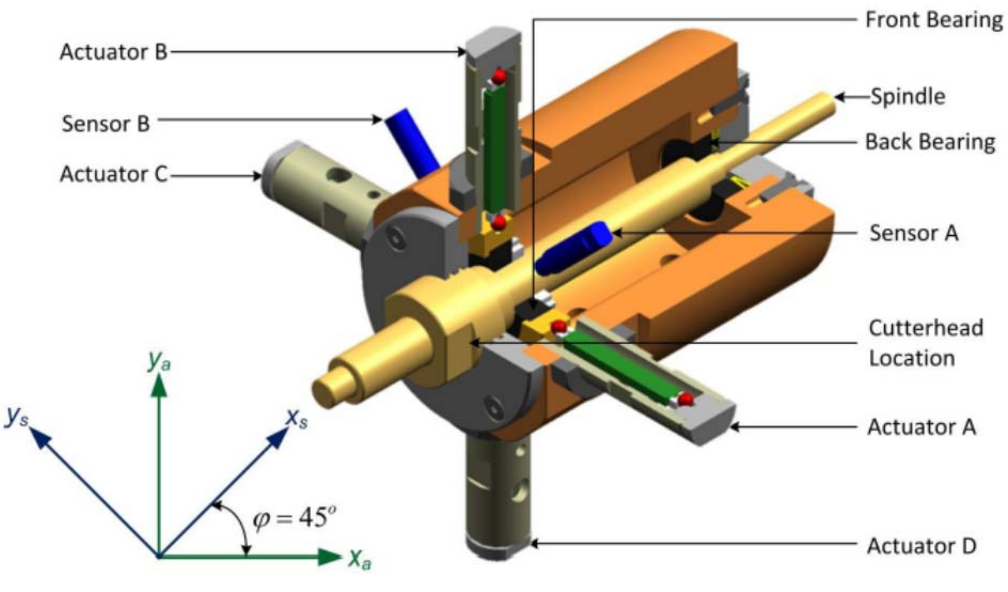
Actuator B
Sensor B
Actuator C
Front Bearing
Spindle
Back Bearing
Sensor A
Cutterhead Location
Actuator A
Actuator D
y_s
y_a
x_s
$\varphi = 45^o$
x_a

Figure 5-8 - Smart Spindle Unit Arrangement

The chosen actuators specification is shown in Table 5-3.

Table 5-3 - Actuator Specification (same as Table 5-1)

Max input voltage	V	150	V
Actuator stiffness	k_p	14	N/µm
Zero load displacement @ 150V	y_0	40	µm
Blocked force	F_{p0}	0.56	kN
Actuator capacitance	C_p	2.3	µF
Cross-sectional area	A	25	mm^2
Length	L	19.5	mm

The analysis of the piezo actuator setup is shown schematically in Figure 5-9 below.

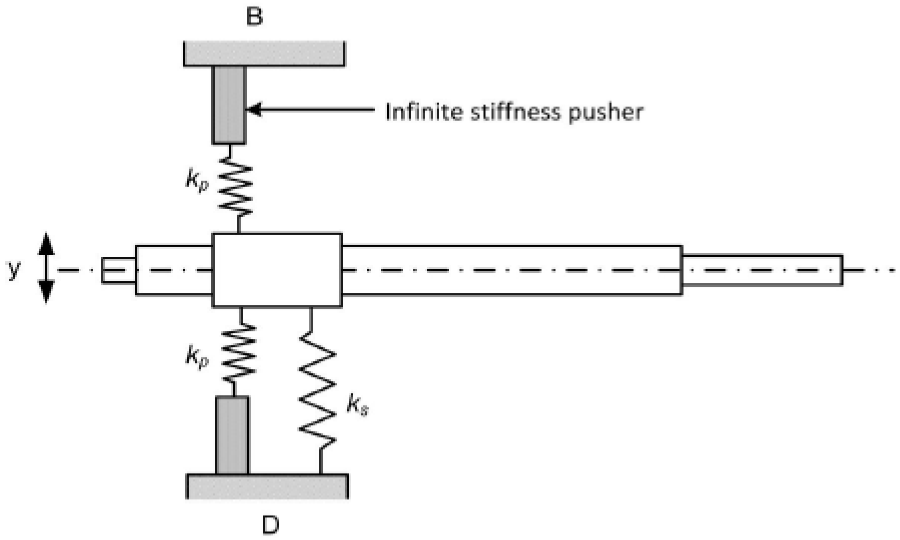

Figure 5-9 - Actuator Arrangement

The piezo actuators are arranged in a push pull configuration. The actuators are modelled as infinite stiffness pushers and a spring connected in series (k_p = 14N/µm). In parallel with the actuator model is a further spring that represents the combined support stiffness of the spacers (k_s = 2N/µm). Therefore the overall stiffness of the actuator is 16N/µm. The use of two actuators in this manner does increase the cost and complexity of the design as additional power amplifiers are required but overcomes the fragility of the actuators when exposed to tensile stress. The ratio between these two stiffness's is calculated as follows

$$\gamma = \frac{k_s}{k_p} \tag{5-3}$$

The influence of the spacers therefore provides an increase to the displacement resistance felt by the actuators. The influence depends on the ratio γ as shown in Figure 5-10. The amplifier voltage corresponds to the input to the piezo actuator. It is clear that as the ratio γ increases the response to a given voltage reduces. It is therefore desirable to have a low ratio γ to maximise the displacement capability of the actuators.

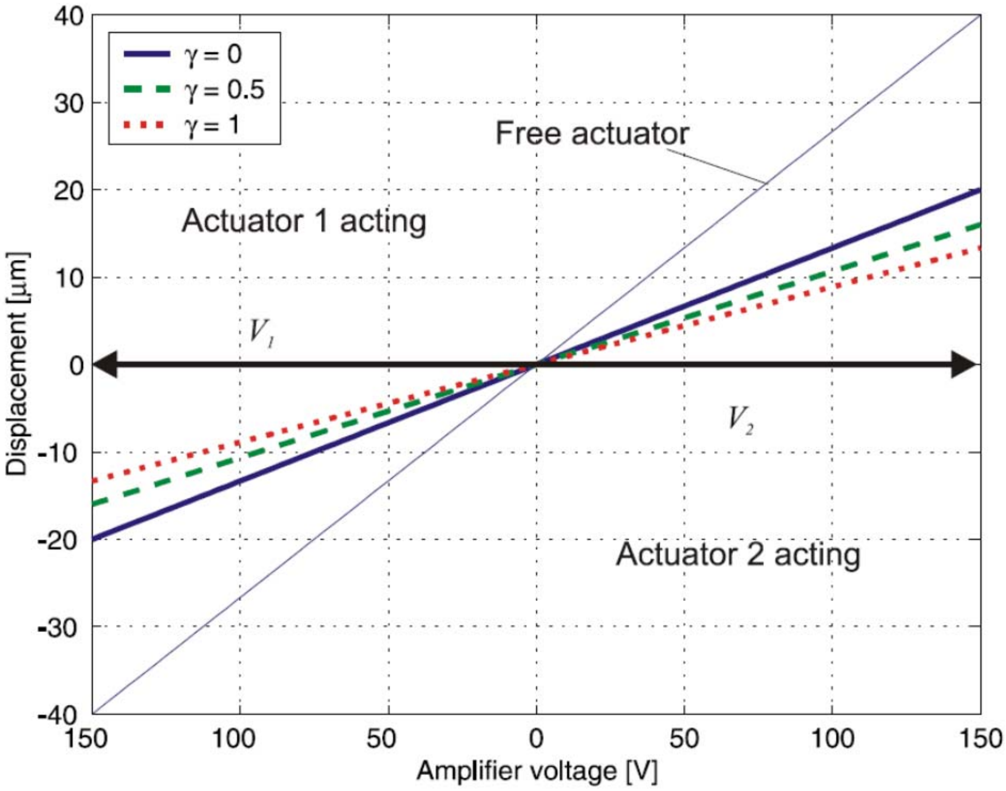

Figure 5-10 - Displacement versus Voltage, (Hynek 2004)

The actuators themselves can only be stressed axially. Other types of forces, such as shearing or torsion may cause damage to the actuators and should therefore be avoided. Methods to avoid particular forces are available. Tension can be avoided through preloading of the actuator. Ball tips of flexures have been introduced to decouple the lateral and bending forces, as seen in Figure 5-11.

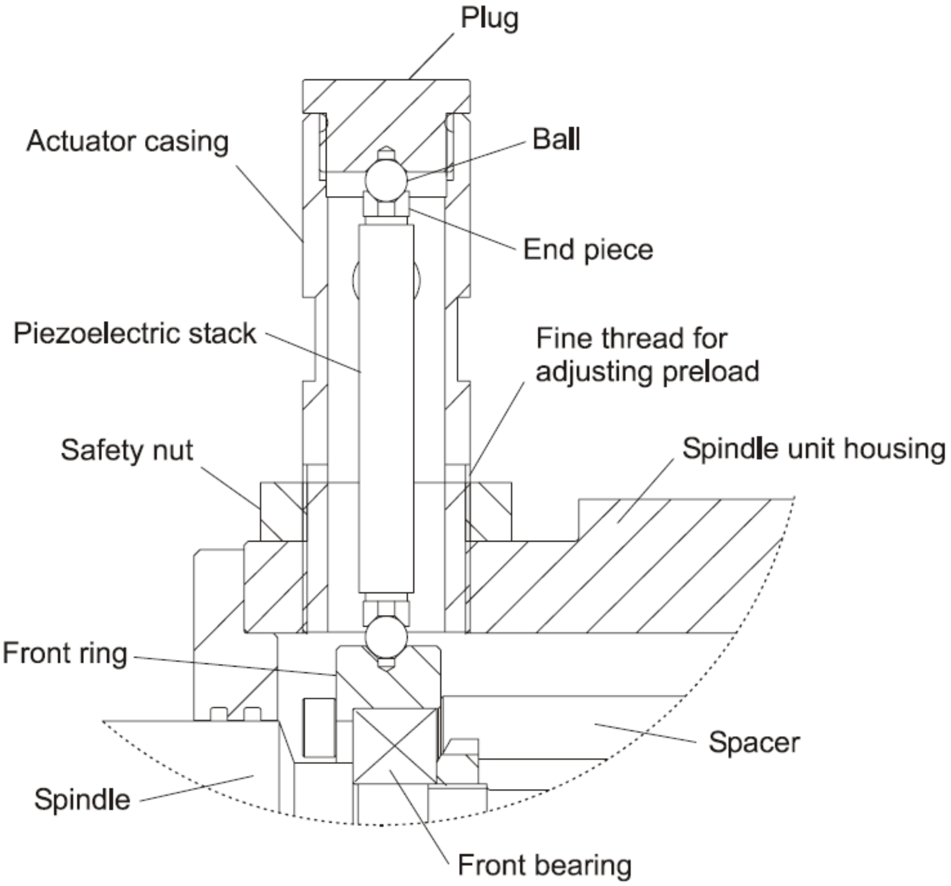
Plug
Actuator casing
Ball
End piece
Piezoelectric stack
Fine thread for adjusting preload
Safety nut
Spindle unit housing
Front ring
Spacer
Spindle
Front bearing

Figure 5-11 - Actuator Mounting, (Hynek 2004)

As the system is used in a push-pull configuration the actuators are then preloaded using the outer casing and locked in place with the safety nut. This preload does not alter the available displacement, (Hynek 2004), rather it causes an initial offset in the spindle position. However, as both the upper and lower actuators are preloaded this offset can be reduced to zero. It is also possible to deliberately offset the spindle from the neutral position if desired. This offset is shown graphically in Figure 5-12.

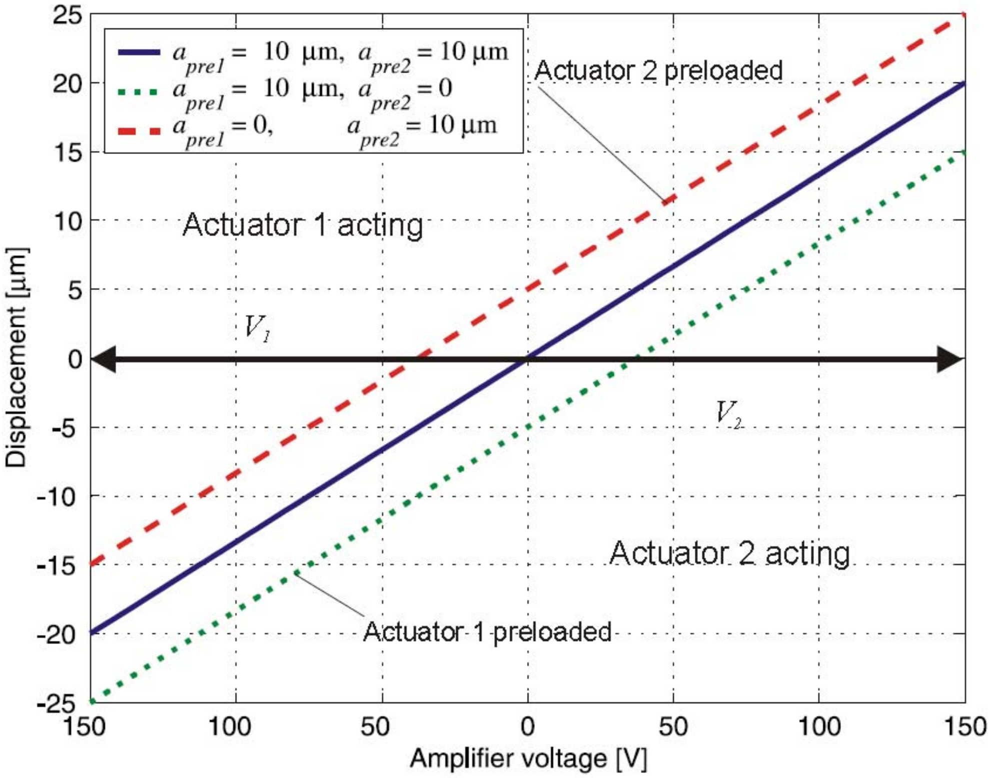

Figure 5-12 - Effect of Preload, γ=0, (Hynek 2004)

5.3.3 Sensor Arrangement

The principal employed within this research is to displace the cutterhead in the vertical axis in order to improve the surface quality of the machined timber. This movement is to be part of a closed loop control system and therefore the displacement must be measured. Two eddy current probes and utilised to measure the displacement. These are located at 45° to the piezo actuators due to space constraints, Figure 5-13.

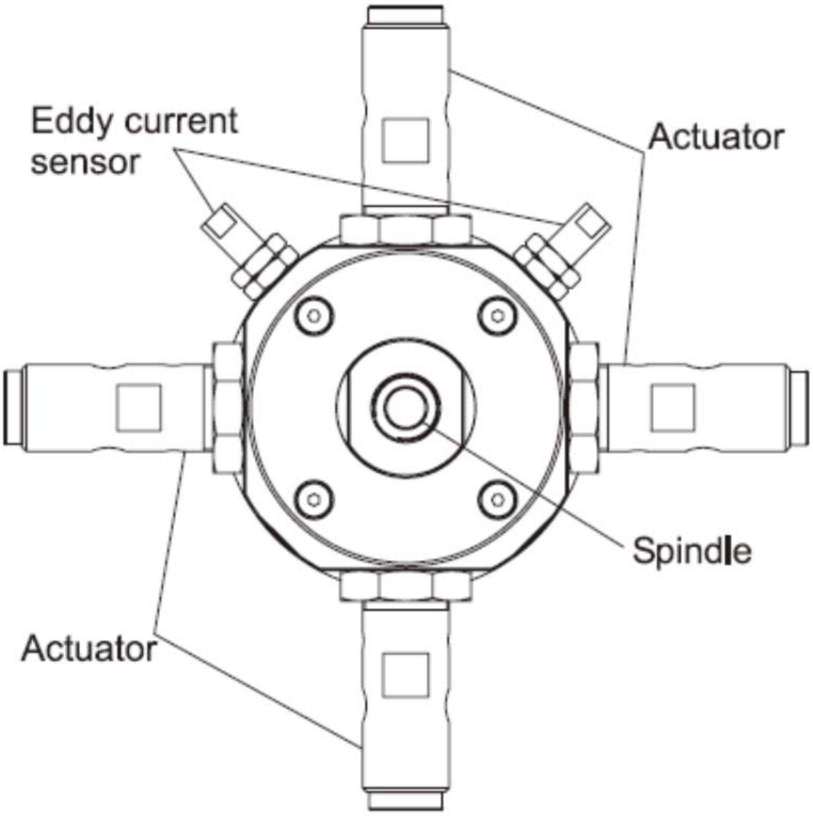
Eddy current sensor
Actuator
Spindle
Actuator

Figure 5-13 - Spindle Sensor Arrangement, (Hynek 2004)

In order to account for this rotation an arithmetic transformation must be carried out.

$$\begin{bmatrix} x_a \\ y_a \end{bmatrix} = \begin{bmatrix} \cos\varphi & -\sin\varphi \\ \sin\varphi & \cos\varphi \end{bmatrix} \begin{bmatrix} x_s \\ y_s \end{bmatrix} \quad (5\text{-}4)$$

Where x_a and y_a are the spindle centre point deflections and x_s and y_s are the measurements from the eddy current probes. Φ is 45°.

$$\sin(45°) = \cos(45°) = \frac{\sqrt{2}}{2} \tag{5-5}$$

Inserting equation (5-5) into (5-4) yields

$$y_a = \frac{\sqrt{2}}{2}(x_s + y_s) \tag{5-6a}$$

$$x_a = \frac{\sqrt{2}}{2}(x_s - y_s) \tag{5.6b}$$

5.3.3.1 Spindle Deflection Test

However the cutterhead displacement cannot be easily directly measured, but the front ring displacement is relatively easy to measure. Due to the overhang of the cutterhead outside the front ring, the relative displacement of the front ring will be lower than that of the cutterhead itself. Using the geometrical relationships shown in Figure 5-4, and the known dimension for the overhang, 47mm, and the spindle length of 87mm, this ratio between measured displacement at the front ring and the actual cutterhead displacement should be approximately 1.54. To verify this assumption differing voltages were applied to the piezo actuator and both the eddy current measurements and an independent measurement using a digital dial gauge were taken. The experimental setup for verification is shown in Figure 5-14 and the results in Table 5-4.

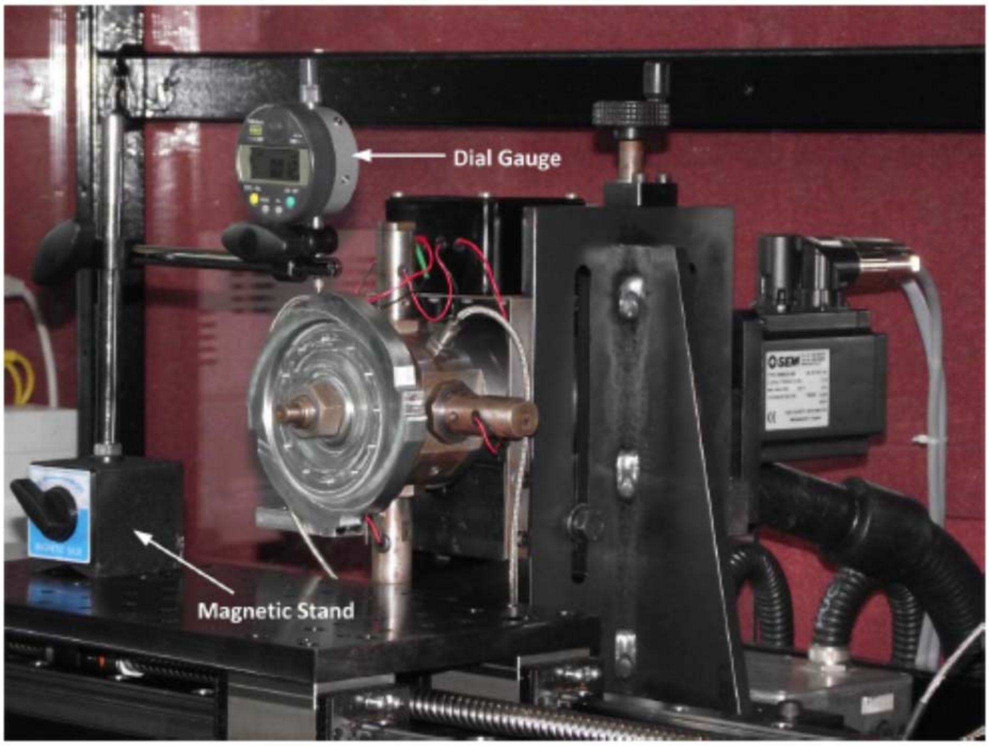

Figure 5-14 - Spindle Deflection Testing Setup

Table 5-4 - Spindle Displacement Results

Voltage (V)	Sensors Reading, y_v (µm)	Dial Gauge Reading, y_b (µm)	y_b/y_v
40	5.30	7.00	1.32
75	10.00	13.00	1.30
76	10.05	13.00	1.29
107	14.30	18.00	1.26
124	16.50	20.00	1.21
-80	-10.70	-13.00	1.21
-83	-11.06	-14.00	1.27
-116	-15.44	-19.00	1.23
-117	-15.60	-19.00	1.22

The results in Table 5-4 clearly do not match the geometric assumptions. The difference between the average reading of 1.26 could be attributed to eddy current probe calibration errors, their mountings and the material used in the test rig. These potential sources of error could have led to an incorrect original calibration of the eddy current probes calibration factor. As such the dial gage readings were used to recalibrate the system.

5.4 Small Scale Planer Modifications

The original test rig was primarily used for no load tests, testing different vibration control algorithms and approaches. Although the test rig was satisfactory for these tests the further work carried out here, primarily cutting tests, modifications were required. The primary modifications necessary for this were to upgrade the motors, both for the cutterhead motor and the timber feed motor.

5.4.1 Feed Table Length

In order to extend the capabilities of the small scale planer and enhance the quality of the research undertaken, modifications to the rig have been undertaken. The first of these modifications was to extend the length of the feed table and accompanying mechanisms. This modification is to allow for future development of the system, and further integration with the Wood Surface Measuring System, WSMS. The principal being that once complete, the timber passing under the cutterhead will be long enough to allow for an uncompensated area of timber to pass to the WSMS, measurements taken and then the compensation applied to the system and the timber machined with the compensation. This will allow for a graphic demonstration of the system in action, such that within the same piece of timber there will be both an area outside the required tolerance, and then once the compensation has been applied an area within specification.

The extension of the feed table length has also necessitated extensions to both the linear rails and the ball screw assembly. The feed motor has been positioned such that as the carriage is drawn across the cutterhead, the ball screw is in tension, rather than compression. This reduces the vibration in the ball screw, and therefore the amplitude of vibration put into the carriage. This reduces the uncontrolled process disturbance input into the total system.

5.4.2 Cutterheads

A further modification was to produce a new set of cutterheads. The previous cutterheads unfortunately were not suitable for experimentation as the difference in radii between knives was far greater, circa 60µm, than the available displacement of the cutterhead. There were also inaccuracies with knife tilt, and knife twist. Three new cutterheads were wire cut, each with different deliberate inaccuracies. These cutterheads were produced externally using electro discharge machining, in particular a wire erosion machine. One cutterhead had a single proud knife, the second cutterhead has two opposing proud knives, and the third has all knives at different radii. This allows for different cuttermark patterns to be easily generated and further more in depth testing of the system. Table 5-5 shows the measurements of the three cutterheads as measured on the Alicona measurement system, Appendix B – Alicona Infinate Focus Machine.

Table 5-5 - Cutterhead Knife Tip Radii Measurements

	Knife 1	Knife 2	Knife 3	Knife 4
Cutterhead 1	57.0666	57.0654	57.0688	57.0646
Cutterhead 2	57.0637	57.0706	57.0681	57.0645
Cutterhead 3	57.0712	57.0677	57.0725	57.0671

5.4.3 Motor Upgrades

However, the most important upgrades to the small scale planer has been the replacement of the two motor units. The previous system did not provide accurate speed control of the cutterhead as the speed was controlled through a variac. This produced a constant no load speed, such as 600rpm, but when load was applied, such as when cutting the timber, the speed rapidly reduced leading to a stall situation on many occasions. In order to make a step change in system performance, and bring the system closer to a real world wood planing machine, the specification was changed demanding that the system be capable of running a four knife cutterhead at a rotational speed of 6000rpm.

Data collected by, (Jackson 1986), shows that for birch timber the tangential force, for our width of cutter and a depth of cut of 1mm, is 630N, and the normal force is 70N. This equates to a resultant force of 634N. The radius of the cutterhead is a nominal 60mm, and the total torque required will be 37.8 Nm ≈ 40Nm. However the knives are not in constant contact with the timber surface, rather the torque signature is far more discrete.

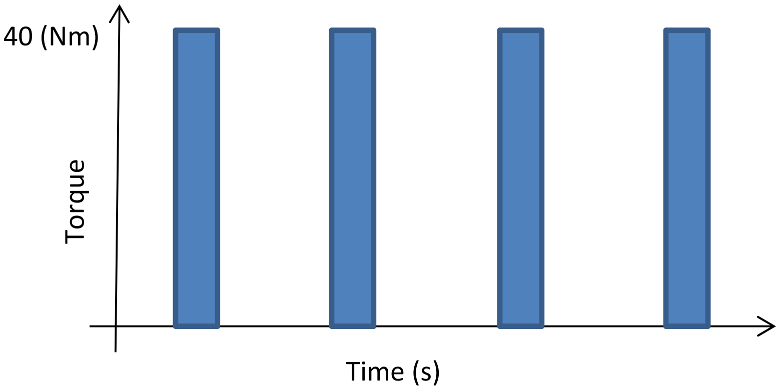

Figure 5-15 - Example Torque Vs Time Graph at 6000rpm

The actual knife contact times are in the order of 0.5ms, (Jackson 1986). In order to average the torque required at 6000rpm;

$$4Knives \times 40Nm \times 0.0005seconds \times 100rps = 8Nm$$

To achieve this a new servo motor was selected and accompanying componentry redesigned to accept it. Further motor specifications of this can be found in Appendix C – Purchased Components.

As shown in section 3 the pitch of the wave produced on the timber surface is dependent on the number of knives on the cutterhead, the rotational speed of the cutterhead and the feed speed. Therefore with the requirement of the system to now operate at 6000rpm with a four knife cutterhead, the feedspeed needs to be matched to the cutting speed. This required a new motor to be selected, such that it could provide the required torque to accelerate the workpiece carriage to the required speed in the available space and provide an accurate constant speed. Again a new servo motor was selected for this and further details can be found in Appendix C – Purchased Component.

Both of the new motors are now run through industry standard SERAD motor controllers controlled via serial link from developed C# software. Further details on the motor controllers can be found in Appendix C – Purchased Component.

5.4.4 WSMS Integration

As a final change to the small scalar planing test rig, the WSMS has been integrated onto the same platform as the cutting rig. This has allowed for dynamic measuring in real-time, rather than having to remove the timber and take it to another measuring station. The WSMS assembly has been designed such that it is a separate frame, and as such can be moved and used with other test rigs/areas, but has been placed as close as possible to the cutterhead, Figure 5-16.

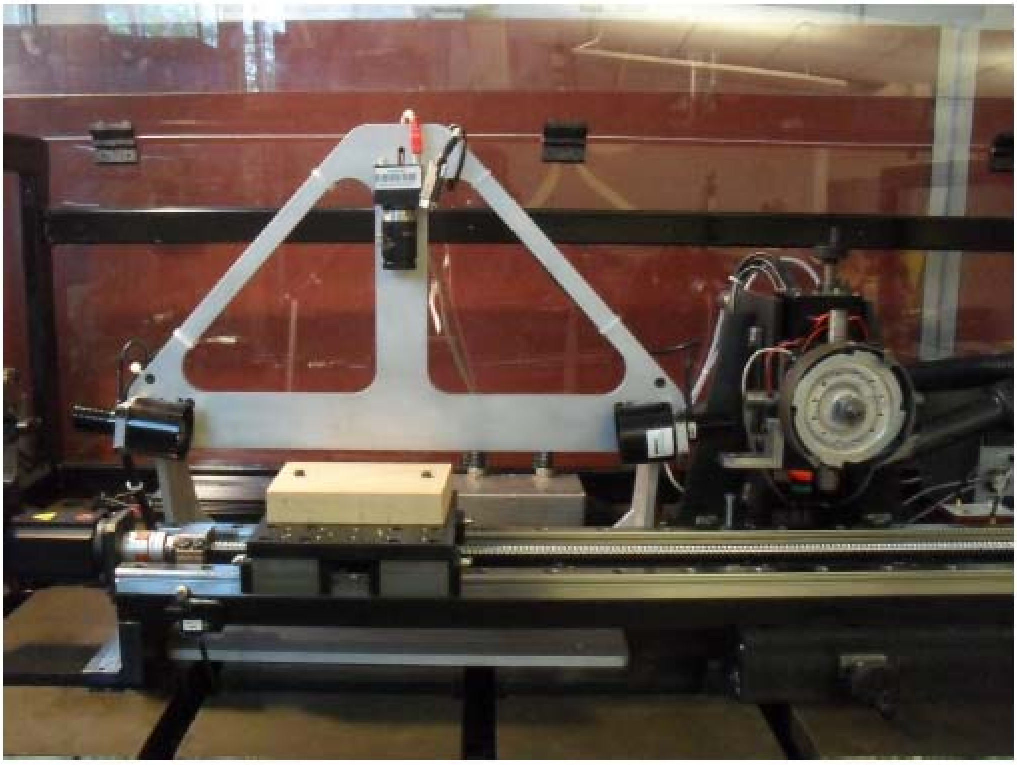

Figure 5-16 - Integration of WSMS to the Small Scalar Planing Machine

5.5 New Small Scale Planer Test Rig

Figure 5-17 shows the updated small scale planer test rig. The key new components are shown is their positions. For this image the guarding has been removed as well as the extraction system used to remove the wooden chips and dust generated during the planing process.

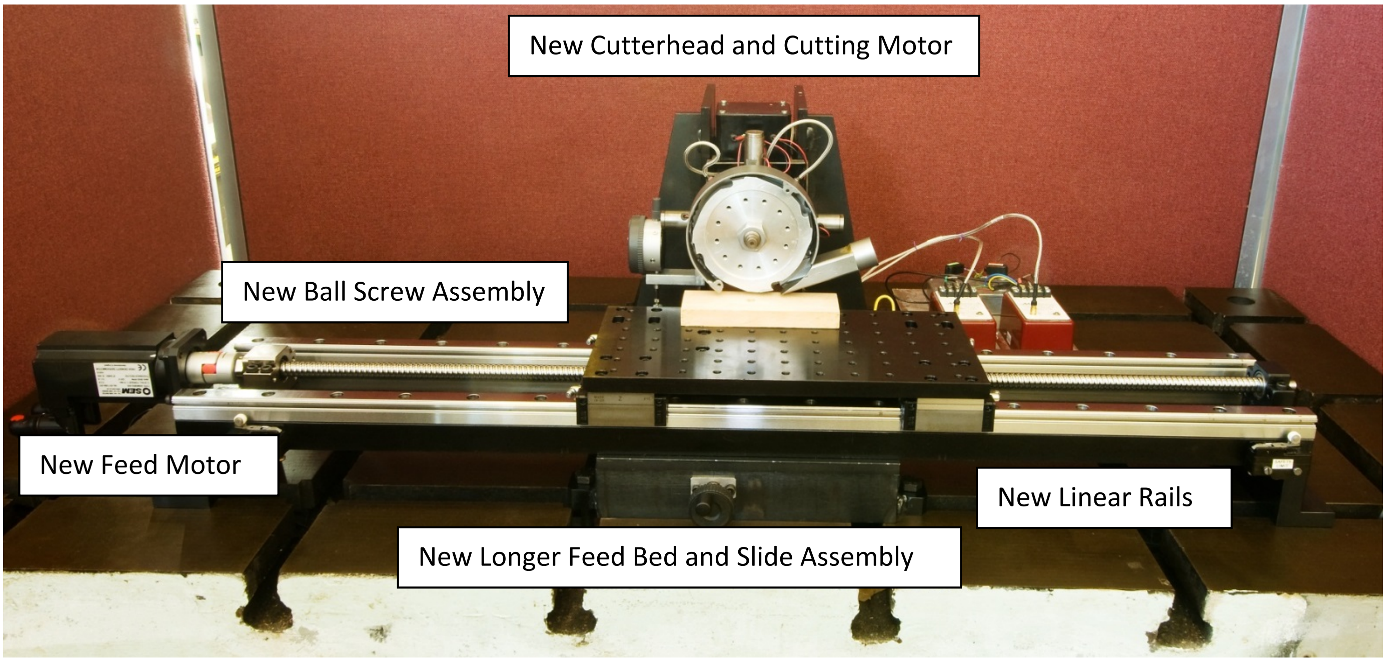
New Cutterhead and Cutting Motor
New Ball Screw Assembly
New Feed Motor
New Linear Rails
New Longer Feed Bed and Slide Assembly

Figure 5-17 - Updated Small Scale Planer Test Rig

5.6 Commissioning Testing

In order to commission the new motors simple tests were carried out. The motor controllers allow for a specific speed demand to be placed upon the motor and once tuned the controllers are designed to maintain that speed. The controllers can be run in other modes but for this application a simple constant speed mode has been selected.

5.6.1 Motor Speed Tests

To test the cutterhead motor speed control the spindle unit has an independent speed measuring device on the spindle, a quadrature encoder. This device is read independently of the motor speed by the PC via a dedicated input line with a sample time of 150µs. The system was tested across the entire speed range, running in a no load situation, and the motor controller was found to control the speed to a very high degree, circa 5rpm.

A similar test was carried out for the feed motor, both when disconnected to the ball screw and when connected to the ball screw, and again similar results were recorded. However as a further test the acceleration of the system needed to be tested. To do this the speed of the system, with the carriage and ball screw connected to the motor, was recorded during a single pass and plotted against time, Figure 5-18. During this test the speed is sampled at 200Hz as beyond this speed the data processing failed, due to the speed of the data acquisition card within the pc and the required processing time. Each sample required a total time of approximately 0.005seconds to fully process, although this value was different for each type of input. No independent measurements of friction of the assembly were made as it was considered that these were insignificant when compared to the mass of the carriage and the overall performance of the system was the important factor.

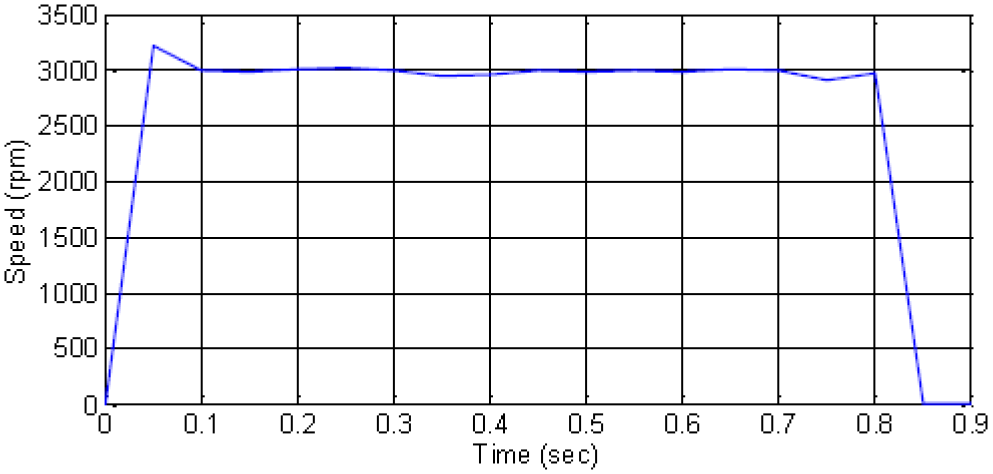

Figure 5-18 - Speed-Time Graph for Feed Motor

Figure 5-18 shows that the system accelerated from stationary conditions in approximately 50ms to a speed of 3000rpm, which equates to a traverse speed of the table of 500mms^{-1} and an acceleration of 10000mms^{-2}. The distance that the system has to accelerate in before the knives will make contact with the timber is 90mm. Using equations of motion

$$v^2 = u^2 + 2as \qquad (5\text{-}7)$$

$$s = 12.5mm$$

This is clearly well within acceptable as the actual distance required is significantly less than the available distance.

5.6.2 Cutterhead Vibration Tests

In order to ascertain whether the new cutterheads were likely to cause large unwanted vibrations another test was carried out. It should be noted that the cutterheads have tapped holes around the diameter in order to deliberately bolt out of balance masses to achieve deliberate out of balance forces when rotating at speed. The processed signals from the eddy current probes were plotted against time with the cutterhead rotating at 3000rpm and the signal sampled at 10KHz, Figure 5-19

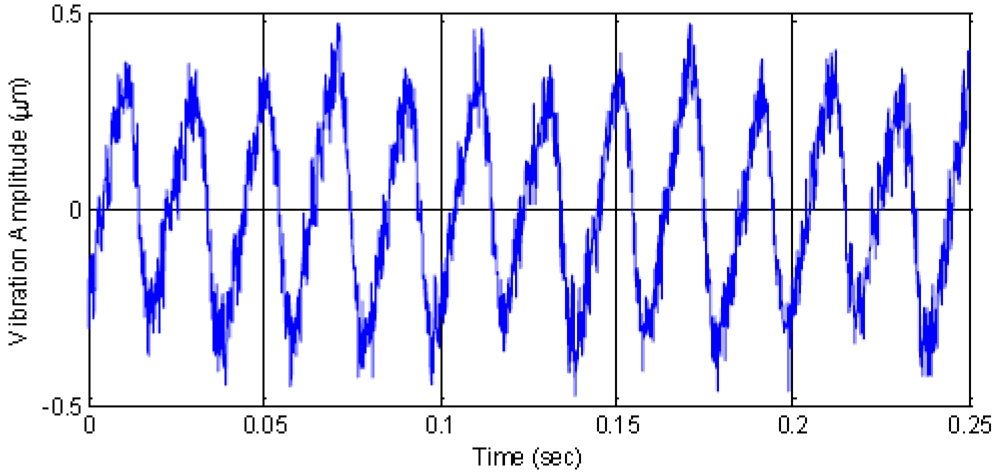

Figure 5-19 - Spindle Vibration Test at 3000rpm

The spindle vertical displacement at this speed, 3000rpm, is approximately 0.4µm, which is again satisfactory as the value is well within the limits of both the measurement system and the repeatability of the apparatus. The test was repeated at different speeds both with and without the cutterhead bolted to the spindle, Table 5-6.

Table 5-6 - Spindle Vibration Amplitude due to Imbalance

Speed (rpm)	Displacement Amplitude, Spindle only (µm)	Displacement Amplitude, Spindle and Cutterhead (µm)
600	0.31	0.31
1000	0.32	0.33
1500	0.35	0.36
2000	0.36	0.37
3000	0.38	0.39
4000	0.41	0.42

6 Chapter 6 – Model Based Tuning

This chapter describes the new inner control architecture, Figure 1-9, employed with the small scale planer and adaptive techniques used to select the various tuning parameters used within the hybrid controller. The effect of the different parameters on system performance is also shown in graphical form, and an overview of the capabilities of the adaptive techniques employed with differing network sizes and shapes. Lastly the effects of different dataset sizes is also investigated.

6.1 Inner Control Architecture

The inner 'tighter' control structure, driving the cutterhead to the required position to overcome cutterhead inaccuracies and out of balance forces, is shown in Figure 6-1. This has been designed by other members of this research group but is shown here for completeness as well as brief explanation of its operation.

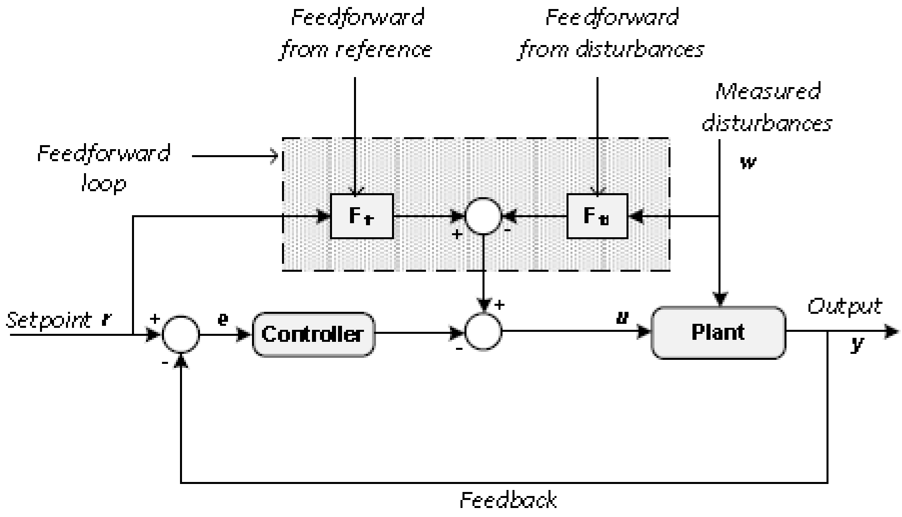

Feedforward from reference
Feedforward from disturbances
Measured disturbances
w
Feedforward loop
F_r
F_u
+
-
+
Setpoint r
+
-
e
Controller
-
u
Plant
Output
y
Feedback

Figure 6-1- Inner Control System Using both Feedforward and Feedback Control (Ogun, Jackson et al. 2012, Ogun 2012)

At the core of the control system is a Linear Quadratic Gaussian, LQG, tracking controller with setpoint action. Although this type of controller design is normally used to drive the output of the system to zero, within this application it has been modified for tracking a reference signal. (Elmas 2008) proposed and implemented an LQG controller on the small scale planer to operate as an active vibration controller. This LQG controller was operated in the more conventional manner whereby the vertical position of the spindle was driven to a reference path, the zero position.

Due to the digital nature of the control computer used within this research and the discrete nature of both the eddy current sensors and the applied voltage to the piezo electric actuators, state based models of the plant are obtained through system identification.

A time invariant system can be described through state based equations;

$$\dot{x}\,(k) = Ax(k) + Bu(k) \tag{6-1a}$$

$$y(k) = Ax(k) \tag{6.1b}$$

Where:

x is the state vector $[x_1,x_2,\ldots x_n]$

y is the output vector $[y_1,y_2,\ldots y_n]$

u is the input vector $[u_1,u_2,\ldots u_n]$

A is the state matrix (n by n)

B is the output matrix (n by p)

(YOUNG, WILLEMS 1972) describe an increase in performance if the control law also applies both the nominal state law and the integral of the error between the reference and the actual output. To implement this, the actual vertical position of the spindle, y(k), is compared to the reference signal, γ(k) and the error integrated. The output of this integration is in the following form:

$$i(k) = \sum_{k=0}^{N} \gamma(k) - y(k) = \sum_{k=0}^{N} \gamma(k) - Cx(k) \tag{6-2}$$

The augmented state vector $\hat{x}$ is given as follows:

$$\hat{x}(k) = \begin{bmatrix} x(k) \\ i(k) \end{bmatrix} \tag{6-3}$$

The state equation for the augmented system is given as follows: (YOUNG, WILLEMS 1972):

$$\hat{x}(k+1) = \underbrace{\begin{bmatrix} A & 0 \\ -C & 0 \end{bmatrix}}_{\hat{A}} \hat{x}(k) + \underbrace{\begin{bmatrix} B \\ 0 \end{bmatrix}}_{\hat{B}} u(k) \tag{6-4a}$$

$$y(k) = \underbrace{\begin{bmatrix} C & 0 \end{bmatrix}}_{\hat{C}} \hat{x}(k) \tag{6.4b}$$

An optimal control law that includes feedback of both the nominal state variables and the added state variables is as follows:

$$u(k) = -K\hat{x}(k) = K\begin{bmatrix} x(k) \\ i(k) \end{bmatrix} \tag{6-5}$$

The gain K is calculated such that the objective function, (6-6) , is minimised. This objective function is a compromise between tracking performance and control effort.

$$J(0,N) = \sum_{k=0}^{N} \hat{x}^T\,(K).Q.\hat{x}(k) + u^T(k).R.u(k) \tag{6-6}$$

Where:

$\hat{x}^T$ is the transpose of the augmented state vector

u^T is the transpose of the input vector

Q is a square, symmetric matrix called the state weighing matrix

R is a square, symmetric matrix called the cost matrix

The augmented state feedback gain matrix K is calculated from:

$$K = R^{-1}B^T M_0 \tag{6-7}$$

M is the solution to an algebraic the Riccati equation

$$0 = A^T M_0 + M_0 A - M_0 B R^{-1} B^T M_0 + Q \tag{6-8}$$

The final control law including the reference signal is as follows:

$$u(k) = -[K_x \quad K_i]\begin{bmatrix} x(k) \\ i(k) \end{bmatrix} + K_\gamma \gamma(k) \tag{6-9}$$

$$u(k) = -K_x x(k) - K_i i(k) + K_\gamma \gamma(k) \tag{6-10}$$

Where:

K_x is the nominal state feedback gain

K_i is the steady state error integral gain

K_γ is the reference signal feedforward gain

6.2 System Identification

The LQG tracker employed requires the system be represented in a linear time-invariant state form. The state based form represents the relationships between inputs and outputs and the state variables of the system as a set of first order or difference equations.

Previous work carried out by (Elmas 2008, Hynek 2004) both developed separate models of the spindle unit using finite element analysis modelling, and a linear model of the actuator systems, including the driver and the actuator. These two models were then combined to form the state based model of the system. To overcome issues with unknown specifications, such as accurate stiffness and capacitance of the actuators and driving amplifier output impedance, (Ogun 2012) extended these principals and used system identification to generate the state based system model, using MATLAB system identification toolbox.

The principal of system identification is to generate the state based model from measured data, without any prior knowledge of the actual system. This overcomes the issues of unknown system characteristics, such as assembly stiffness, and any governing mathematical relationships. This generates a ‘black box’ model of the system, which represents the system only as far as the input output data. The actual mathematical representations inside this model may not bare resemblance to the system modules themselves.

In order to generate a suitable model three main steps are carried out:

- Recording the system response to an input signal
- Estimation of the state input and output matrices of the model
- Evaluation of the estimated model

A general state space representation of a linear is system is as follows:

$$\dot{x}(t) = A(t)x(t) + B(t)u(t) \tag{6-11a}$$

$$y(t) = C(t)x(t) + D(t)u(t) \tag{6.11b}$$

System identification is used to estimate the values of A, B, C and D. These matrices can then be used within the LQG controller as described in section 6.1.

6.3 Input-Output Data

In order to collect the input-output data a linear sine sweep is used. This allows the various resonate frequencies of the structure to be tested. This input-output data provides information about the natural frequencies and damping co-efficients of the assembly which may also be useful when considering various machining aspects, such as cutting speeds.

The frequency of the sine sweep has a maximum value of 1KHz due to limited bandwidth of the piezo amplifiers. (Elmas 2008) carried out testing and determined the maximum frequency of the amplifiers to be 1424Kz at 3Db. At higher frequencies the author reported large roll off. The newly increased specification of the small scale planer requires a maximum cutting speed of 6000rpm, which equates to 100Hz, with a four knife cutter the maximum required frequency is equal to 400Hz which is well within the limits of the piezo amplifiers available operating range.

(Ogun 2012) reported that a change of rate of frequency used of 0.5Khzs^{-1} gave a reasonable trade-off between accuracy and subjection of the actuators to potentially harmful levels of vibration, so this rate of change of frequency has been used here also.

The output data was recorded using the eddy current probes mounted within the spindle unit, Figure 5-13. These signals were recorded at a sampling frequency of 1KHz, as were the input signals. Each test lasted six seconds, thereby repeating the vibration input three times. During all tests the spindle unit was stationary, (Lauffer, Regelbrugge et al. 1998) reports that the non-rotating cutterhead will not have a significant effect on the influence of the system dynamics.

The effect of different masses of the cutterhead was also investigated. In order to introduce out of balance forces the cutterheads were designed such that masses could be bolted around the circumference of the cutterhead. These masses would then introduce sinusoidal forces as the cutterhead rotates. In order to achieve the same displacement of the cutterhead at differing speeds different masses are required, Figure 6-2.

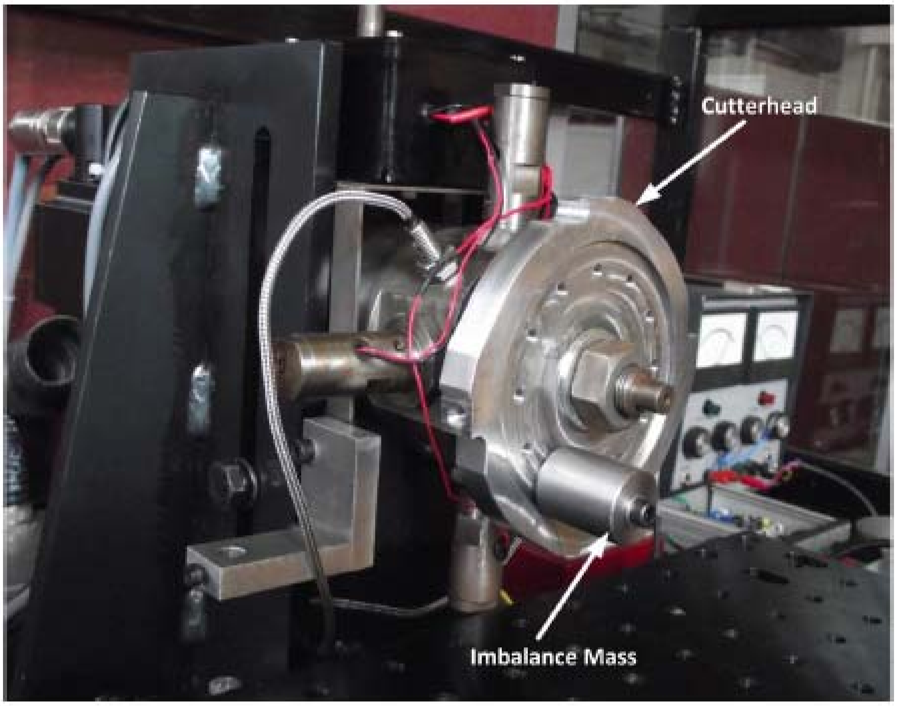
Cutterhead
Imbalance Mass

Figure 6-2 - Imbalance Mass attached to the Cutterhead

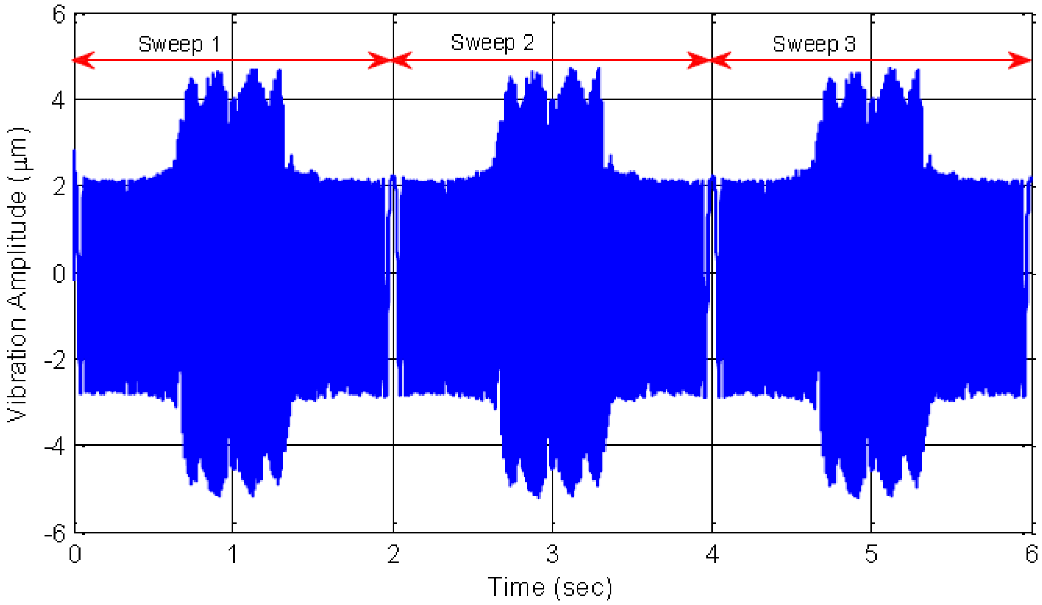

Figure 6-3- Time Domain Response - 106g Cutterhead

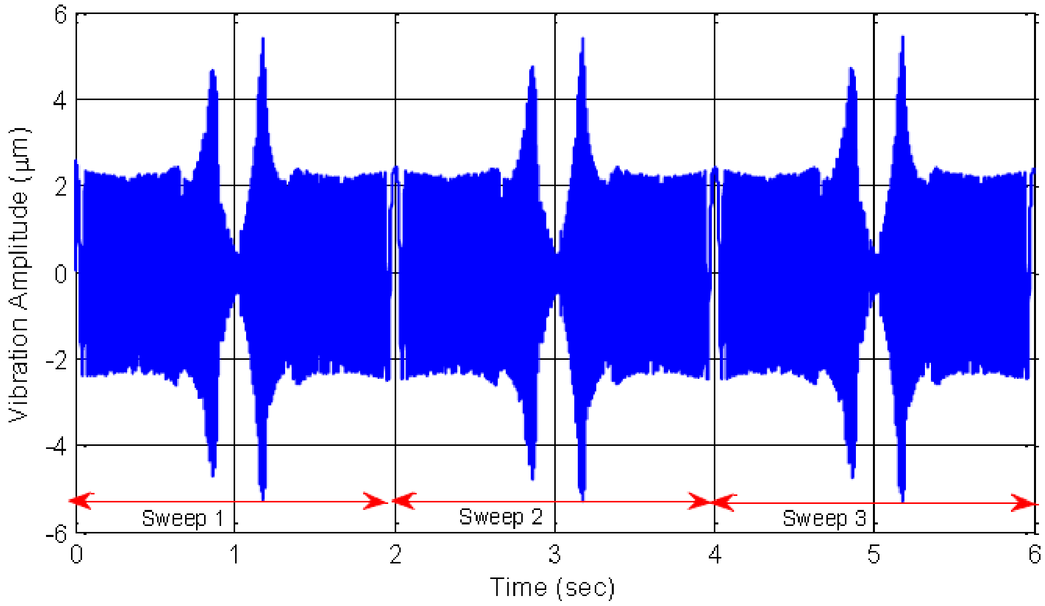

Figure 6-4 - Time Domain Response - 190g Cutterhead

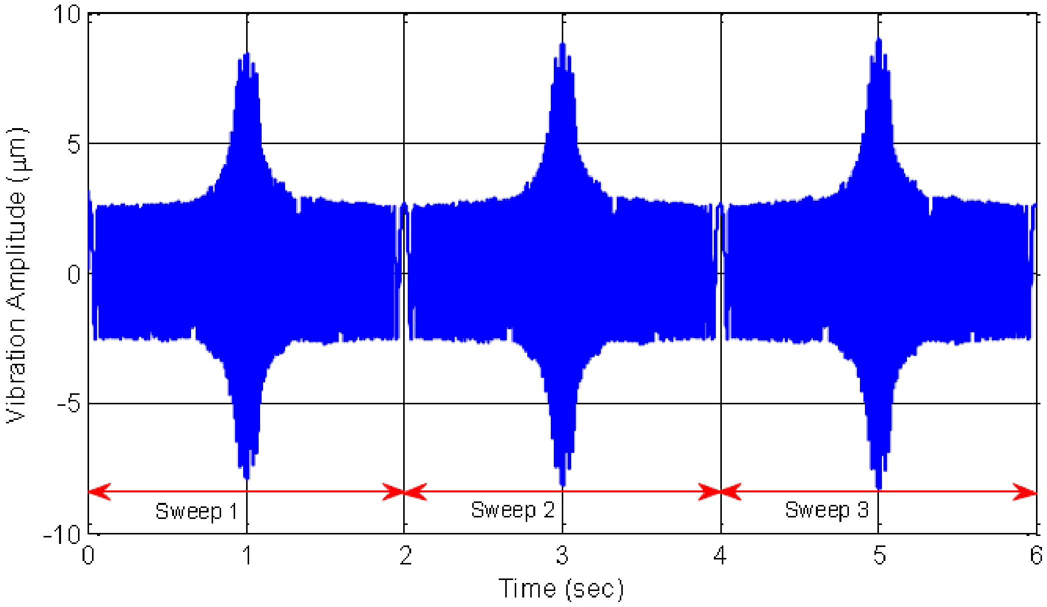

Figure 6-5 - Time Domain Response - 293g Cutterhead

The above figures, Figure 6-3, Figure 6-4 and Figure 6-5, show the dramatic effect the differing cutterhead masses have on the response to a similar sine sweep input, with all other components remaining the same. These differing responses highlight the advantages of using the system identification technique over the previously employed finite element analysis technique. If the system is modified it is a quick test re-run to estimate the state-space model rather than the more laborious previously employed techniques. These changes are not limited to the small scale planer itself but also the supporting hardware such as the piezo amplifiers and actuators.

6.4 State Based Model Parameter Estimation

In order to estimate the state based model parameters used within the LQG controller, as stated in section 6.2, the MATLAB System Identification Toolbox is used. The toolbox uses the prediction-error minimisation, PEM, algorithm to estimate the model matrices from the input output data, using the following objective function:

$$V = \frac{1}{N}\sum_{t=1}^{N}\frac{1}{2}e^{2}(t) \tag{6-12}$$

Where:

e(t) is the difference between the measured output and the predicted output of the model

N is the number of samples

Mathworks, the provider of MATLAB, report that the accuracy of the estimated model depends on the number of data samples and becomes more accurate with increased numbers of data samples, therefore the increased number of data samples through sweeping the system three times should give an increase in estimated model accuracy.

However, the parameter with the largest effect on the estimated model accuracy is the order of the model. The model order needs to be capable of fully capturing the dynamics of the small scale planer. In order to ascertain the accuracy of the model the input data is split into two, half being used to generate the model estimate and the second half being used to validate this model. In order to validate the model, the second half of the input data is fed into the estimated model and compared to the original output data.

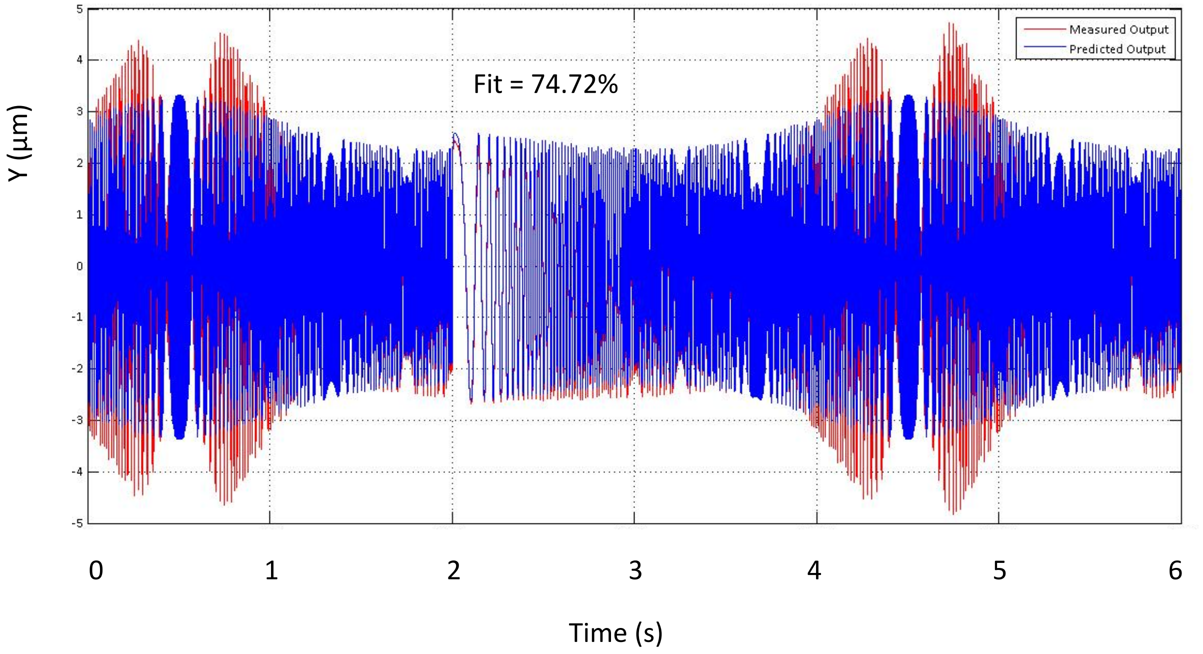

Figure 6-6- Measured and Predicted Outputs for Second Order Model

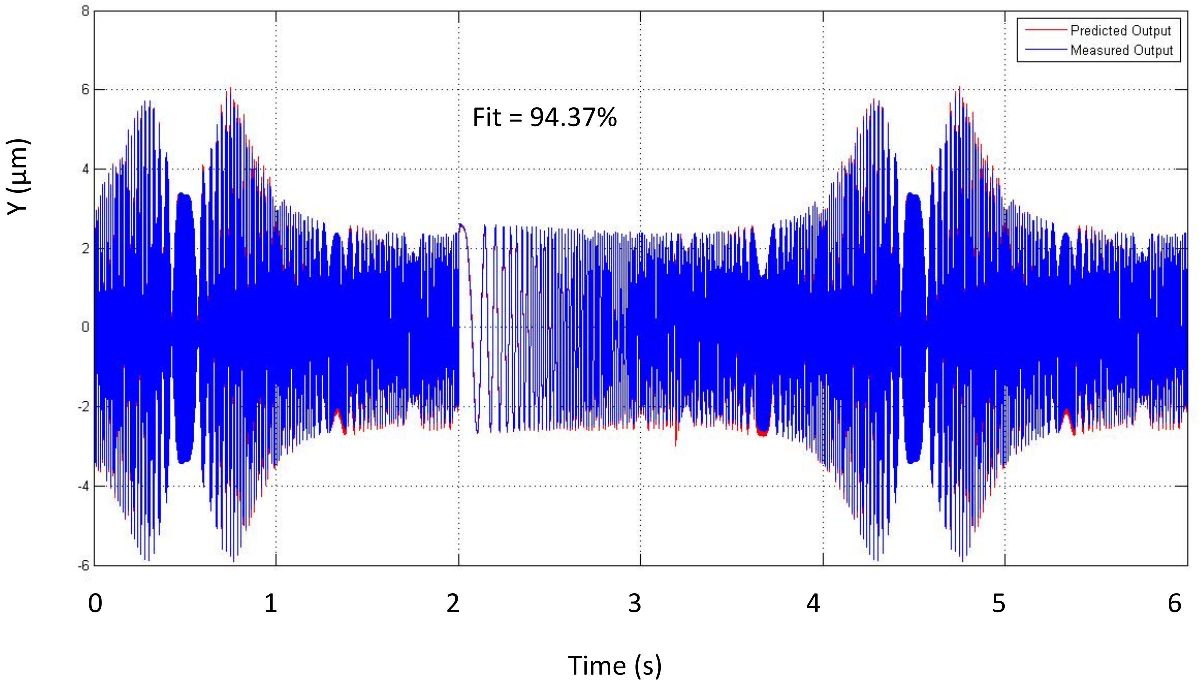

Figure 6-7 - Measured and Predicted Outputs for Fourth Order Model

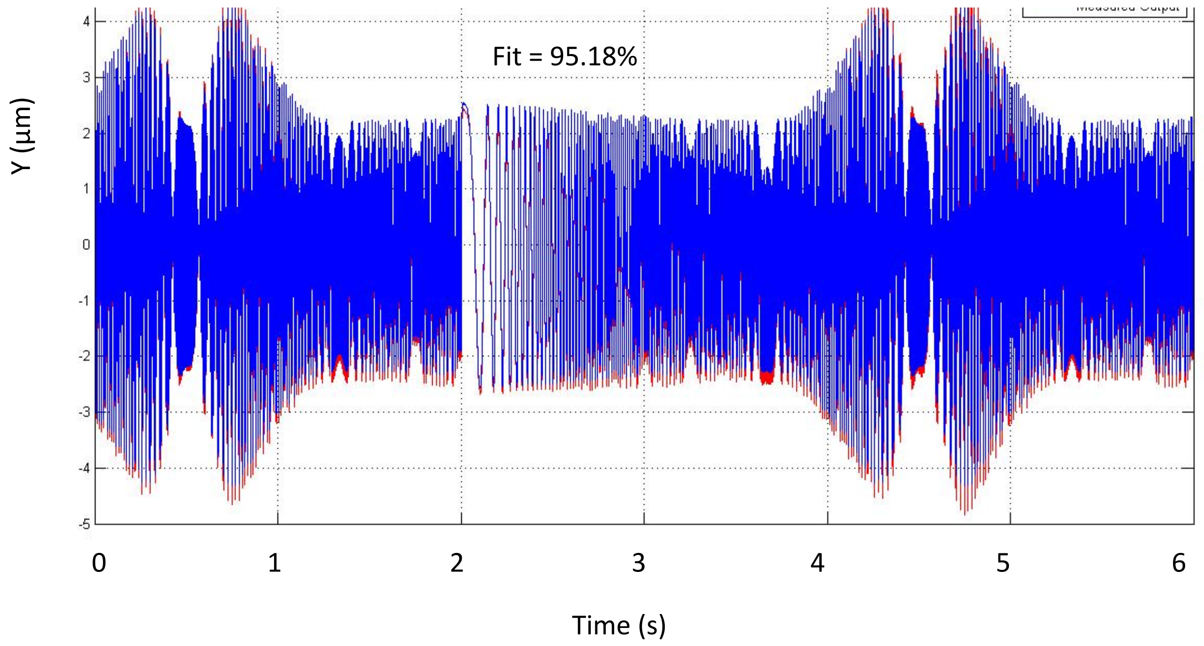

Figure 6-8 - Measured and Predicted Outputs for Sixth Order Model

Figures,

Figure 6-6, Figure 6-7 and

Figure 6-8 shows the increased correlation between the measured data and the model estimated output with an increase in model order. However the increase in accuracy is far reduced when going from a model order of four to six rather than from two to four. Above a model order of six the increase in estimated model performance is reduced even further and becomes negligible. A fourth order model has been selected to balance the requirements of system accuracy and computational requirements. With every increase in model order the computational requirements increase significantly, so the advantages with minimal accuracy improvements are offset by the dramatic increase in computing overhead required. If the model order chosen is not sufficiently accurate, the synthesized model may radically fail to describe the actual system behaviour, (Sjövall, Abrahamsson 2007). Within this experimentation a computer with 2GB of RAM running a 2GHz Pentium processor was successfully used with a fourth order model generated as described above.

6.5 LQG Controller Parameter Tuning

Since the LQG controller provides a trade-off between optimal tracking, Q, and the minimisation of the control force, R, it is the ratio between these matrices that is important rather than the actual values. However there are conditions for the existence of a solution to the Riccati equation, the matrix Q must be symmetric and positive semi-definite where R must be symmetric and positive definite. To satisfy both of the requirements the matrices can both be said to be the result of a scalar multiplication with the identity matrix;

$$Q = Q_a \times I \qquad (6\text{-}13)$$

$$R = R_a \times I$$

This allows the value of R_a to be fixed and the value of Q_a to be tuned to achieve optimal control. Within the controller there is also a feedback gain, k_{ff}, which has a very strong influence on the system performance. A Simulink model of the setpoint tracker can be found in Section 12.1.

The values of R_a, Q_a and k_{ff} can be tuned using an iterative gradient descent method each time the system is powered up. In a factory situation this may be at the start of the day. Gradient descent attempts to find the local minimum of the gradient of the objective function, in order to find the solution. However this can take valuable time away from the process of machining timber if using a variable learning rate, whereas using a fixed learning rate can yield poor results. An intelligent system may be implemented here to yield a potential benefit.

This leads to the implementation of either a single or multiple intelligent systems, thereby perhaps generating a form of validation of the result, where one system can validate the other. This is not however totally infallible as if a certain set of conditions ‘corrupt’ all of the intelligent systems involved the validation may be lost. However to generate these systems a certain amount of a-priori knowledge needs to be generated in order to train and test the systems, using the real plant.

6.6 System Tracking Performance

In order to understand the effect the different parameters have on the system tracking performance at different operating conditions a number of system tests were carried out. The following plots show the effect of altering a single controller parameter by plotting both the desired and actual vertical position of the cutterhead throughout a number of full rotations, whilst not machining timber. The performance is a measure of the output signal accuracy to that of the reference signal, where a larger distance between the two profiles corresponds to a larger error and therefore a lower system performance. It is important to note that due to the non-continuous cutting regime, due to the discrete nature of the cutting knives, the performance of the system is a measure of the accuracy of the displacement only during the cutting period for each knife. For the remaining duration of the revolution the position of the cutting head is less important, although a large displacement may lead to errors for the subsequent pulses.

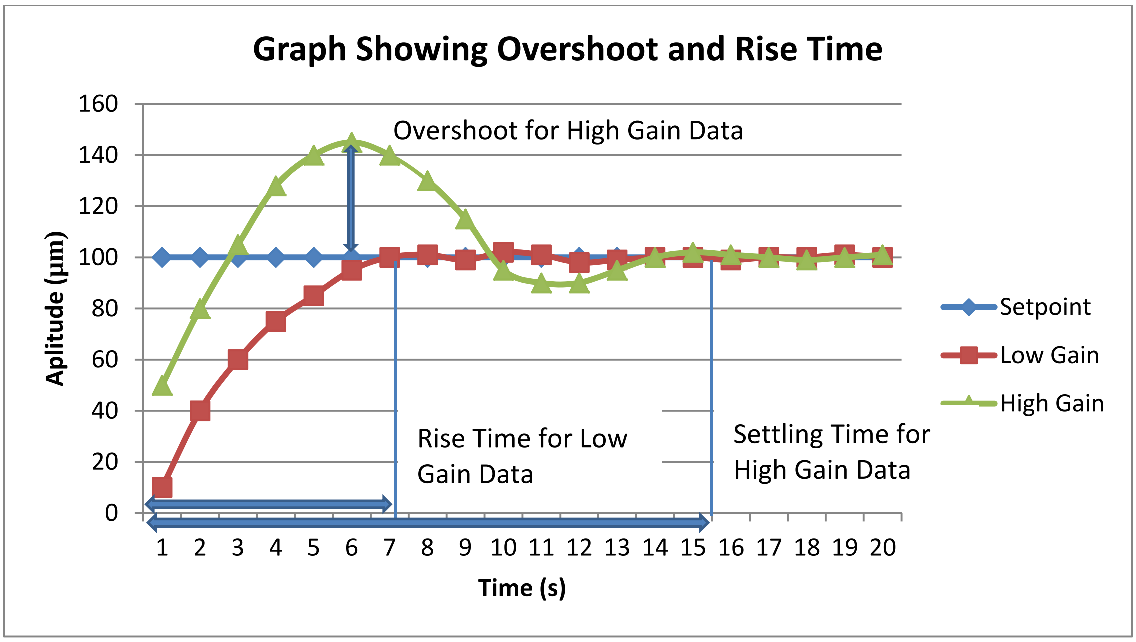

Figure 6-9 - Graph Showing Overshoot, Settling Time and Rise Time Examples

Figure 6-9 graphically shows the definition of the terms overshoot, settling time and rise time used here. Overshoot being the level to which the controller overshoots the set point position, settling time being the time taken by the controller to settle at the set point and rise time to time taken by the controller to reach the set point within 5% of the set point position.

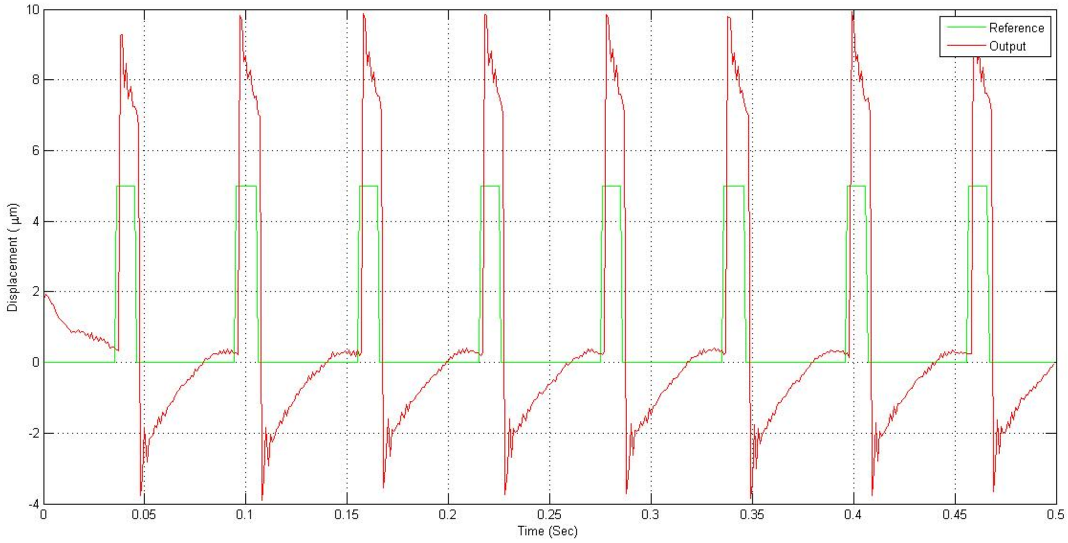

Figure 6-10 - Measured vs Desired Cutterhead Positions, TIR 0.005m, 1000rpm, High Feedback Gain (K_{ff} = 15)

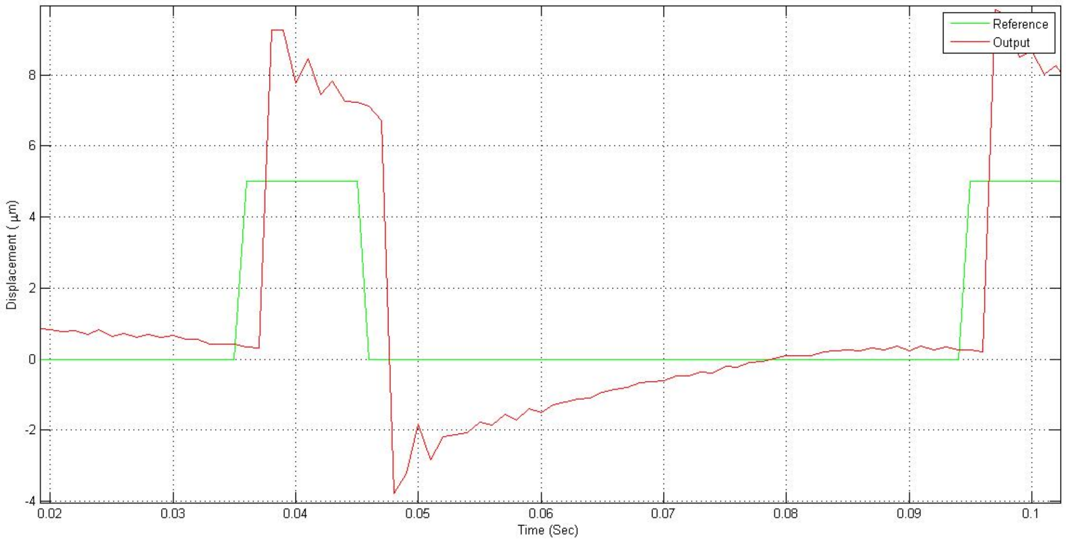

Figure 6-11 - Measured vs Desired Cutterhead Positions, TIR 0.005m, 1000rpm, High Feedback Gain (K_{ff} = 15) Zoomed

Figure 6-10 and Figure 6-11 show the effect of a high feed forward gain, k_{ff} = 15, on the system tracking performance. It can be seen that there is a high level of overshoot of the actual vertical spindle position relative to the reference position. However the system has a fast response to the step input due to this high level of gain. The apparent lag of the system from the step input is caused by the processing time of the computers and associated electronics. This was measured at a constant 2ms.

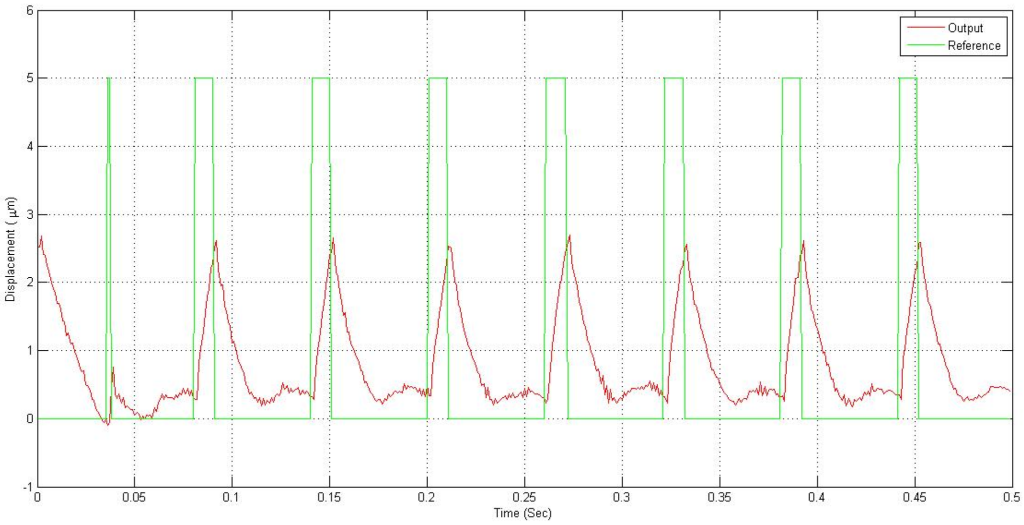

Figure 6-12 - Measured vs Desired Cutterhead Positions, TIR 0.005m, 1000rpm, Low Feedback Gain (K_{ff} = 1)

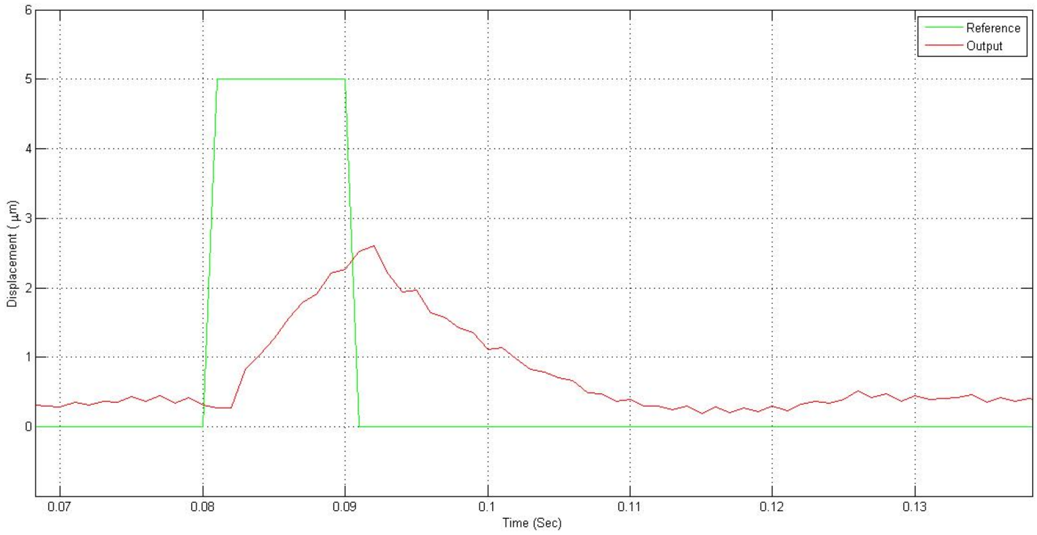

Figure 6-13 - Measured vs Desired Cutterhead Positions, TIR 0.005m, 1000rpm, Low Feedback Gain (K_{ff} = 1), Zoomed

Figure 6-12 and Figure 6-13 show the effect of a low feed forward gain , k_{ff} = 1, on the system tracking performance. It can be seen that the rise time is quite large and the vertical position of the spindle does not reach the desired reference position.

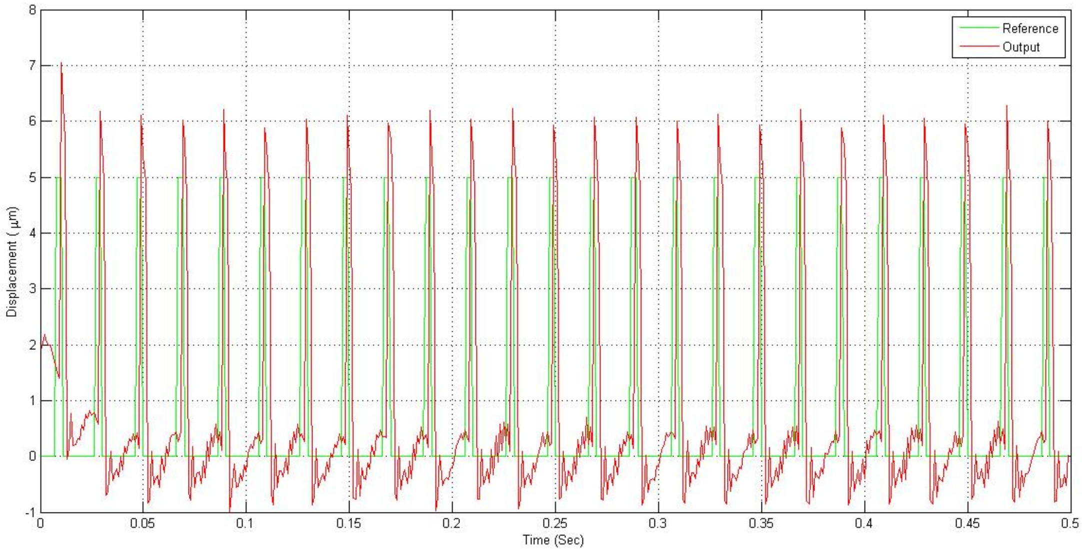

Figure 6-14 - Measured vs Desired Cutterhead Positions, TIR 0.005m, 3000rpm, Poorly Tuned

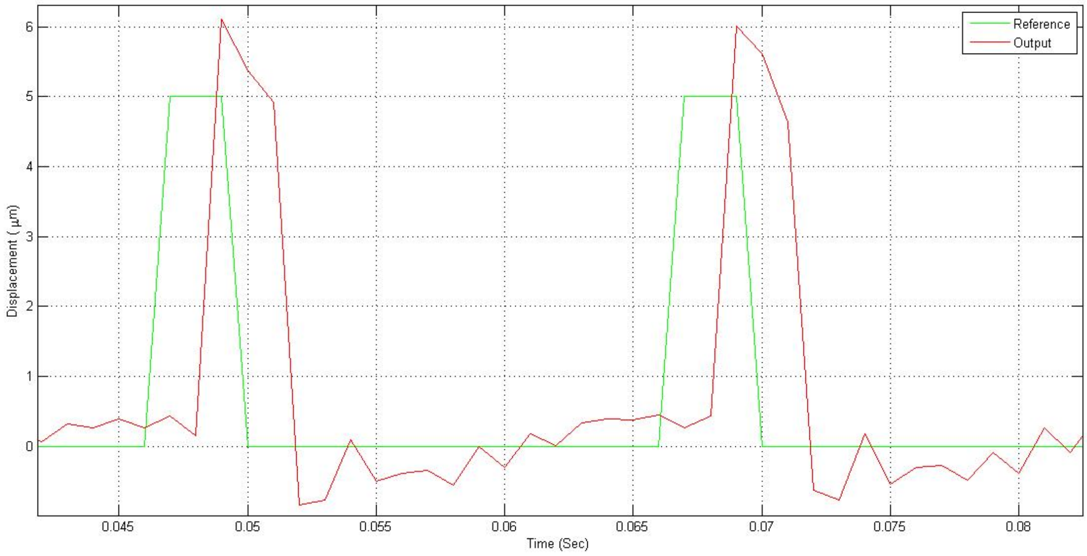

Figure 6-15 - Measured vs Desired Cutterhead Positions, TIR 0.005m, 3000rpm, Poorly Tuned, Zoomed

Figure 6-14 and Figure 6-15 show the effect of a poorly tuned LQG controller on the vertical position of the spindle. The tuning parameters deployed when obtaining this graph were a k_{ff} of 9.5 and a Q value of 57000. It can be seen that the system overshoot is circa 1 micron but that there is almost a negligible settling time. The settling time being very low is a positive quality for this set of control parameters, however the overshoot is not. The overshoot, although a very small actual value, when considering the effects this will have on the machined timber surface, is too large and therefore this set of parameters cannot be considered to produce an acceptable machine operation.

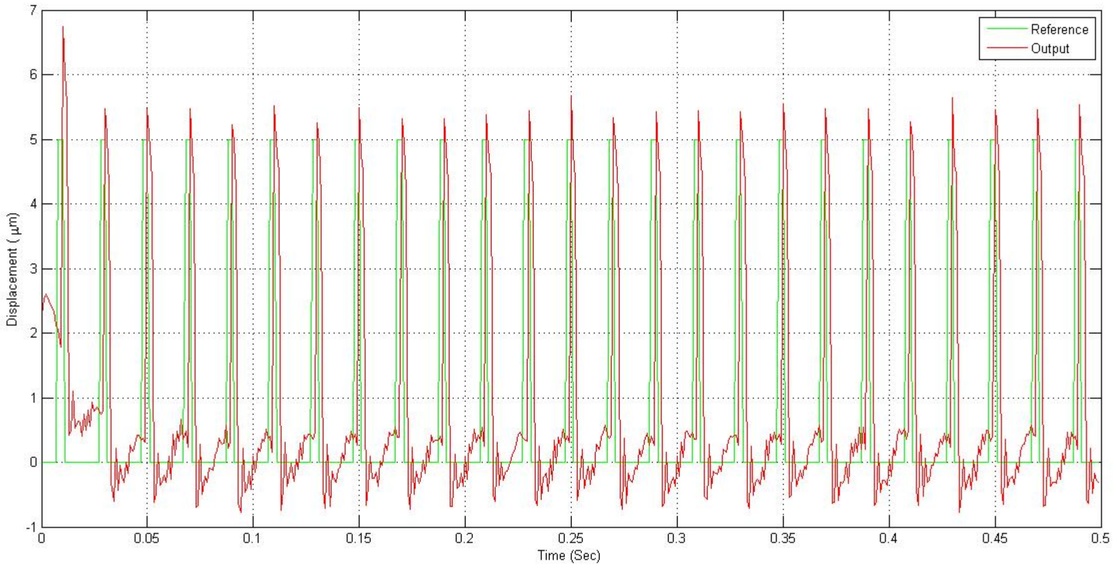

Figure 6-16 - Measured vs Desired Cutterhead Positions, TIR 0.005m, 3000rpm, Tuned

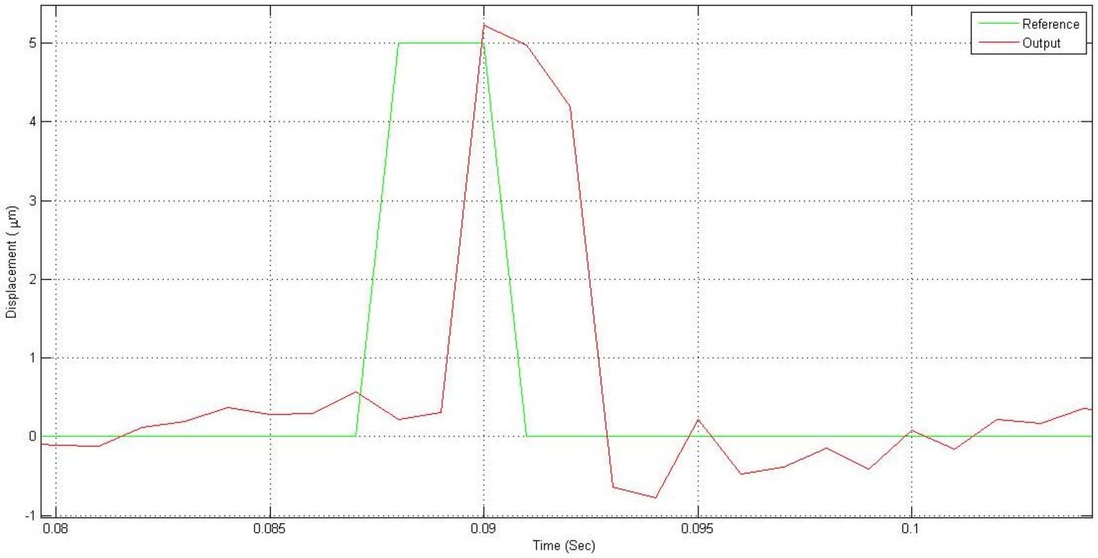

Figure 6-17 - Measured vs Desired Cutterhead Positions, TIR 0.005m, 3000rpm, Tuned, Zoomed

By altering the ratio of Q to R and the feed forward gain the performance of the tracker can be modified and improved, as shown in Figure 6-16 and Figure 6-17. The controller parameters deployed to obtain this improved system tracking performance were a k_{ff} value of 9.0 and a Q value of 59600.

6.6.1. An Adaptive Approach

Unfortunately the tuned values of both controller parameters, Q to R ratio and k_{ff}, change with both speed and required spindle displacement. A multi-input multi-output neural network has been implemented to generate the required values of Q and k_{ff} for the LQG controller to provide optimal tracking of the spindle to the reference path.

A set of input-output data is required to train the network. This data is generated through experience of machine capability, in terms of actuation speeds and forces, whilst at the same time producing a high quality surface finish. Using the internal model, generated though the system identification toolbox, un-tuned versions of both Q, R and k_{ff} are tuned to achieve optimal tracking performance. This data is then stored in the a-priori knowledge base. The operating conditions are then changed and the process repeated.

6.6.2 Data Generation

In order to achieve optimal tracking of the reference signal, optimal tracking, when discussed within this thesis, needs to be defined. The three attributes used here to ascertain the quality of the tuned controller are the rise-time of the spindle, the overshoot of the spindle and the settling time of the spindle to the input reference pulse signal. Arbitrary magnitudes, based on experience with the rotary wood planing test rig have been selected. Table 6-1 states these characteristics used here to designate optimal control.

It must be stated that in most cases not all of these characteristics were able to be consistently achieved for every reference signal pulse on every revolution of the cutterhead. These discrepancies between revolutions, or perhaps the inability to achieve a certain attribute on any revolution of the cutterhead, may be real, or may be artificially created by the resolution of the sampling time of the vertical measurements for the spindle displacement. At higher speeds the sampling frequency was not increased, as this is not possible with the current equipment, and so higher frequencies of the spindle displacement may have been lost. This would be particularly relevant to the rise time of the cutterhead not accurately being measured and being extended by potentially the sampling time period.

Table 6-1 - Optimal Control Characteristics

Rise Time	<0.002 seconds
Settling Time	<0.05 seconds
Overshoot	<0.5µm

Figure 6-18 shows a flowchart of how the training data was generated. This was a purely manual technique and based heavily on user experience, in a similar fashion to tuning a PID controller, (Åström, Hägglund 2004). The data generated also has encoded within, although not directly accessible, machine characteristics as well as operating conditions.

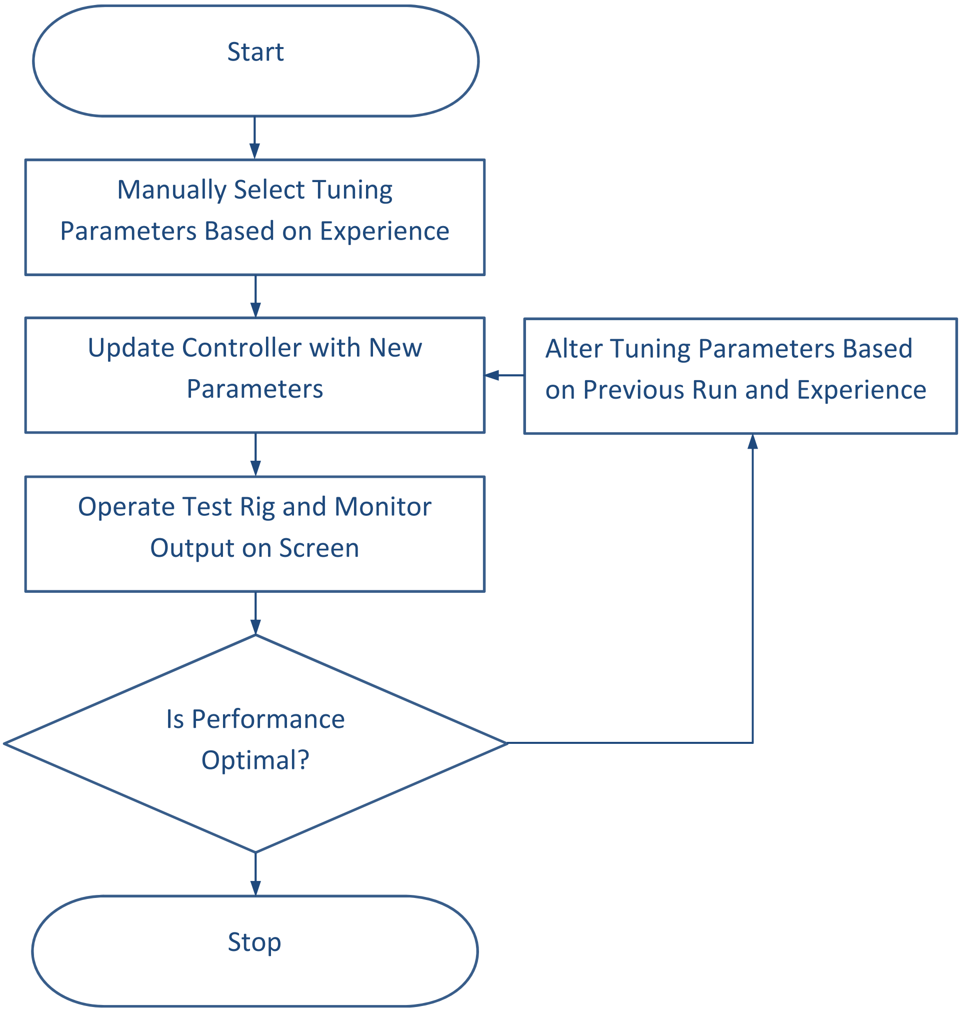
Start
Manually Select Tuning Parameters Based on Experience
Update Controller with New Parameters
Alter Tuning Parameters Based on Previous Run and Experience
Operate Test Rig and Monitor Output on Screen
Is Performance Optimal?
Stop

Figure 6-18 - Manual Parameter Generation for Optimal Control

6.6.3 Network Training

A single, multi-input multi-output neural network has been trained and implemented to generate the LQG controller parameters. Four different networks were tested to ascertain which network features would provide a more improved parameter generation performance. There are two different size data sets that have been used to train two different size neural networks.

The networks were all trained within the MATLAB neural network toolbox using a gradient descent back propagation method. The gradient descent method updates the network weights and biases in the direction in which the performance function decreases most rapidly, the negative of the gradient. The performance function used to train all the networks was the mean squared error. This has been selected as it is a commonly implemented performance function and is the default function used within MATLAB, (Wilson, Martinez 2003, Nakama 2009). The mean squared error is calculated as follows;

$$F = mse = \frac{1}{N}\sum_{i=0}^{N}(e_i)^2 = \frac{1}{N}\sum_{i=0}^{N}(t_i - a_i)^2 \tag{6-14}$$

Where:

e_i is the error of the network

t_i is the target output

a_i is the network output

The gradient descent methods works to minimise the performance function, mean squared error. An iteration of this function can be written as;

$$x_{k+1} = x_k - \alpha_k g_k \qquad (6\text{-}15)$$

Where:

x_k is a vector of current weights and biases

g_k is the current gradient

α_k is the learning rate

The networks are trained until one of any of the below target is attained:

- The maximum number of training epochs is reached
- The maximum amount of time is exceeded
- The performance is minimised to the goal
- The performance gradient falls below a set target

6.7 Network Parameter Generation Performance

In order to ascertain the performance of each of the networks graphs have been created showing the original training data and the network generated parameter value. Figure 6-19, Figure 6-20, Figure 6-27 and Figure 6-28 show the performance of the smaller network with twenty hidden neurons, trained with the smaller data set. Figure 6-23, Figure 6-24, Figure 6-31 Figure 6-32 show the performance of the same size network, twenty hidden neurons, but trained with a larger data set, across the full operating range of the small scale planer both in terms of speed and TIR. Figure 6-21, Figure 6-22, Figure 6-29 Figure 6-30 show the performance of a larger network, fifty hidden neurons, but trained with the exact same smaller data set. Figure 6-25, Figure 6-26, Figure 6-33 Figure 6-34 show the performance of the larger network, fifty hidden neurons, but this time trained with the larger data set.

Table 6-2 gives the split of graphs generating the K_{ff} values.

Table 6-2 - K_{ff} Generation Network Figures

	Smaller Training Set (5 Entries)	Larger Training Set (21 Entries)
Smaller Network Size (20 Hidden Neurons)	Figure 6-19 Figure 6-20	Figure 6-23 Figure 6-24
Larger Network Size (50 Hidden Neurons)	Figure 6-21 Figure 6-22	Figure 6-25 Figure 6-26

Table 6-3 gives the split of graphs generating the Q values.

Table 6-3 - Q Generation Network Figures

	Smaller Training Set (5 Entries)	Larger Training Set (21 Entries)
Smaller Network Size (20 Hidden Neurons)	Figure 6-27 Figure 6-28	Figure 6-31 Figure 6-32
Larger Network Size (50 Hidden Neurons)	Figure 6-29 Figure 6-30	Figure 6-33 Figure 6-34

Table 6-4 - Different Network Sizes and Inputs

	Smaller Training Set (5 Entries)	Larger Training Set (21 Entries)
Smaller Network Size (20 Hidden Neurons)	Network A	Network C
Larger Network Size (50 Hidden Neurons)	Network B	Network D

Table 6-4 gives the different networks an arbitrary designation showing how each network is both providing a K_{ff} value and a Q value.

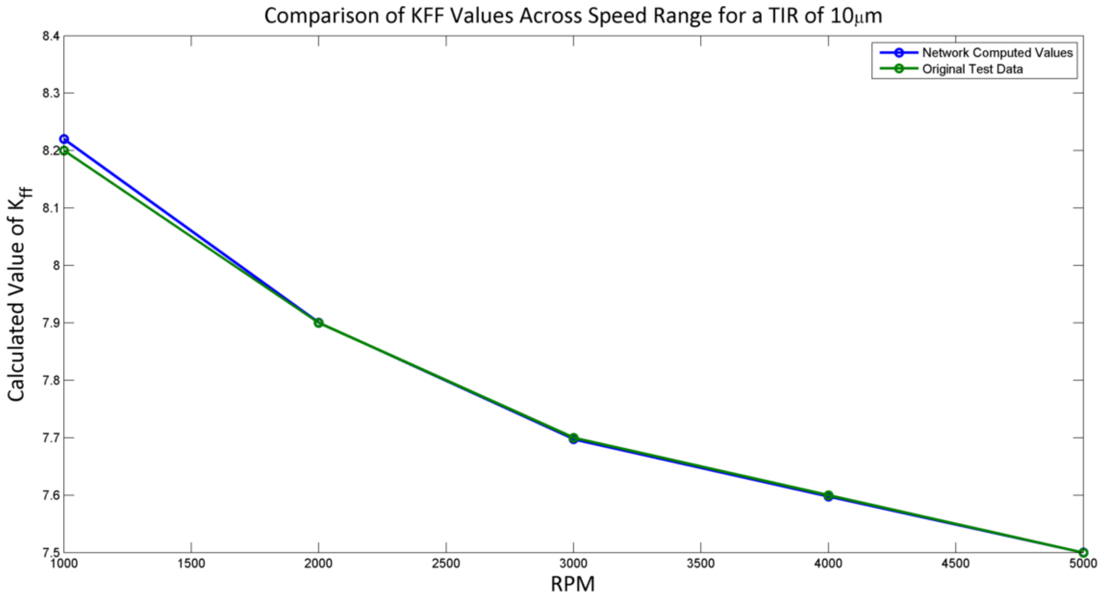

Figure 6-19 - Small Network (20 Hidden Nodes) K_{ff} Generation Performance using Smaller Data Set (5 Entries) for TIR of 10μm

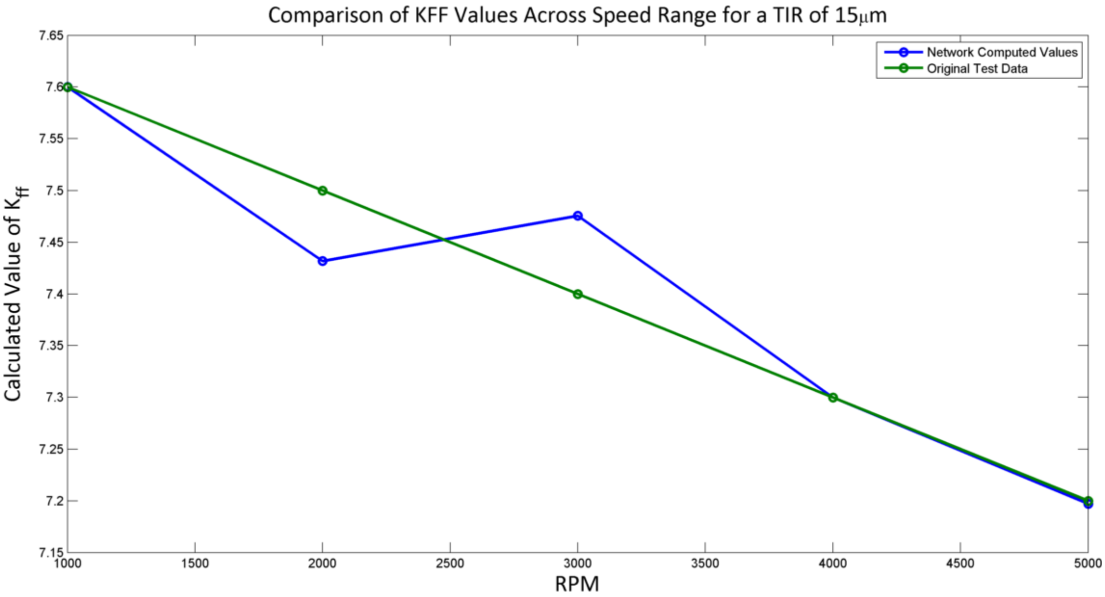

Figure 6-20 - Small Network (20 Hidden Nodes) K_{ff} Generation Performance using Smaller Data Set (5 Entries) for TIR of 15μm

Figure 6-19 and Figure 6-20 show the smaller network, network A, 20 internal hidden nodes, trained with the smaller data set, 5 different operating conditions each repeated 5 times, performance when considering K_{ff} generation across a range of operating speeds. It can be seen that for both a TIR value of 10µm and 15µm the general trend is for a decreasing k_{ff} value, and the network essentially follows this trend. The network performance for a TIR value of 10µm is quite good, the maximum error of 0.02 corresponds to a percentage error of the full range of 3%, whereas when considering the maximum error for a TIR value of 15µm the maximum error of 0.07 corresponds to a full range error of 17%.

Figure 6-19 shows not only a lower maximum error but also a more consistent accuracy in parameter generation than that of Figure 6-20 for the increase TIR value of 15µm over 10µm. It is hypothesized at this time that the oscillation seen in Figure 6-20 is caused by the very small training data set. However even with this small training data set the network is able to generate potentially useful parameters.

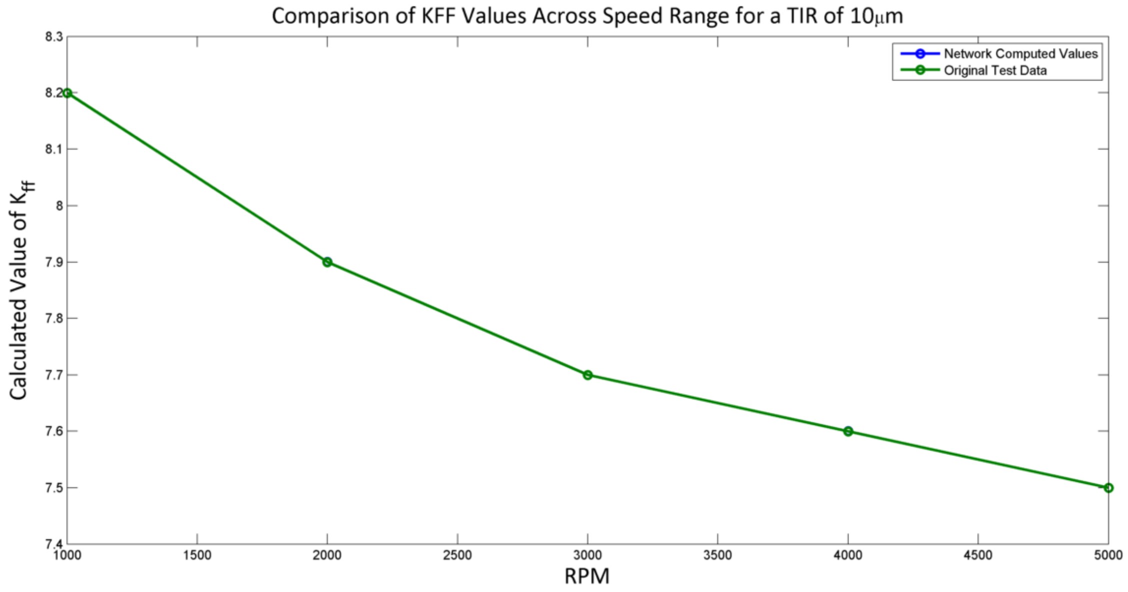

Figure 6-21 - Large Network (50 Hidden Nodes) K_{ff} Generation Performance using Smaller Data Set (5 Entries) for TIR of 10μm

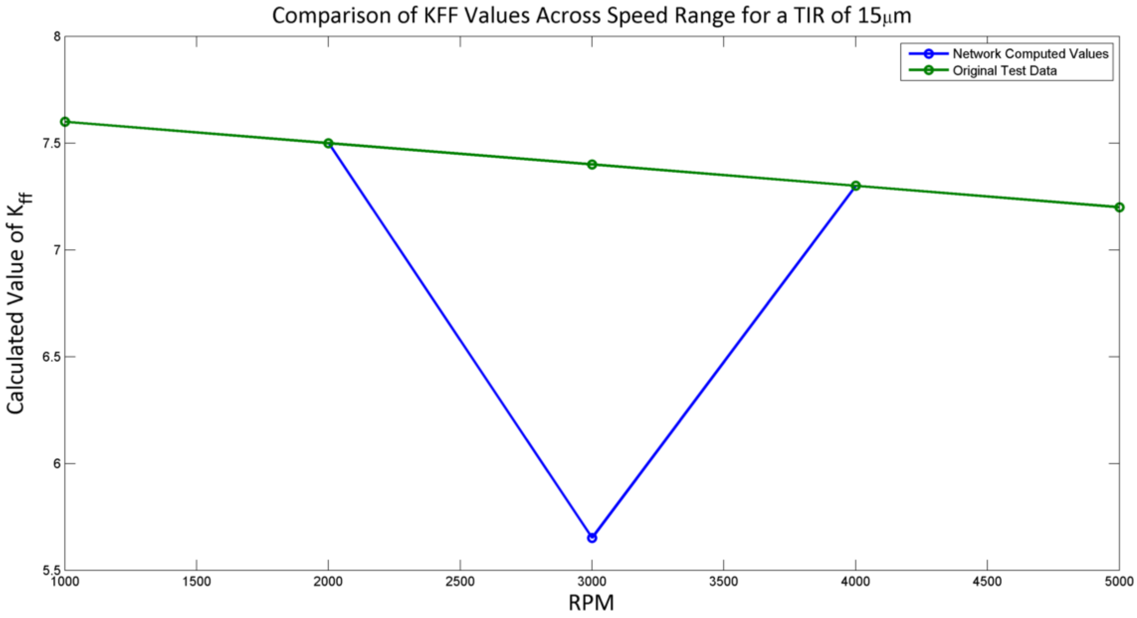

Figure 6-22 - Large Network (50 Hidden Nodes) K_{ff} Generation Performance using Smaller Data Set (5 Entries) for TIR of 15μm

Figure 6-21 and Figure 6-22 show the performance of the larger network, network B, 50 hidden neurons in the single hidden layer, when again trained with the smaller training data set, 5 data entries. Figure 6-21 shows the performance on the network for a TIR value of 10μm and Figure 6-22 for a TIR value of 15μm. Again the network fits the trend of decreasing k_{ff} value as the rotational speed of the cutterhead increases.

For a TIR value of 10μm the network has zero error and conforms to the training data set very well, as shown in Figure 6-21, however the performance for a TIR value of 15μm is considerably lower when considering the maximum error. The maximum error of 1.8 corresponds to an error when considering the range in the training data of 450%. However this anomaly only occurs in a single region of the parameter generation, circa 3000rpm of the cutterhead, and the remaining areas of parameter generation are producing acceptable results.

When comparing the results for the larger network and those for the smaller network it can be said, that for these particular input-output data sets the larger network has a generally higher performance that that of the smaller network, when trained with the very limited training data set.

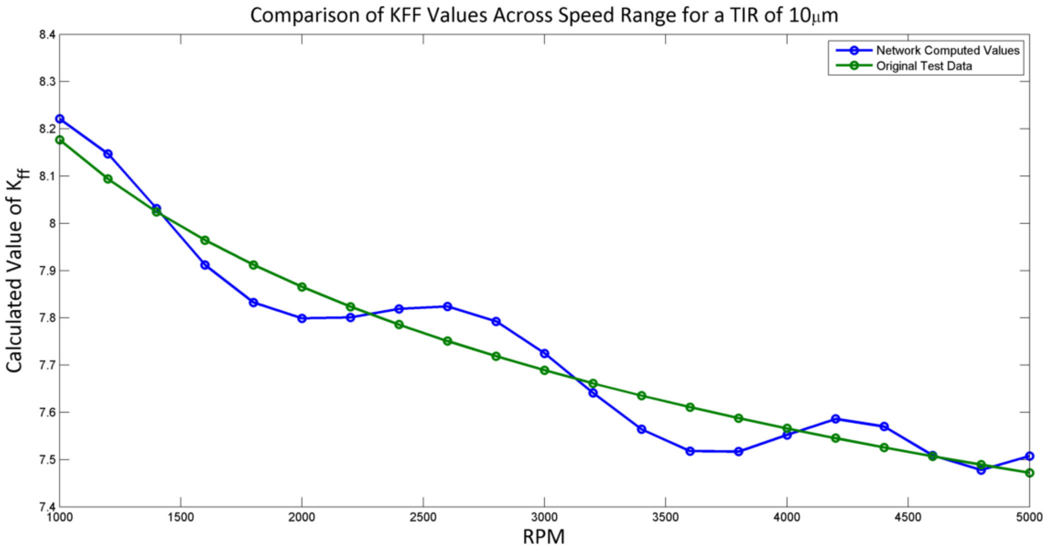

Figure 6-23 - Small Network (20 Hidden Nodes) K_{ff} Generation Performance using Larger Data Set (21 Entries) for TIR of 10µm

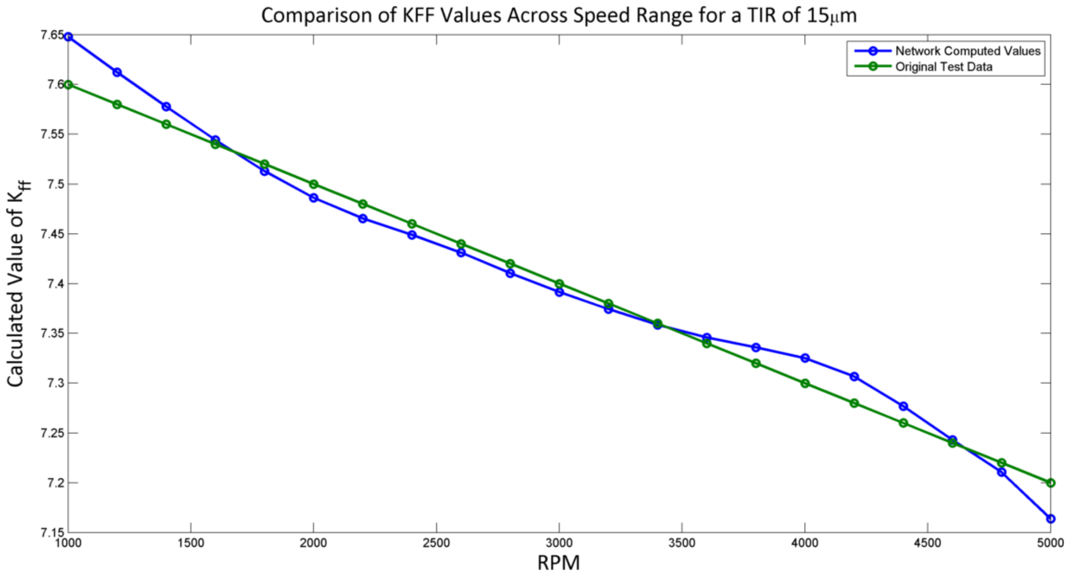

Figure 6-24 - Small Network (20 Hidden Nodes) K_{ff} Generation Performance using Larger Data Set (21 Entries) for TIR of 15µm

Figure 6-23 and Figure 6-24 show the network, network C, parameter generation performance for a smaller network, 20 hidden neurons in the single hidden layer, when trained with a larger, although still relatively small, training data set, 21 entries. Although for both TIR values, 10μm and 15μm, the general trend of the network matches that of the training data, the performance of the network has decreased with the larger training data set, when compared to the earlier results for the smaller training data set of 5 data entries.

For a TIR value of 10μm the maximum error of 0.095 corresponds to a range error of 13.5%, and for a TIR value of 15μm the maximum error of 0.05 corresponds to a range error of 12.5%. At this stage the oscillatory behaviour of the network, as shown in Figure 6-23 is not understood, although it may be due to the network having 5 hidden neurons and as the input data activates these more or less across the range the generation performance reduces, in a similar manner to fuzzy logic and the activation of the different membership functions.

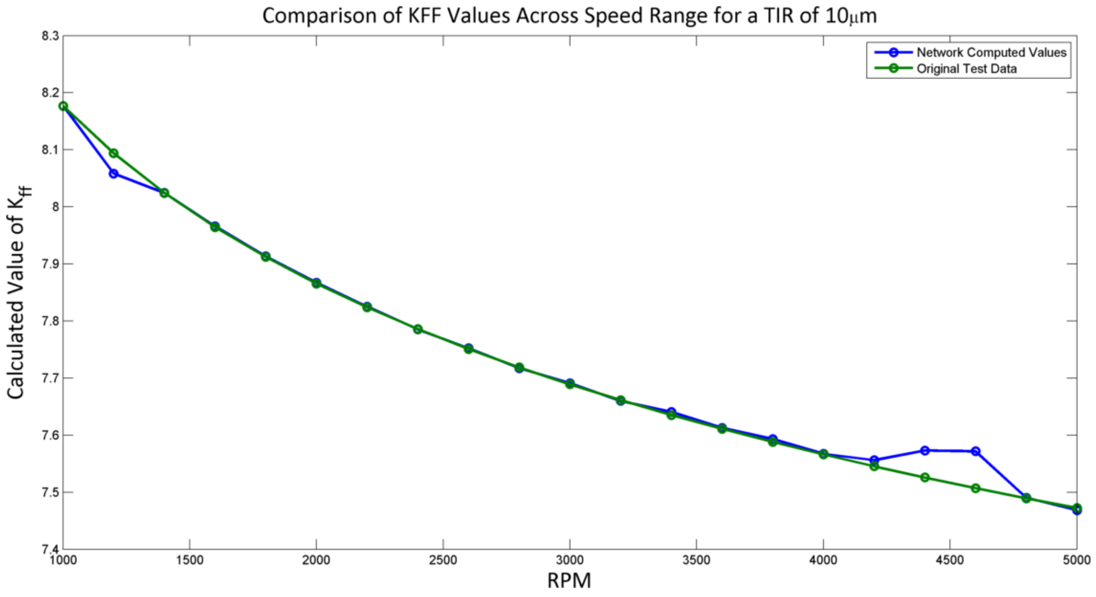

Figure 6-25 - Large Network (50 Hidden Nodes) K_{ff} Generation Performance using Larger Data Set (21 Entries) for TIR of 10μm

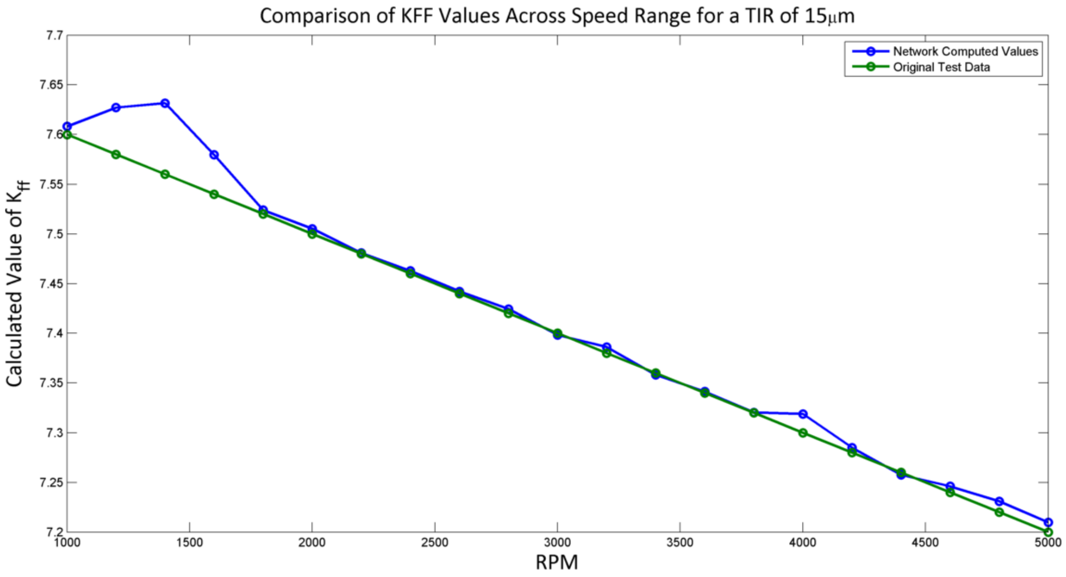

Figure 6-26 - Large Network (50 Hidden Nodes) K_{ff} Generation Performance using Larger Data Set (21 Entries) for TIR of 15μm

Figure 6-25 and Figure 6-26 show the network, network D, performance for a larger network, 50 hidden neurons in the hidden layer, when trained with the larger training data set, 21 entries. Again the general trend of decreasing k_{ff} with increasing rotational cutterhead speed is matched by the network output.

The maximum error for a TIR value of 10µm of 0.05 corresponds to a full range error of 7% and for a TIR value of 15µm the maximum error of 0.065 corresponds to a full range error of 11%. These errors however appear to be located in specific regions of the operating window and for the main the performance is considerably improved than these maximum figures would suggest.

If these results are compared to all of the other network sizes and input data entry sizes, the general network performance appears to be improved with an increase in hidden layer size and training data entry volume.

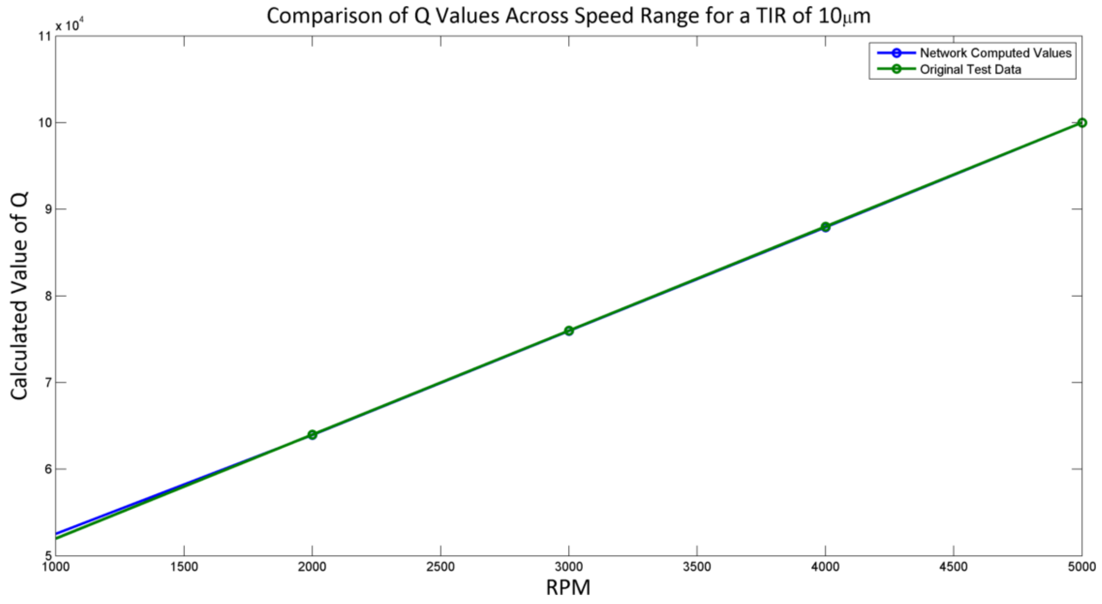

Figure 6-27 - Small Network (20 Hidden Nodes) Q Generation Performance using Smaller Data Set (5 Entries) for TIR of 10µm

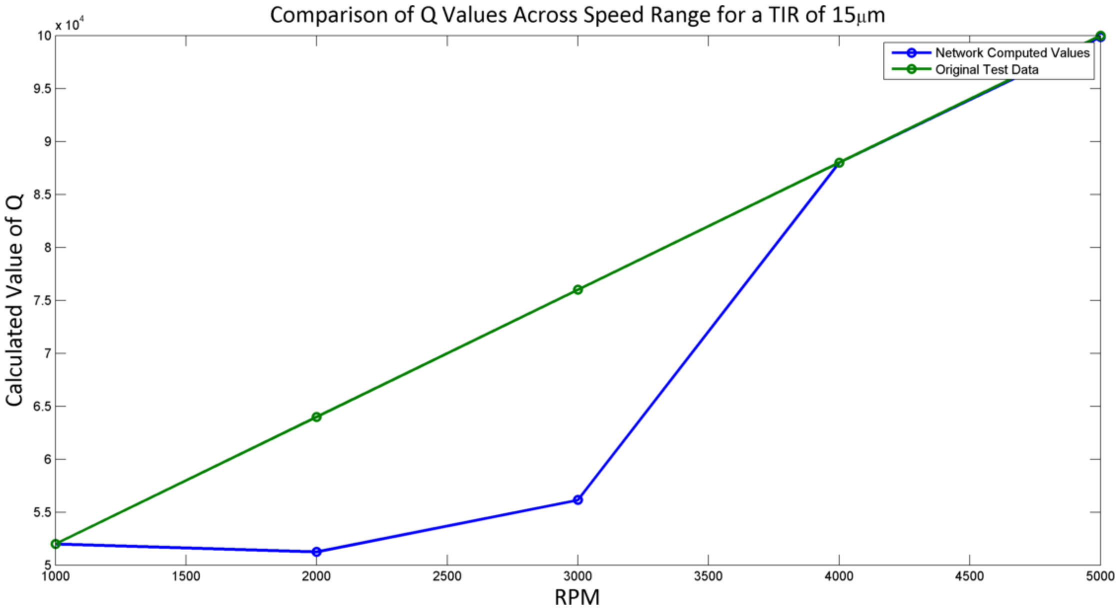

Figure 6-28 - Small Network (20 Hidden Nodes) Q Generation Performance using Smaller Data Set (5 Entries) for TIR of 15µm

Figure 6-27 and Figure 6-28 show the network, network A, performance for the generation of a suitable value of Q across a range of cutterhead rotational speeds. As the cutterhead rotational speed increases the general trend is for the value of Q to increase also, and in general the smaller network, 20 hidden neurons in the hidden layer, trained with the smaller data set, 5 data entries, corresponds with this trend.

For a TIR value of 10μm the maximum error shown in Figure 6-27 of 0.1×10^4 corresponds to a range error of 2%. However this error is at the edge of the operating window and in the main the system performance is superior to this value. Figure 6-28 shows that for a TIR value of 15μm the maximum error is 1.4×10^4 which corresponds to a full range error of 26%. As shown in Figure 6-28 although the trend of increasing Q value with increasing cutterhead rotational speed is similar the curve shape is quite different as predicted by the network when compared to the actual data. This is most likely caused by the network having limited training data and attempting to generate both values for k_{ff} and Q.

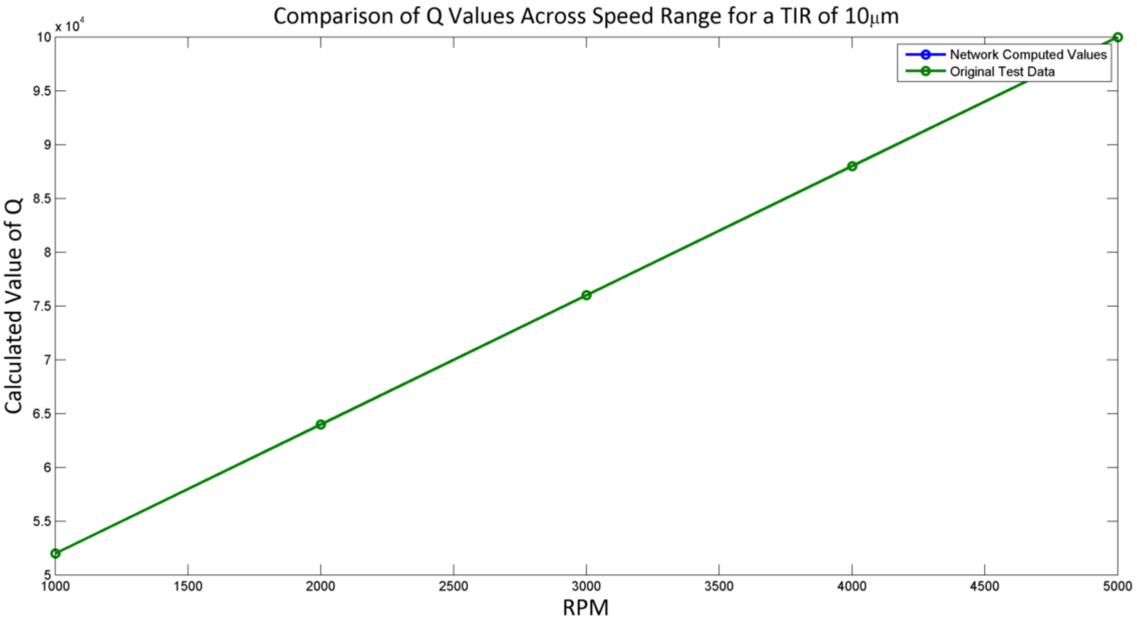

Figure 6-29 - Large Network (50 Hidden Nodes) Q Generation Performance using Smaller Data Set (5 Entries) for TIR of 10μm

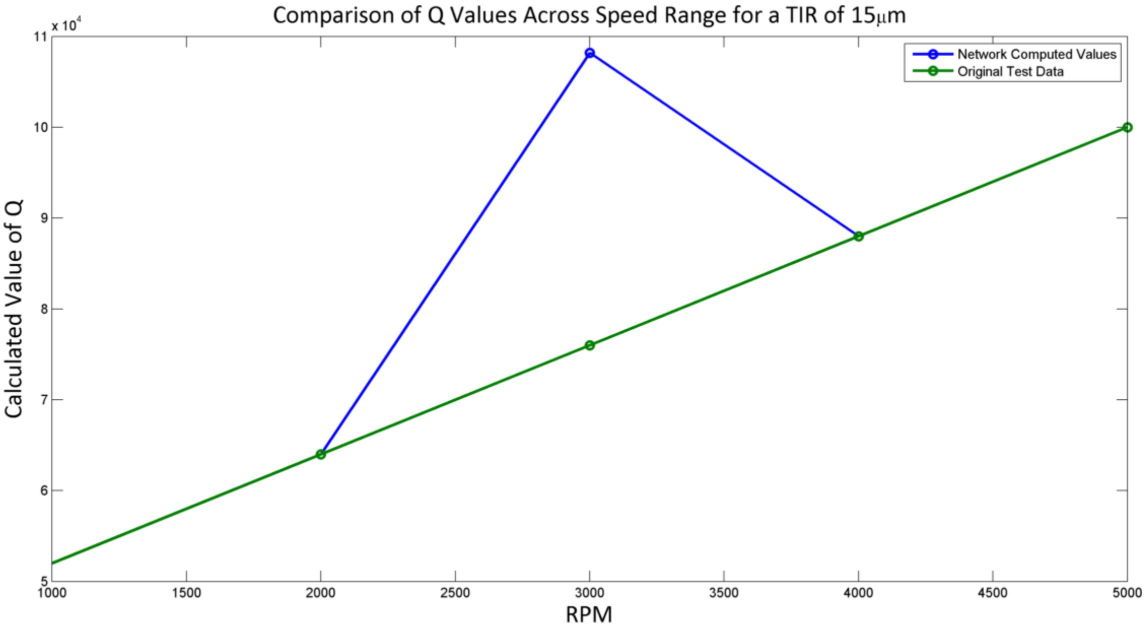

Figure 6-30 - Large Network (50 Hidden Nodes) Q Generation Performance using Smaller Data Set (5 Entries) for TIR of 15μm

Figure 6-29 and Figure 6-30 show the performance of the larger network, network B, with 50 hidden neurons in the hidden layer, when generating suitable values of Q with the smaller training set, 5 entries, for two different values of TIR. Again the trend of increasing Q value for increasing rotational speed of the cutterhead is matched and for a TIR value of 10μm the maximum error of the network appears to be zero. In this case the network is matching the training data. However with a larger TIR value, 15μm, the network performance decreases significantly. Here the maximum error of 3.4×10^4 corresponds to a full range error of 71%.

Interestingly the error is again there for the larger TIR value of 15 μm as for the smaller network trained with the same training data, but rather than the network generating a significantly lower value of Q, the network has generated a significantly larger value of Q. This anomaly point is again located around a rotational speed of the cutterhead of 3000rpm. This may be a coincidence but further research effort should be expended to investigate this.

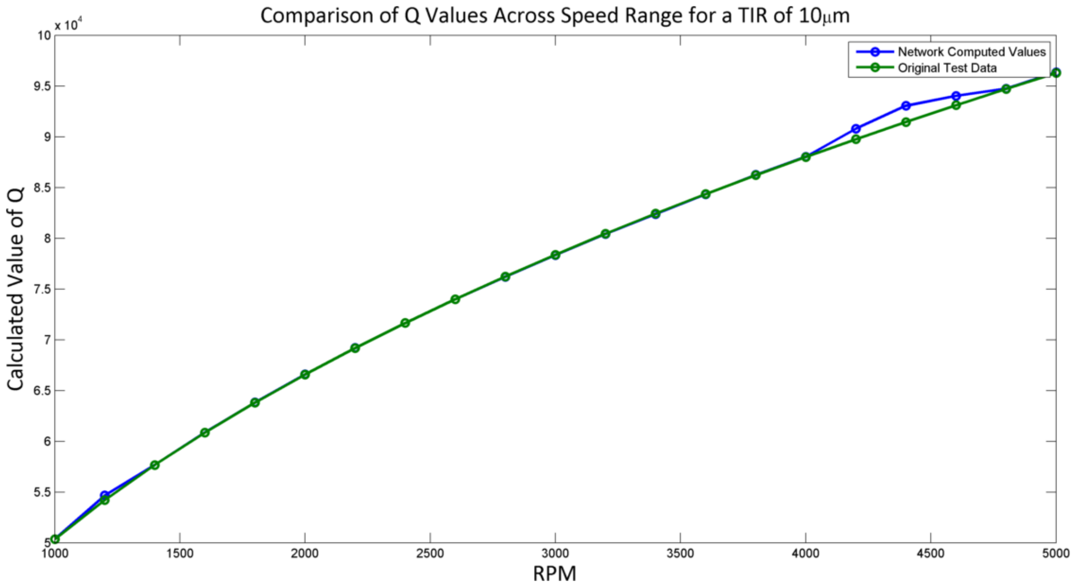

Figure 6-31 - Small Network (20 Hidden Nodes) Q Generation Performance using Larger Data Set (21 Entries) for TIR of 10μm

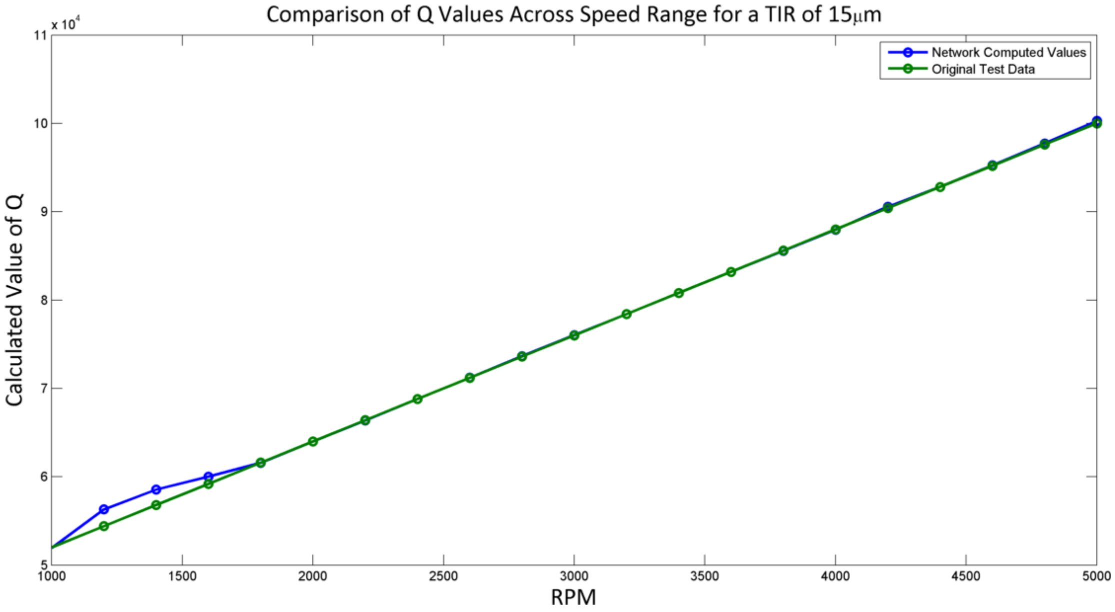

Figure 6-32 - Small Network (20 Hidden Nodes) Q Generation Performance using Larger Data Set (21 Entries) for TIR of 15μm

Figure 6-31 and Figure 6-32 show the performance of the smaller network trained with the larger dataset, network C. This network again matches the trend of Q value with increasing rotational cutterhead speed, however does not appear to have the anomalous results around the 3000 rpm region.

The maximum error in Q prediction for a TIR of 10μm of 0.25×10^4 corresponds to a full range error of 5.3% and the maximum error for a TIR of 15μm of 0.2×10^4 corresponds to a full range error of 4.2%. If the complete trace is considered though the network performance is again considerably improved over the majority of the operating ranges. The majority of the errors as seen in the previous plots appear to be localised around specific points rather than an offset, although some are oscillating around the manually tuned values.

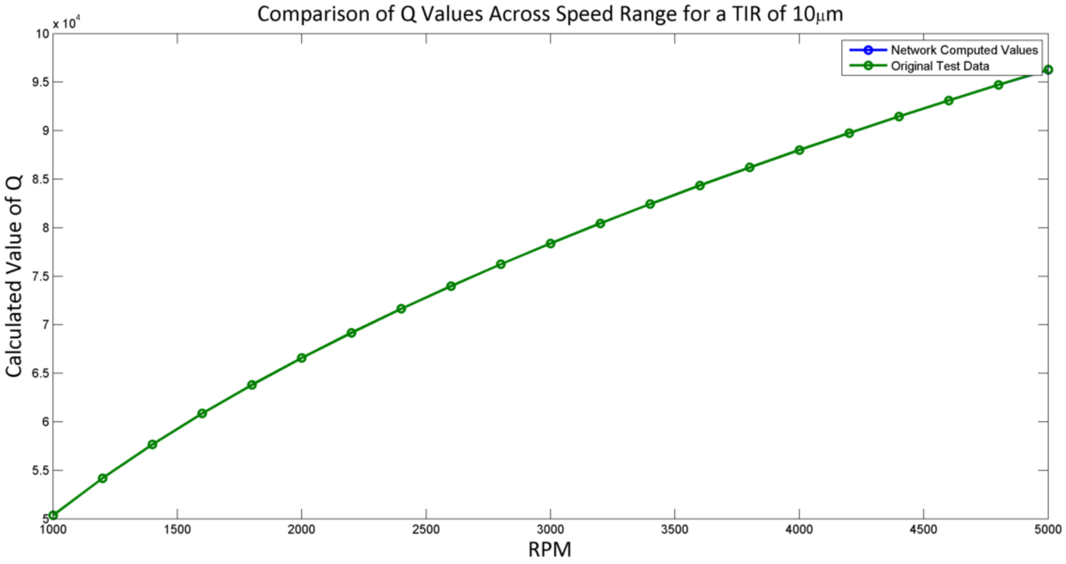

Figure 6-33 - Large Network (50 Hidden Nodes) Q Generation Performance using Larger Data Set (21 Entries) for TIR of 10μm

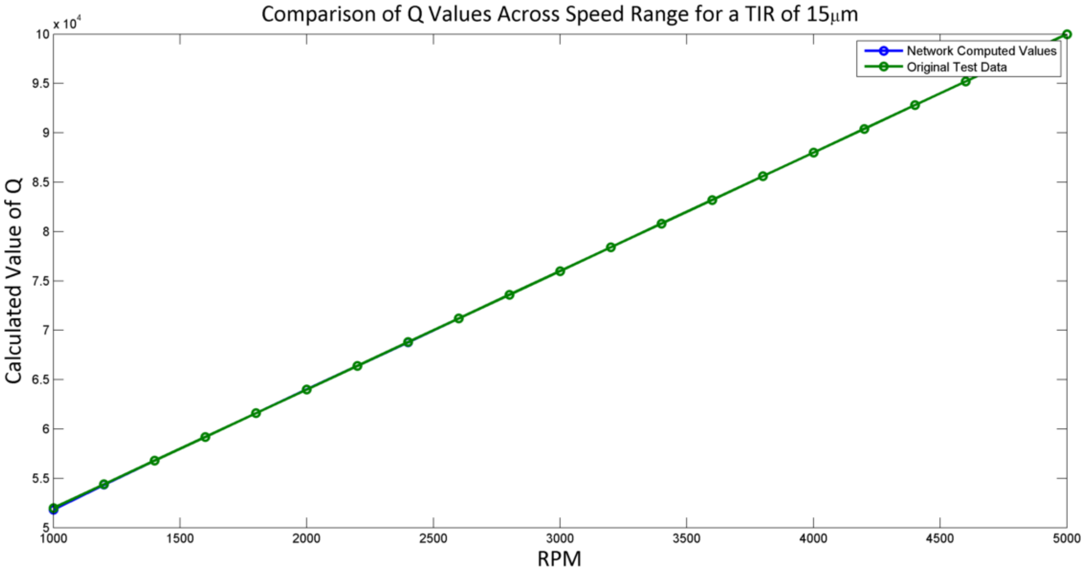

Figure 6-34 - Large Network (50 Hidden Nodes) Q Generation Performance using Larger Data Set (21 Entries) for TIR of 15μm

Figure 6-33 and Figure 6-34 show the results for network D, the larger network trained with the larger training data set. Here the errors are almost zero and the maximum error for a TIR of 15μm of 0.04× 10^4 corresponds to a full range error of 0.8%

The above figures show two general trends in network performance in generating the parameters required by the LQG tracking controller to produce optimal path tracking. As, in this case, a single network is being tasked with providing parameters for all operating ranges of the small scale planer, such as the full speed range and TIR range, it is likely to be a more complex task than if multiple networks were being tasked with providing a single parameter each. The above figures show the trend that as the number of hidden neurons increases the parameter generation performance increases, that is that the error between the original training data and the network computed values reduces.

It is also a fair assessment that as the training data size increased the performance of the network also increased. When comparing Figure 6-28 to Figure 6-32, the error with the larger training data set was again significantly lower. This may be due to the extreme small size of the training data and the manner in which the network is trained. During the training phase the data is split up and half used for network training and half used for validation purposes. However with such as small number of data points, the network training input resolution is very low and may be causing these distortions in the network performance.

Although some trends, such as those shown in Figure 6-26 and Figure 6-34 are an approximation to a linear response, others such as those in Figure 6-33 are very non-linear in response to changing RPM. These results would tend to suggest that networks trained with larger data sets perform more admirably than those trained with smaller data set, and that for this application a larger number of hidden neurons in the hidden layer allowed the network to match more closely the original training data. For the small scale planer application the larger sized network trained with the larger data set was successfully implemented throughout the remainder of this work.

6.8 Summary and Conclusion

This chapter describes the techniques used to model the small scale planer test rig using system identification techniques to develop mathematical models. The aim of the system identification is the estimate the state space models of the small scale planer without any a-priori knowledge of the system. The estimation of the state space models is made purely from input output data collected from the small scale planer through the excitation of the piezo actuators. A sine sweep is used with a frequency range of 0-1KHz with a step size of 0.5Hz. A fourth order model has been used to represent the system, giving a reasonable trade-off between accuracy of the model and the computational complexity of the model.

Other research carried out on the test rig has developed an LQG controller to track a desired cutterhead path to overcome cutterhead inaccuracies and vibration of the spindle unit. However the Q/R ratio and feed forward gains within the model require tuning dependant on the rotational speed of the cutterhead and the run out of the cutterhead knives. A multi input, multi output neural network has been created to generate the required parameter values to achieve optimal tracking of the reference path. Four different networks were created with differing sizes of hidden layer and trained database sizes. For this particular application it was found that a network with fifty hidden neurons and a training database size of sixty three total entries performed adequately, and has been applied to the small scale planer successfully.

7 Chapter 7 – Defect Measurement and Classification Techniques

Assuming full control of the vertical position of the cutterhead spindle assembly, the subsequent element to the control system is the generation of the reference path signal. The generation of the reference path requires the accurate measurement of the machined timber surface, as well as a-priori knowledge concerning cutterhead defects and their appearance on the timber surface. This a-priori knowledge can then be used to characterise the surface defect pattern from the machined surface.

This chapter analyses briefly the Wood Surface Measurement System, WSMS, the subsequent data produced and its transformation using the principal component analysis, PCA, technique. PCA is also briefly discussed and the format of the data output. This output from the PCA is then passed to a pattern characterisation system. Two different types of pattern characterisation techniques are discussed and analysed. The defect cause is then passed to a following algorithm to generate the reference path, this is discussed further in chapter 7.

As this work forms parts of a collaborative effort, some of the work reported here, used to put the authors work into context, is mainly based on the efforts of other group members. Some of this research effort may be an extension to the initial concepts of others, but in these cases there will be a significant expansion and/or modification to that work.

7.1 Measurement Techniques

In order for the defects on the machined timber surface to be correctly characterised, surface geometric data needs to be gathered. Investigations have been carried out utilising the shape from shading, SFS and photometric stereo, PS to gather this geometric data, (Yang 2006, Jackson, Yang et al. 2007). (Yang 2006) implemented two image photometric stereo and single image SFS. All images were however taken using static workpieces, overcoming the common issues involved with position matching with moving workpieces.

(Ogun, Jackson et al. 2012) have implemented a system known as temporal multiplexing on the WSMS at Loughborough University but rather than assuming a negligible offset in multiple images through rapid picture capture, an encoder has been used on the moving surface to determine the pixel offset between the images. This has then allowed accurate matching of the images to reduce any distortion to the measured surface.

Other work carried out has focused on the photometric stereo method, and indeed has been implemented within this work by other members of the research group. Therefore only the two image photometric stereo method will be briefly explained within this body of work.

7.1.1 Wood Surface Measurement System Principals of Operation

The wood surface measurement system employed within this research utilises a two image photometric stereo type approach to determine the surface features on the machined timber surface. To apply the photometric stereo underlying algorithms it is assumed that the machined surface exhibits diffuse behaviour. (Maristany, Lebow et al. 1993) investigated the properties of unfinished timber and reports that, due to both its heterogeneous and anisotropic nature, unfinished timber exhibits approximately diffuse behaviour.

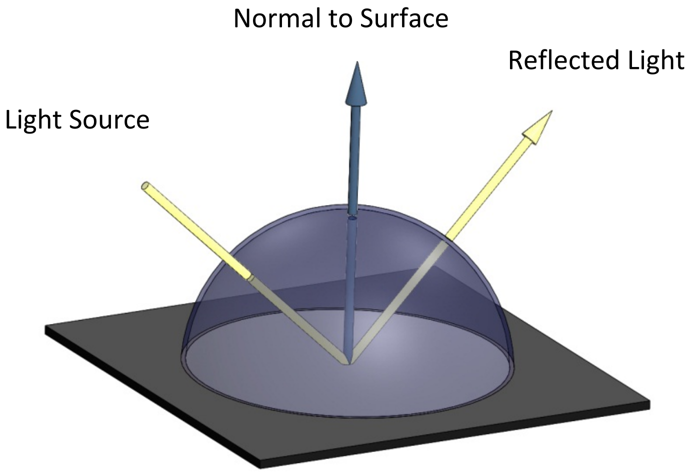

Figure 7-1 - Idealised Specular and Diffuse Reflection - A Lambertian Surface - (Jackson, Yang et al. 2007)

A Lambertian reflection is one that exhibits reflection as shown in Figure 7-1. The reflection has a directional component combined with a uniform diffuse dome, and the surface is known as a Lambertian surface. Reflection from a Lambertian surface is shown in Figure 7-2.

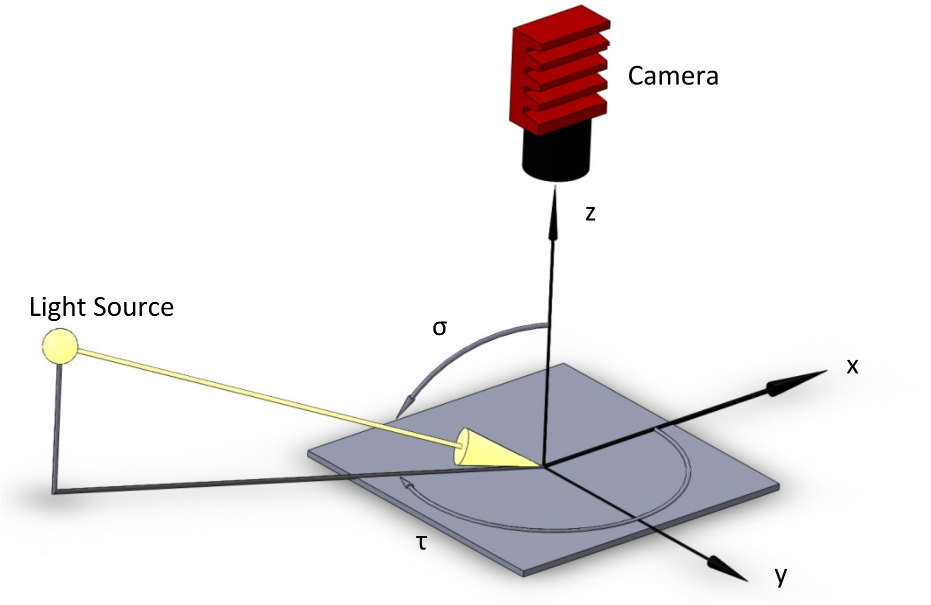

Figure 7-2 - Schematic of Lambertian Reflection

Where

σ is the zenith, or angle, of the light source

τ is the azimuth, tilt angle, of the light source

According to Lamberts law, reflection at a surface point (x, y) is determined by

$$i(x,y) = i_o\rho(x,y)\frac{-p(x,y)\cos\tau\sin\sigma}{\sqrt{p^2(x,y) + q^2(x,y) + 1}} - \frac{q(x,y)\sin\tau\cos\sigma + \cos\sigma}{\sqrt{p^2(x,y) + q^2(x,y) + 1}} \qquad (7\text{-}1)$$

Where

i(x, y) is the intensity reflected at the point *(x, y)*

i_0 is the incident intensity

ρ(x, y) is the surface albedo, a coefficient that represents the proportion of light reflected from the point *(x, y)* with respect to the incident light *p* and *q* are the gradient of the surface at any local point in the x and y directions

Potential issues with this type of measurement surround the reflectivity of the surface due to a variability in the albido of the wood. However (Lebow, Brunner et al. 1996) have developed a technique using principal component analysis of the spectral reflectance curves to classify different features of the wood structure, such as Loose knots, tight knots, earlywood, latewood, pitch pockets and pitch streaks. With this ability these areas of the timber may be excluded from the classification as the WSMS may return false positive results of surface waviness or results that would skew the classification.

Due to the geometry of the machining process it is assumed that there is no variation in the height of the cuttermarks along the y axis, *q(x, y) = 0*. The cutterheads have been wire cut with the knife mounting faces parallel to the axis of revolution. This reduces equation (7-1) to;

$$i(x) = i_o \rho(x) \frac{-p(x)\cos\tau\sin\sigma + \cos\sigma}{\sqrt{p^2(x)+1}} \qquad (7\text{-}2)$$

For the experimental arrangement employed at Loughborough, as detailed in section 0, the two light sources are arranged opposite each other and both along the waviness direction, $\tau_1 = 180^\circ$ and $\tau_2 = 0^\circ$ This then simplifies the arrangement in Figure 7-2 to that in Figure 7-3.

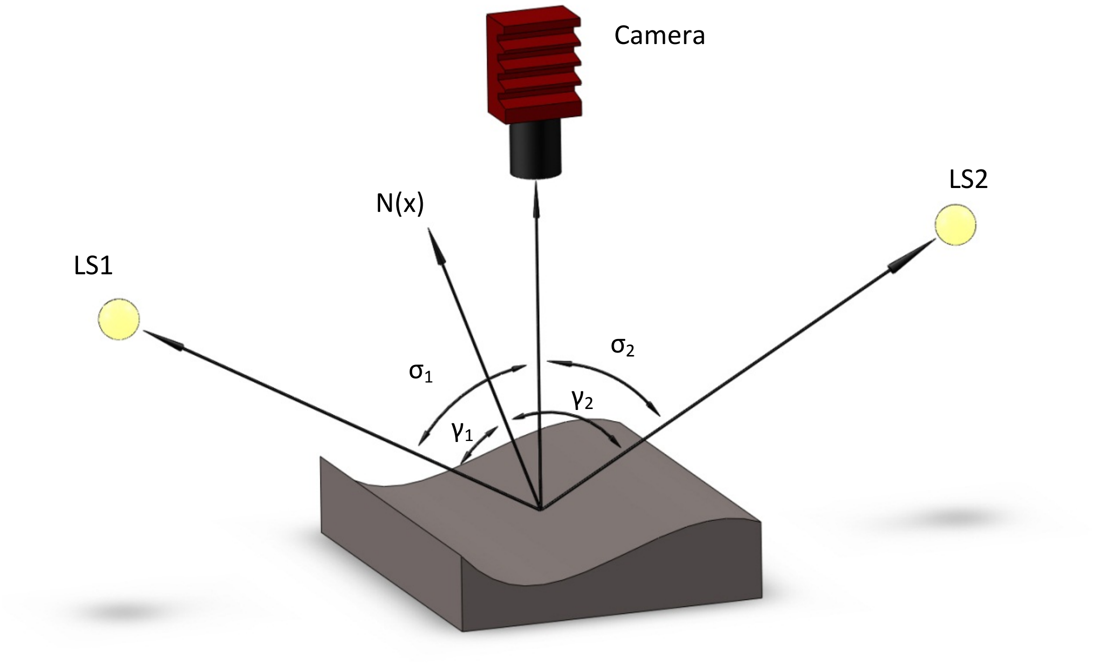

Figure 7-3 - Schematic of the two image photometric stereo method, (Jackson, Yang et al. 2007)

Where

S is the surface normal, coincident with the Z axis and the optical axis of the camera

x is a point on the surface profile

n(x) is the normal to the point

L1 is the vector pointing from the point x to LS1

L2 is the vector pointing from the point x to LS2

σ_1 and σ_2 are the angles between the surface normal S and L1, and S and L2. Since these angles are equal, σ is used.

γ_1 is the angle between the normal n(x) and L1

γ_2 is the angle between the normal n(x) and L2

Substituting the light source angles, $\tau_1 = 180^{\circ}$ and $\tau_2 = 0^{\circ}$, into equation (7-2) gives;

$$i_1(x) = i_{01}\rho(x)\frac{p(x)\sin\sigma + \cos\sigma}{\sqrt{p^2(x)+1}} \tag{7-3a}$$

$$i_2(x) = i_{02}\rho(x)\frac{-p(x)\sin\sigma + \cos\sigma}{\sqrt{p^2(x)+1}} \tag{7-4b}$$

Where

i_{01}=i_{02}, as LS1 and LS2 are identical in intensity

Dividing equation (7-3a)by equation (7-4b) gives;

$$p(x) = \frac{i_1(x) - i_2(x)}{i_1(x) + i_2(x)}.\frac{1}{\tan\sigma} \tag{7-5}$$

Equation (7-5) shows that two images are required to calculate the gradient of the surface under investigation. (Yang 2006) describe the requirements for these images to be converted to intensity profiles and implemented the equation shown below, (7-6), to calculate these intensity profiles.

$$c(j) = \frac{\sum_m g_{ij}}{m} \tag{7-6}$$

The intensity profiles c(j) for the two timber surface images are then substituted for i_1 and i_2 in equation (7-5) to give p(x). After substituting the intensity profiles into equation (7-5), the first derivative of the surface, the slope, is given by;

$$p(x) = \frac{ds}{dx} \tag{7-7}$$

In order to extract the height data, the gradient data has to be integrated. (Jackson, Yang et al. 2007) describe a global integration technique, frequency integration, which is considered to be the most relevant technique for this application.

The Fourier transformation of equation (7-7) gives;

$$P(u) = 2\pi i u S(u) \tag{7-8}$$

$$S(u) = \frac{P(u)}{2\pi i u S(u)} \tag{7-9}$$

$$s(x) = F^{-1}(S(u)) \tag{7-10}$$

7.2 Principal Component Analysis

The output from the WSMS system is a complete normalised surface profile of a section of the machined timber. This normalised x-y plot of the surface contains a considerable amount of data in the form of data points, typically 280 data points per 0.1mm. When considering large a-priori knowledge bases containing numerous timber surface examples and the computing required to analyse this, with particular considerations to the speed of solution, a compressed form of data is required.

Principal component analysis, PCA, is used as a method to reduce the number of observed variables by generating a smaller number of artificial ones. PCA, also known as the Karhunen-Loève transform, KLT, is a standard data reduction technique which extracts relevant data, attempts to remove redundant data, thereby highlighting hidden features and relationships that exists between observations, (Yang, Ren 2011). PCA is a technique for reducing the dimensionality of the data. These lower dimensioned data sets are known as principal components, (Abdi, Williams 2010).

Principal component analysis is a mathematical procedure that employs an orthogonal transformation of the observed data set from a high dimensional space to a lower dimensional space. The variances of the data lie on the principal components such that the first principal component has the largest variance and subsequent principal components have reducing variance.

7.2.1 Principal Component Analysis Implementation

The surface profile, with respect to timber length l, s(l) is recorded using the WSMS as previously discussed. The local maxima and minima are connected using a cubic spline approximation, (Ogun 2012), to create the upper envelope, $e_{upper}(l)$, and lower envelope, $e_{lower}(l)$. The PCA is employed to reduce the dimensionality of the envelopes. These two envelopes, the upper and lower, are then said to be two variables of the same size x and y.

To produce data with a zero mean, each data point within the dataset has the mean of that dataset subtracted from it giving;

$$x_m = x - \bar{x} \tag{7-11a}$$

$$y_m = y - \bar{y} \tag{7-12b}$$

This mean centring process is required to ensure that the primary principal component does not represent the mean of the dataset, (Miranda, Borgne et al. 2008).

Co-variance is a measure of the linear relationship between two random variables and is then calculated for the data set. For this x_m and y_m are combined, such that they form the columns of the resultant matrix, giving a matrix X. As the data is two dimensional the co-variance matrix will be a two by two matrix.

$$cov(X,Y) = \sum_{i=1}^{n} \frac{(X_i - \bar{X})(Y_i - \bar{Y})}{n-1} \tag{7-13}$$

Where

n = number of elements in X

The co-variance matrix is formed as below;

$$C = \begin{bmatrix} cov_{xx} & cov_{xy} \\ cov_{yx} & cov_{yy} \end{bmatrix} \tag{7-14}$$

It is evident that for an n dimensional data set the co-variance matrix will be an n by n sized matrix.

Since the co-variance is square, eigenvectors and eigenvalues can be calculated for the matrix. These eigenvectors are then re-arranged in order of decreasing eigenvalues, giving the principal components in order of significance.

7.2.2 Use of Principal Components

The principal components represent the variation between the upper and lower envelopes of the surface profile. Rather than working with full datasets comprising of x-y plots of the surface profile, PCA allows a two by two matrix to represent the surface. Upon inspection of the principal components, implemented on different ranges of surface defects, distinct patterns start to emerge.

To show the patterns in the principal components, a number of simulations have been carried out where the surface profile is shown as well as the upper and lower envelopes. During these simulations it is assumed that the knives are all accurately ground and there is zero unwanted vibration, unless otherwise stipulated. The principal components are shown along with the surface profile. The diagonals of the principal components are the same and so have been omitted.

7.2.2.1 Four Knife Finish with Once Per Revolution Vibration

The simulated surface profile and upper and lower envelopes for a four knife finish with a once per revolution vibration are shown below in Figure 7-5 and the principal components, along with relevant cutting data, are shown in Table 7-1. For the below simulation the out of balance mass was positioned such that it aligns with knife two, φ = 0, as per Figure 7-4. It is arranged such that knife 1 is the first to come into contact with the timber surface.

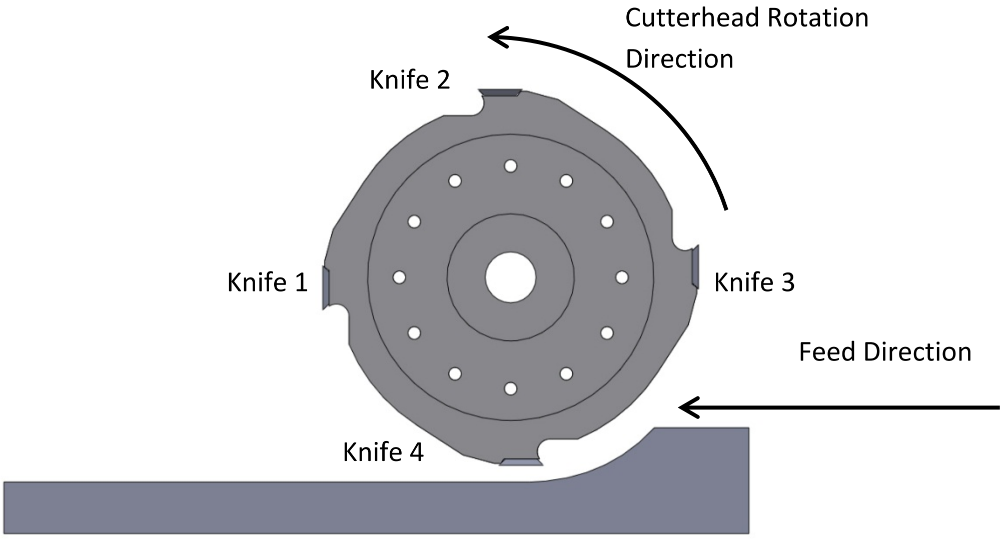

Figure 7-4 - Cutterhead Numbering Convention

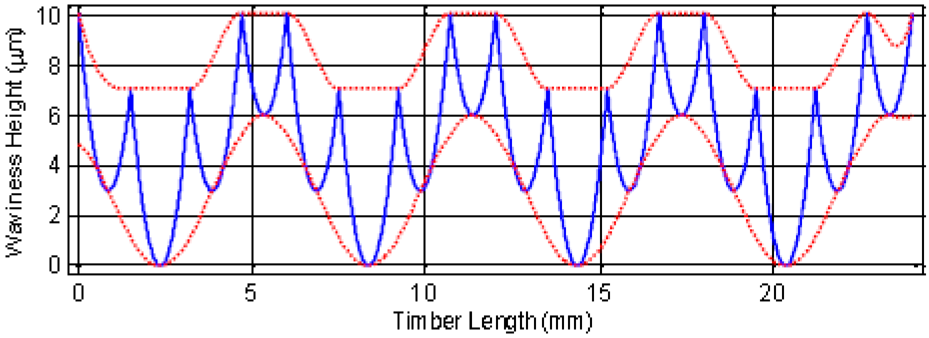

Figure 7-5 - Four knife finish with once per revolution vibration (φ = 0)

Here the red lines are the upper and lower splines fitted to the local minima and maxima of the blue line, representing the machine timber surface.

Table 7-1 - Principal Components for four knife finish with once per revolution vibration

Cutting Speed (rev min^{-1})	Feed Speed (mm s^{-1})	Knife Radius (mm)	Vibration Amplitude (mm)	Principal Components
3000	300	50	0.003	0.5105, 0.8599
3000	400	60	0.006	0.5108, 0.8597
3000	500	70	0.008	0.5113, 0.8594
2800	450	65	0.005	0.5119, 0.8590

In order to ascertain the robustness of the PCA further simulation has been carried out with varying position of the out of balance mass.

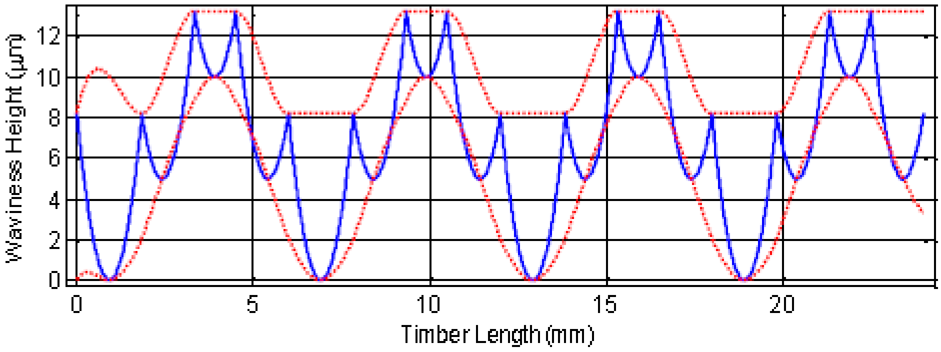

Figure 7-6 - Four knife finish with once per revolution vibration (φ = π/2)

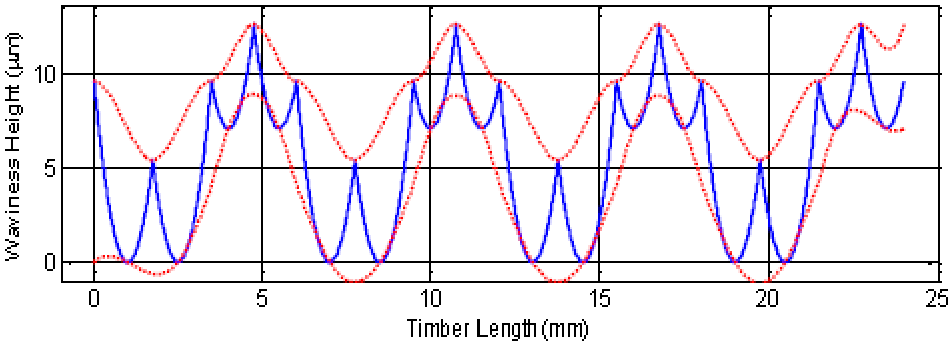

Figure 7-7 - Four knife finish with once per revolution vibration (φ = π/4)

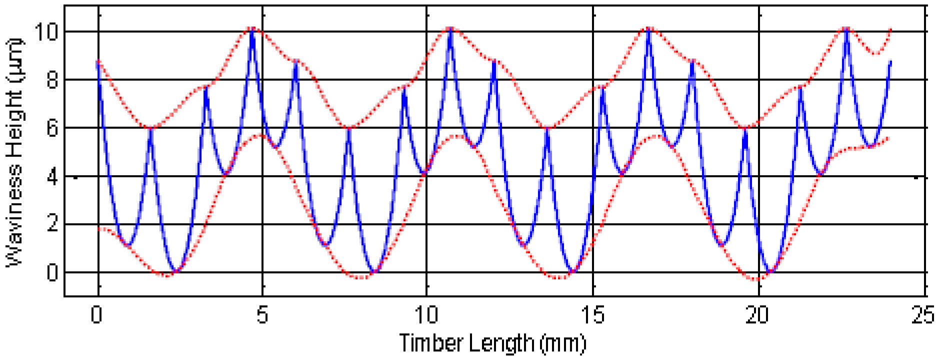

Figure 7-8 - Four knife finish with once per revolution vibration (φ = π/6)

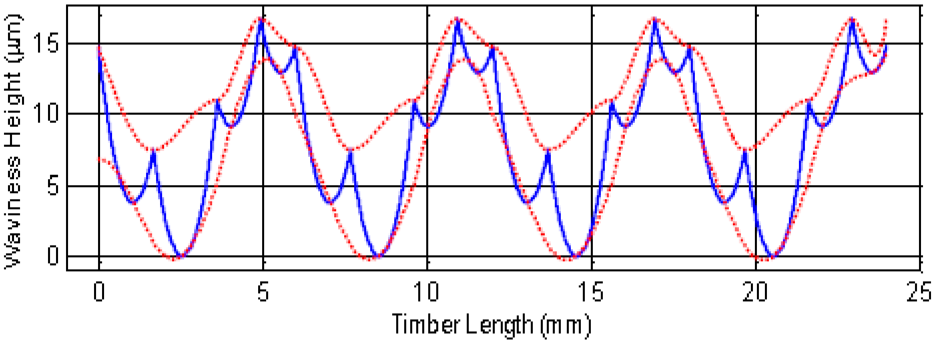

Figure 7-9 - Four knife finish with once per revolution vibration (φ = π/8)

Table 7-2 - Principal Components for four knife finish with once per revolution vibrations at varying out of balance positions

Vibration Amplitude, peak to peak (mm)	φ (radians)	Principal Components
0.005	π/2	0.5050, 0.8631
0.005	π/4	0.5252, 0.8510
0.003	π/6	0.5279, 0.8493
0.007	π/7	0.5200, 0.8542

Figure 7-6, Figure 7-7, Figure 7-8, Figure 7-9 clearly show that although the same defect cause has been active, a once per revolution vibration, the surface form is quite different. This may make classification based upon the surface form itself difficult to achieve as all of these surface forms would need to be classified within the same group. However Table 7-2 shows that the output of the principal component analysis technique does not change a great deal. This has large added benefits as not only is the amount of data greatly reduced, to a two by two matrix, but the values within the matrix remain reasonably constant, making classification a simpler process.

However for this to be a universal application, as it cannot be used as a classification tool if the compressed data does not show a wide enough difference between samples, further simulation has been carried out to test PCA on a range of different defect types.

7.2.2.2 Four Knife Finish with Twice Per Revolution Vibration

In a similar manner to the once per revolution vibration a four knife finish with twice per revolution has been simulated, the envelopes generated and the principal component analysis carried out. The vibration positions have been varied, again in a similar manner to the once per revolution vibration, but always diametrically opposite across the cutterhead.

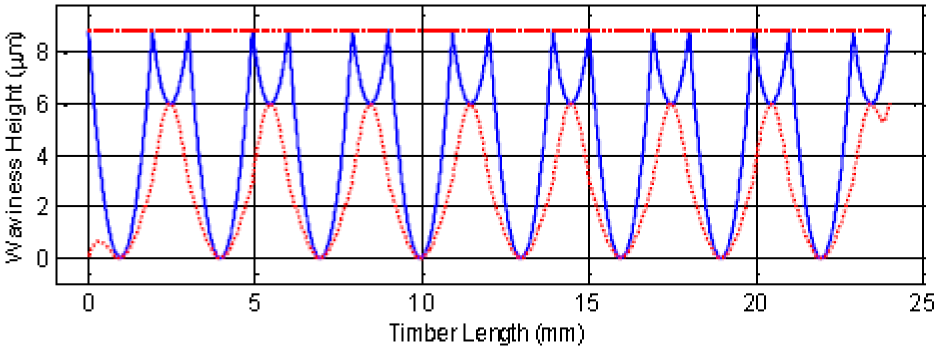

Figure 7-10 - Four knife finish with twice per revolution vibration

Table 7-3 - Principal components for a four knife finish with twice per revolution vibration

Cutting Speed (rev min^{-1})	Feed Speed (mm s^{-1})	Knife Radius (mm)	Vibration Amplitude (mm), φ (rad)	Principal Components
3000	300	50	0.003, 0, π	0, 1
3000	400	60	0.006, π/2, 3π/2	0, 1
3000	500	70	0.008, π/4, 5π/2	0, 1
2800	450	65	0.005, π/8, 9π/2	0, 1

Figure 7-10 shows the surface profile generated by the simulations. This profile is very different to that produced with the once per revolution vibration, and this is reflected by the principal components calculated for the differing cutting parameters, shown in Table 7-3.

7.2.2.3 Extended Principal Component Analysis and Data Structure

The limited amount of data produced using the principal component analysis, as applied here, is not sufficient when considering larger numbers of knives on the rotary cutterhead. (Ogun 2012) has simulated a ten knife cutterhead and found that the change of the principal components was only very small, circa (0.02, 0.01). To generate more data the application of the principal component analysis has been modified slightly. Rather than just an upper envelope and a lower envelope and average of these two envelopes is also included. This additional input to the principal component analysis generate a three by three matrix rather than a two by two matrix. This additional data does indeed provide additional information which can be used to aid in the classification process.

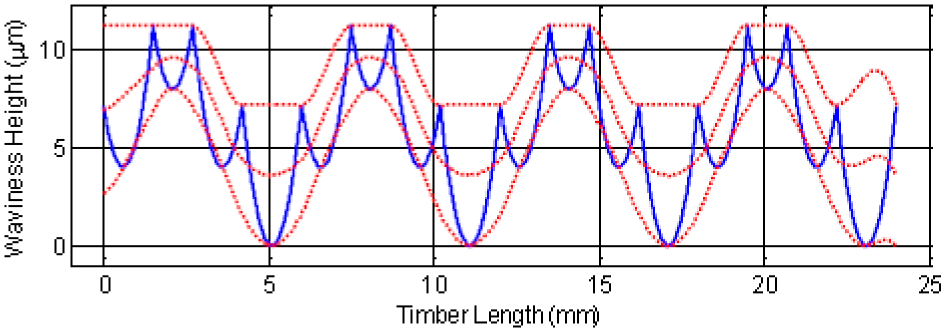

Figure 7-11 - Extended principal component analysis to include a third input data stream, the average of the upper and lower envelopes

Table 7-4 - Extended PCA Results for four knife finish with once per revolution vibrations at varying out of balance positions using simulated data, based on simulation data

Cutting Speed (rev min^{-1})	Feed Speed (mm s^{-1})	Knife Radius (mm)	Vibration Amplitude (mm)	φ (radians)	Principal Components
3000	300	50	0.003	π/2	0.4308, 0.8048, 0.4082, 0.7074, 0.5831, 0.4082, 0.5666, 0.1109, 0.8165
3000	400	60	0.006	π/4	0.4318, 0.8043, 0.4082, 0.7017, 0.5839, 0.4082, 0.5667, 0.1102, 0.8165
3000	500	70	0.008	π/6	0.4471, 0.7959, 0.4082, 0.6904, 0.5973, 0.4082, 0.5687, 0.0993, 0.8165
2800	450	65	0.005	π/7	0.4443, 0.7974, 0.4082, 0.6925, 0.5948, 0.4082, 0.5684, 0.1013, 0.8165

Comparing the results in Table 7-2 and Table 7-4, for similar operating conditions, we can see very similar trends produced for certain elements on the analysis. Of note is the final column always being the same values. This is similar to the diagonals always remaining the same for the original PCA.

Table 7-5 - Extended PCA Results for four knife finish with differing operating conditions

Cutting Speed (rev min^{-1})	Feed Speed (mm s^{-1})	Knife Radius (mm)	Vibration Amplitude (mm)	φ (radians)	Principal Components
3000	400	50	0	N/A	0.8944, 0.4472, 0, 0, 0, 1, 0.4472, 0.8944, 0
3000	400	60	0.006 (twice per revolution)	π/2	0.0009, 0.9129, 0.4082, 0.8942, 0.1835, 0.4082, 0.4476, 0.3647, 0.8645

Table 7-5 shows the extended PCA results for two further operating conditions, the ideal, and a twice per revolution vibration. These results are clearly different to the results for a once per revolution vibration and the ideal has the same type of format as for the original PCA, with a number of 0's and 1's. These results remain constant over all operating conditions while there is a four knife finish.

7.3 A-Priori Knowledge Base

Recognising the potential of the principal component analysis technique to produce data patterns with trends based on surface waveforms and hence some information concerning defects, a synthetic a-priori knowledge base has been generated, similar in concept, although different in realisation, to that described by (Khairy 1996).This database was generated using algorithms based on the circular arc theory rather than recorded from real specimens as to save time. The principal component analysis was applied to these synthetic surfaces as well as the defect cause.

In order to overcome any defects on the machined timber surface, the first step taken within this body of work is to attempt to ascertain the cause of the defect. The defects under investigation are both out of balance forces and run out of the knives. These two types can also be mixed together to generate a pseudo third type of defect cause. Once the defect cause has been correctly and fully identified corrective action can then be implemented.

The intention is to implement a system capable of interrogating the output of the principal component analysis and classify the defect into pre-defined real world categories. However to categorise the defects into pre-defined categories there is a requirement to obtain an a-priori knowledge base in order to compare and contrast the measured surface to. This database must cover a wide range of defects and operating parameters of the small scale planer test rig. A range of pitches from 1mm to 5mm has been selected as 1mm is the minimum pitch that the WSMS is capable of detecting and 5mm is a poor quality surface finish. This range of pitches is covered using 1mm increments. At each pitch a total of four different proud knife situations are simulated. Each knife has been simulated with a maximum run out of seven micrometres, due to a limitation of the algorithm used to simulate the machined timber surface. Vibration has also been added to the cutterhead with a maximum amplitude of two micrometres at 45° increments.

These values were selected as they are all within the scope of the small scale planer test rig and allowed the use of the existing simulation tool developed for this research. The dataset was specified only for a four knife cutterhead as it was assumed that the number of knives on the cutterhead would be known prior to machine operation and an appropriate dataset selected and used, therefore it was not necessary to mix datasets with differing numbers of knives on the cutterhead. The knives were assumed to be spread equidistantly around the cutterhead, and during the initial testing and development phase, no noise has been added to the surface profiles produced. The final a-priori knowledge base stores the three by three matrices as row vectors and then a textual based cause for the defect.

7.4 Defect Classification Tools

With a wide range of data within the a-priori knowledge base covering a number of different defects, the subsequent process is to classify the defects. The principal here being that patterns can be picked out from the principal component data in order to classify the defect cause.

7.4.1 K-Nearest Neighbor

K-nearest neighbor, KNN, is a commonly used method for classification in pattern recognition. KNN is sometimes known as a lazy learning algorithm as all of the computation is deferred until the actual process of classification. Classification is based upon the entire training set. This has both advantages, such as the ability to easily add new data to the data set without any retraining time, and disadvantages such as the requirement to continually maintain the dataset, and the actual classification phase can become quite computationally demanding.

KNN assumes that the data is in a feature space where each pattern data point is represented as a point in n-dimensional space. In this case the data points are the modified output of the PCA, a nine by one row vector.

7.4.1.1 Principals of K-Nearest Neighbor

K-nearest neighbor is a simple classification technique based on a majority rate of its neighbours, where the object is classified based on its closest k neighbours. Unlike other adaptive techniques there is no real training phase, just the storing of the a-priori knowledge base which contains both data points and classifiers. During this research the distance metric employed is the squared Euclidean distance.

Squared Euclidean distance has been chosen as it places progressively greater weight on points that are further apart. Although not strictly a metric as it does not satisfy the triangle inequality for a Euclidean geometry, however to compare (Wang, Zhang et al. 2005) have used the squared Euclidean distance transform, SEDT, directly upon image analysis tasks. One potential failure of this type of algorithm, KNN, is that the number of samples of each type will tend to dominate the classification of the test vector. However the synthetic A-Prior Knowledge Base, APKB, generated has equal number of all defects under investigation, such that no one type of defect will dominate the classification task.

At the time of classification the query vector distance is measured to all the other nodes within the space. The nearest k nodes are then selected and the query node is classified to the modal classification of these k nodes.

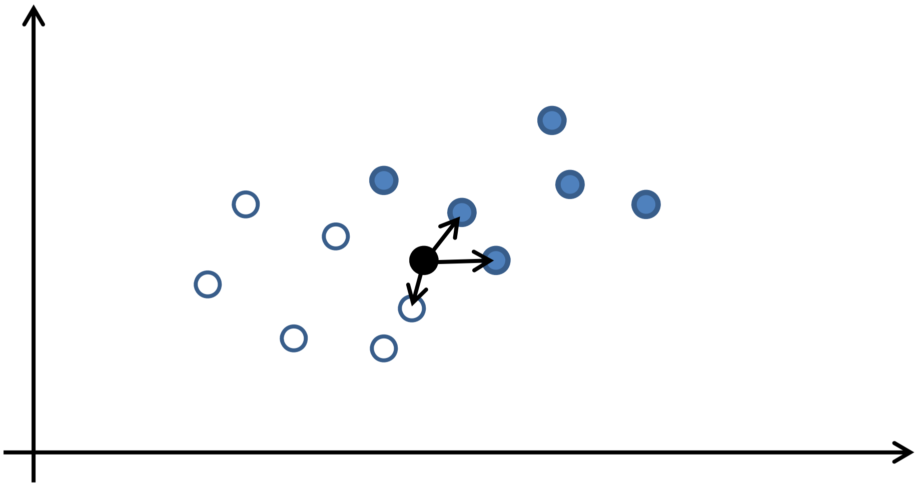

Figure 7-12 - K-nearest neighbor graphical example, k = 3

Figure 7-12 gives an example to the classification technique itself. The query node, solid black, is measured to all surrounding nodes. The three nearest nodes are selected and the query node is classified based on the modal nearest nodes, (Laguı´a, Castro 2008) in this case the solid blue classifier. This type of classification, although very simplistic, is logical, and could be said to approximate the manner in which a human may attempt the problem.

In order to assign some form of confidence to the classification, the distance metric has been used further with some additional post processing, (Mitchell, Remmel et al. 2008). The assumption here is that if the distance to a known set of samples is very low then there should be a higher confidence in the classification than if the distance to the closest known data points is large. To achieve this the distance to the nearest k nodes of each type is measured and then compared to the other remaining known classifiers.

A further extension to the KNN technique has also been implemented. If k approaches the total number of nodes of each classification, attempts to find the centre of each classification area can be made, and the classification can be carried out based on the centre location of each classification type distance to the query node, rather than the modal classification of the nearest k nodes.

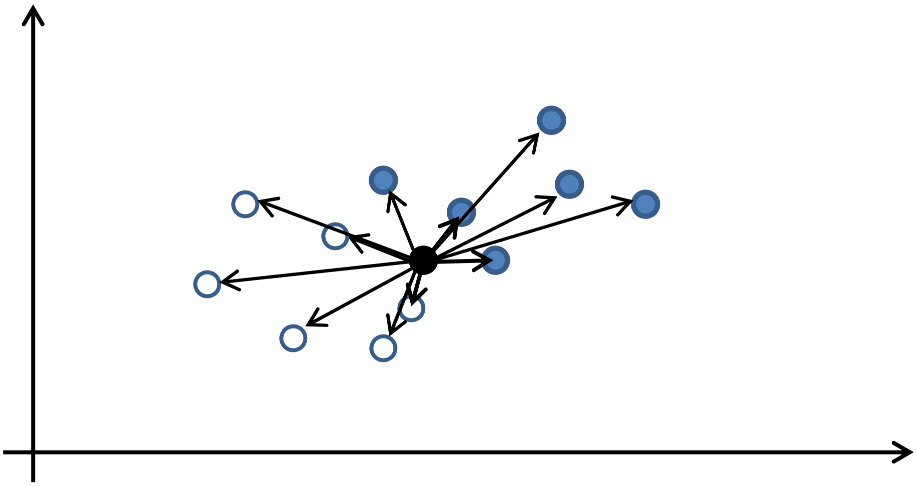

Figure 7-13 - Modified K-nearest neighbor approach

This approach does increase the level of computation required by a small amount, although with the speed of modern desktop computers this speed difference is insignificant to the overall success of the classification technique. This adaption of the technique attempts to overcome any outlier issues and is a more heuristic approach to the problem of classification, utilising all of the available data rather than being restricted to a small slice of the total available data.

7.4.2 Pattern Recognition Neural Network

A second technique has been implemented within this research. A pattern recognition neural network has been implemented using the inbuilt MATLAB ‘patternnet’ function. The patternnet function describes a feedforward neural network trained to classify inputs according to target inputs. The feedforward structure of the network consists of three layers. The first layer is connected to the input, and here has nine neurons as the output of the principal component analysis is a three by three matrix. The centre layer consists of a number of neurons, this value has been modified to realise the network potential, and the final layer produces the network output. The number of neurons in the final layer is equal to the number of classification cases. In an ideal situation only a single neuron in the output layer is activated when the network is presented with a full set of input data. With all the other output neurons output becoming zero and the activated neuron becoming one. However in reality this is not the case and a number of the output neurons are semi-activated. Depending on the activation level this can become a source of uncertainty. If for example a number of output neurons are activated to a similar degree it becomes difficult to have full confidence in the classification output presented by the network, shown schematically in Figure 7-14.

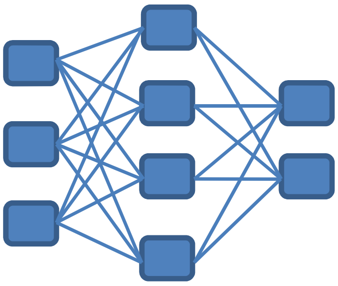

Ideal Output	Real Type Output
1	0.55
0	0.45

Figure 7-14 - Simplified Patternnet Network showing both ideal and real type outputs

7.4.3 Performance Differences between K-Nearest Neighbour and Pattern Recognition Neural Network

Multiple size neural networks have been produced, the hidden layer size was varied, as well as multiple types of k nearest neighbour algorithm, the value of k was altered as well as the voting technique employed. In order to test the systems a selection of one hundred data points were taken from the a-priori knowledge base and shown to the particular system. The same data points were used in all cases. The classification was then carried out and the result recorded.

The results are presented below in Table 7-6 and Table 7-7.

Table 7-6 - K Nearest Neighbour Classification Results

k	Majority Case % Correct	Distance Weighted (1/d) % Correct	Distance Weighted ($1/d^2$) % Correct
1	63	62	64
3	76	79	81
5	94	96	95
Full Dataset	97	98	97

Two different distance weighting metrics were implemented as shown in Table 7-6. These were selected as they are some of the most common used within the research community. Of high importance was the length of time taken to compute the classification when using the full dataset size for the value of k. Even when using modern high speed computers the system took up to an hour to compute the classification. This is clearly not a suitable solution when trying to work in real time. This system may be operating within the slower outer loop, as described in section 2.8.1, the classification will need to be computed in a number of seconds rather than an extended duration, otherwise the quantity of wood passing through the machine that may be outside the required specification could be immense.

Table 7-7 - Neural Network Classification Results

Number of Hidden Neurons	% Correct
5	40
9	92
10	85
15	84
20	87

Of interest was the strength of classification with the neural network type solution. With the number of hidden neurons set at five, activation levels of the different output neurons were spread across all the output neurons rather than there being a modal output neuron. Whereas as the number of hidden neurons was increased to nine, to match the input layer size, the spread was reduced and the confidence in the classification increased. It was also noted that the classification time of the K-nearest neighbour technique was measured in minutes, a similar duration to the training time of the neural network type approach. However this is a single hit when considering the neural network approach rather than a wait on each and every classification operation with the K-nearest neighbour approach. This deficit for the K-nearest neighbour is offset by the ease of implementing additional data to the dataset, when the additional training requirements of the neural network is taken into account.

7.5 A-Priori Data Considerations

When looking at more detail at the random data points used to test the different classification approaches, a number of trends can be seen. These trends have a bearing on the classification result and on the a-priori knowledge dataset used within the techniques themselves.

Where the test data node, the set of data to be classified, lies within the boundaries of a classification area the classification is more easily carried out than when the test node lies at the boundary between two or more different classification areas. This observation is perhaps simplistic but can have an effect on this particular application. The final application of the classification type needs to be brought into consideration. If the classification is to be used solely for the purpose of actual knowledge about the defect cause then the classification itself needs to be precise. However, as it is in this case, the classification is to be used by a subsequent sub section, some inaccuracies or simplifications can be made.

Of crucial importance to this work is the observation that both defect conditions under consideration here, proud knives and out of balance forces may be overcome with similar actions, the vertical movement of the cutterhead. With this in mind the classification requirements can be modified such that, rather than absolutely identifying the absolute cause, which can lead to potential errors in classification where two cases can lead to the same surface waveform;

1. Proud knife in position one and short knife in position three.
2. Out of balance mass located at knife one

To a classification of the corrective action;

1. Lift at position one and plunge at position three

This type of technique reduces the possible number of classifications, but does reduce the ability of the user to have a definite cause of the cutterhead inaccuracies. If this can be made to generate separation of the datapoints between the different classification regions the classification success may be improved, as shown in Table 7-8.

Table 7-8 - K-Nearest Neighbour Classification Success Based on Modified A-Priori Knowledge Base

k	Majority Case % Correct	Distance Weighted (1/d) % Correct	Distance Weighted ($1/d^2$) % Correct
1	82	81	81
3	89	86	87
5	97	96	97
Full Dataset	99	100	99

It was again noted that errors occurred when the test node were on the border of the classification region area. Within the dataset not all regions were possible to separate but the reversed approach to the classification has made a significant improvement to the performance of the system.

7.6 Conclusions

This chapter has briefly described the vision system employed within this research. The principal component technique of data size reduction has also been explained, as has the data shape and size produced by the technique. This data has been used as a form of a-priori knowledge base for a number of different classification techniques successfully. Based on the final use of the classification result, and using the important observation that for the rotary wood planing process both defects under investigation are overcome using the similar actions, the vertical movement of the cutterhead, a reversed method of interpreting the data has been used to further improve the system performance.

The following chapter describes how the classification results are utilised and the novel approach employed to maintain a high quality surface finish on the machined timber surface in real time.

8 Chapter 8 – A New Approach, Subtle Changes

This chapter describes a new heuristic subtle change approach to control the reference signal for the controller. The approach described uses a-priori knowledge about both the rotary wood planing machine and the cutterhead geometry. A-priori knowledge regarding previous experience of the cutting process is also used. If therefore this a-priori knowledge is not known, or proven to be incorrect, this approach may fail to generate a correct reference signal. However these requirements do not render the approach useless for other applications. The approach can be modified to be applied to other machining and manufacturing processes with suitable a-priori knowledge.

In this application, the geometry, in simple terms, of the cutterhead must be known. For the test shown within this thesis the cutterhead has four cutting knives spaced equidistantly around the circumference of the cutterhead, as shown in Figure 8-1.

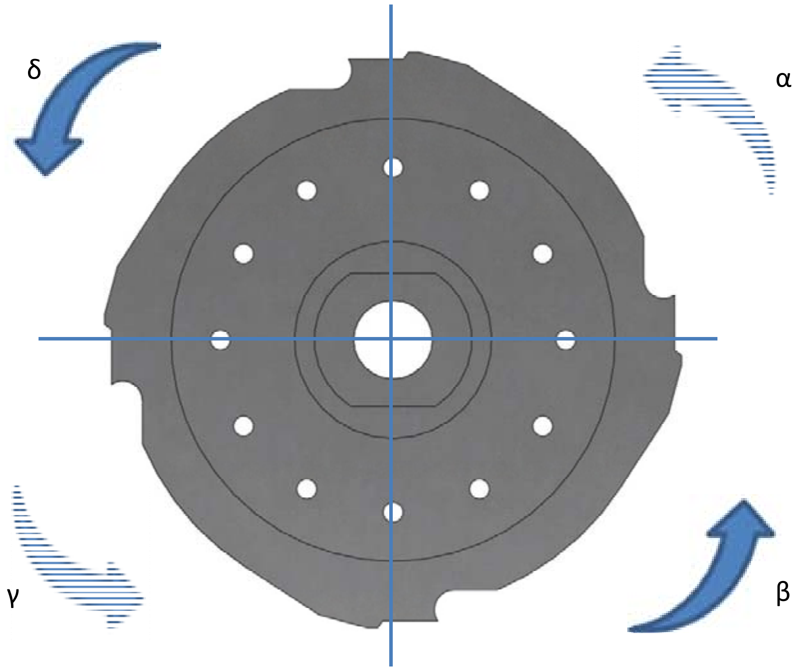

Figure 8-1 - Example Cutterhead Geometry

Where;

$\alpha=\beta=\gamma=\delta=90°$

The exact radius of the cutterhead and knives need not be known accurately, as long as the difference between the radii of the different knives is within the movement limit of the actuation technique, in this case the piezo actuators. One goal of this technique is to overcome the differing radii of the four cutter knives whilst producing a higher surface timber finish.

8.1 Corrective Action Complication

This section will describe some of the complications associated with the application of corrective action on the rotary wood planing machine.

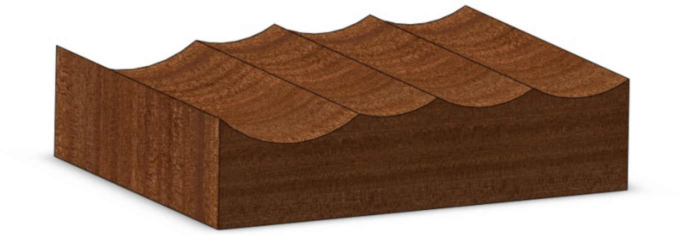

Figure 8-2 - Example Timber Surface Cut with a Single Proud Knife on a Four Knife Cutterhead

If presented with the surface profile in Figure 8-2, and with a-priori knowledge concerning the number of knives on the cutterhead, it can be deduced that the surface profile is the result of a single proud knife around the four-knife cutterhead. However, to apply the correct corrective action to lift the proud knife such that an ideal surface profile is produced, a link needs to be generated between particular knives to particular cuttermarks. Without this link the definite solution allowing the correct corrective action to be applied cannot be found and there is a 75% chance of applying the corrective action to an incorrect knife.

In some applications known datum points or fiducials are present which aid in positioning, such as printed circuit board manufacture. These allow vision systems to take corrective action for board positioning tolerance errors. This type of solution is not utilised for rotary wood planing machines, as it would require the production of another, possibly unwanted, surface feature, such as a notch, to identify and link the cuttermarks to particular cutting knives. Using the test rig at Loughborough we could accurately locate the timber edge using the rotary encoder within the motor, and the cutterhead using the rotary encoder in the motor. Using these two positions it would be possible to create the link between the knives and cuttermarks by counting the cuttermarks from the edge. This type of approach however is not suitable to a production machine as it would require time consuming setups of the timber which would reduce the amount of timber produced across a production time. Therefore a more intelligent approach is sought in order to match the cuttermarks to particular knives through a mix of a-priori knowledge and knowledge created in real time.

8.2 Generation of Further Data in Real Time

The approach described later in this chapter, section 8.4, relies upon the generation of further data in real time mixed with a-priori knowledge concerning the cutterhead geometry. Using these two data streams allows the generation of suitable corrective action, in the form of a reference path, and then applied to the controller to position the cutterhead.

Although the initial defect cause may not be fully identified, the positions of the knives around the cutterhead does not alter during the cutter process. At the core of this approach is the concept that making a subtle change to the reference path, and therefore to the cutterhead rotation centre, will attempt to generate a known link between particular knives around the cutterhead and specific cuttermarks on the timber surface.

However, altering the centre of rotation position of the cutterhead may potentially have a negative effect on the machined timber surface, if not moved in line with the geometry of the cutterhead. In order not to generate quantities of waste timber, these trial modifications of the reference path need to be within the allowable tolerance of wave pitch, but remaining large enough to be easily distinguishable from any run-out of the cutterhead.

8.3 Requirements for Subtle Change Approach

In this application, rotary wood planing, the overriding requirement, for the subtle change approach to operate correctly, is that the system operates in a repetitive manner, both in the depth and pitch of the cuttermarks on the timber surface, given a stable reference path to the controller, Figure 8-3.

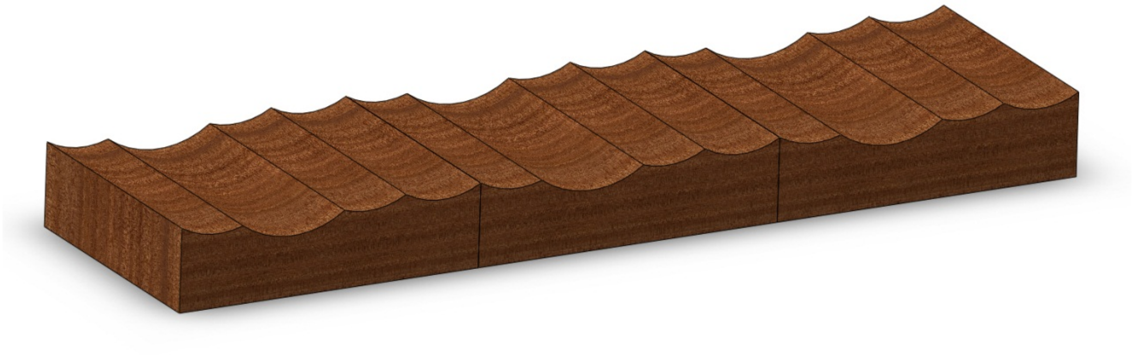

Figure 8-3 - Required Repetitive Cuttermarks on Timber Surface

Figure 8-3 shows an example of this repetitive requirement. This is an example of a four knife cutterhead with a single proud knife. The approach relies on the repetitive action of the process in order to generate accurate additional information about the cutterhead in real time. If, for example, the surface form in Figure 8-4 were cut into the timber surface, attempting to identify the surface defect corrective action, through the generation of a suitable reference path, and therefore cut a higher surface quality into the timber, becomes far more difficult.

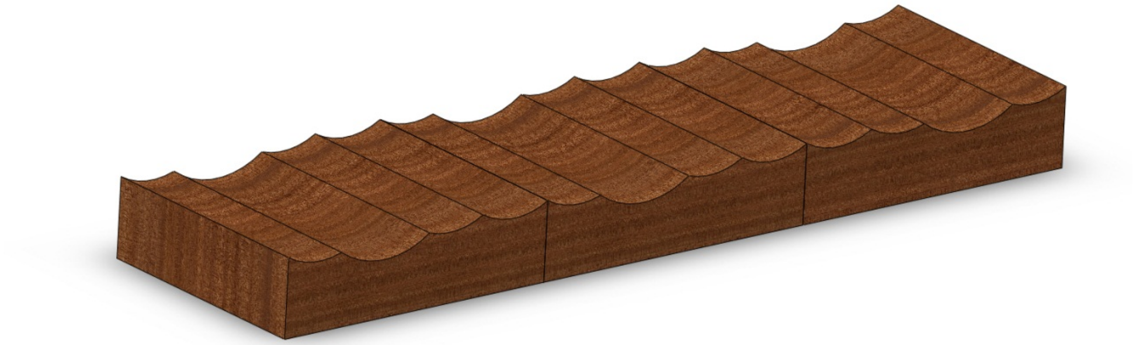

Figure 8-4 - Non Repeating Surface Form

If this application is transposed to other rotary applications, such as metal grinding, this requirement also holds true. However, the technique, in principal, can be applied to other applications where this is no longer a requirement. This is discussed in more detail in section 8.6.

8.4 Principal of Subtle Change Technique

This section describes briefly the steps involved in this subtle change approach.

Step 1:- Carry out cutting operation with ‘zero reference path’. A zero reference path is a path with zero amplitude such that it does not affect the cutterhead path.

Step 2:- Carry out surface waveform analysis and save result to memory with a note of reference path.

Step 3:- Modification of reference path such that knife 1 is displaced a known level (+10μm)

Step 4:- Carry out new cutting operation with new reference path

Step 5:- Carry out surface waveform analysis and save result to memory with a note of reference path

Step 6:- Can the change be identified? If yes, carry out appropriate modifications to reference path to counter original defects, and carry out new cutting operation, carry out surface waveform analysis and inspect new surface. If no go to step 7.

Step 7:- Modification of reference path such that the subsequent knife is displaced a known level (+10µm). Go to step 5.

A flow diagram of this new approach is shown in Figure 8-5.

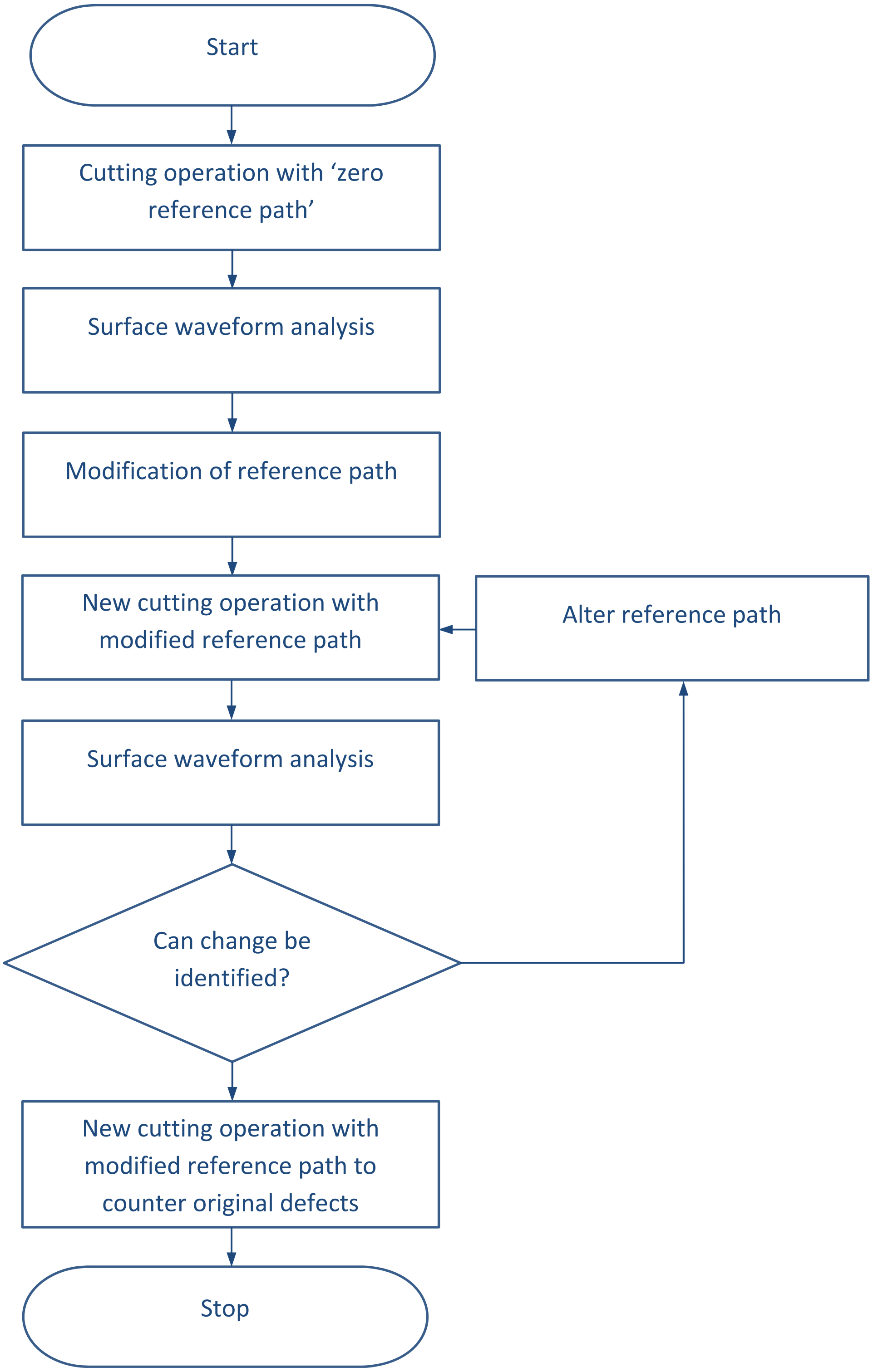
Start
Cutting operation with 'zero reference path'
Surface waveform analysis
Modification of reference path
New cutting operation with modified reference path
Alter reference path
Surface waveform analysis
Can change be identified?
New cutting operation with modified reference path to counter original defects
Stop

Figure 8-5 - Flow diagram of heuristic approach

The crux to this approach is that both knife run-out and out of balance forces on the cutterhead or drivetrain, causing oscillation of the cutterhead, or external forces, are all countered through the same correction action, vertical movement of the centre of rotation of the cutterhead. Section 6 described a system of defect classification and a modified system outputting the type of action required to overcome the defect, without actually identifying the actual defect cause, such as;

“Lift knife 1 & plunge knife 3”

Rather than

“Out of balance mass at knife 1” or “Proud knife 1 and shallow knife 3”

This simplification to the analysis of the surface waveform classification also simplifies the subtle change technique, in that the full description of the cause of the defect needs to be transposed to a corrective action, but this step is no longer required. It does however mean that as an operator the full cause is no longer known, but a second classification technique, operating in parallel may be used to inform the operator independently of the system used to pass information to this approach.

This approach can be said to be iterative, depending on the geometry of the cutterhead. Steps 5 to 7 may be looped around a number of times, until the system can identify a link each knife to a particular cuttermark. Once this link is made, the system is able to apply corrective action to the cutterhead through the generation of a suitable reference signal.

8.4.1 Step 1 – Initial Cutting Test

This first simple step in the process is to perform a cutting test without any displacement of the cutterhead via a modified reference path.

8.4.2 Step 2 – Initial Surface Waveform Analysis

This step of the process allows a fuller understanding of the cutterhead, including, although not distinguishable from, any vibration input into the cutterhead and/or system as a whole. A note of the reference path is also made. In certain conditions, such as when iterating through the scenario for a second time due to unknown heights of the cuttermarks, the initial cut may be made with a previously generated reference path. In this scenario this reference path is made known as the default unmodified reference path.

8.4.3 Step 3 – Modification of reference path

A modification is made to the reference path. This modification is to a single cutting knife around the cutterhead, when compared to the default reference path. The position of the modification is known, such that the knife number that is plunged deeper into the timber surface is known. This will allow for a partial discreet match between the initial machined surface and the secondary machined timber surface to be found

8.4.4 Step 4 – Second Cutting Test

A secondary cutting test is then carried out. This test uses the modified reference path, with a single knife plunged deeper into the timber surface.

8.4.5 Step 5 – Secondary Surface Waveform Analysis

The secondary timber surface is then analysed and the defect classified. The defect classification when combined with the previous defect classification and the known changes to the reference path, will potentially allow the link to be found.

8.4.6 Step 6 – Identification and Generation of Link

Step 6 is the key novelty to the approach. Although this approach is based on pattern matching between two surface profiles, this implementation within this body of work is purely a logical implementation. The inputs to this body of research, from the previous steps, are the outputs from the defect classification.

‘Plunge Knife 1’

‘Lift Knife 2’

The approach, as implemented here, uses these output phrases to generate idealised defective surface forms. Figure 8-6 gives an example of these idealised surface forms.

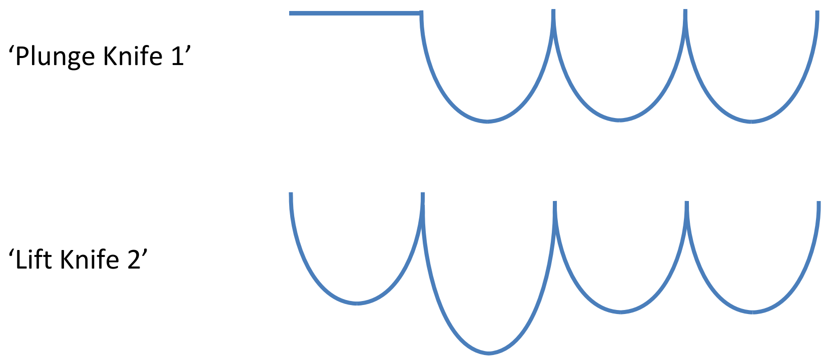

Figure 8-6 - Example Idealised Surface Defects

Using a series of case based arguments the logical heuristic approach will ascertain whether a link between cutting knives and cuttermarks can be made. If this link can be made, the known change to the reference path will be the cuttermark position that does not overlap between the two surface profiles.

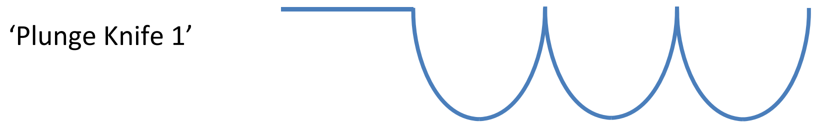

Figure 8-7 - Example Initial Surface Form

Using the surface plots in Figure 8-7, the initial defect classification would have returned;

‘Plunge Knife 1’

It is key that the system will provide the same classification if any of the four cutting knives require plunging.

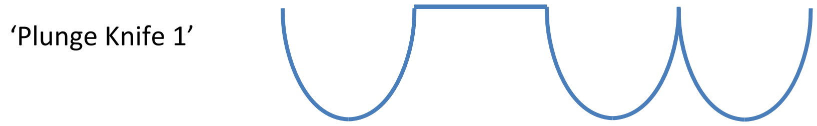

Figure 8-8 - Plunge Knife 1 Surface Defect Example

In order to generate the required link between specific cutting knives and their cuttermarks, a single discreet position of overlap must be found.

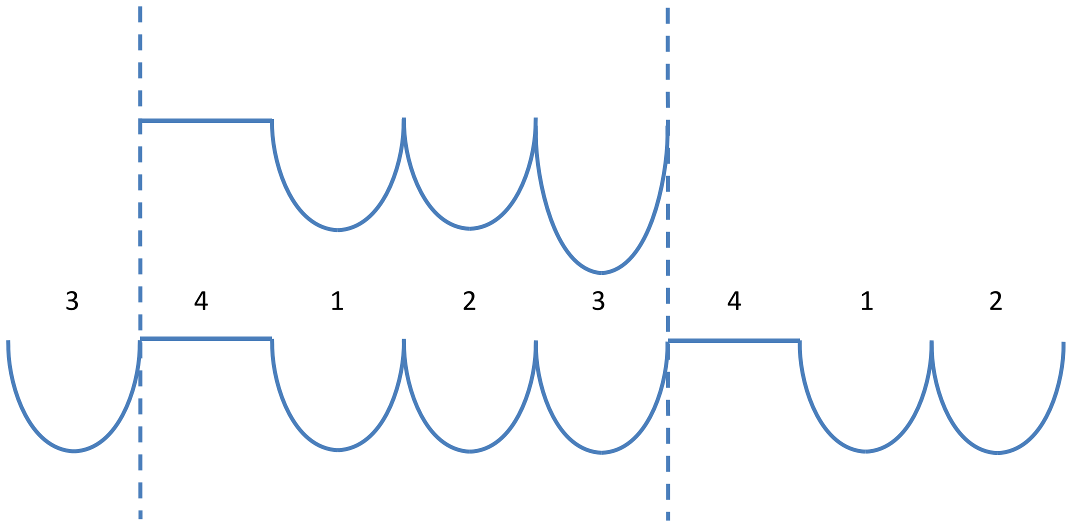

Figure 8-9 - Matched Idealised Surface Defects

In Figure 8-9 the only cuttermark that does not match between the original surface profile, lower profile in figure, and the changed reference path profile, upper profile in figure, is the cuttermark for the knife where the displacement was modified by the reference path, cutter 3 in the classification profile in Figure 8-9, although the actual knife modified by the reference path was knife 1. There are no other positions where the upper profile can be matched to the lower profile. This allows a definite link between cuttermarks and cutting knives to be created.

Once this link has been made, the original surface profile is re-evaluated. During this re-evaluation however the relative surface heights are measured. Due to limitations with the WSMS system, relative heights of the surface waves are given rather than absolute heights. Once measured the heights are scaled such that the maximum displacement is 7µm. This value has been arbitrarily selected based on experience with the system.

In Figure 8-9 the new reference path link would be calculated as follows;

- Matched knife through classification is knife 3, K_{mc}
- However the knife displacement modified through the modified reference path is knife 1, K_{mp}
- Therefore actual knife numbers are $K_{act} = K_{mc}+(K_{mc}-K_{mp})$
- Therefore the knife that originally required plunging is 4+(3-1) = 6. Which due to a four knife cutterhead the actual knife is the remainder when all complete revolutions are removed, which in this case is 2

8.5 Potential Complications

This section of text describes some potential complications of the approach as it has been implemented here. Some of these complications are brought on by limited information about the timber surface, such as the depth of the cuttermarks, whereas other complications are part of this new approach, such as the high dependency on the accuracy of both the measured timber surface and the classification of the defects.

8.5.1 Measurement Dependency

At this stage of development this approach relies heavily on the surface measurements. The surface measurements are key to the successful deployment of the technique and are used both at the initial stage and throughout when matching cuttermarks to particular knives. If the surface measurement technique, here the stereoscopic vision system but on other applications contact methods may be more appropriate, fails to give reliable data, then the algorithms underpinning the approach may not be able to generate a suitable reference path to produce the desired timber surface finish.

8.5.2 Lost Links

Once the system has overcome any cutterhead inaccuracies and/or out of balance forces and the desired surface finish is produced, if a knife wears or the system changes, the entire process of generating the link between knives and cuttermarks, through known subtle changes, is required to repeat. At this stage of development it is not possible to instantly isolate the cause behind the generation of the new defect.

8.5.3 Number of Knives Around the Cutterhead

A further complication is linked to the number of knives around the cutterhead. As the number of knives increases the number of possible outcomes from a single subtle change increases and the possibility of not generating the required link between cuttermarks and knives may not be created. If the cutterhead has two knives and the original surface profile indicates that knife A is required to be plunged, there is a 50% chance that the knife required to be plunged is in position 1. If a reference path plunges knife 1 and the surface form is improved then it holds that it was indeed knife 1 that needed to be plunged. If however the surface waveform is not improved then it holds that the knife that requires plunging was actually knife 2. Therefore a single change is able to generate the required link.

8.5.4 Missing Cuttermarks

The system currently uses the input from the defect classification. If however a cuttermark is cut out by a subsequent knife, due to a large run-out on that particular knife, the defect classification technique will not be able to classify the surface profile correctly, as one of the cuttermarks will be missing. This is currently only a complication due to the classification a-priori knowledge base method of organisation. In principal the pitch of the cuttermarks could be measured, which would highlight that one of the cuttermarks was significantly larger than the others. The heuristic approach could then be implemented as usual. Once the link had been created, there would then be a 50% chance selecting the correct knife to lift. There would be no way, currently, of recognising, for example, if knife three had cut out knife four, or if knife four had cut out knife 3. However in order to overcome this a further iteration can be carried out in order to check if the first knife lifting selection is correct.

8.5.5 Input Geometry

However if the cutterhead holds four knives, then the number of possible outcomes increases to four, Figure 8-10

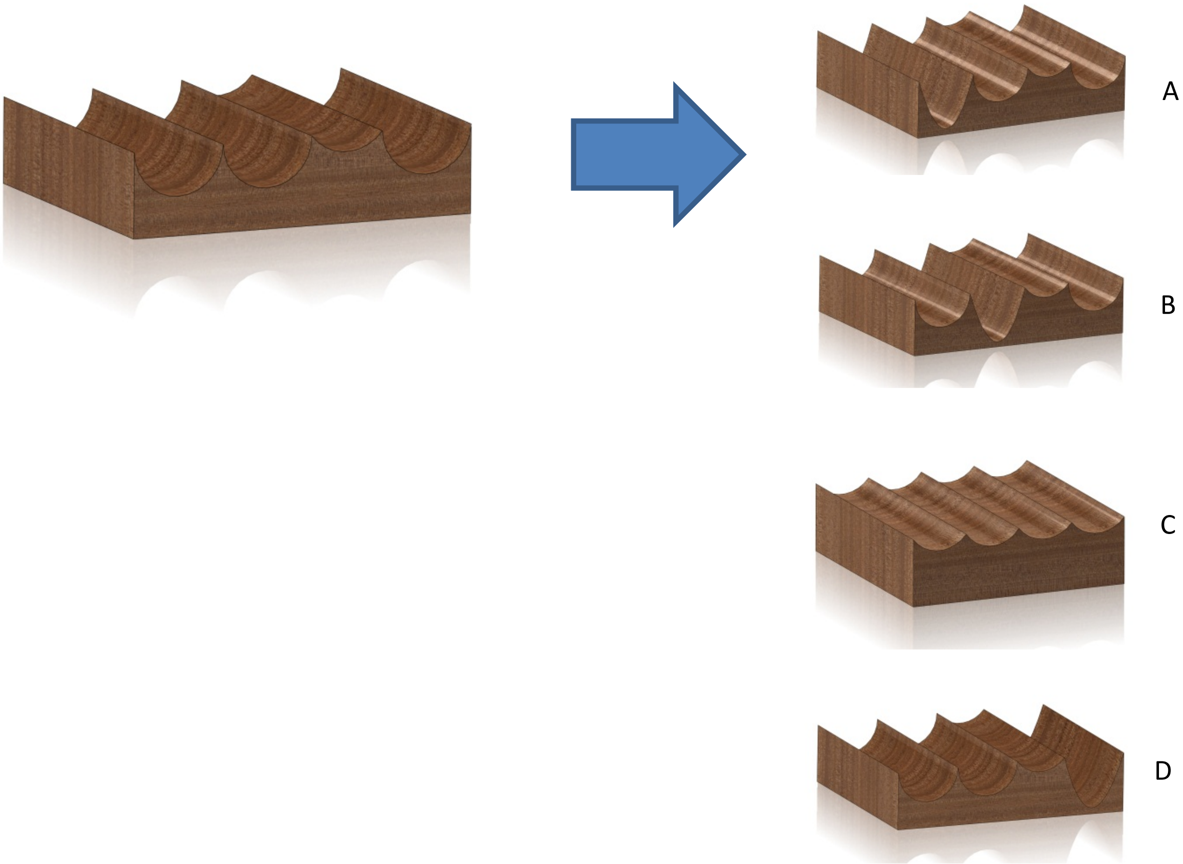

Figure 8-10 - Possible Surface Forms Produced By a Single Plunged Knife Reference Path

Figure 8-10 shows the outcome of a single knife plunge type reference path, given the single shallow knife shown on the right hand side of the figure. Each of the outputs, A, B C and D, represent a different reference path, each plunging a different knife. In this example all of the four reference paths result in a link between cuttermarks and knives.

If output A is measured, it is clear that the reference path is plunging the incorrect knife as the surface form is not an ideal profile. However, using the known geometry of the cutterhead, the deepest cuttermark is opposite, on the cutterhead, the original shallow knife, which allows an accurate reference path can be created, where the correct knife is plunged deeper into the timber.

If output B is measured, again it is clear that the original reference path is not plunging the correct knife into the timber. Again, however, the surface form, when combined with the known cutterhead geometry, is sufficient to create a new reference path to overcome the cause of the surface defects, assuming the level of plunge is within the capabilities of the rig. The knife that has been plunged into the timber is the knife preceding the knife that caused the original shallow cuttermark. Therefore a modified reference path plunging the knife following the original plunged knife should be used to improve the surface profile.

If output C is measured, an ideal surface profile, the most likely reason is that the original subtle change to the reference path, is aimed at the correct knife. At this point the depth of plunge of the knives needs to be altered to generate the most ideal surface form possible.

If output D is measured, the opposite situation to that as if output B is measured, in that the reference path has not plunged the correct knife, but the knife plunged into the timber in this case is the following knife, rather than the preceding knife in output B, to the knife which is producing the shallow cuttermarks.

Therefore, for the input profile as that in Figure 8-10, all possible single knife subtle changes to the reference path result in the required link between cuttermarks and particular knives. However this is not always the case.

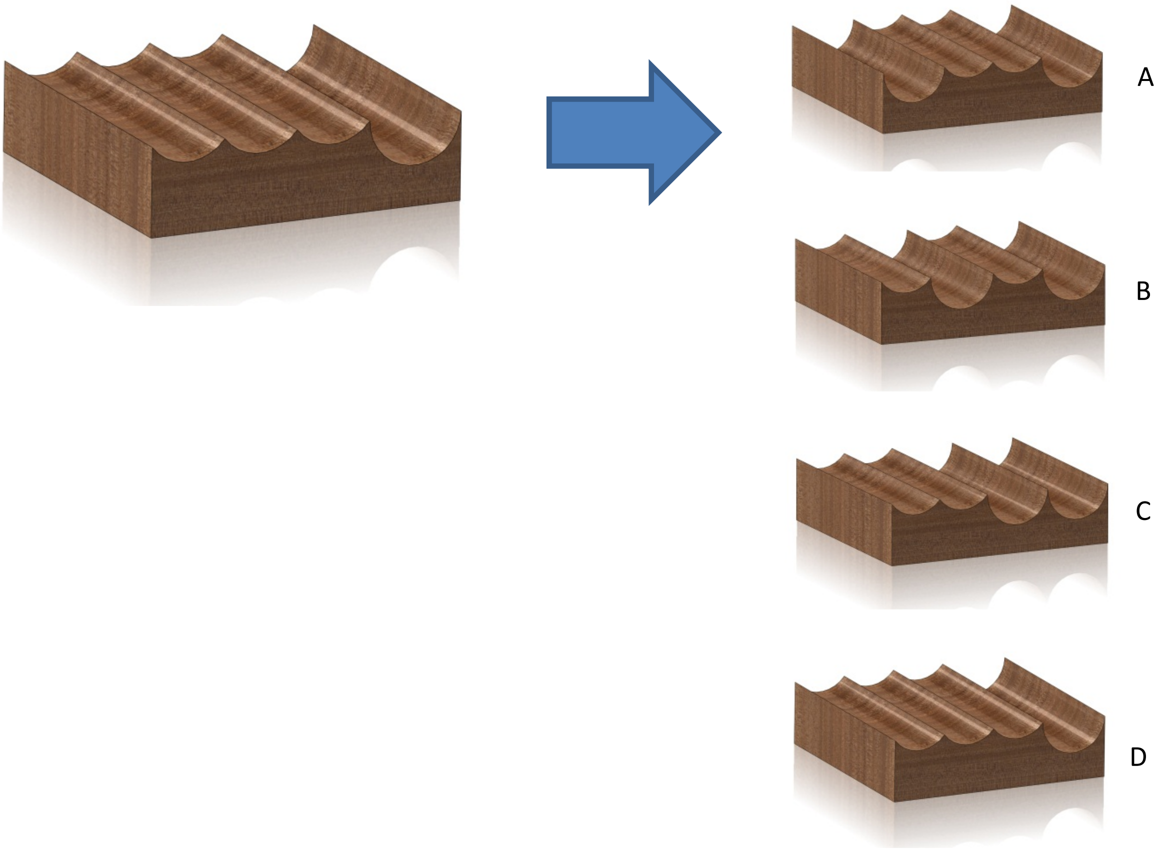

Figure 8-11 - Further Possible Surface Forms Produced By a Single Plunged Knife Reference Path

Using the input surface profile from Figure 8-11 a differing scenario is played out.

If output A is measured, due to the repetitive nature of the rotary planing technique, a link between the cuttermarks and articular knives cannot be made. Although at first glance it would appear that it can be, Figure 8-12 shows the surface form based on output A. Based on this surface profile, it is not possible to ascertain whether the knife plunged is the knife before or after the original deep cutting knife. In this case a different subtle change is required to generate the required link.

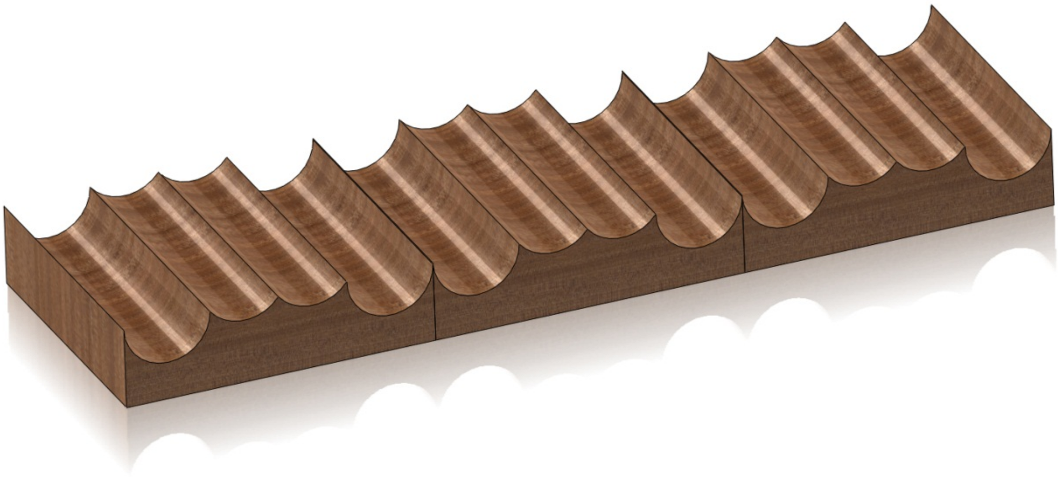

Figure 8-12 – Timber Surface Based on Output A

If the surface profile measured is similar to output B, a similar situation to output A from Figure 8-11 is reached. The new surface profile, when combined with the a-priori knowledge of the cutterhead geometry, is able to generate the required link between cuttermarks and particular knives. The change to the surface profile indicates that the knife opposite, when using a four knife cutterhead, the original proud knife is now producing deep cuttermarks. This allows a new reference path to be generated to lift the original proud knife.

If a surface profile similar to output c is measured, the actual full surface profile will be similar to that in Figure 8-12, and the same reasoning as for a surface profile A holds true, and the different subtle change to the reference path needs to be used to generate the required link.

If the surface profile measured is similar to output D, similar to the original surface form, then the conclusion drawn is that the knife that has been plunged into the timber surface, was the same knife as the originally proud knife. Assuming this conclusion then a modified reference path can be generated and implemented to lift this knife, and generate an improved timber surface quality.

For these two different input surface forms, there are differing levels of success for the four, based on a four knife cutterhead as in Figure 8-1, different possible subtle changes using the reference path. In principal the maximum number of required subtle change is as follows;

$$c = n - 1 \tag{8-1}$$

Where;

c = maximum number of subtle changes

n = number of knives

This equation assumes that all knives cuttermarks are clearly visible and subsequent knives have not cut out any cuttermarks. If this is the case the current solution will not succeed in generating the required link between particular knives and their cuttermark, as the assumption is that all knives generate a particular cuttermark on the timber surface.

8.5.6 Knife Displacement Magnitude

A current complication of the approach concerns the actual knife displacements and their effect on the approach. The WSMS does not give actual heights of the waves on the surface form, rather it produces relative heights. Although the approach is able to overcome, after a number of trials, the differing wave height complications, it does have to do this in an iterative approach, rather than creating an ideal solution initially.

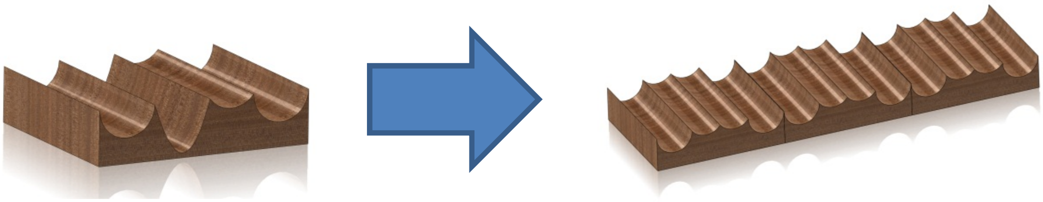

Figure 8-13 - Knife Displacement Complication Example

Figure 8-13 gives an example of this type of complication. In this example a link exists between particular knives and their cuttermarks already. If the knife creating the second cuttermark was lifted by 10µm and the knife cutting the fourth cuttermark was lifted 5µm, the output of this operation may be that shown. In this example the link that was initially created between particular knives and their cuttermarks, has now been lost. This is indeed the case for almost all operations of the principal on the cutting operation after the link has been sought. In some cases, where for example three knives are at exactly the same radius, if the resultant surface form shows a single proud or shallow knife, it holds that this cuttermark is still being cut by the originally different radius knife. This loss of the link however can be overcome by iterating through the deployment procedure a number of times, however on subsequent iterations, rather than initially running with a zero magnitude reference path, the resultant reference path from the previous iteration is used, and the subtle changes are mapped onto this reference path. If however the measurement system was capable of producing absolute waviness height, rather than relative height, this prolonged operation would contract down to simply generating the link and then applying a reference path based totally on actual waviness measurements.

8.6 Alternative Applications for the Technique

An important aspect to this approach is the ability to implement it onto other applications. As the approach has been developed on a rotary wood planing machine, the most obvious alternative applications are those with a similar operation, such as surface grinding of metals.

8.6.1 Rotary Machining Applications

The current solution has been developed on a rotary wood planing machine, and in this case the majority of work has been carried out using a four knife cutterhead. However, this approach can be applied to other rotary machining processes, such as conventional milling of materials, dependant on cutter geometry, and surface grinding. Figure 8-14 shows a comparison between the four-knife cutterhead used within this research, and a generic grinding wheel.

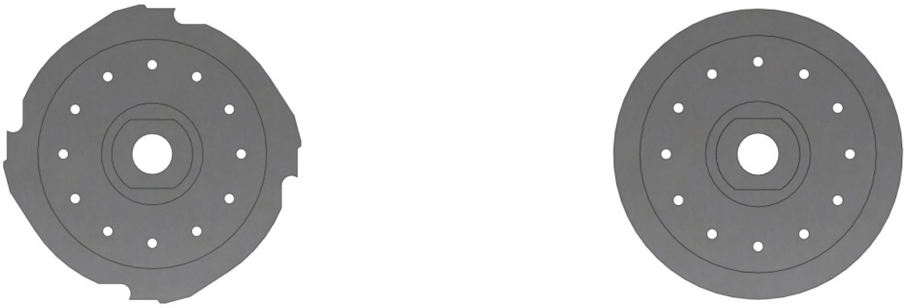

Figure 8-14 - Comparison Between Discrete and Non Discrete Cutting Positions, Left - Wood Planing Machine Four Knife Cutterhead, Right - Surface Grinding Wheel

A major difference between the two 'cutterheads' is in the nature of the cutting surfaces. In the wood planing cutterhead there are four discrete cutting surfaces, the knives, whereas the entire circumference is the cutting surface in the grinding wheel. The current implementation of this approach would not work due to the lack of discrete locations of the knives. However with some small modifications these issues may be overcome. As a potential solution to this issue, the grinding wheel could be artificially split into sections and treated as having discrete cutting surfaces and then using the approach as described in this chapter.

8.6.2 Further Applications

However, other non-rotary machining applications could have similar approaches implemented, or aspects of this approach implemented to achieve separate goals. An example of this would be the application of pushing a subtle change in order to generate further data about the process, when combined with an a-priori knowledge base, in real time could be the a robotic system picking parts from a specific parts from a bin of random of parts. In this case the principal of generating additional information in real time is exploited, perhaps by the robotic system disturbing the parts within the bin in order to allow further information, perhaps regarding position and orientation, to be gained through the use of a vision system.

If the robotic system utilised a vision system to detect features on the parts within the bin. These features could then form the input to a classification system using the a-priori data to match these features to known parts. However if no parts can be successfully detected a solution may be to change the image viewed by the vision system in order to generate new data regarding the parts within the bin. In order to do this, the solution may involve disturbing the bin of parts.

A further application of this type of technique could involve overcome drift within a system, where sufficient changes are available to change specific system parameters. This drift may be due to temperature changes or wear of components, but if only the output is easily measurable, rather than all the components and individual sub operations. In this case, subtle changes could be applied to individual processes and the changes to the final output measured. This type of application could involve almost any machining operation where there are numerous system parameters.

A key requirement, due to the iterative nature of the approach, is that there is accurate feedback, such that small changes to the system parameters can be measured. If these small changes cannot be measured consistently then the system will not be able to accurately apply changes to improve the output quality, through a combination of the additional short term knowledge and the a-priori knowledge.

9 Chapter 9 – The Connected Solution

This chapter describes how the different work packages carried out in this research fit together and shows two different cutterhead examples, a two knife cutterhead and a four knife cutterhead. Each step of the process is briefly described and any parameters generated shown.

9.1 Two Knife Cutterhead

The first example is the simple case of a two knife cutterhead. Although this is a trivial case in terms of the application of the correct compensation, but it shows the versatility of the system to cope with multiple different cutterheads.

9.1.1 Cutting Parameters

The initial stage within this adaptive rotary timber machining process is the selection of the cutting parameters. Often an important characteristic is the pitch of the waves on the timber surface. In this two knife cutterhead example, due to a large TIR of 70µm, measured with a dial gauge rigidly mounted onto the cutting guard, the pitch was set a 5mm. With a lower value for the pitch , the finish on the timber surface would become a single knife finish as the proud knife would remove the cuttermarks created by the shorter cutting knife. To achieve this desired pitch of 5mm, a cutting speed of 1200rpm was selected and a timber feedspeed of 200mms^{-1} were used.

9.1.2 System Identification

The following step is to carry out the system identification, as per section 6.2. This generates a state based model of the system which is used within the LQG controller designed by (Ogun 2012).

This state based model, combined with the cutting parameters are passed to the neural network described in section 1. This network output the values of Q and K_{ff}, which are also passed to the LQG controller in order to achieve optimal reference path tracking.

9.1.3 Initial Cutting Test

An initial cutting test is then carried out. The result of which is shown in Figure 9-1. Here it can be seen the effect of a non-optimised reference path.

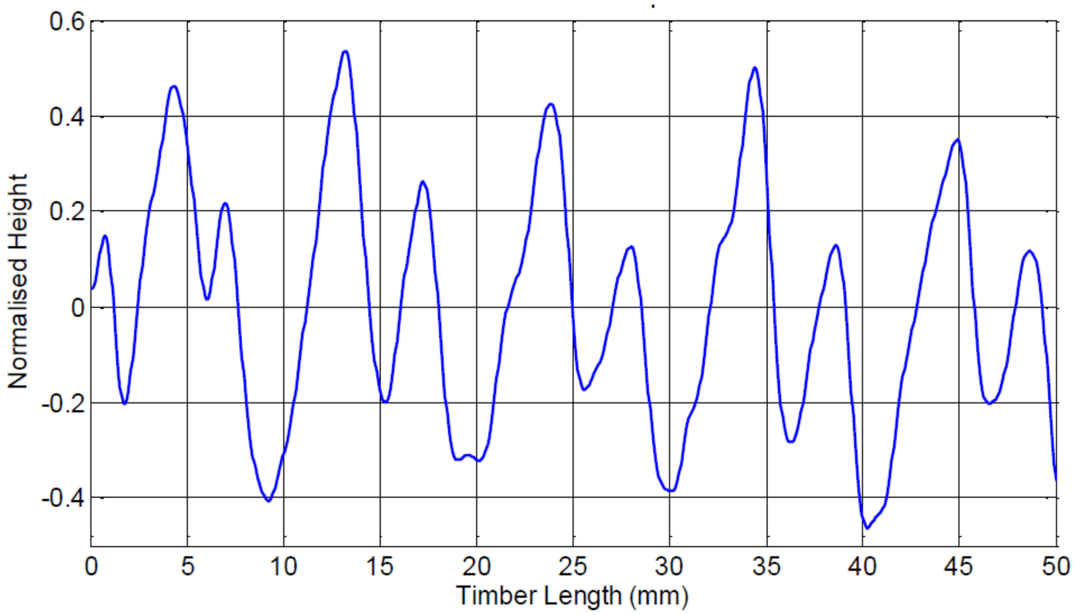

Figure 9-1 - 2 Knife Cutting Test without Compensation

A principal component analysis is then carried out and the results passed to the defect classification technique. The result of this classification is

---

‘Plunge Knife 1’

This is of course not surprising, and is actually the only response available. It may be that the required technique is actually to plunge knife 2, but there is no link between the knives and cuttermarks in order to distinguish between knife 1 and knife 2.

9.1.4 Heuristic Approach

Using a two knife cutterhead actually complicates the approach described in chapter 8. As there are only two cutting knives, in order to make a suitable link between cutting knives and cuttermarks, for this specific case only, the depth, or relative depth, of the cuttermarks alone is used to isolate the change to the reference path. A known knife is plunged deeper into the timber surface and this change will show in the relative heights of the cuttermarks. Once the link has been found corrective action is applied through the reference path. Figure 9-2 shows the final surface form once corrective action had been applied to the cutterhead. Knife 1 was lifted 18µm and knife two plunged 18µm. Although this was not enough to counteract the TIR of the cutterhead, it is the maximum displacement allowable by the piezoelectric actuators and the arrangement employed in the small scalar planing machine. However the surface profile is significantly improved over the initial surface profile.

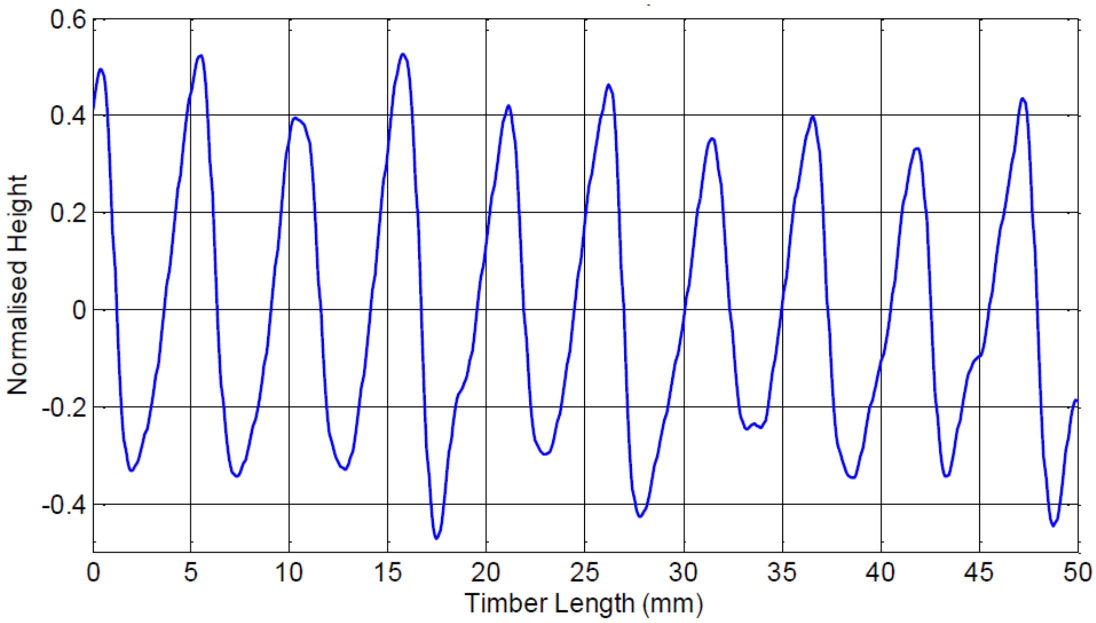

Figure 9-2 - 2 Knife Cutting Test with Compensation

9.2 Four Knife Cutterhead

The second example is that of a four knife cutterhead. The processes are the same as for the two knife cutterhead, however the cutting parameters are different. During the four knife cutting tests, due to an on-going upgrade of the WSMS system, to measure the timber surface, an Alicona Infinate Focus Machine was used, see Appendix B for further details.

9.2.1 Cutting Parameters

In this four-knife cutterhead example the aim pitch is 2mm. To achieve this pitch a cutterhead rotational speed of 4000rpm has been chosen, and a feedspeed of 533mms^{-1} has been calculated.

9.2.2 Initial Cutting Test

Figure 9-3 is the resultant surface profile from the initial cutting test.

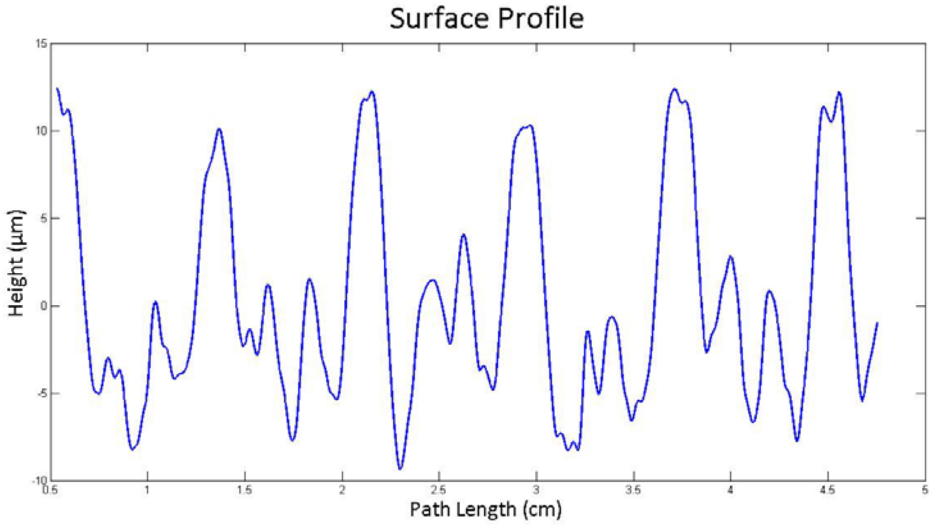

Figure 9-3 - Initial Cutting Test Surface Profile

9.2.3 Heuristic Approach

The surface profile shown in Figure 9-3, returned from the defect classification;

‘Plunge Knife 1, Plunge Knife 2, Lift Knife 3’

In order to gain an understanding of which knives around the cutterhead these are the heuristic approach was implemented. The first change to the reference path simply plunges and arbitrary knife, knife 3. The resultant surface profile is shown in Figure 9-4.

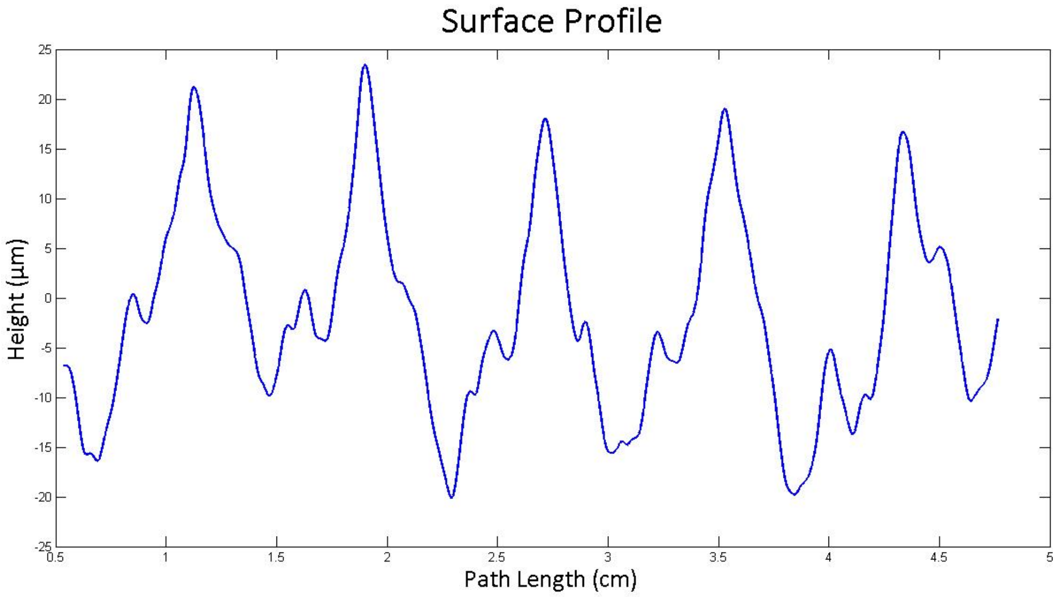

Figure 9-4 - Surface Profile with Knife 3 plunged 14µm

Using this surface profile, when combined with the original surface profile a link could be made. The result from the defect classification was as follows;

‘Plunge Knife 1, Lift Knife 3’

At this point the link between cuttermarks and knives could be made. The final reference path used became;

[0, -0.012, -0.002, 0.001]

As the timber surface was measured using an Alicona measuring device, rather than relative surface heights, absolute heights are provided. This did reduce the complexity as rather than iterating through the process in order to achieve optimal displacement levels, the levels were able to be simply read from the plots.

Figure 9-5 shows the final machined timber surface.

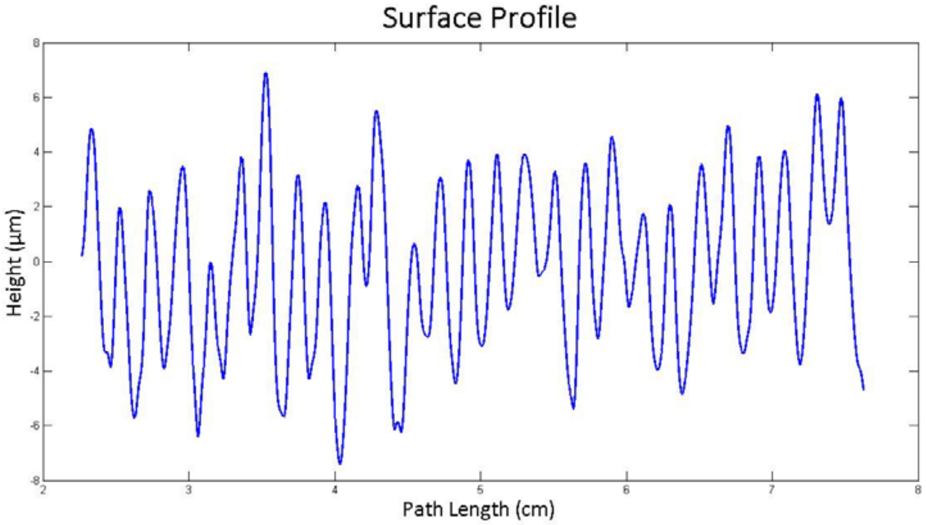

Figure 9-5 - Final Machined Timber Surface

9.3 Surface Quality Assessment

In order to assess the surface quality of the timber surface, a simple standard deviation test is carried out.

$$SD = \sqrt{\left(\frac{1}{N_c}\sum_{i=1}^{N_c}(S_i - \bar{S})^2\right)} \qquad (9\text{-}1)$$

Where

N_c is the number of cuttermarks

$\bar{S}$ is the desired waviness pitch

S_i is the width of the ith cuttermark

The aim of the technique is to achieve a lower standard deviation, indicating that the cuttermarks are close to the desired pitch. A lower standard deviation indicates a higher quality surface finish of the timber.

Table 9-1- Standard Deviation Results

Surface	Standard Deviation (mm)
Uncompensated four-knife cutterhead	1.26
Compensated four-knife cutterhead	0.25

The results shown in Table 9-1 show that the system has been able to generate a reference path that significantly improves the surface quality of the machined timber surface.

10 Chapter 10 – Conclusions and Recommendations

A novel new machining control architecture has been created in this thesis. This new architecture, and the control strategies within the architecture, is capable of improving the surface finish of machined timber. The particular successes in this thesis are given below.

10.1 Achievements from Aims

For clarification, the achievements have been split into sections according to the aims previously set out in section 1.3.

10.1.1 Test Rig Upgrade

The existing small-scale planer test at Loughborough has been upgraded and expanded. The improvements are listed below;

- Increased rotational speed range of cutterhead to a maximum of 6000rpm
- Increased feed speed capability to a maximum of 1333 mms^{-1} allowing for a pitch of 1 mm at a cutterhead rotational speed of 6000rpm
- Fully integrated WSMS system to rotary wood planing machine, which allows for a timber surface to be measured whilst still being machined further
- Increased slide length to allow real time changes to parameters

10.1.2 Real-Time Controller Adjustment

Investigations into the effect of altering certain controller parameters to suit the current system operating conditions have been carried out. These have allowed for a wider range of operating conditions to be attainable based on the LQG controller employed within this work.

- Modification of the Q/R ratio alters the characteristics of between the rise time and the overshoot of the knife tip to a step change within the reference signal driving the cutterhead to the required vertical displacement to produce an increased surface quality.

- The effect of modifying the feedback gain of the controller has also been investigated.
- The data recorded from both the modifications to the Q/R ratio and the feedback gain has been used to create an a-priori knowledge base referencing the controller. This a-priori knowledge base has been used to create a neural network capable of specifying the parameters used within the controller that will produce the highest quality surface finish on the timber surface. These values also change with TIR of the cutterhead and the displacement caused by out of balance forces. This new network is capable of accounting for these different displacement requirements.

10.1.3 Defect Classification Software Tool Development

Two different defect classification techniques have been developed, a pattern recognition neural network and a K-nearest neighbors approach. Both techniques utilise an a-priori knowledge base using the output from a principal component analysis in order to reduce the data size. In order to increase the computation speed, rather than the inputs to these techniques being a plot of the surface form, perhaps consisting of many thousands of data points, a 3 by 3 matrix is used as the input. Both techniques performed successfully however the K nearest neighbor technique was able to correctly classify, when tested, the defects more accurately than the pattern recognition neural network.

However when the output was modified such that rather than outputting the cause of the defects, to a corrective action, the classification success increased. Both systems had an improved classification success when dealing with data sets towards the centre of spread for a specific condition. Due to the spectrum of input data, and certain levels of overlapping data, the success tended to drop at the edges of these groups.

10.1.4 Real-Time Reference Path Modification

A novel new approach to controlling the wood planing machine has been developed. Due to complications concerning the lack of information linking specific knives to their cuttermarks, the application of corrective action is difficult. The heuristic approach developed within this body of work is able to artificially force subtle changes to the timber surface. The subtle changes are produced at specific positions around the cutterhead, specific knives, and then using the surface form produced, combined with the original surface form, new information regarding the cutterhead and the run-out, or displacement produced by out of balance forces, can be attained.

This approach uses a logical heuristic approach, based on the knowledge and experience gained by the author during this body of work. Using this approach the limitations of the WSMS, the inability to measure the actual depth of the cuttermarks, can be overcome. A drawback of this approach is that the new information regarding the specific run outs of particular knives is potentially temporary knowledge. That is, due to the lack of absolute depth knowledge when a link between knives and cuttermarks has been made, and a full corrective reference path has been implemented, the link is lost and the approach has to iterate through once again.

10.1.5 Overall Assessment

In order to maximise the potential of existing wood planing machines, expand the operating scope of these machines and potentially increase the performance of other rotary machining processes a new active machining approach has been developed. This approach uses periodic real-time modification of the cutterhead trajectory to compensate for the cutterhead inaccuracies and vibrations. The system employs eddy current displacement sensors and piezoelectric actuators.

Experimental results show that the overall approach, and new control strategies, as well as the upgraded small planer test rig are capable of increasing the surface performance of the machined timber surface. The new approach is also capable of overcoming unknown run out values of a number of different cutterheads available to the research department. This new approach has direct benefits over the traditional jointing technique in terms of lower machining cost, increased performance and lower downtime of the machine due to the redundancy of the jointing process.

10.2 Recommendations for Further Work

The work carried out within this thesis has highlighted a number of areas of future interest. These areas of interest will benefit future development of this work but may also benefit others areas of research.

10.2.1 Measurement System

The current surface measurement system produces a surface plot, but with relative surface heights. Although this output form is suitable for defect classification, it does require the approach discussed in chapter 8 to iterate around a number of times in an attempt to overcome this inability. If the measurement system was capable of producing actual height data, the overall performance of the complete approach would be improved with a lower time to optimisation

10.2.2 Defect Characterisation

The approached employed to perform defect classification use the surface plot data, once a principal component analysis has been performed, to classify the defect. This may be continually employed during the cutting process, and the subsequent modification of control parameters will maintain optimal tracking performance of the set point at all times, giving a significant improvement over previous research work carried out in this area, (Elmas 2008).However certain defects can produce similar or identical surface profiles. These similarities in the data can lead to incorrect defect classifications. Further research in this area may be the most profitable area to expend research effort in order to achieve an improved overall system capability.

10.2.3 Heuristic Subtle Change Approach

The newly developed novel heuristic subtle change control technique employs a logical approach to generate the links between specific knives and their cuttermarks. Currently this approach has only been programmed to generate these links for a two or four knife cutterhead in order to prove out the technique. This has led to a relatively large programming overhead, which as the number of knives increases will become increasingly large. This may lead to slower system as the technique is coded to overcome rotary planing machines with high numbers of knives. Further research to reduce the overall code overhead may lead to a more practical implementation of the principals

11 References

ABDI, H. and WILLIAMS, L.J., 2010. Principal component analysis. *Wiley Interdisciplinary Reviews: Computational Statistics,* **2**(4), pp. 433-459.

ABELE, E., ALTINTAS, Y. and BRECHER, C., 2010. Machine tool spindle units. *CIRP Annals - Manufacturing Technology,* **59**(2), pp. 781-802.

ADKINS, C.A., ZHIMING HUANG, WONG, B.W., WALCOTT, B.L. and ROUCH, K.E., 1996. Active vibration control using an electromagnetic absorber with two degrees of freedom, *Southeastcon '96. Bringing Together Education, Science and Technology., Proceedings of the IEEE,* 1996, pp175-178.

ALTUG, S., 1999. Fuzzy inference systems implemented on neural architectures for motor fault detection and diagnosis. *IEEE Transactions on Industrial Electronics,* **46**(6), pp. 1069-1079.

AMEN, M., 2001. Heuristic methods for cost-oriented assembly line balancing: A comparison on solution quality and computing time. *International Journal of Production Economics,* **69**(3), pp. 255-264.

AMEN, M., 2000. Heuristic methods for cost-oriented assembly line balancing: A survey. *International Journal of Production Economics,* **68**(1), pp. 1-14.

AN, Q.L., FU, Y.C. and XU, J.H., 2011. Experimental study on turning of TC9 titanium alloy with cold water mist jet cooling. *International Journal of Machine Tools and Manufacture,* **51**(6), pp. 549-555.

ANDERSON, J.D., LEE, D.J. and ARCHIBALD, J.K., 2005. FPGA implementation of vision algorithms for small autonomous robots, D.P. CASASENT, E.L. HALL and J. RONING, eds. In: *Society of Photo-Optical Instrumentation Engineers (SPIE) Conference Series; Society of Photo-Optical Instrumentation Engineers (SPIE) Conference Series,* oct 2005, pp401-411.

ANDERSON, B.D.O. and DEHGHANI, A., 2008. Challenges of adaptive control–past, permanent and future. *Annual Reviews in Control,* **32**(2), pp. 123-135.

ÅSTRÖM, K.J. and HÄGGLUND, T., 2004. Revisiting the Ziegler–Nichols step response method for PID control. *Journal of Process Control,* **14**(6), pp. 635-650.

BALAZINSKI, M., 2002. Tool condition monitoring using artificial intelligence methods. *Engineering Applications of Artificial Intelligence,* **15**(1), pp. 73-80.

BEER, P., SINN, G., GINDL, M. and TSCHEGG, S., 2005. Work of fracture and of chips formation during linear cutting of particle-board. *Jorurnal of Materials Processing Technology,* **159**, pp. 224-224-228.

BRECHER, C., SPACHTHOLZ, G. and PAEPENMÜLLER, F., 2007. Developments for High Performance Machine Tool Spindles. *CIRP Annals - Manufacturing Technology,* **56**(1), pp. 395-399.

BROWN, N., 1999. *Modification Of The Rotary Machining Process To Improve Surface Form*.

BROWN, N. and PARKIN, R.M., 1999. Improving wood surface form by modification of the rotary machining process—a mechatronic approach. *Proceedings of the Institution of Mechanical Engineers, Part B: Journal of Engineering Manufacture,* **213**(3), pp. 247-260.

CAO, X., LIN, B. and ZHANG, X., 2013. A study on grinding surface waviness of woven ceramic matrix composites. *Applied Surface Science,* (0),.

CARPENTER, G., 1992. FUZZY ARTMAP - A NEURAL NETWORK ARCHITECTURE FOR INCREMENTAL SUPERVISED LEARNING OF ANALOG MULTIDIMENSIONAL MAPS. *IEEE Transactions on Neural Networks,* **3**(5), pp. 698-713.

CHAUVIN, Y., 1990. Generalization performance of overtrained back-propagation networks. *EURASIP,* , pp. 46-55.

CHEN, Y., WANG, X.G., SUN, C., DEVINE, F. and DE SILVA, C.W., 2003. Active Vibration Control with State Feedback in Woodcutting. *Journal of Vibration and Control,* **9**.

CLARK, W.W., 2000. Vibration Control with State-Switched Piezoelectric Materials. *Journal of Intelligent Material Systems and Structures,* **11**(4), pp. 263-271.

CUS, F. and ZUPERL, U., 2008. <br />Model reference adaptive force and surface roughness control in milling. *Journal of Achievements in Materials and Manufacturing Engineering,* **26**(2), pp. 178-182.

CUTRI, F.A., 1991. *Production Enhancemnt In The Planing And Spindle Moulding Process Utilising A Mechatronic Approach*.

DENAI, M.A., PALIS, F. and ZEGHBIB, A., 2004. ANFIS based modelling and control of non-linear systems : a tutorial, *Systems, Man and Cybernetics, 2004 IEEE International Conference on,* 2004, pp3433-3438 vol.4.

DENAUD, L.E., BLERON, L., RATLE, A. and MARCHAL, R., 2007. Online control of wood peeling process: Acoustical and vibratory measurements of lathe checks frequency. *Annals of Forest Science,* **64**(5), pp. 569-575.

DIETZSCH, M., GRÖGER, S., GERLACH, M. and KRYSTEK, M., 2007. Extraction of the Mechanical Surface in Measurement of Nano Structures. *CIRP Annals - Manufacturing Technology,* **56**(1), pp. 537-540.

DINIZ, A.E., LIU, J.J. and DORNFELD, D.A., 1992. Correlating tool life, tool wear and surface roughness by monitoring acoustic emission in finish turning. *Wear,* **152**(2), pp. 395-407.

ELMAS, S., 2008. Active Vibration Control And Real-Time Surface Profile Monitoring System For A High Performance Machining Process.

ELMAS, S., ISLAM, N., JACKSON, M.R. and PARKIN, R.M., 2011. Analysis of profile measurement techniques employed to surfaces planed by an active machining system. *Measurement,* **44**(2), pp. 365-377.

FAN, L.P., 2006. Internal model based iterative learning control for linear motor motion systems. *ISDA 2006: Sixth International Conference on Intelligent Systems Design and Applications, Vol 3, ,* pp. 62-66.

FIERRO, R., 1998. Control of a nonholonomic mobile robot using neural networks. *IEEE Transactions on Neural Networks,* **9**(4), pp. 589-600.

GANGULI, A., DERAEMAEKER, A. and PREUMONT, A., 2007. Regenerative chatter reduction by active damping control. *Journal of Sound and Vibration,* **300**(3–5), pp. 847-862.

GAO, Y., ZHANG, D. and YU, C.W., 2001. Dynamic modeling of a novel workpiece table for active surface grinding control. *INTERNATIONAL JOURNAL OF MACHINE TOOLS & MANUFACTURE,* **41**, pp. 609-609-624.

GAO, D., YAO, Y.X., CHIU, W.M. and LAM, F.W., 2002. Accuracy enhancement of a small overhung boring bar servo system by real-time error compensation. *Precision Engineering,* **26**(4), pp. 456-459.

GARRATT, J.D. and NETTLETON, D.J., 1992. A stylus instrument for roughness and profile measurement of ultra-fine surfaces. *International Journal of Machine Tools and Manufacture,* **32**(1–2), pp. 233-238.

GONZALEZ, A. and PEREZ, R., 1999. SLAVE: a genetic learning system based on an iterative approach. *Fuzzy Systems, IEEE Transactions on,* **7**(2), pp. 176-191.

GONZALEZ, A. and PEREZ, R., 1996. A Learning system of fuzzy control rules. *Genetic Algorithms and Soft Computing, ,* pp. 202-225.

GONZALEZ, A. and PEREZ, R., 1993. Learning the structure of a fuzzy rule: A genetic approach. *Congress Fuzzy Intelligence,* **2**, pp. 57-70.

GONZALEZ, A. and PEREZ, R., 1998. Completeness and consistency conditions for learning fuzzy rules. *Fuzzy Sets and Systems,* **96**(1), pp. 37-51.

GOODCHILD, R., 1963. <br />Investigating Finish in Rotary Planing. *Engineering, ,* pp. 172-173.

GORECKI, C., 1990. Optical classification of machined metal surfaces by Fourier spectrum sampling. *Wear,* **137**(2), pp. 287-298.

GRÖGER, S., DIETZSCH, M., GERLACH, M. and JE, S., 2005. `Real mechanical profile' — the new approach for nano-measurements. *Journal of Physics: Conference Series,* **13**(1), pp. 13.

GUSCHINSKAYA, O. and DOLGUI, A., 2009. Comparison of exact and heuristic methods for a transfer line balancing problem. *International Journal of Production Economics,* **120**(2), pp. 276-286.

HAMAMOTO, K., 2001. An iterative learning control algorithm within prescribed input-output subspace. *Automatica,* **37**(11), pp. 1803-1809.

HECKER, R.L. and LIANG, S.Y., 2003. Predictive modeling of surface roughness in grinding. *International Journal of Machine Tools and Manufacture,* **43**(8), pp. 755-761.

HUGHES, A., BURRIDGE, J., FREEMAN, C., CHAPPELL, P., LEWIN, P. and ROGERS, E., 2008. Robotic trajectory tracking for neurological rehabilitation. *Progress in Neurology and Psychiatry,* **12**(3), pp. 22-24.

HYNEK, P., 2004. *Wood Surface Form Improvement by Real Time Displacement of Tool Trajectory*, Loughborough University.

IKONEN, V., KELLOMÄKI, S. and PELTOLA, H., 2003. Linking tree stem properties of Scots pine (Pinus sylvestris L.) to sawn timber properties through simulated sawing. *Forest Ecology and Management,* **174**(1–3), pp. 251-263.

ISKRA, P. and HERNANDEZ, R.E., 2009. The Influence of Cutting Parameters on the Surface Quality of Routed Paper Birch and Surface Roughness Prediction Modeling. *Wood and Fiber Science,* **41**(1), pp. 28-37.

ISKRA, P. and HERNANDEZ, R.E., 2012. Toward a process monitoring of CNC wood router. Sensor selection and surface roughness prediction. *Wood Science and Technology,* **46**(1-3), pp. 115-128.

ISKRA, P. and TANAKA, C., 2006. A comparison of selected acoustic signal analysis techniques to evaluate wood surface roughness produced during routing. *Wood Science and Technology,* **40**(3), pp. 247-259.

ISLAM, N., PARKIN, R.M., JACKSON, M.R. and KESY, Z., 2011. Development of a novel profile measurement system for actively planed surfaces. *Measurement,* **44**(2), pp. 466-477.

JACKSON, M.R., 1986. *Some Effects of Machine Characteristics on the Surface Quality of Planed and Spindle Moulded Wooden Products*.

JACKSON, M.R., PARKIN, R.M. and BROWN, N., 2002. Waves on wood. *PROCEEDINGS OF THE INSTITUTION OF MECHANICAL ENGINEERS PART B-JOURNAL OF ENGINEERING MANUFACTURE,* **216**(4), pp. 475-497.

JACKSON, M.R., YANG, D. and PARKIN, R.M., 2007. Analysis of wood surface waviness with a two-image photometic stereo method. *System and Control Engineering,* **221**.

JAIN, A.K., DUIN, R.P.W. and JIANCHANG MAO, 2000. Statistical pattern recognition: a review. *Pattern Analysis and Machine Intelligence, IEEE Transactions on,* **22**(1), pp. 4-37.

JALILI, N., 2002. A Comparative Study and Analysis of Semi-Active Vibration-Control Systems. *Journal of Vibration and Acoustics,* **124**(4), pp. 593-605.

JAVADPOUR, R., 2003. A fuzzy neural network approach to machine condition monitoring. *Computers & Industrial Engineering,* **45**(2), pp. 323-330.

KAVLICOGLU, N.C., KAVLICOGLU, B.M., LIU, Y., EVRENSEL, C.A., FUCHS, A., KOROL, G. and GORDANINEJAD, F., 2007. Response time and performance of a high-torque magneto-rheological fluid limited slip differential clutch. *Smart Materials and Structures,* (1), pp. 149.

KHAIRY, A.B., 1996. A knowledge-based system for electrochemical machining procedure. *Journal of Materials Processing Technology,* **58**(1), pp. 121-130.

KILIC, D.S. and RAMAN, S., 2007. Observations of the tool–chip boundary conditions in turning of aluminum alloys. *Wear,* **262**(7–8), pp. 889-904.

KIRAN, M.B., RAMAMOORTHY, B. and RADHAKRISHNAN, V., 1998. Evaluation of surface roughness by vision system. *International Journal of Machine Tools and Manufacture,* **38**(5–6), pp. 685-690.

KORI, J.G. and JANGID, R.S., 2009. SEMI-ACTIVE MR DAMPERS FOR SEISMIC CONTROL OF STRUCTURES. *Bulletin of the New Zealand Society for Earthquake Engineering,* **42**(3), pp. 157-166.

LAGUI´A, M. and CASTRO, J.L., 2008. Local distance-based classification. *Knowledge-Based Systems,* **21**(7), pp. 692-703.

LARA-PRIETO, V., PARKIN, R., JACKSON, M.R., SILBERSCHMIDT, V. and KESY, Z., 2010. Vibration characteristics of MR cantilever sandwich beams: experimental study. *Smart Materials and Structures,* .

LAUFFER, J.P., REGELBRUGGE, M.E., DOHNER, J.L., HINNERICHS, T.D., KWAN, C.M., LIN, Y. and XU, R., 1998. Smart spindle unit for active chatter suppression of a milling machine: II. *Dynamics and control,* **167**.

LEACH, R., GIUSCA, G.L. and NAO, K.I., Development and characterization of a new instrument for the traceable measurement of areal surface texture. *Measurement Science and Technology,* (12), pp. 125102.

LEBOW, P.K., BRUNNER, C.C., MARISTANY, A.G. and BUTLER, D.A., 1996. Classification of Wood Surface Features By Spectral Reflectance. *Wood and Fiber Science,* **28**, pp. 74-74-90.

LEE, C.S., KIM, S.W., YIM, D.Y. and TÖNSHOFF, H.K., 1987. An In-Process Measurement Technique Using Laser for Non-Contact Monitoring of Surface Roughness and Form Accuracy of Ground Surfaces. *CIRP Annals - Manufacturing Technology,* **36**(1), pp. 425-428.

LEE, H.S., 1996. Study on robustness of iterative learning control with non-zero initial error. *International Journal of Control,* **64**(3), pp. 345-359.

LEI, S. and LIU, W., 2002. High-speed machining of titanium alloyes using the driven rotary tool. *INTERNATIONAL JOURNAL OF MACHINE TOOLS & MANUFACTURE,* **42**, pp. 653-653-661.

LEMASTER, R.L., LU, L. and JACKSON, S., 2000. <br />Use of process monitoring techniques on a CNC wood router. Part 2. Use of vibration accelerometer to monitor tool wear and workpiece quality. *Forest Products Journal,* **50**(9), pp. 59-64.

LIM, S., PARK, S. and KIM, K., 2005. AI vibration control of high-speed rotor systems using electrorheological fluid. *Journal of Sound and Vibration,* **284**(3–5), pp. 685-703.

LIU, Y., CHANG, K. and LI, W., 2010. Model reference adaptive control for a piezo-positioning system. *Precision Engineering,* **34**(1), pp. 62-69.

LU, X.D., PAONE, M.P., USMAN, I., MOYLS, B., SMEDS, K., ROTHERHOFER, G. and SLOCUM, A.H., 2009. Rotary-axial spindles for ultra-precision machining. *CIRP Annals - Manufacturing Technology,* **58**, pp. 323-323-326.

MADADY, A., 2008. A SELF-TUNING ITERATIVE LEARNING CONTROLLER FOR TIME VARIANT SYSTEMS. *ASIAN JOURNAL OF CONTROL,* **10**(6), pp. 666-677.

MALKOÇOĞLU, A., 2007. Machining properties and surface roughness of various wood species planed in different conditions. *Building and Environment,* **42**(7), pp. 2562-2567.

MARISTANY, A.G., LEBOW, P.K., BRUNNER, C.C., BUTLER, A.D. and FUNCK, J.W., 1993. Classifying wood-surface features using dichromatic reflection, DESHAZER J. A. and {MEYER G. E., eds. In: *Proc. SPIE Vol. 1836, p. 56-64, Optics in Agriculture and Forestry, James A. DeShazer; George E. Meyer; Eds.* May 1993, pp56-64.

MARX-GÓMEZ, J., RAUTENSTRAUCH, C., NÜRNBERGER, A. and KRUSE, R., 2002. Neuro-fuzzy approach to forecast returns of scrapped products to recycling and remanufacturing. *Knowledge-Based Systems,* **15**(1-2), pp. 119-128.

MCKONE, T.E., 2005. Can fuzzy logic bring complex environmental problems into fucus? *Environmental science & technology,* **39**(2), pp. 42A-47A.

MIRANDA, A.A., BORGNE, Y.A. and BONTEMPI, G., 2008. New Routes from Minimal Approximation Error to Principal Components. *Neural Process.Lett.,* **27**(3), pp. 197-207.

MITCHELL, S.W., REMMEL, T.K., CSILLAG, F. and WULDER, M.A., 2008. Distance to second cluster as a measure of classification confidence. *Remote Sensing of Environment,* **112**(5), pp. 2615-2626.

NAGARJUNA, N., MAHESH, O. and RAJAGOPAL, K., 2006. A heuristic based on multi-stage programming approach for machine-loading problem in a flexible manufacturing system. *Robotics and Computer-Integrated Manufacturing,* **22**(4), pp. 342-352.

NAGATA, F., KUSUMOTO, Y. and WATANABE, K., 2009. Intelligent machining system for the artistic design of wooden paint rollers. *Robotics and Computer-Integrated Manufacturing,* **25**(3), pp. 680-688.

NAKAMA, T., 2009. Theoretical analysis of batch and on-line training for gradient descent learning in neural networks. *Neurocomputing,* **73**(1–3), pp. 151-159.

NISHIO, S. and MARUI, E., 1996. Effects of slots on the lateral vibration of a circular saw blade. *International Journal of Machine Tools and Manufacture,* **36**(7), pp. 771-787.

NOËL, M., SODHI, M.S. and LAMOND, B.F., 2007. Tool planning for a lights-out machining system. *Journal of Manufacturing Systems,* **26**(3-4), pp. 161-166.

OGUN, P.S., 2012. Real-Time Intellignet Control of a High Performance Production Machine. PhD edn. Loughborugh University.

OGUN, P.S., JACKSON, M.R. and PARKIN, R.M., 2012. In-process surface profile assessment of rotary machined timber using a dynamic photometric stereo technique. *Proceedings of the Institution of Mechanical Engineers, Part I: Journal of Systems and Control Engineering,* .

OGUN, P.S., 2012. *Modelling and real-time control of a high performance rotary wood planing machine*, © Philips Ogun.

ÖZÇIFÇI, A. and YAPICI, F., 2008. Effects of machining method and grain orientation on the bonding strength of some wood species. *Journal of Materials Processing Technology,* **202**(1–3), pp. 353-358.

PARK, K.S. and KIM, S.H., 1998. Artificial intelligence approaches to determination of CNC machining parameters in manufacturing: a review. *Artificial Intelligence in Engineering,* **12**(1–2), pp. 127-134.

PARK, B., 2001. Generation and evolutionary learning of cutting conditions for milling operations. *International Journal of Advanced Manufacturing Technology,* **17**(12), pp. 870-880.

PARKIN, R.M. and JACKSON, M.R., 1996. A mechatronic approach for analysing timber surfaces. *Mathematics and Computers in Simulation,* **41**(5–6), pp. 445-450.

POMERLEAU, D.A., 1991. Efficient training of artificial neural networks for autonomous navigation. *Neural Comput.,* **3**(1), pp. 88-97.

RAMARATNAM, A. and JALILI, N., 2006. A switched stiffness approach for structural vibration control: theory and real-time implementation. *Journal of Sound and Vibration,* **291**(1–2), pp. 258-274.

REKDALSBAKKEN, W., 2006. Feedback Control of an Inverted Pendulum with the use of Artificial Intelligence.

RIDGE, B., SKOCAJ, D. and LEONARDI, A., 2008. A System for Learning Basic Object Affordances using a Self-Organising Map, *International Conference on Cognitive Systems,* 2008 2008, .

ROOKS, B., 2003. Machine Tending on the Modern Age. *Industrial Robot: An Internation Journal,* **30**(4), pp. 313-318.

SANDAK, J. and TANAKA, C., 2003. Evaluation of surface smoothness by laser displacement sensor 1: effect of wood species. Springer Japan.1435-0211.

SATHIANARAYANAN, D., KARUNAMOORTHY, L., SRINIVASAN, J., KANDASAMI, G.S. and PALANIKUMAR, K., 2008. Chatter Suppression in Boring Operation Using Magnetorheological Fluid Damper. *Materials and Manufacturing Processes,* **23**(4), pp. 329-335.

SJÖVALL, P. and ABRAHAMSSON, T., 2007. Component system identification and state-space model synthesis. *Mechanical Systems and Signal Processing,* **21**(7), pp. 2697-2714.

SMITH, M.L. and SMITH, L.N., 2005. Dynamic photometric stereo—a new technique for moving surface analysis. *Image and Vision Computing,* **23**(9), pp. 841-852.

SOLIMAN, E. and ISMAIL, F., 1998. A control system for chatter avoidance by ramping the spindle speed. *Journal of Manufacturing Science and Engineering, Transactions of the ASME,* **120**(4), pp. 674-683.

SULAIMAN, O., HASHIM, R., SUBARI, K. and LIANG, C.K., 2009. Effect of sanding on surface roughness of rubberwood. *Journal of Materials Processing Technology,* **209**(8), pp. 3949-3955.

SUN, M. and WANG, D., 2001. Iterative Learning Control With Initial Rectifying Action. *Automatica,* **38**, pp. 1177-1182.

TAYLOR J, B., CARRANO A, L. and LEMASTER R, L., 1999. Quantification of process parameters in a wood sanding operation. Madison, WI, ETATS-UNIS: Forest Products Society.

TIAN, Y., ZHANG, D. and SHIRINZADEH, B., 2011. Dynamic modelling of a flexure-based mechanism for ultra-precision grinding operation. *Precision Engineering,* **35**(4), pp. 554-565.

VAHEBI NOJEDEH, M., HABIBI, M. and AREZOO, B., 2011. Tool path accuracy enhancement through geometrical error compensation. *International Journal of Machine Tools and Manufacture,* **51**(6), pp. 471-482.

WANG, L., ZHANG, Y. and FENG, J., 2005. On the Euclidean distance of images. *Pattern Analysis and Machine Intelligence, IEEE Transactions on,* **27**(8), pp. 1334-1339.

WILSON, D.R. and MARTINEZ, T.R., 2003. The general inefficiency of batch training for gradient descent learning. *Neural Networks,* **16**(10), pp. 1429-1451.

YANG, D., 2006. *Measurement of cutter marks on planed wood surfaces with machine vision methods*, Loughborough University, UK.

YANG, D., JACKSON, M.R. and PARKIN, R.M., 2006. Inspection of wood surface waviness defects using the light sectioning method. *Proceedings of the Institution of Mechanical Engineers, Part I: Journal of Systems and Control Engineering,* **220**(7), pp. 617-626.

YANG, R. and REN, M., 2011. Wavelet denoising using principal component analysis. *Expert Systems with Applications,* **38**(1), pp. 1073-1076.

YOUNG, P.C. and WILLEMS, J.C., 1972. An approach to the linear multivariable servomechanism problem†. *International Journal of Control,* **15**(5), pp. 961-979.

YU, J. and SARKER, B.R., 2003. Directional decomposition heuristic for a linear machine-cell location problem. *European Journal of Operational Research,* **149**(1), pp. 142-184.

ZADEH, L.A., 1973. Outline of new approach to the analysis of complex systems and decisions processes. *IEEE Transactions On Systems, Manufacturing and Cybernetics,* **3**, pp. 28-44.

ZHANG, Y. and SIMS, N.D., 2005. Milling workpiece chatter avoidance using piezoelectric active damping: a feasibility study. *Smart Materials and Structures,* **14**(6), pp. N65.

ZHOU, Y., 2002. A new fuzzy neural network with fast learning algorithm and guaranteed stability for manufacturing process control. *Fuzzy Sets and Systems,* **132**(2), pp. 201-216.

ZILIANI, G., 2007. Iterative learning explicit hybrid force/velocity control for contour tracking. *2007 IEEE/ASME INTERNATIONAL CONFERENCE ON ADVANCED INTELLIGENT MECHATRONICS, VOLS 1-3,* , pp. 871-876.

ZUPERL, U., KIKER, E. and JEZERNIK, K., 2006. Adaptive Force Control in High-Speed Machining by Using a System of Neural Networks, *Industrial Electronics, 2006 IEEE International Symposium on,* 2006, pp148-153.

12 Appendix A – Computational Models

12.1 Simulink Model for Setpoint Tracker Controller

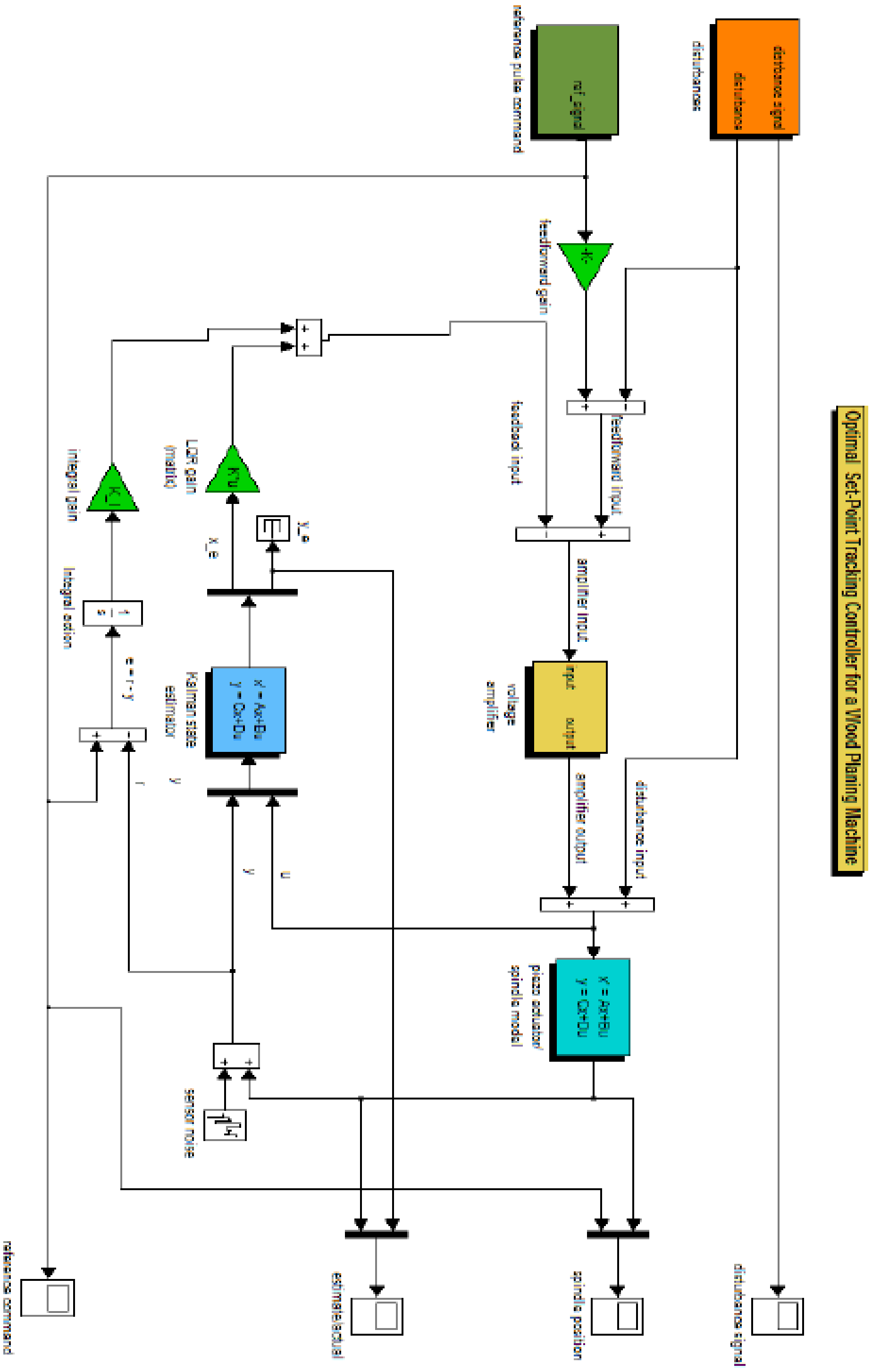
Optimal Set-Point Tracking Controller for a Wood Planing Machine
reference pulse command
ref_signal
disturbance
disturbance signal
disturbance
feedforward gain
-K-
feedback input
feedforward input
amplifier input
input
output
voltage amplifier
amplifier output
disturbance input
x' = Ax+Bu
y = Cx+Du
piezo actuator/ spindle model
x' = Ax+Bu
y = Cx+Du
Kalman state estimator
x_e
y_e
LQR gain (matrix)
K*u
K_I
integral gain
1/s
Integral action
e = r - y
r
y
y
u
sensor noise
reference command
estimate/actual
spindle position
disturbance signal

13 Appendix B – Alicona Infinate Focus Machine

alicona
INFINITEFOCUS

The Alicona InfiniteFocus is a high resolution optical system (non-contact) for 3D surface form and roughness measurement. The operating principle of InfiniteFocus is based on the variation of focus technique (Focus-Variation). The Focus-Variation technique uses small depth of focus of an optical system, combined with continuous vertical scanning, to generate 3D topographic model of the surface. The wood samples were measured using the following parameters:

Objective Lens Magnification	5x
Working distance	23.5mm
Field of View	2858µm x 2175µm
Vertical Resolution	410nm

The Alicona InfiniteFocus has a motorised X-Y table and seamless image stitching algorithm, which allowed the desired sample length to be measured. It is also equipped with a module for the calculation of area-based 2D surface profile measurement.

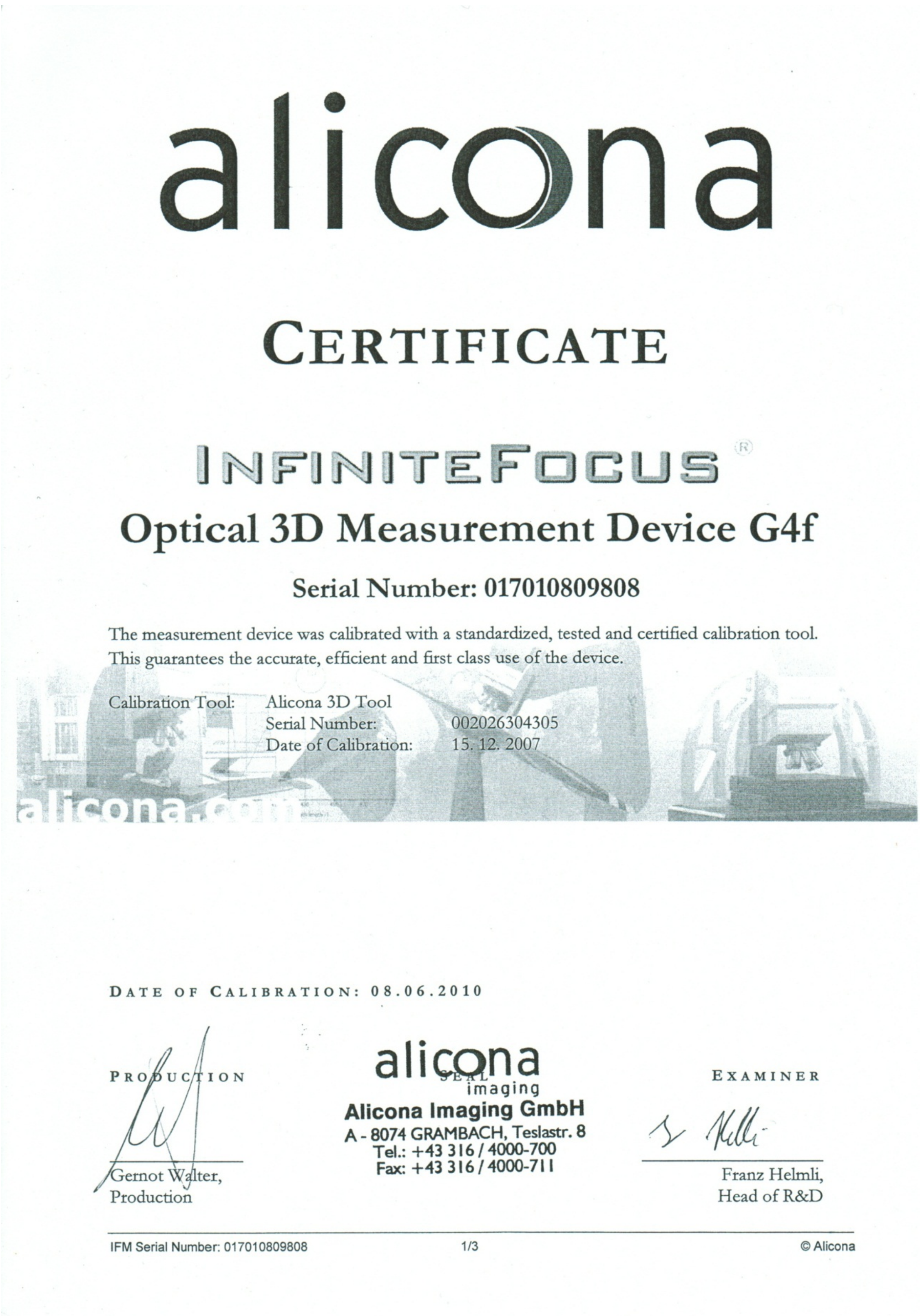

alicona

CERTIFICATE

INFINITEFOCUS®

Optical 3D Measurement Device G4f

Serial Number: 017010809808

The measurement device was calibrated with a standardized, tested and certified calibration tool. This guarantees the accurate, efficient and first class use of the device.

Calibration Tool:	Alicona 3D Tool	
	Serial Number:	002026304305
	Date of Calibration:	15. 12. 2007

alicona.com

DATE OF CALIBRATION: 08.06.2010

PRODUCTION

SEAL

alicona
imaging
Alicona Imaging GmbH
A - 8074 GRAMBACH, Teslastr. 8
Tel.: +43 316 / 4000-700
Fax: +43 316 / 4000-711

EXAMINER

Gernot Walter,
Production

Franz Helmli,
Head of R&D

IFM Serial Number: 017010809808 1/3 © Alicona

14 Appendix C – Purchased Components

14.1 Table of Suppliers

Item	Supplier
Codewheel	Avnet
24V Power Supply	OneCall Farnell
Eddy Current Probe	Monitran
Cutting Knife Tips	NLS Tools
Motors and Drives	Norwin Electronics
Steel Shim	Repco Technology ltd
Components for guarding	RS Components
Torque Wrench	Screwfix Direct

14.3 Component Data Sheets

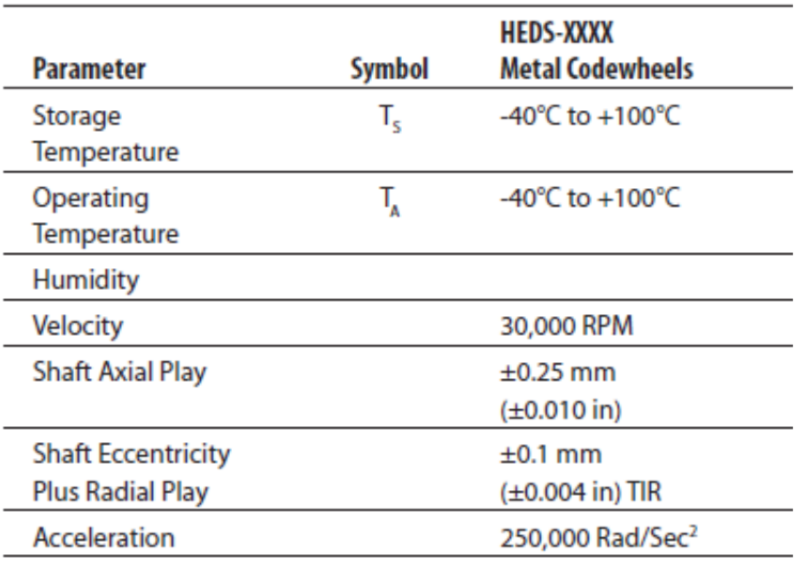

Parameter	Symbol	HEDS-XXXX Metal Codewheels
Storage Temperature	T_S	-40°C to +100°C
Operating Temperature	T_A	-40°C to +100°C
Humidity		
Velocity		30,000 RPM
Shaft Axial Play		±0.25 mm (±0.010 in)
Shaft Eccentricity Plus Radial Play		±0.1 mm (±0.004 in) TIR
Acceleration		250,000 Rad/Sec^2

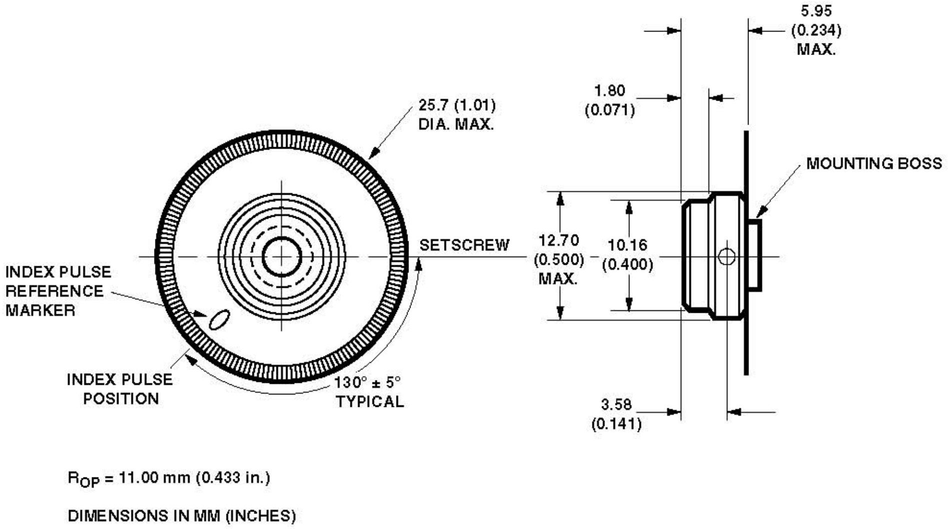
5.95
(0.234)
MAX.
1.80
(0.071)
25.7 (1.01)
DIA. MAX.
MOUNTING BOSS
SETSCREW
12.70
(0.500)
MAX.
10.16
(0.400)
INDEX PULSE
REFERENCE
MARKER
INDEX PULSE
POSITION
130° ± 5°
TYPICAL
3.58
(0.141)
R_{OP} = 11.00 mm (0.433 in.)
DIMENSIONS IN MM (INCHES)

gure 6. HEDS-5140 Codewheel Used with HEDS-9140.

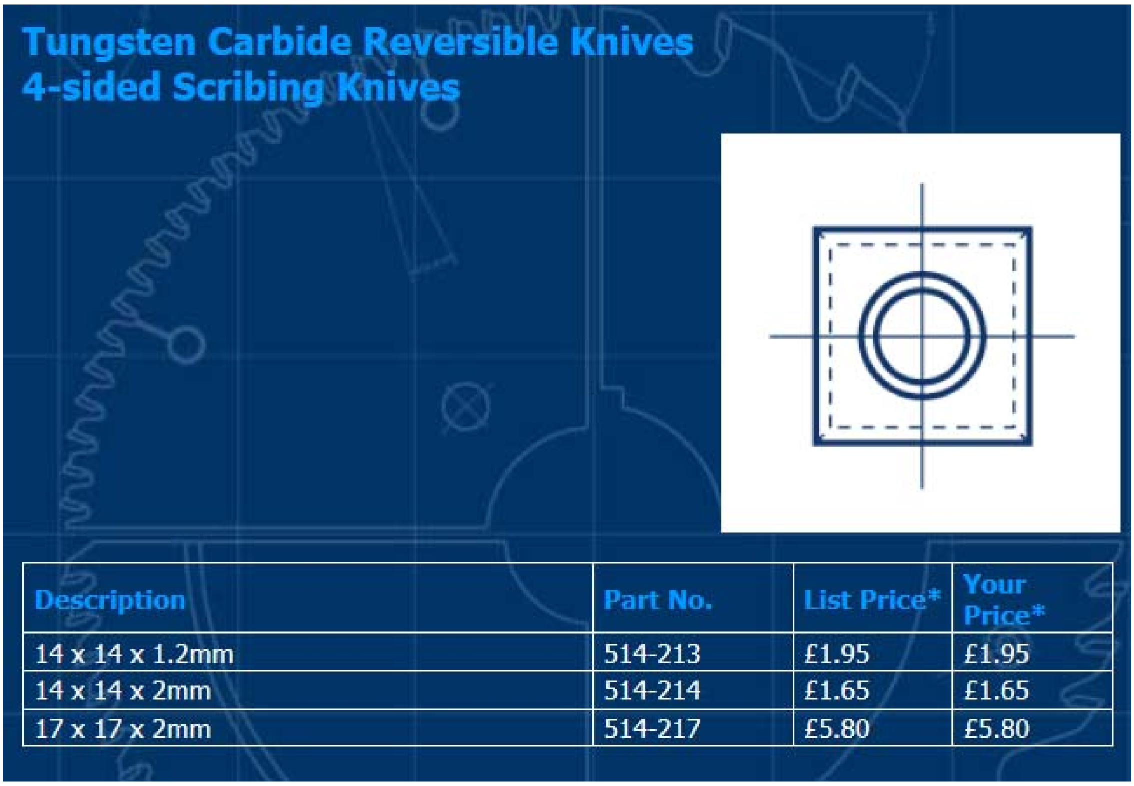

Tungsten Carbide Reversible Knives
4-sided Scribing Knives

Description	Part No.	List Price*	Your Price*
14 x 14 x 1.2mm	514-213	£1.95	£1.95
14 x 14 x 2mm	514-214	£1.65	£1.65
17 x 17 x 2mm	514-217	£5.80	£5.80

8.3 HDM82E8

HDM COMPACT SERVOMOTORS

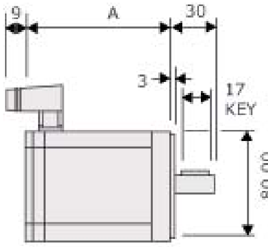

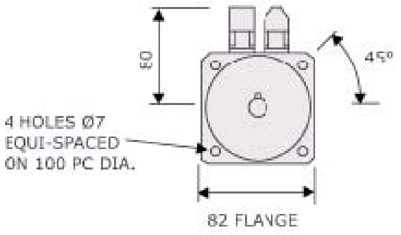

Outline Drawing.

Technical Data.

HDM82 HDM82 HDM82 Parameter Units E8-30S E8-38S E8-76S

Continuous Stall Torque [1] Nm 2.3 2.3 2.3 Continuous Stall Current [1] A 6.6 5.2 2.6

Rated Torque [1] Nm 2.1 2.1 2.1 Rated Current [1] A 6 4.7 2.3 Rated Speed rpm 4500 4500 3000

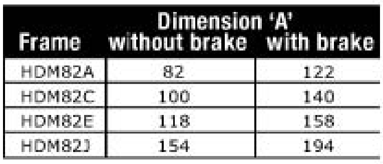

Frame	Dimension 'A' without brake	Dimension 'A' with brake
HDM82A	82	122
HDM82C	100	140
HDM82E	118	158
HDM82J	154	194

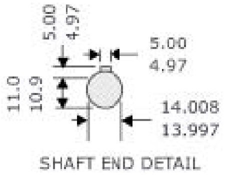

Continuous Stall Torque (HR/HJ)[6] Nm 2.2 2.2 2.2

Notes

[1] - Motors are tested on an aluminium heatsink with dimensions 255x255x6mm and with a temperature rise 'T of 100K on the windings. The maximum temperature of the windings is therefore 140°C.

[2] - Where no motor speed is specified, optimal performance may not be achieved on 560V DC link.

[3] - At 25ºC.

[4] - Inductance values based on nominal current.

[5] - At rated values Torque = Kt x rms current.

[6] - Continuous Stall Torque (HR/HJ) is for use in comparisons with SEM's HR and HJ servomotors only.

Max. Speed (300V DC link)	rpm	8000 -----	7800 -----	3900
Max. Speed (560V DC link)²	rpm			7300
Peak Stall Torque Peak Current	**Nm A**	**6.9 35**	**6.9 28**	**6.9 14**
Resistance Line-Line3 Inductance Line-Line4	: mH	0.912.2	1.5 3.4	5.8 13.5
Voltage Gradient No Load Max. Motor EMF Line – Line	V Volts	30 240	38 300	76 610
Torque Constant Kt3,5 Number of Poles **THERMAL** Insulation Class Max. Ambient Temperature Thermal Time Constant Thermal Resistance	Nm/A°C minutes °C/W	0.35 8 F 40 26 1.18	0.45 8 F 40 26 1.18	0.9 8 F 40 26 1.18
MECHANICAL Rotor Polar Moment of Inertia Static Friction Torque Cogging Torque Motor Weight Motor Weight with brake fitted	kgcm²N m Nm kg kg	0.88 0.04 0.075 2.9 TBA	0.88 0.04 0.075 2.9 TBA	0.88 0.04 0.075 2.9 TBA

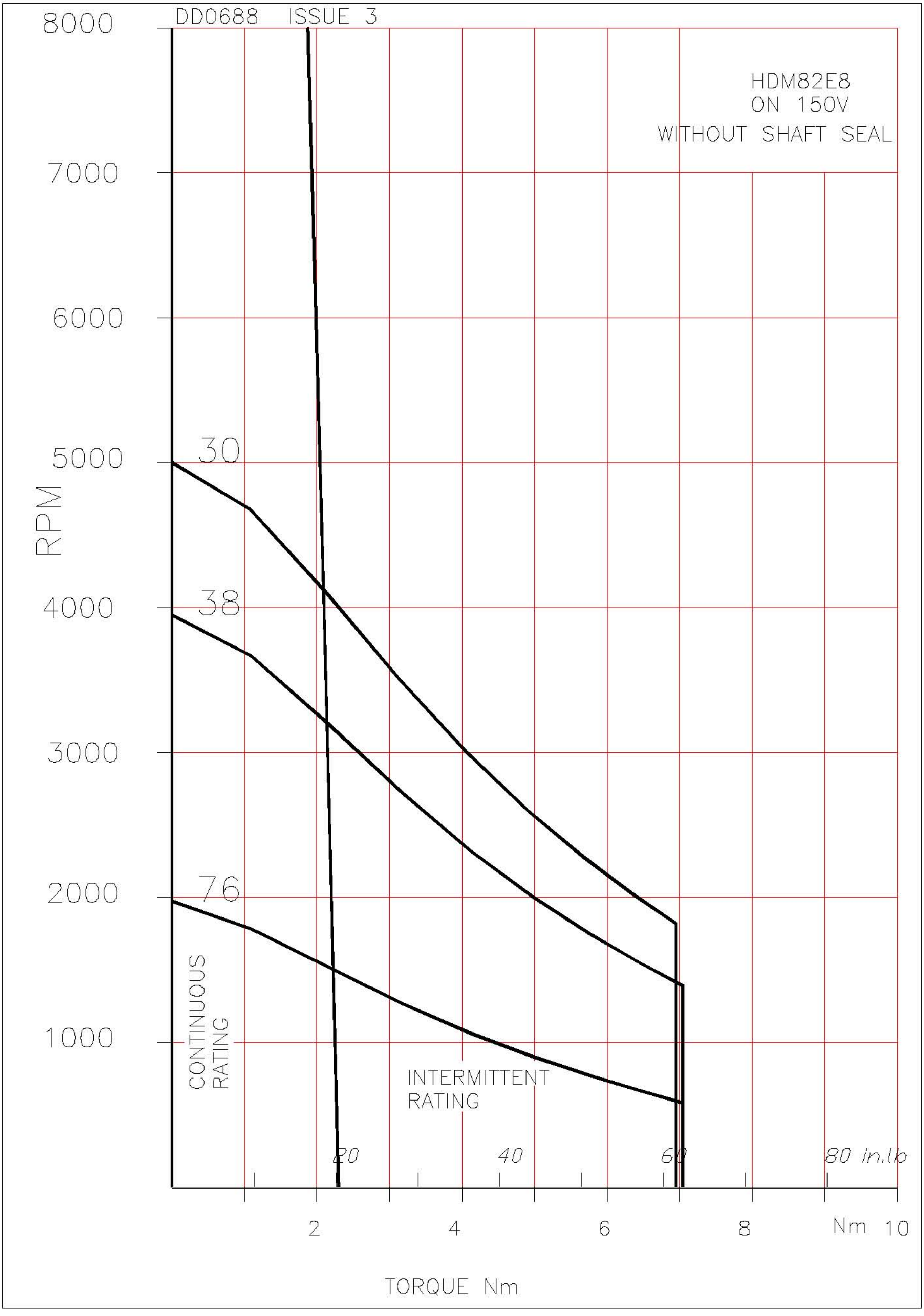
DD0688 ISSUE 3
HDM82E8
ON 150V
WITHOUT SHAFT SEAL
RPM
8000
7000
6000
5000
4000
3000
2000
1000
30
38
76
CONTINUOUS
RATING
INTERMITTENT
RATING
20
40
60
80 in.lb
2
4
6
8
Nm 10
TORQUE Nm

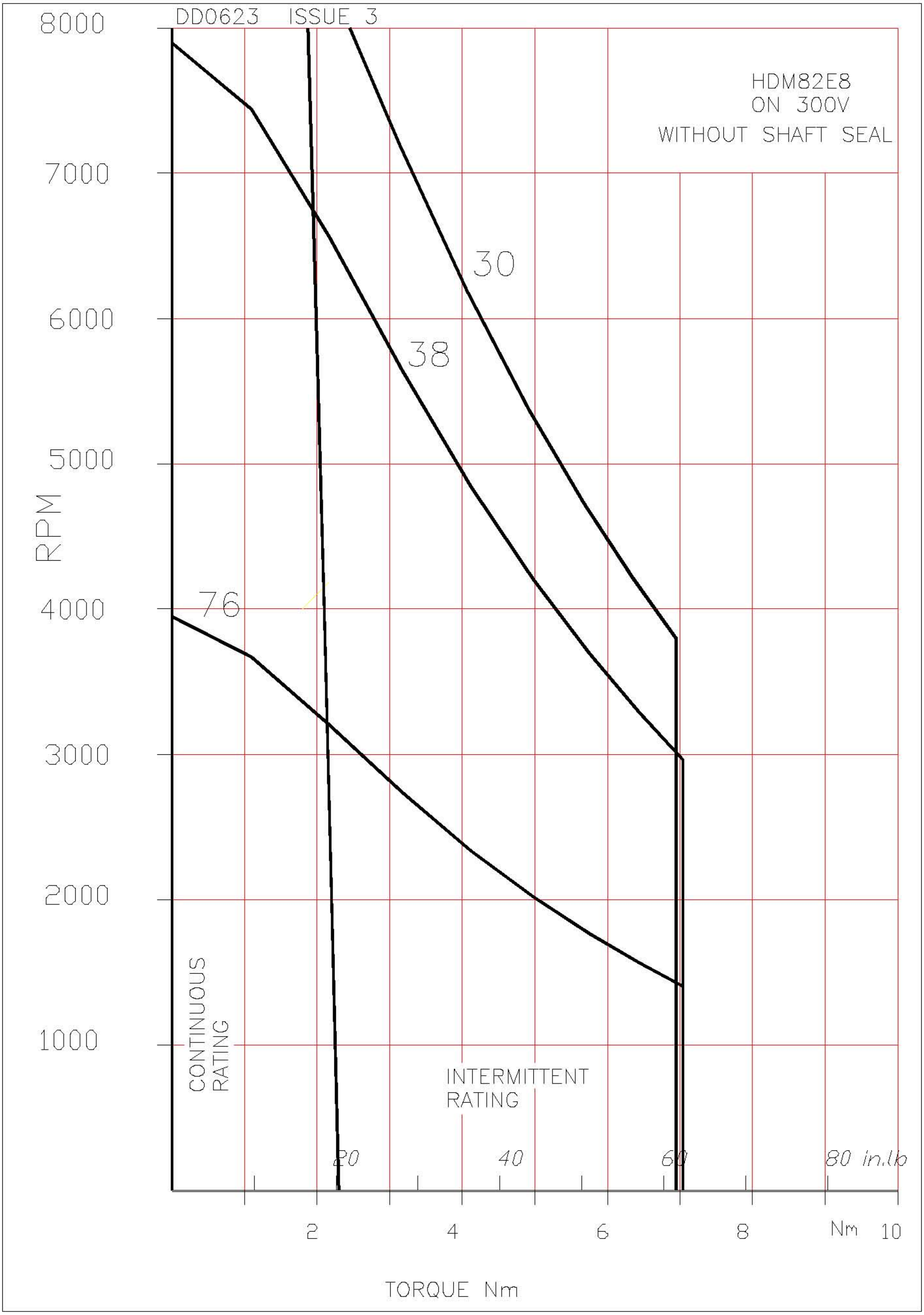
DD0623 ISSUE 3
HDM82E8
ON 300V
WITHOUT SHAFT SEAL
8000
7000
6000
5000
4000
3000
2000
1000
RPM
30
38
76
CONTINUOUS RATING
INTERMITTENT RATING
20
40
60
80 in.lb
2
4
6
8
Nm
10
TORQUE Nm

FIRST ANGLE PROJECTION

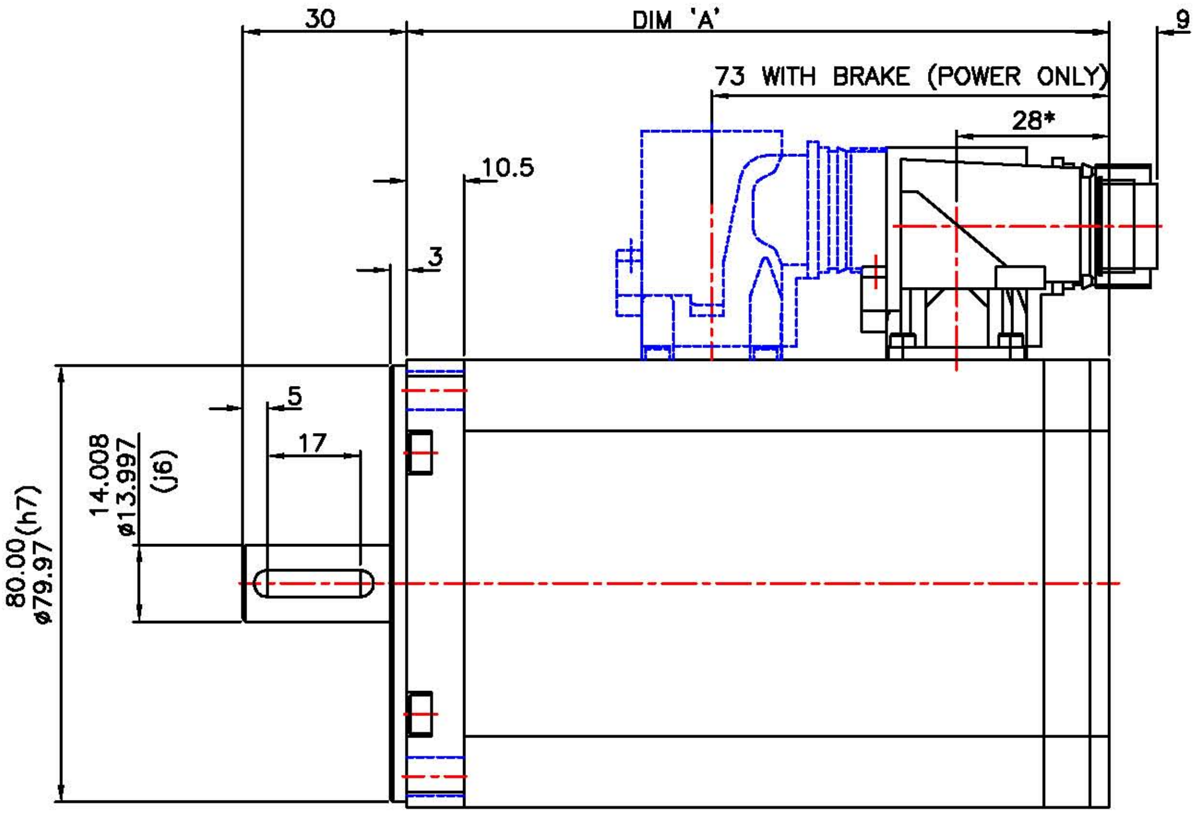

30
DIM 'A'
9
73 WITH BRAKE (POWER ONLY)
28*
10.5
3
5
17
80.00 ø79.97 (h7)
14.008 ø13.997 (j6)

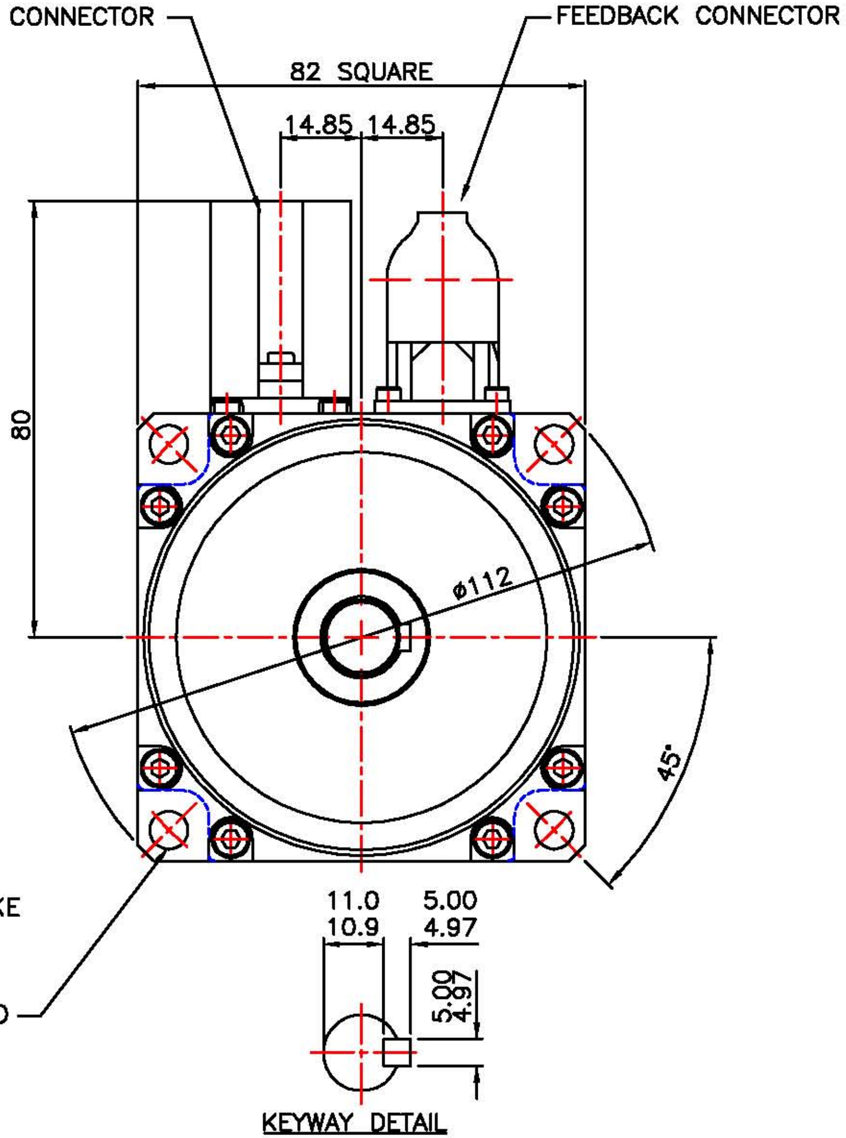

MOTOR CONNECTOR
FEEDBACK CONNECTOR
82 SQUARE
14.85
14.85
80
ø112
45°
11.0
10.9
5.00
4.97
5.00
4.97

KEYWAY DETAIL

*F/B CONNECTOR BRAKE & NON BRAKE, POWER CONNECTOR NON BRAKE

4-FIXING HOLES ø7 EQUI-SPACED ON 100 PCD

FOR CONNECTORS FACING DE SEE 664-7-06548

FRAME	DIM 'A'	
	NO BRAKE	WITH BRAKE
HDM82A	82	122
HDM82C	100	140
HDM82E	118	158
HDM82J	154	194

2 12JUL06 MR3798 CONNECTORS CHANGED OVER
3 12MAR07 MR4005 F/B CONNECTOR ON BRAKE MOTOR MOVED

ALL DIMENSIONS IN MILLIMETRES
TOLERANCES UNLESS OTHERWISE STATED ANG: ±0.5° DIM: ±0.25mm

TITLE: HDM82 STD MET WITH M23 & M17 CONNS FACING NDE

MATERIAL	AS STATED	CODE	
SPEC		FORM	
FINISH		PATTERN No.	

DRAWING NO.
664-7-06498

SEM
LONDON ENGLAND

SCALE	1:1
ISSUE No.	3
DR.	PFS
DATE	22MAY06

A06498C1

7.3 HDM58E6

HDM COMPACT SERVOMOTORS

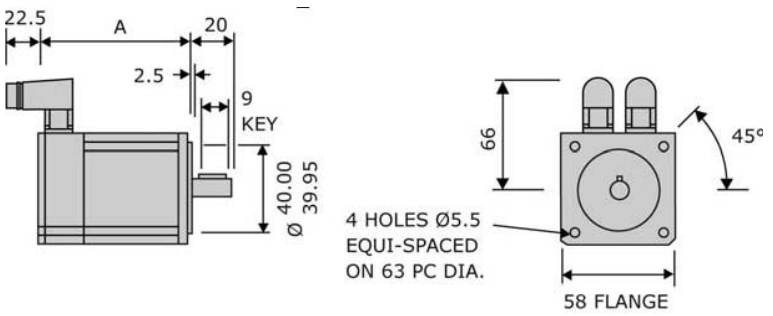

Outline Drawing. Technical Data.

Rated Torque [1] Nm 1.1 1.1 1.1 Rated Current [1] A 2.3 1.36 0.94 Rated Speed rpm 4500 4500 4500
Max. Speed (300V DC link) rpm 7500 4300 3000 Max. Speed (560V DC link)[2] rpm 8000 8000 5600
Peak Stall Torque Nm 3.5 3.5 3.5

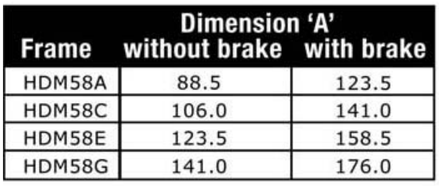

Frame	Dimension 'A' without brake	Dimension 'A' with brake
HDM58A	88.5	123.5
HDM58C	106.0	141.0
HDM58E	123.5	158.5
HDM58G	141.0	176.0

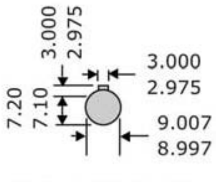

SHAFT END DETAIL

Peak Current A 13.1 7.5 5.2

HDM58 Parameter	Units	E6-40S	HDM58 E6-70S	HDM58 E6-100S
Continuous Stall Torque 1	**Nm**	**1.15**	**1.15**	**1.15**
Continuous Stall Current 1	**A**	**2.5**	**1.4**	**0.98**

[1] - Motors are tested on an aluminium heatsink with dimensions 255x255x6mm and with a temperature rise 'T of 100K on the windings. The maximum temperature of the windings is therefore 140°C.

[2] - Where no motor speed is specified, optimal performance may not be achieved on 560V DC link.

[3] - At 25ºC.

[4] - Inductacne values are based on nominal current.

[5] - At rated values Torque = Kt x rms current.

[6] -Continuous Stall Torque (HR/HJ) is for use in comparisons with SEM's HR and HJ servomotors only.

Resistance Line-Line[3] Inductance Line-Line[4]	: mH	5.26.1	16 18.5	33 38
Voltage Gradient No Load Max. Motor EMF Line – Line	V Volts	40 320	70 560	100 700
Torque Constant Kt[3,5] Number of Poles	Nm/A	0.48 6	0.81 6	1.17 6
THERMAL Insulation Class Max. Ambient Temperature	°C	F 40	F 40	F 40
Thermal Time Constant Thermal Resistance	minutes °C/W	30 1.6	30 1.6	30 1.6
MECHANICAL Rotor Polar Moment of Inertia Static Friction Torque Cogging Torque Motor Weight Motor Weight with brake fitted Continuous Stall Torque (HR/HJ)[6]**Notes**	kgcm² Nm Nm kg kg Nm	0.2 0.02 0.045 1.4 TBA 1	0.2 0.02 0.045 1.4 TBA 1	0.2 0.02 0.045 1.4 TBA 1

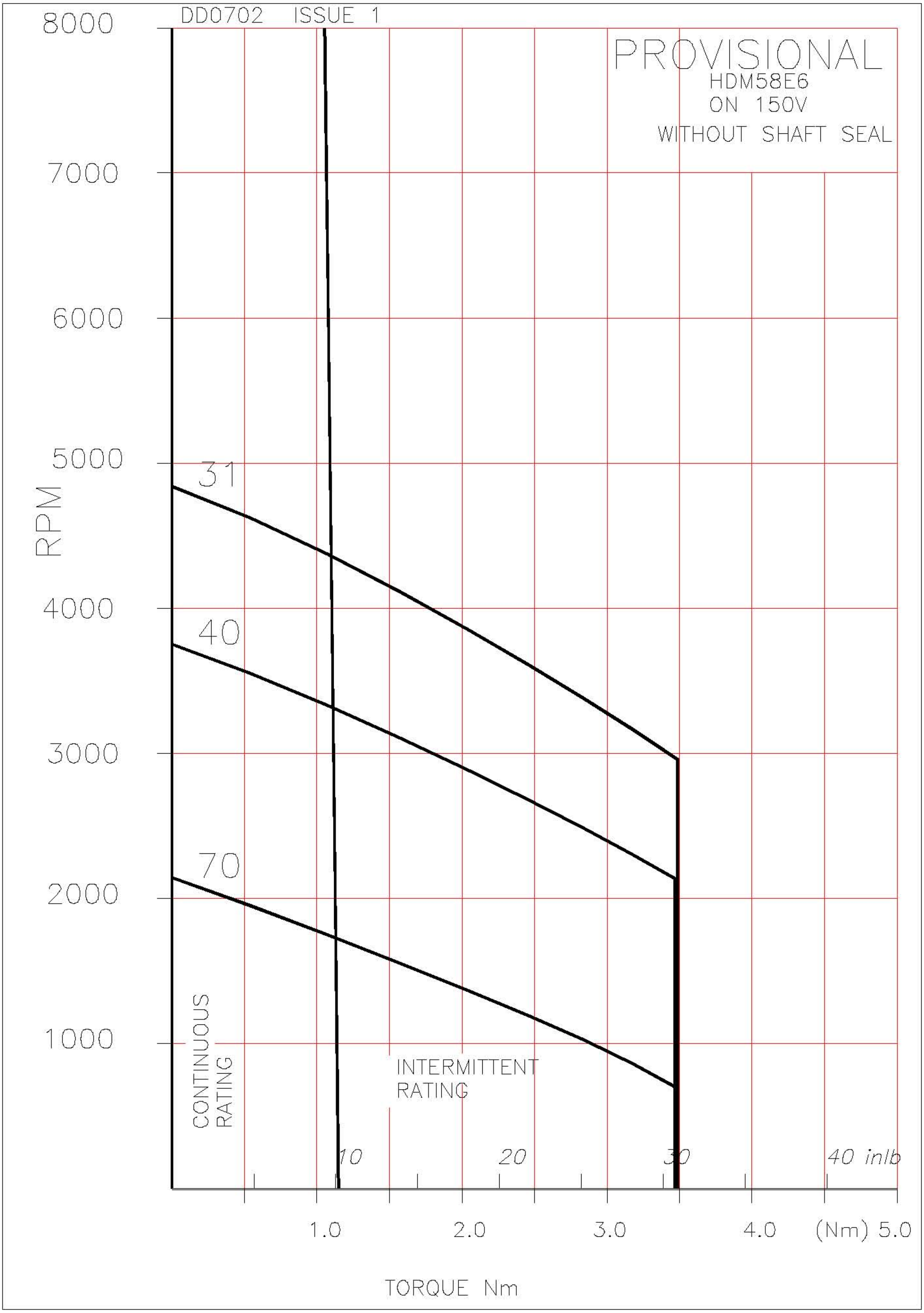
DD0702 ISSUE 1
PROVISIONAL
HDM58E6
ON 150V
WITHOUT SHAFT SEAL
8000
7000
6000
5000
4000
3000
2000
1000
RPM
31
40
70
CONTINUOUS
RATING
INTERMITTENT
RATING
10
20
30
40 inlb
1.0
2.0
3.0
4.0
(Nm) 5.0
TORQUE Nm

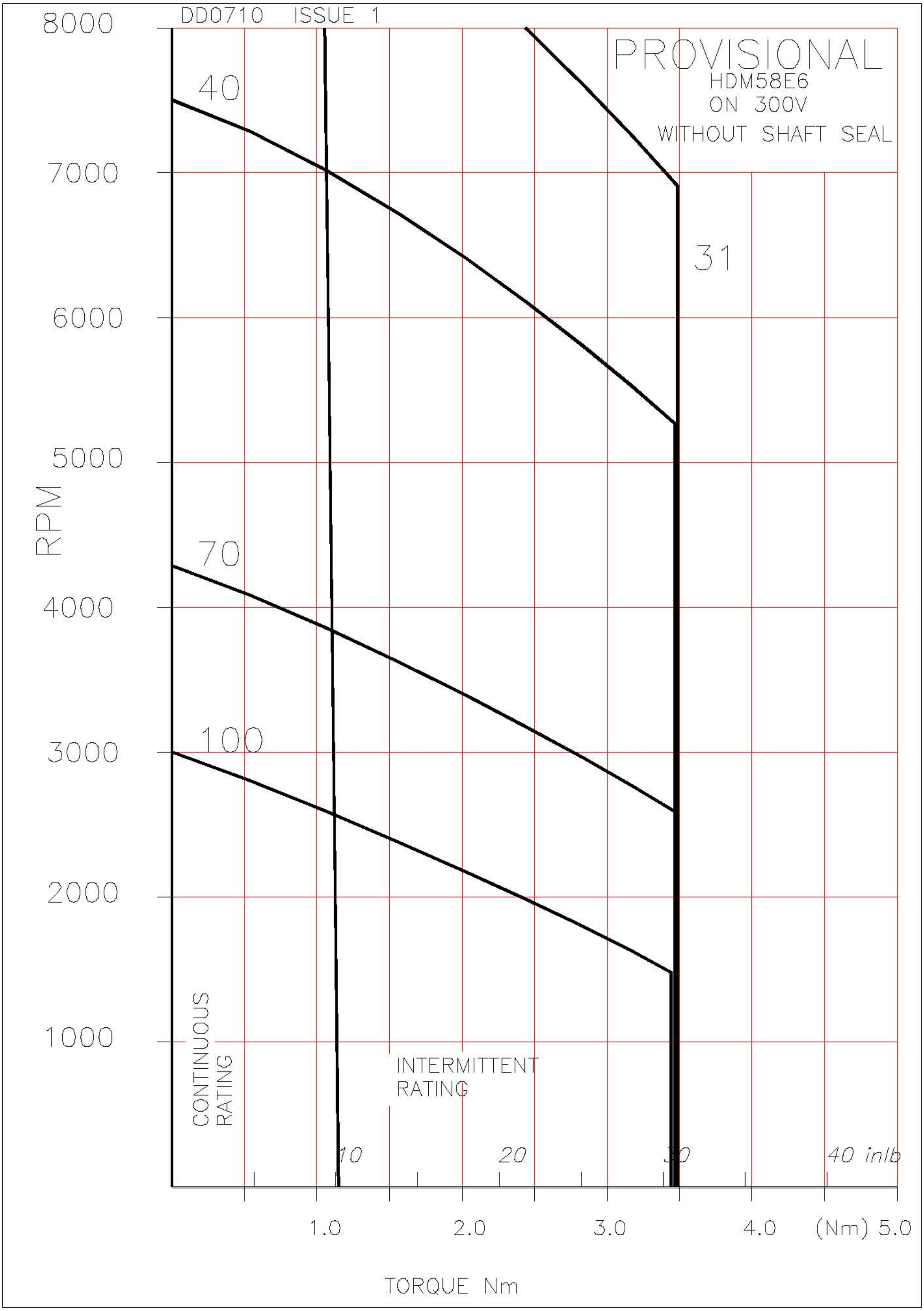
DD0710 ISSUE 1
PROVISIONAL
HDM58E6
ON 300V
WITHOUT SHAFT SEAL
RPM
8000
7000
6000
5000
4000
3000
2000
1000
40
70
100
31
CONTINUOUS RATING
INTERMITTENT RATING
10
20
30
40 inlb
1.0
2.0
3.0
4.0
(Nm) 5.0
TORQUE Nm

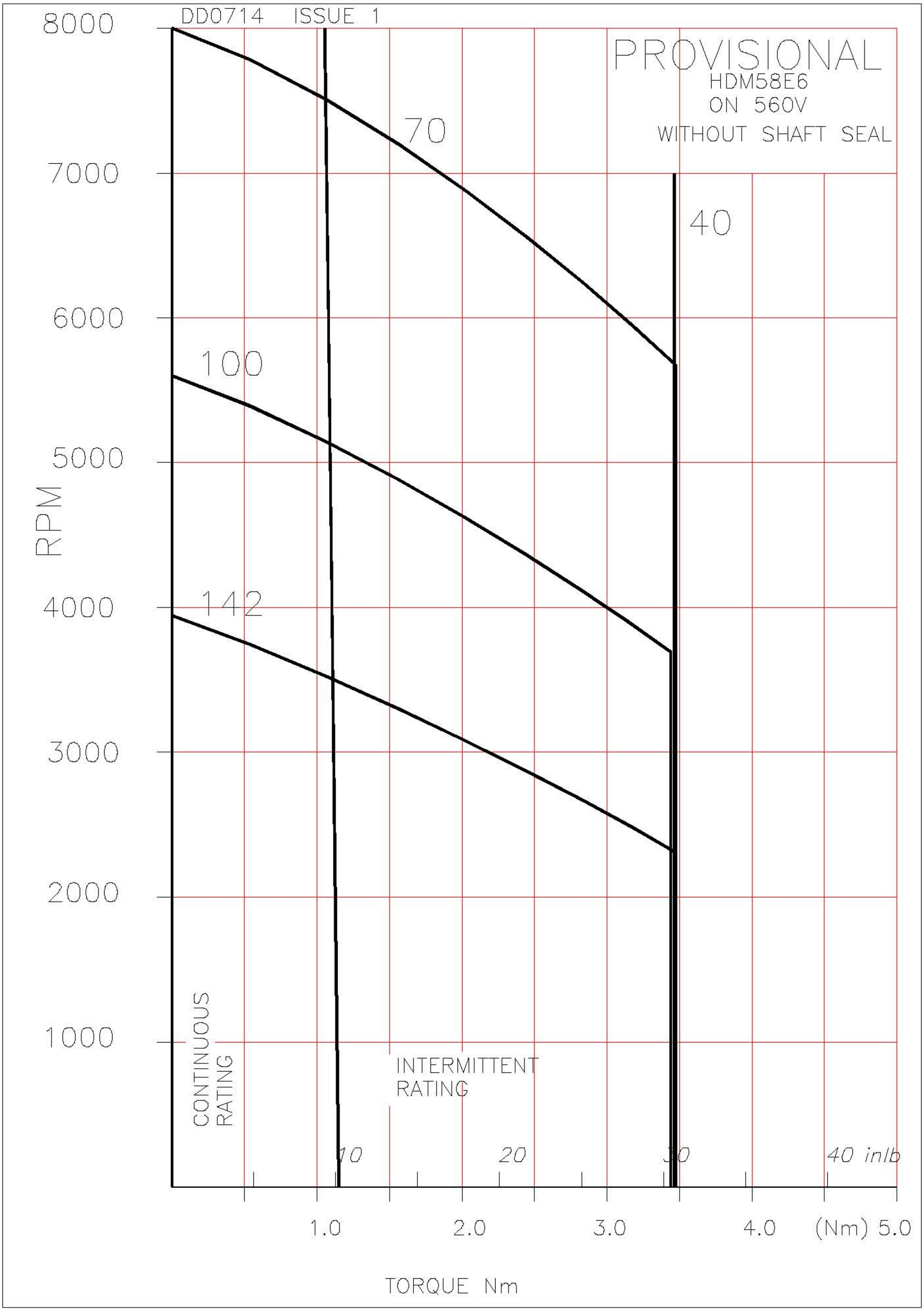
DD0714 ISSUE 1
PROVISIONAL
HDM58E6
ON 560V
WITHOUT SHAFT SEAL
8000
7000
6000
5000
4000
3000
2000
1000
RPM
70
40
100
142
CONTINUOUS
RATING
INTERMITTENT
RATING
10
20
30
40 inlb
1.0
2.0
3.0
4.0
(Nm) 5.0
TORQUE Nm

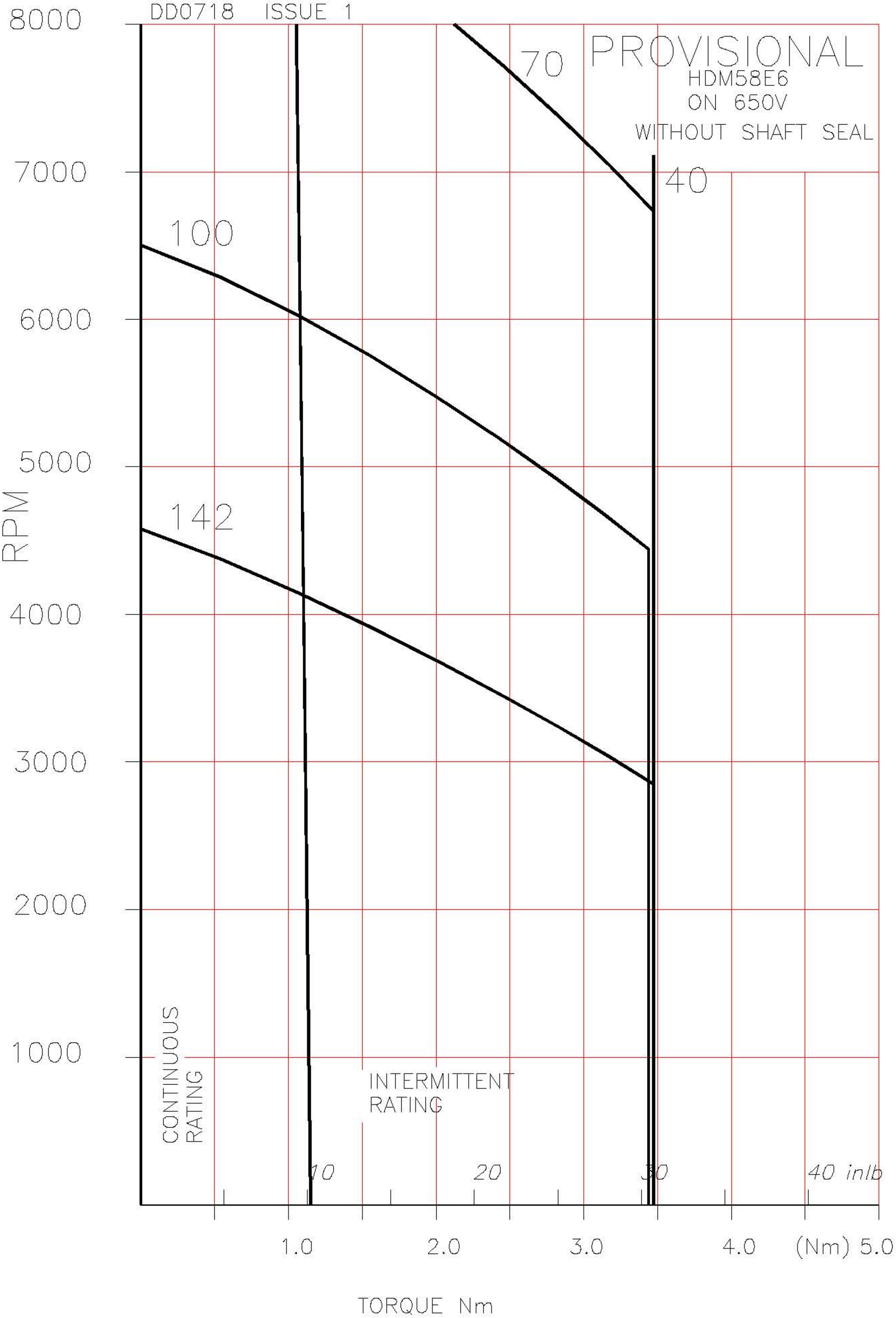
DD0718 ISSUE 1
PROVISIONAL
HDM58E6
ON 650V
WITHOUT SHAFT SEAL
70
40
100
142
8000
7000
6000
5000
4000
3000
2000
1000
RPM
CONTINUOUS RATING
INTERMITTENT RATING
10
20
30
40 inlb
1.0
2.0
3.0
4.0
(Nm) 5.0
TORQUE Nm

HDM58 PERMITTED RADIAL SHAFT LOADINGS

(If axial loads are to be applied, the equivalent radial loading must be calculated as described on next page)

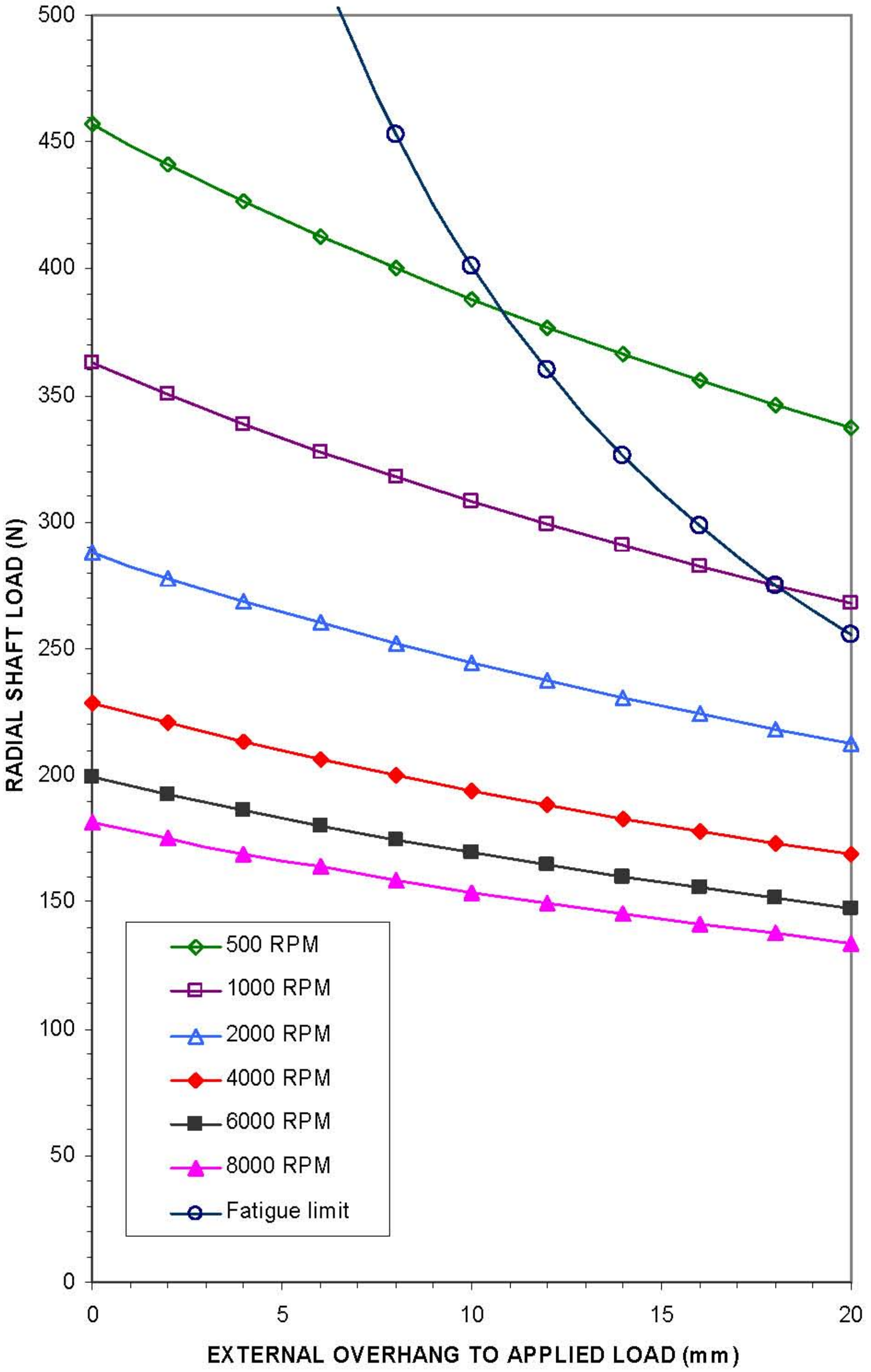

Shaft Loading Information for SEM Standard Servomotors

General notes:-

1 All loadings are based upon An L10 bearing life expectancy of 30,000 hours.

2 Separate graphs are usually supplied to indicate maximum axial loads which are applicable. However, for motors with locked drive end bearings, a graph is used to illustrate the maximum allowed radial shaft loadings together with a simplified calculation to provide a compensated figure for when radial and axial loadings are to be applied in combination.

3 It may occur, in certain circumstances, that loading outside the scope of the published information is deemed necessary. In these cases it is desirable that SEM Ltd should be consulted and all relevant information made available, in order that due consideration can be given to finding a satisfactory solution.

4 Should motors be required to operate under abnormal conditions, such as excessive vibration or shock, this should also be referred to SEM Ltd as noted above.

HDM58 COMBINATION OF AXIAL AND RADIAL LOADING

Calculated combined load must NOT EXCEED the Radial Shaft loadings as per Radial Loading Chart

Equivalent radial load (Pr) = 0.56Fr + Yfa
or = Fr (Whichever is the larger)

Where Fr = Applied radial load
Fa = Applied axial load (232N Max)
Yfa = Value taken from chart

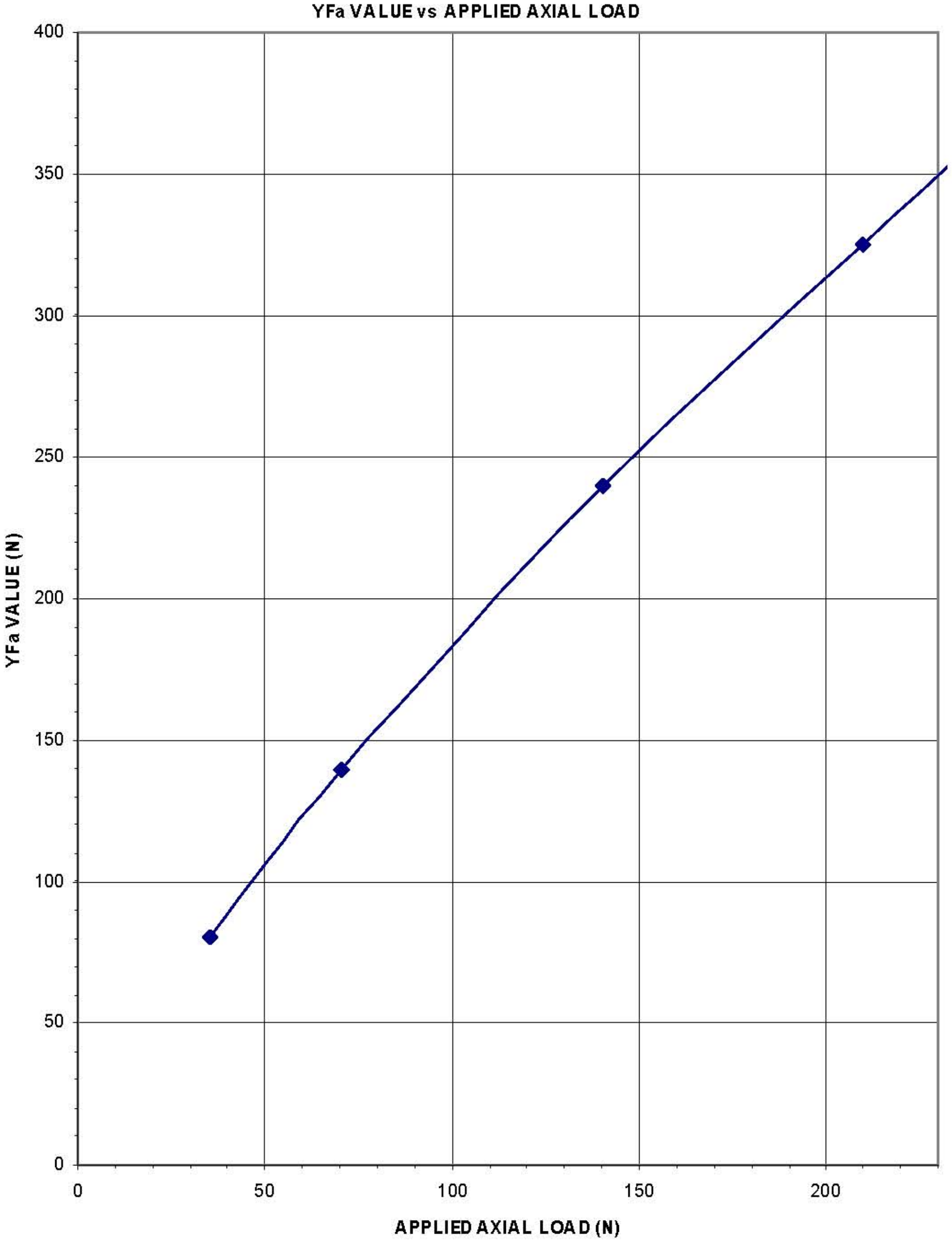

Shaft Loading Information for SEM Standard Servomotors

General notes:-

1 All loadings are based upon An L10 bearing life expectancy of 30,000 hours.

2 Separate graphs are usually supplied to indicate maximum axial loads which are applicable. However, for motors with locked drive end bearings, a graph is used to illustrate the maximum allowed radial shaft loadings together with a simplified calculation to provide a compensated figure for when radial and axial loadings are to be applied in combination.

3 It may occur, in certain circumstances, that loading outside the scope of the published information is deemed necessary. In these cases it is desirable that SEM Ltd should be consulted and all relevant information made available, in order that due consideration can be given to finding a satisfactory solution.

4 Should motors be required to operate under abnormal conditions, such as excessive vibration or shock, this should also be referred to SEM Ltd as noted above.

FIRST ANGLE PROJECTION

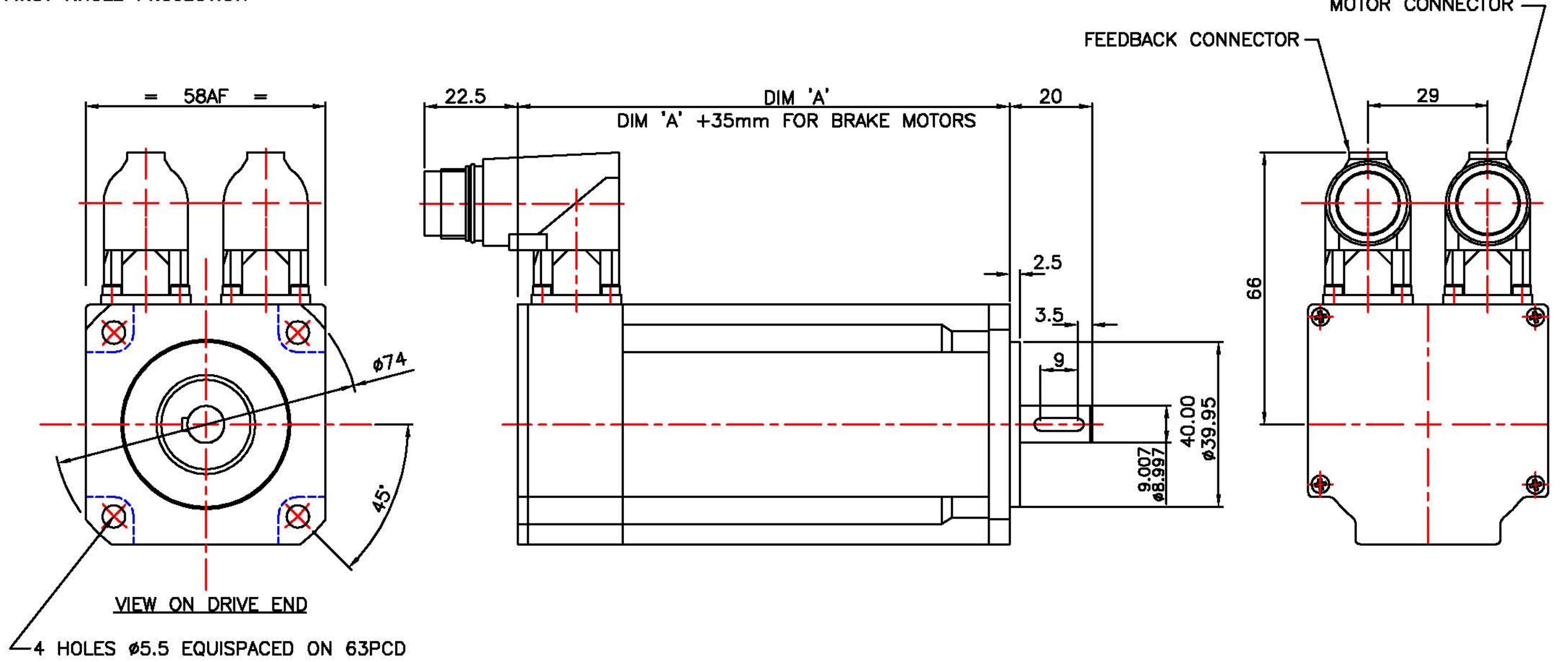
MOTOR CONNECTOR
FEEDBACK CONNECTOR
= 58AF =
22.5
DIM 'A'
DIM 'A' +35mm FOR BRAKE MOTORS
20
29
2.5
3.5
9
66
40.00
ø39.95
9.007
ø8.997
ø74
45°
VIEW ON DRIVE END
4 HOLES ø5.5 EQUISPACED ON 63PCD

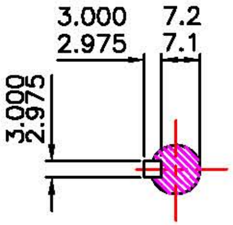
3.000
2.975
7.2
7.1
3.000
2.975

SHAFT DETAIL AT DE

FRAME	DIM'A'
HDM58A	88.5
HDM58C	106.0
HDM58E	123.5
HDM58G	141.0

FOR CONNECTORS FACING DE SEE 664-7-06522

2 NOW SHOWN WITH WITH CAST BODY/DE
(PRE-ISSUE CHANGE)

ALL DIMENSIONS IN MILLIMETRES
TOLERANCES UNLESS ANG: ±0.5°
OTHERWISE STATED DIM: ±0.25mm

TITLE: OUTLINE HDM58 STD MET WITH M17 CONNS FACING NDE

MATERIAL		**CODE**	
SPEC		**FORM**	
FINISH		**PATTERN No.**	

DRAWING No.
664-7-06455

SEM
LONDON ENGLAND

SCALE	1:1
ISSUE No.	2
DR.	SIH
DATE	04JAN06

A06455B1

IMD Series User Manual

Digital drive for brushless ac servomotors

IMD series
Intelligent Motion Drive
SERAD

The manual covers the installation and use of the following drive types:

- **IMD / 1**
- **IMD / 2**
- **IMD / 5**
- **IMD / 10**

Manufacturer :

Serad S.A.
271 routes des crêtes
44440 Teillé
France

Phone: +33 2 40 97 27 04
Fax: +33 2 40 97 27 04

web: www.serad.fr
email: info@serad.fr

UK Distributor :

Norwin Electronics Ltd
Unit 6, Industrial Estate
Station Road, Gamlingay
Nr. Sandy, Bedfordshire
SG19 3HB

Phone: 01767 651485
Fax: 01767 651623

web: www.norwin.co.uk
email: sales@norwin.co.uk

We reserve the right to make changes to all or part of the specification without prior notice.

1.2.2 Technical data

Supply : 230 to 400V AC ±10% three phase

Auxiliary supply : 24V DC ±10%, 0.4A typical (0.7A max with all options fitted)

Supply filter : Integral

Switching frequency : 6.67 kHz sine-wave PWM

DC Bus voltage : 310V to 680V

Braking resistor : Integral: 75 ohms, 60W

Facility to add an external resistor:

Min. value	Max. cont. power	Max. pulse power
60 Ω	5kW	10kW

Protection :
Short circuit between phases, phase to earth,
Over current, I2t
Over voltage, under voltage
Motor feedback fault

Motor feedback :
Resolver (16 bit resolution)
Absolute resolver accuracy ± 0.7°
SinCos encoder Hiperface (option)

Master encoder input :
Incremental: A, /A, B, /B, Z, /Z
Absolute: SSI
SinCos encoder Hiperface (option)
Vitual

Encoder emulation : Incremental: A, /A, B, /B, Z, /Z 1 to 100,000 points per rev

Diagnostic display : 7 segment LED

Communication :
RS232 Modbus RTU
RS485 Modbus RTU (option)
IMDBUS for master / slave applications
CANopen (option)
Ethercat (option)

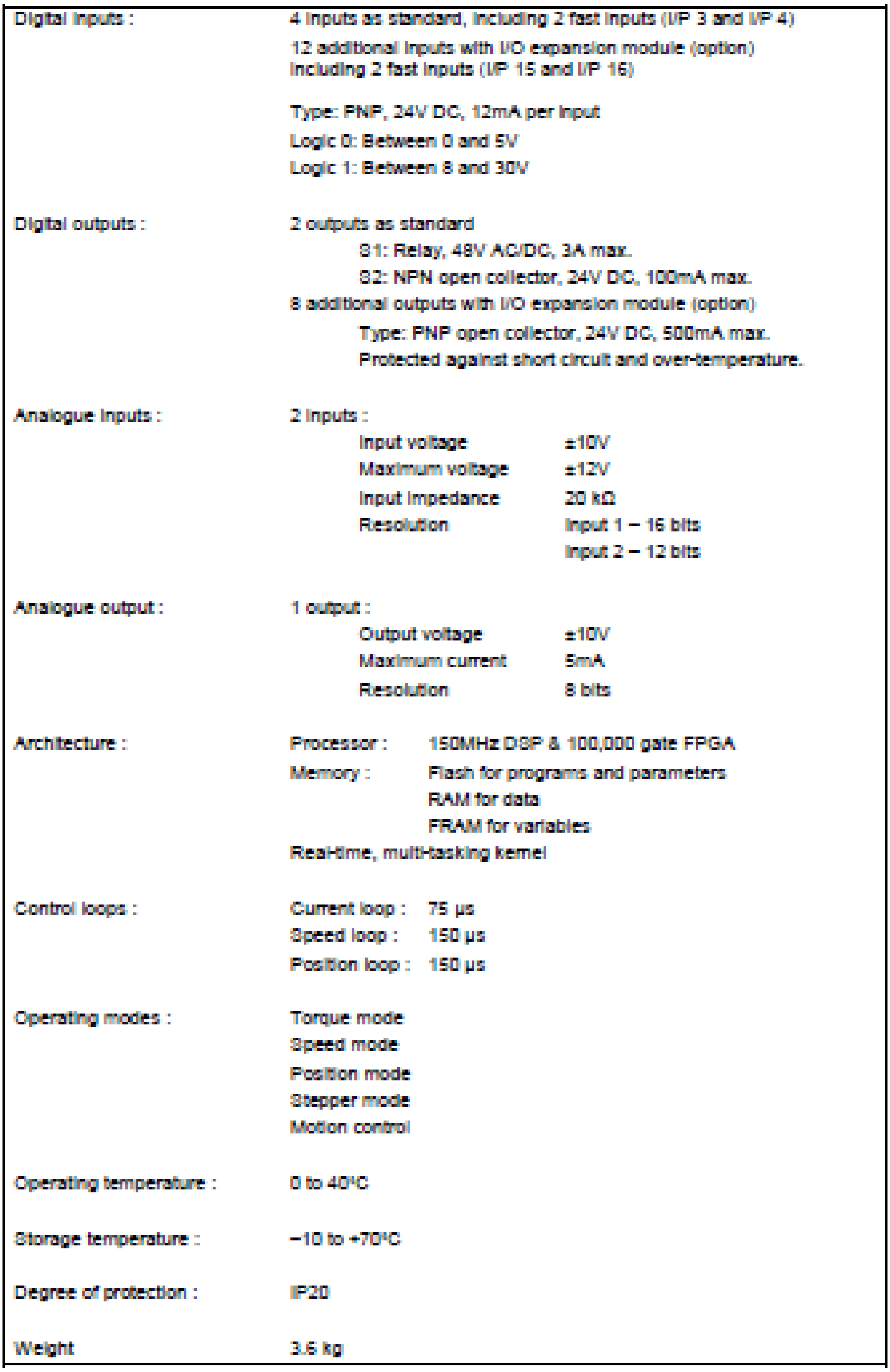

Digital inputs :	4 inputs as standard, including 2 fast inputs (I/P 3 and I/P 4) 12 additional inputs with I/O expansion module (option) including 2 fast inputs (I/P 15 and I/P 16) Type: PNP, 24V DC, 12mA per input Logic 0: Between 0 and 5V Logic 1: Between 8 and 30V
Digital outputs :	2 outputs as standard S1: Relay, 48V AC/DC, 3A max. S2: NPN open collector, 24V DC, 100mA max. 8 additional outputs with I/O expansion module (option) Type: PNP open collector, 24V DC, 500mA max. Protected against short circuit and over-temperature.
Analogue inputs :	2 inputs : Input voltage ±10V Maximum voltage ±12V Input impedance 20 kΩ Resolution Input 1 – 16 bits Input 2 – 12 bits
Analogue output :	1 output : Output voltage ±10V Maximum current 5mA Resolution 8 bits
Architecture :	Processor : 150MHz DSP & 100,000 gate FPGA Memory : Flash for programs and parameters RAM for data FRAM for variables Real-time, multi-tasking kernel
Control loops :	Current loop : 75 µs Speed loop : 150 µs Position loop : 150 µs
Operating modes :	Torque mode Speed mode Position mode Stepper mode Motion control
Operating temperature :	0 to 40°C
Storage temperature :	–10 to +70°C
Degree of protection :	IP20
Weight	3.6 kg

15 Appendix D – Technical Drawings

16 Appendix E – Publication

Chamberlain, M. R., Jackson, M. R. and Parkin, M. R. (2011).Some Effects of Database Corruption in System Prediction Performance. The 15th International Conference on Mechatronics Technology (ICMT 2011), Nov 30 – Dec 2, 2011, Melbourne, Australia

Some Effects of Database Corruption in System Prediction Performance

Matthew R. Chamberlain, Michael R. Jackson, Robert M. Parkin

Mechatronics Research Centre, Wolfson School of Mechanical and Manufacturing Engineering, Loughborough University, Loughborough UK

Corresponding: - m.r.chamberlain@lboro.ac.uk

Abstract – Many types of intelligent adaptive systems use vast databases of a-priori knowledge during training phases. These systems are then reliant on both the accuracy of this data and on the breadth of the data. It is assumed whilst training that the data encompasses the total operating window for the system in enough detail to generate an accurate 'black box' model of the plant under control. It may be that under certain unforeseen operating conditions, or in a scenario where there is little prior knowledge, the system may be forced to operate outside the scope of the original a-priori knowledge. Lastly the data gathered into the a-priori source may have been unintentionally corrupted. This paper aims to examine some of these effects upon two common adaptive intelligent tools, neural networks and an adaptive neuro-fuzzy inference system, ANFIS, network.

Keywords – A-priori, neural network, ANFIS, data corruption, PID, motor control.

1 INTRODUCTION

One common control tool employed in motor control is the PID controller.[1][2] This is a widely known and used controller. The system uses three different gains, proportional, integral and derivative, and the weighted sum of these three gains is used to modify the system output in order to minimise the error.

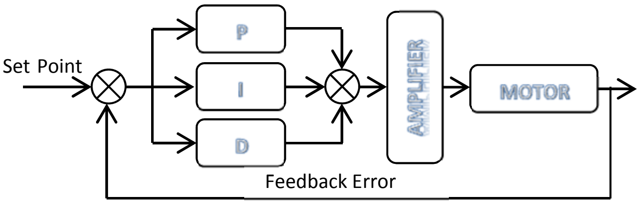

Figure 1 - PID Controller Schematic

In this paper the controller output is modelled by both a neural network and an ANFIS network. Ultimately all three gains could be controlled using an adaptive intelligent tool such as these but in order to simplify the results shown here, only the proportional gain effects are shown.

It is common to assess the performance of a PID controller through three separate conditions, rise time, settle time and overshoot.[3] Depending on the plant under control of the controller the importance of each of these characteristics is modified. For example in a situation where accuracy is of higher importance than speed, the controller gains could be modified to reduce the overshoot whilst at the same time having a detrimental effect on the settling time. Within this paper the results displayed highlight the maximum overshoot of the plant. It is therefore appropriate to consider this a case where the plant, a motor in this case, is situated in a condition where accuracy is the key important factor, outweighing speed.

It is reasonable to accept that if the adaptive technique can predict the performance of the DC motor, with respect to overshoot, that it can be used to control it. Overshoot and settle time are graphically shown in Figure 2. Within this paper overshoot is defined as the maximum speed above the set point speed and settle time is defined as the time from the initial step input to the time that the motor speed has settled to within a constant band about the set point level. Either a user, or an algorithm, is able to define the output system performance requirement, and the adaptive technique is then able to generate a set of parameters to achieve the desired overall characteristics, thereby using the predictive ability of the adaptive technique to effectively control the overall mechanical system.

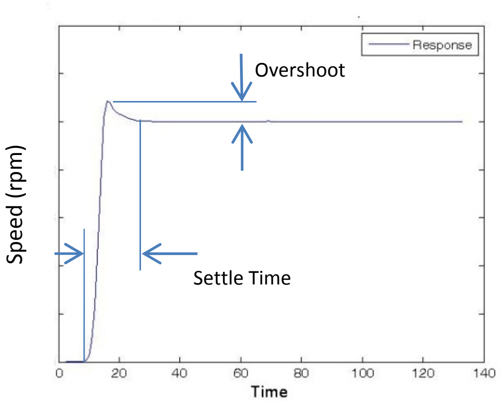

Figure 2 - Graphical Definition of Overshoot and Settling Time

The plant under investigation is a simple DC motor, modelled within MATLAB, and as mentioned above the results highlight the effect of changing the P gain on the system overshoot performance. This paper investigates the effect of differing training data corruption types, noise and anomaly data errors, on the system prediction performance of the DC motor characteristics. Also under investigation is the performance of two different neural network systems when operating outside the a-priori knowledge training database. This condition may be crucial when a machine operating window is expanded through some different technique and the input-output data is now not available as these conditions were not originally foreseen, or in cases where there is simply not a full a-priori knowledge base covering all operating conditions, such as in the development of new technologies.

2 NETWORKS

This paper focuses on two types of adaptive techniques, neural networks and ANFIS networks. These have been selected due to their popularity and implementation in both research and industrial applications.[4], [5],[6]. Other methods that have been classified as intelligent and/or adaptive such of genetic algorithms; probabilistic reasoning and Bayes theorem are not considered within the scope of this paper, [7].

A neural network is a network made up of interconnected neurons in layers. Much work has been undertaken to investigate these networks, [8], and it is generally accepted that increasing the number of neurons within the hidden layers is a law of diminishing returns, and that often a satisfactory result can be obtained with a relatively low number of neurons [9]. Considerable research effort has been expended on neural network implementation into real world problems, with particular effort spent on preserving previous training iterations to prevent the system from overtraining to a particular set of restricted data, rather than training to the underlying control problem. [10] .

An ANFIS model is similar to a neural network with a number of membership functions and rules with adjustable parameters. These parameters are chosen to tailor the membership functions to the a-priori knowledge to best represent the data. This tuning is often carried out using back propagation, sometimes in conjunction with a least squares method, to generate a fuzzy inference system, FIS. The inputs to the network are then mapped through input membership functions and associated parameters, and then through output membership functions.

The fuzzy nature of the ANFIS, where a single input may adhere to multiple membership functions, potentially allows the system to better handle uncertainty by attaching degrees of certainty to the answer, [11]. This paper also investigates whether this ability aids the ANFIS network to overcome data corruption, and to be able to effectively decipher the underlying correlation between the input-output data.

3 SYSTEM TRAINING

Whilst creating both the ANFIS and neural networks data sets are required, sometimes referred to as a-priori knowledge. These data sets should cover the entire operating scope of the system, such that a full ‘picture’ can be produced. The data should also have a high enough resolution such that there are no large gaps in the data set. This allows the effect of any error in the training data to be reduced. This data is commonly split into two separate data sets, often referred to as training data and validation data. The training data is then used to train the network and the validation data used to validate the performance of the network.

Two different types of training data error are considered. Noise errors, where the amplitude of the signals within the training database is corrupted through the addition of a random signal, this may be a positive or negative signal, and anomaly errors; these are large single point errors. Noise errors can enter into signals from a wide range of conditions. These can be from pure pickup along the length of any signal cabling, to degradation of electrical components. Anomaly errors are more commonly caused by signal conditioning elements clipping the amplitudes of signals or a mismatch in sampling frequencies.

However, in cases where there is limited data there may not be enough data to reduce the effects of these types of data corruptions. If this is the case it is important to know the effect these corruptions will have on the eventual system performance. Therefore to investigate this, a number of test cases have been created, using ideal and corrupted data in a controlled scenario. This has allowed the effect of specific types of data corruption to be isolated and investigated without any other possible effects having occurred.

A simple MATLAB Simulink model of a DC motor has been created to provide a set of input-output data to train the different network types. The proportional gain of the PID controller was altered from a value of 1 to 1200 and the maximum speed overshoot, in revolutions per minute, for each condition recorded. The data sets consisted of a single data point for each condition, and this is referred to as the ideal/original data set. (Error in the following graphs is defined as the network predicted response subtracted from the ideal/original response.)

This ideal/original data set was then corrupted through differing levels of anomaly and noise error. These levels were set at 5%, 10% and 50%, where a 50% error level denotes a noise signal of up to 50% of the original output amplitude in the data set and 50% of the data points having been corrupted with an anomaly data error. The anomaly value was set to a high peak value, which although with any amount of database inspection could be filtered out; it has been left to assess its effects on the network performance.

4 DATABASE CORRUPTION EFFECTS

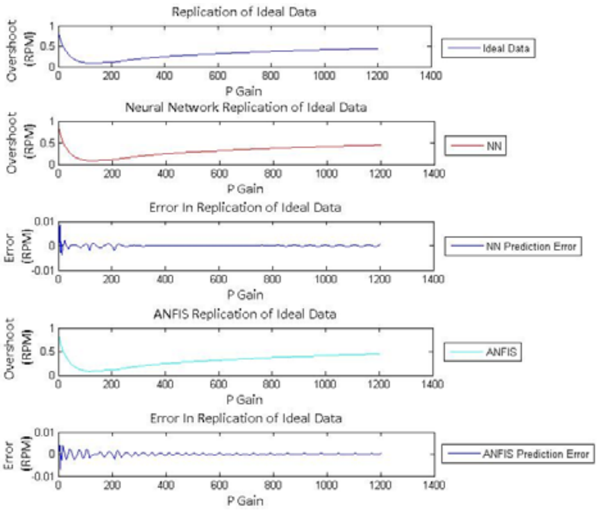

Figure 3 - Replication of Ideal Data

Figure 3 shows that both an ANFIS model and a neural network are more than adequate in modelling a DC motor overshoot performance. It can be seen that both the neural network and the ANFIS systems have almost no appreciable error. These error levels are shown in more detail in Figure 4.

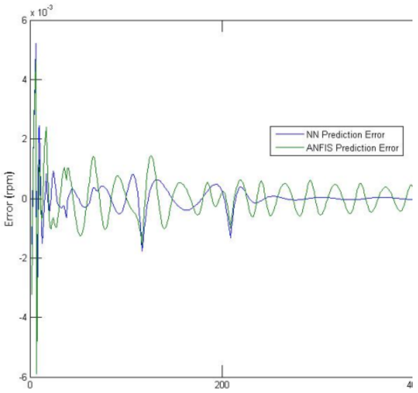

Figure 4 - Ideal Data Replication Error

Figure 4 shows that at a very low proportional gain both systems have some level of prediction error but that the actual level is still very low, as shown in Figure 4, in the order of 1%. It is of note that the ANFIS prediction appears to oscillate around a zero error level whereas the neural network is of an order of magnitude more accurate. These figures are provided as a control to compare to subsequent corrupted database figures.

If the training database for both the ANFIS system and neural network system is now corrupted with a noise type error of 5% amplitude differences, start to become apparent between the two different system performances, as shown in Figure 5.

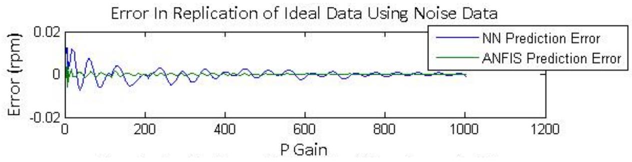

Figure 5 - Replication Errors with 5% Noise Errors

At this 5% noise error level the neural network performance appears to be more affected than the ANFIS type network. One likely cause for the increased performance of the ANFIS network is the key makeup of the ANFIS network, the fuzzy nature of the system overcoming to a certain degree the noisy nature of the training data.

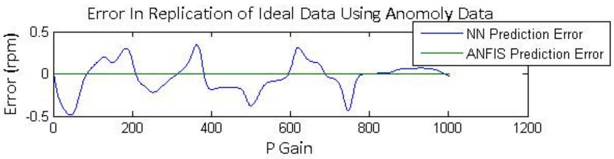

Figure 6 - Replication Errors with 5% Anomaly Data

Figure 6 shows the error of both systems when using the anomaly data set to train the systems. It can be seen that the results are similar, if more extreme, than with the noise data. Again the ANFIS system has a much higher system performance than that of the neural network. The peak error value of 0.38 at a proportional gain of 390, when compared to the real peak value of 0.5 is an error percentage of 76% and even with this low level of data corruption the neural network based system is not performing to any level of acceptable accuracy.

Interestingly if Figure 6, the outputs of the neural network and ANFIS systems, is compared to Figure 7 the output of the systems, there is a correlation between the neural network predicted overshoot and the volume of anomaly data stacked on that particular side of the ideal data line.

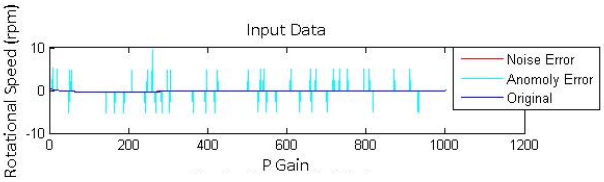

Figure 7 - 5% Training Data Set

This trend is to be expected to some degree as it is the network mapping more accurately the input data, however in this case this is actually a negative outcome as this more accurate mapping, is being driven away from the real system response by the database corruption.

As the level of database corruption is increased the prediction error with respect to noise error does not dramatically increase, see Figure 8. This shows that as the noise level is increased there is no real increase in prediction error for either the neutral network based system, or the ANFIS based system. Again however the ANFIS system outperforms the neural network based one by an order of magnitude.

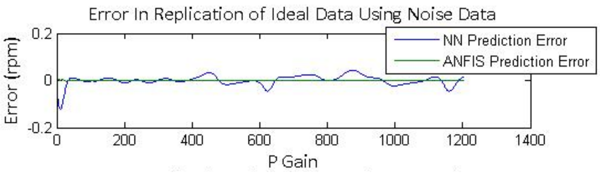

Figure 8 - Replication Errors with 50% Noise Errors

Conversely, when considering the performance of the systems trained with anomaly data the picture is rather different. Again the ANFIS system has overcome the errors and performs adequatly, as can be seen in Figure 9. This figure shows that although the ANFIS prediction performance continues at a high level the performance of the neural network has dramatically reduced. The peak value of an error of 2.1, at the proportional gain of 600, is 400% of the maximum real value. This figure graphically shows the difference in performance of the neural network and ANFIS techniques and the advantages of the ANFIS system when considering both noise and anomoly type error corruptions of the the a-priori knowledge base.

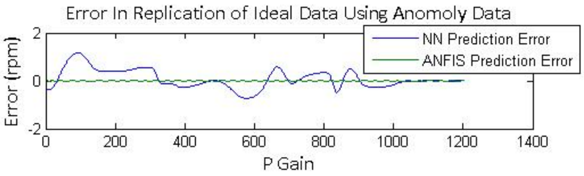

Figure 9 - Replication Errors with 50% Anomaly Errors

When considering any system there must be a scope of operation. The training data must cover this entire scope such that the system used to control the plant has ‘experience’ of all possible operating conditions. Two different neural networks have been trained using the same a-priori knowledge base as training data, the ideal/original data. Both networks have the same simple three layer structure, with a single neuron in both the input and output layers. The first network however has two hidden neurons in the hidden layer whereas the second network has five hidden neurons. The hidden layer populous were selected arbitrarily but were kept low to reduce training times. The training data scope was reduced for both networks to a proportional gain of 700, beyond this point neither network had any a-priori knowledge.

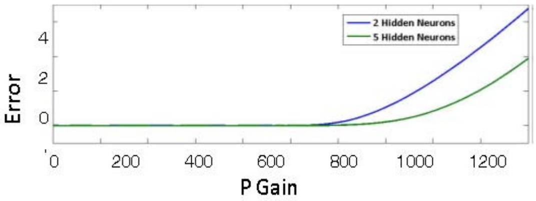

Figure 10 - Out of Scope Performance

As seen in Figure 10, the results correlate well with the previous work carried out by [9] as both networks have low actual number of hidden neurons and a high system prediction performance over the entire scope of the training data, which is to be expected. However once beyond the training data scope the performance of the different networks begins to diverge. This divergence accelerates further beyond the edge of the training data. Interestingly the network with 5 hidden neurons appears to model the real world behaviour more accurately beyond the edge of the training data than the network with 2 hidden neurons.

Although the training data should encompass the total operating conditions, it is a crucial acknowledgement that the networks will give responses to unsupported input conditions. This may have implications where the operating scope of the machine using a neural network is expanded but the underlying neural network controlling the machine is not retrained for the expanded scope. The network would still give a prediction for the out of scope conditions which could be incorrect, leading the machine to potentially produce waste.

5 CONCLUSIONS

In this paper two common network types have been investigated for robustness against two training database corruption types, noise and anomaly type. The main focus of the work has been systems with sparse training databases as those with both full and deep a-priori knowledge will most likely overcome these types of corruptions more significantly. ANFIS networks appear to be able to overcome the difficulties of database corruptions more adequately, including up to 50% corruption rates as described in section 4, whereas the non-fuzzy architecture of the pure neural network is not able to overcome these types of errors with to the same level.

Two neural networks have also been forced to work beyond the scope of their training data, and the evidence suggests that networks with a higher number of hidden neurons in the hidden intermediate layers have a lower prediction, and thereby ability to control, error level, although this condition should be avoided if possible as the error level rapidly increases once operating conditions are outside the a-priori knowledge base.

Further work is focused on involving different corruption types, including mixed type of corruption and alternative adaptive techniques.

6 REFERENCES

[1]Visual servoing based on fuzzy adaptive PID with Modified Smith Predictor for micromanipulation. ; 2 - 5 July; ; 2008.

[2]Mori S, Sakaguchi A, Yamamoto T. Design and experimental evaluation of a data-driven skill-based PID controller. Advanced intelligent mechatronics, 2007 ieee/asme international conference on 2007:1-5.

[3]Chen M. A hybrid neuro-fuzzy PID controller. Fuzzy Sets Syst. 1998;99(1):27-36.

[4]Javadpour R. A fuzzy neural network approach to machine condition monitoring. Comput.Ind.Eng. 2003;45(2):323-330.

[5]Tsai Y, Chen JC, Lou S. An in-process surface recognition system based on neural networks in end milling cutting operations. Int.J.Mach.Tools Manuf. 1999 4;39(4):583-605.

[6]Monostori L. AI and machine learning techniques for managing complexity, changes and uncertainties in manufacturing. Engineering Applications of Artificial Intelligence 2003;16:277-277-291.

[7]De Silva CW. The Role of Soft Computing in Intelligent Machines. Philosophical Transactions: Mathematical, Physical and Engineering Sciences 2003;361:1749-1749-1780.

[8]Marinai S. Artificial neural networks for document analysis and recognition. IEEE Trans.Pattern Anal.Mach.Intell. 2005;27(1):23-35.

[9]Balazinski M. Tool condition monitoring using artificial intelligence methods. Eng Appl Artif Intell 2002;15(1):73-80.

[10]Pomerleau DA. Efficient training of artificial neural networks for autonomous navigation. Neural Comput. 1991;3(1):88-97.

[11]McKone TE. Can fuzzy logic bring complex environmental problems into focus? Environ.Sci.Technol. 2005;39(2):42A-47A.